THESIS
1
2000

This is to certify that the

dissertation entitled

Extended Molecular Arrays of transition metal complexes with polynitrile ligands

presented by

Xiang Ouyang

has been accepted towards fulfillment
of the requirements for

Ph.D degree in Chemistry

Kem K Dunn

Major professor

Date 12/15/99

MSU is an Affirmative Action/Equal Opportunity Institution O-12771

LIBRARY
Michigan State
University

PLACE IN RETURN BOX to remove this checkout from your record.
TO AVOID FINES return on or before date due.
MAY BE RECALLED with earlier due date if requested.

DATE DUE	DATE DUE	DATE DUE

11/00 c:/CIRC/DateDue.p65-p.14

EXTENDE

METAL C

EXTENDED MOLECULAR ARRAYS OF TRANSITION METAL COMPLEXES WITH POLYNITRILE LIGANDS

By

Xiang Ouyang

A DISSERTATION

Submitted to
Michigan State University
in partial fulfillment of the requirements
for the degree of

DOCTOR OF PHILOSOPHY

Department of Chemistry

1999

EXTEND
METAL C

The mai
solid-state stru
materials with
quest in this ar
that can beha
magnetization
that may exhib
magnetic prop
systems could
temperatures,
(nanomagnets).

In searc
dimensional p
acceptors. A n
transition met
tetracyanoquin
metal building
TCNQ and sir
structures base

ABSTRACT

EXTENDED MOLECULAR ARRAYS OF TRANSITION METAL COMPLEXES WITH POLYNITRILE LIGANDS

by

Xiang Ouyang

The main goal of this project is to design, synthesize and study the solid-state structures of molecular assemblies and polymeric molecule-based materials with potentially interesting magnetic or electrical properties. The quest in this area of research is not just to obtain molecule-based compounds that can behave as classical solid state magnets, showing spontaneous magnetization below a certain temperature Tc, but also to unearth materials that may exhibit completely new physical properties or those in which the magnetic properties are combined with other properties. Examples of such systems could be materials showing bistability, tunable magnetic ordering temperatures, discrete molecules showing magnetic hysteresis (nanomagnets), or hybrid materials coupling magnetism with conductivity.

In search of new materials, we isolated one-, two- and three-dimensional polymers with paramagnetic metals joined by organic acceptors. A main focus has been to synthesize and crystallize paramagnetic transition metal compounds linked by the stable organic radical tetracyanoquinodimethanide, $TCNQ^{\cdot}$. In one case, quadruply bonded metal-metal building blocks have been introduced into extended networks with TCNQ and similar molecules. Solid-state structures of 1-D polynitrile structures based on diamagnetic Mo_2^{4+} units have been carried out; these

constitute a va

units such as th

Two ma

special attenti

crystallize and

In spite of thi

inspired us to u

the CCD area c

with the avai

opportunities t

been plagued b

issues will be a

In addi

transition meta

have been prep

molecular arra

techniques inc

spectroscopy,

discussed.

constitute a valuable model for other compounds with open shell dimetal units such as those previously reported for mixed-valence Ru_2^{5+} compounds.

Two main obstacles were encountered in the project that required special attention, namely that metal-TCNQ compounds are difficult to crystallize and that they are notorious for their inherent twinning problems. In spite of this, their potential applications in molecular based materials inspired us to undertake crystallographic studies. Fortunately, the advent of the CCD area detector for single crystal X-ray data collection taken together with the availability of sophisticated twinning software provided new opportunities to pursue crystal structure determination. These have long been plagued by twinning, disorder or small crystal size problems. These issues will be addressed in detail in the context of modern CCD methods.

In addition to metal-metal bonded precursors and mononuclear transition metal precursors, polynuclear 3d transition metal halide clusters have been prepared as potential precursors for the construction of extended molecular arrays. Characterization of the compounds by solid-state techniques including single crystal and powder X-ray methods, infrared spectroscopy, and scanning and transmission electron microscopy are discussed.

To my wife Ying and my son Andrew

First, I w
wise guidance
energetically e
having difficu
crystallograph
team", Robert
Hanhua Zhao,
many compou
Juan Modesto
Professor Euge
thank all the pa
Gary, Kemal, C
R. Clerac and S

Many th
Chemistry and
support. I wo
about crystallo
Sparks, for his
to the marvelou
like to thank m
D. Ward for th
advice as a sec
C. Campana of

ACKNOWLEDGEMENT

First, I would like to thank my advisor-professor Kim R Dunbar. Her wise guidance and full support were always with me though the years. She energetically encouraged me to pursue my goal, especially when I was having difficulties. It was she who led me into my new career - crystallography. I would also like to thank our "magnetic and conducting team", Robert Heintz, Guilio Grandinetti, and especially "Han" (Professor Hanhua Zhao, Nanjing Normal University, Nanjing, Chaina), who prepared many compounds for my structural studies. I would also like to thank Dr. Juan Modesto for his help in fitting magnetic data and to our collaborators Professor Eugenio Coronado and late Professor Jerry Cowen. I also want to thank all the past and present Dunbar group members, Staurt, Stacey, Alice, Gary, Kemal, Calvin, Robert, Matt, Paul, Jen H.& Jen S., Cristian, Liz, Dr. R. Clerac and Shannon, for their friendship and help.

Many thanks to Michigan Sate University, the Department of Chemistry and the Center for Fundamental Material Research for financial support. I would like to thank Dr. Don Ward for many long discussions about crystallography and twinning. I would like to thank to Dr. Bob Sparks, for his β–release of the TWINNING 1.0 package that introduced me to the marvelous world of problematic and twinned structures. I would also like to thank my committee: Professor G. Baker, Professor J. Geiger and Dr. D. Ward for their helpful comments, as well as Professor M. Smith for his advice as a second reader on my defense. Finally appreciation goes to Dr. C. Campana of Bruker AXS who taught me the operation of the SMART

CCD diffracto
many helpful d
Last but
their tremendo
for their patien

CCD diffractometer. And to Dr. V. Young of University of Minnesota for many helpful discussions on the treatment of twinning structures.

Last but certainly not least, I want to thank my wife and my son for their tremendous support and understanding and my sister and my parents for their patience and support.

TABLE OF CONTENTS

Page

LIST OF TABLES xviii
LIST OF FIGURES xxiv
LIST OF SYMBOLS AND ABBREVIATIONS xxxi
CHAPTER I
INTRODUCTION 1
1. History of Molecule-Based Materials (Molecular Magnets/Molecular Conductors) 2
A. Molecule-based Conductors 2
B. Molecule-based Magnets 3
2. Interaction of Magnetic Spins 4
A. Orthogonality of Spins 4
B. Orbital Interactions of Dimetal Complexes with Polynitrile Ligands 6
3. Design of Molecule-based Materials from Inorganic/Organic Precursors 6
A. M(TCNQ) and $M(TCNQ)_2$ Materials 7
(1) General background 7
(2) Polymeric metal-TCNQ materials 10
B. Metal-Metal Bonded Precursors in Molecule-Based Materials. 12
C. Soluble Transition Metal Coordination Complexes as Precursors 14
4. Handling Crystallographic Problems with a CCD Detector 15
References 16
CHAPTER II
SYNTHESES AND CHARACTERIZATION OF EXTENDED ARRAYS WITH METAL-METAL BONDED COMPLEXES AND POLYNITRILE ACCEPTOR LIGANDS 24

1. Introducti
2. Experimer
A. Starting
B. Synthes
(1) Prep
(a) 2:1
(b) 2:1
(c) 2:1
(2) Prep
(a) 1:1
be
(b) Gr
(3) Prep
•8C
(a) Re
7&
(b) Re
ro
(c) Sin
te
(i) E
(ii) P
(iii)
(iv) S
(4) Prep
{[M
(a) Ro

1. Introduction 25
2. Experimental Section 27
A. Starting Materials and Reaction Procedures 27
B. Synthesis 28
(1) Preparation of $Mo_2(O_2CCF_3)_4$(TCNQ) (1). 28
(a) 2:1 Reaction of $Mo_2(O_2CCF_3)_4$ with TCNQ in THF. 28
(b) 2:1 Reaction of $Mo_2(O_2CCF_3)_4$ with TCNQ in toluene. 28
(c) 2:1 Reaction of $Mo_2(O_2CCF_3)_4$ with TCNQ in xylenes 28
(2) Preparation of $Mo_2(O_2CCF_3)_4$(DM-DCNQI) (2). 29
(a) 1:1 Reaction of $Mo_2(O_2CCF_3)_4$ with DM-DCNQI in benzene/CH_2Cl_2. 29
(b) Growth of single crystals by slow diffusion reaction. 29
(3) Preparation of {[$Mo_2(O_2CCMe_3)_3$(NC)2CC(CN)CONH] •8CH_2Cl_2 }$_\infty$ (3). 31
(a) Reaction of $Mo_2(O_2CCMe_3)_4$ with TCNE in CH_2Cl_2 at – 78 °C. 31
(b) Reaction of $Mo_2(O_2CCMe_3)_4$ with TCNE in CH_2Cl_2 at room temperature. 31
(c) Single crystal growth of (3) under various low temperature conditions. 32
(i) Ethylene glycol/CO_2(s) bath. 32
(ii) Freezer storage. 32
(iii) Low temperature circulating bath 32
(iv) Solvent diffusion in a fritted H-tube at ~ -12°C. 33
(4) Preparation of {[$Mo_2(O_2CCMe_3)_3$(NC)2CC(CN)CONH]•0.5C_6H_6}$_\infty$ (4). 33
(a) Room temperature reaction. 33

(b) Benzene extraction from the CH_2Cl_2 reaction product (4). 33
(5) Preparation of $[Re_2Cl_4(dppm)_2]_2TCNQ•10THF$ (5) 34
(6) Preparation of $[Re_2Cl_4(dppm)_2]_2DM\text{-}DCNQI•10THF$ (6). 34
C. X-ray Crystallographic Studies 34
(1) $[Mo_2(O_2CCF_3)_4]_2(TCNQ)•2(m\text{-}C_8H_{10})$
$•[Mo_2(O_2CCF_3)_4]•2(m\text{-}C_8H_{10})$ (1). 34
(2) $Mo_2(O_2CCF_3)_4$ DM-DCNQI$•C_6H_6$ (2). 35
(3) $\{[Mo_2(O_2CCMe_3)_3(NC)2CC(CN)CONH]•8CH_2Cl_2\}_\infty$ (3) 36
(a) Data collected on a Siemens P3/V diffractometer. 36
(b) Data collected on a Siemens SMART CCD 1K platform
diffractometer. 37
(4) $\{[Mo_2(O_2CCMe_3)_3(NC)_2CC(CN)CONH]•0.5C_6H_6\}_\infty$ (4). 39
(5) Crystallographic study of $[Re_2Cl_4(dppm)_2]_2TCNQ•10THF$
(5) 40
(6) Crystallographic study of $[Re_2Cl_4(dppm)_2]_2DM\text{-}$
DCNQI•10THF (6). 42
3. Results and Discussion 43
A. Preparation and Characterization 47
(1) Synthesis of the TCNE product of $Mo_2(O_2CCMe_3)_4$. 47
B. Crystallographic Studies. 50
(1) $Mo_2(O_2CCF_3)_4$ TCNQ 50
(2) $[Mo_2(O_2CCF_3)_4(DM\text{-}DCNQI)•C_6H_6]_\infty$ (2) 53
(3) Structural characterization of transformed TCNE with
$Mo_2(O_2CCMe_3)_4$ 61
(a) Data from a P3/V instrument partially solved by DIRDIF. 61
(b) Structure solution and refinement of data from a Siemens
SMART CCD. 63

(i) [
(ii) [
(4) Stru
and
C. Charge
4. Summary
References..
CHAPTER III
PREPARATIO
PROPERTIES
MATERIALS
1. Introducti
2. Experime
A. Synthes
(1) Start
(2) Bulk
(a) Me
(b) Me
(3) Bulk
(4) Thin
(5) Bulk
(6) Bulk
B. Single C
(1) Cu(T
(2) [Mn(
(3) [Mn(
(4) ["Bu
(5) ["Bu

(i) $[Mo_2(O_2CCMe_3)_3(NC)_2CC(CN)CONH)]\bullet 8CH_2Cl_2$ (3) 63
(ii) $[Mo_2(O_2CCMe_3)_3(NC)_2C(CN)CCONH)]\bullet 0.5C_6H_6$ (4) 66
(4) Structural features of $[Re_2Cl_4(dppm)_2]_2TCNQ\bullet 10THF$(5) and $[Re_2Cl_4(dppm)_2]_2DMDCNQI\bullet 10THF$ (6) 72
C. Charge Transfer and Infrared Spectral Data. 76
4. Summary 77
References 78
CHAPTER III
PREPARATION, STRUCTURAL CHARACTERIZATION AND PROPERTIES OF BINARY TRANSITION METAL TCNQ MATERIALS 82
1. Introduction 83
2. Experimental Section 85
A. Synthesis 85
(1) Starting materials and reaction procedures. 85
(2) Bulk syntheses of Cu(TCNQ) phase I (7). 86
(a) Method A. 86
(b) Method B. 86
(3) Bulk synthesis of Cu(TCNQ) phase II (8). 87
(4) Thin films of Cu(TCNQ) 87
(5) Bulk synthesis of $Mn(TCNQ)_2(MeOH)_2$ (9). 88
(6) Bulk synthesis of $Mn(TCNQ)_2(H_2O)_2$ (10). 88
B. Single Crystal Growth. 88
(1) Cu(TCNQ) phase I and phase II (7), (8). 88
(2) $[Mn(TCNQ)(TCNQ\text{-}TCNQ)_{0.5}(MeOH)_2]_\infty$ (9). 89
(3) $[Mn(TCNQ)_2(H_2O)_2]_\infty$ (10). 89
(4) $[^nBu_4N][TCNQ]$ (11). 89
(5) $[^nBu_4N][TCNQF_4]$ (12). 89

(6) $[Zn(H_2O)_4(\eta^1\text{-}TCNQ)_2 \bullet TCNQ \bullet 2MeCN]_\infty$ (13). 89
(7) $[Ni(DMSO)_6][TCNQ]_3$ (14) 89
(8) $[Ni(TCNQ)_2(H_2O)]_\infty$ (15). 91
C. Physical Measurements 91
(1) X-ray crystallography. 92
(a) Cu(TCNQ) phase I (7) 92
(b) Cu(TCNQ) phase II (8) 92
(c) $[Mn(TCNQ)(TCNQ\text{-}TCNQ)_{0.5}(MeOH)_2]_n$ (9) 94
(d) $[Mn(TCNQ)_2(H_2O)_2]_\infty$ (10). 96
(e) $[^nBu_4N][TCNQ]$ (11) 96
(f) $[^nBu_4N][TCNQF_4]$ (12) 97
(g) $\{[Zn(H_2O)_4](\eta^1\text{-}TCNQ)_2 \bullet 2TCNQ \bullet 2MeCN\}_\infty$ (13). 98
(h) Structure of $[Ni(DMSO)_6][TCNQ]_3$ (14) 100
(i) Crystal structure of $[Ni(TCNQ)_2(H_2O)]_\infty$ (15). 102
(2) Powder X-ray diffraction studies. 103
3. Results and Discussion 105
A. Synthetic Methods and Powder X-ray Characterization of Cu(TCNQ). 105
(1) Bulk synthesis of phase I. 105
(2) Conversion of phase I to phase II Cu(TCNQ) in acetonitrile. 106
B. Syntheses of the $Mn(TCNQ)_2(solvent)_2$ phases. 107
C. Spectroscopic Studies. 108
(1) X-ray photoelectron spectroscopy 108
(2) Infrared spectroscopic studies. 111
(3) SEM studies of Cu(TCNQ). 112
(4) Powder X-ray studies of Cu(TCNQ) bulk phases 114
(5) Powder X-ray studies of Cu(TCNQ) films. 119

(a) At room temperature. 119
(b) At elevated temperatures 119
(6) XRD and SEM studies of $M(TCNQ)_2$ and $M(TCNQ)_2L$ 120
(a) Powder patterns of $M(TCNQ)_2$ 120
D. Single Crystal Diffraction Studies. 125
(1) Details of collection and refinement for Cu(TCNQ). 125
(a) Cu(TCNQ) phase I. 126
(b) Cu(TCNQ) phase II. 126
(c) Comparison of the Cu(TCNQ) polymorphs. 127
(d) Further structural analysis of Cu(TCNQ) and a comparison to Ag(TCNQ). 130
(2) Crystallographic studies of $M(TCNQ)_2L_x$ phase (x=solvent). 133
(a) $[Mn(TCNQ)(TCNQ\text{-}TCNQ)_{0.5}(MeOH)_2]_\infty$. 133
(b) $[Mn(TCNQ)_2(H_2O)_2]_\infty$ (10). 136
(c) Structures of $[^nBu_4N][TCNQ]$ (11) and $[^nBu_4N][TCNQF_4]$ (12) salts 140
(d) $\{Zn(H_2O)_4(TCNQ)_3 \cdot 2MeCN\}_\infty$ (13). 140
(e) $[Ni(DMSO)_6][TCNQ]_3$ (14). 143
(f) $Ni(TCNQ)_2(H_2O)$ (15). 155
(3) TCNQ bonding modes in various TCNQ containing compounds. 155
(a) Ring interactions and physical properties. 155
(b) Hydrogen bonding and weak interactions. 157
(c) Bond length relationship and the degree of charge transfer in the TCNQ ligand. 157
E. Magnetic Measurements. 157
(1) Cu(TCNQ) phases. 157

(2) Mn
F. Charge
(1) Cha
G. Conclu
References
CHAPTER IV
STRUCTURA
AND TETR
METAL HAL
1. Introducti
2. Experime
A. Synthe
(1) Prep
(a) Bu
(b) Si
(2) Prep
(a) Bu
(b) Si
(3) Prepa
(4) Prepa
(5) Prepa
(6) Prepa
(7) Prepa
(8) Prepa
(a) Bu
(b) Sin
(c) Co

(2) Mn samples..... 163
F. Charge-Transport Properties TCNQ. 166
(1) Charge-transport properties of Cu(TCNQ). 166
G. Concluding Remarks. 169
References 171
CHAPTER IV
STRUCTURAL AND MAGNETIC STUDIES OF DINUCLEAR AND TETRANUCLEAR CLUSTERS OF 3-D TRANSITION METAL HALIDES 178
1. Introduction 179
2. Experimental Section. 179
A. Synthesis. 179
(1) Preparation of $[Mn_5Cl_{10}(THF)_8]_\infty$ (16). 180
(a) Bulk preparation 180
(b) Single crystal growth 180
(2) Preparation of $[MnBr_2(THF)_2]_\infty$ (17) 180
(a) Bulk preparation 180
(b) Single crystal growth 180
(3) Preparation of crystals of $[MnCl_2(MeOH)_2]_\infty$.(18) 181
(4) Preparation of $[Fe_2Cl_4(bpy)_2]$ from $Fe_4Cl_8(THF)_4$ (19). 181
(5) Preparation of $[FeCl_2(bpy)]_\infty$ from $Fe_4Cl_8(THF)_4$ (20). 181
(6) Preparation of $[ppn]_2[Co_2Cl_6]$ (21). 182
(7) Preparation of $[ppn]_2[Mn_2Cl_6]$ (22). 182
(8) Preparation of $[ppn]_2[NiCl_4]$ (23, 24) 183
(a) Bulk Preparation. 183
(b) Single crystals of phase I (23). 183
(c) Composite crystals of a triclinic phase (24) and orthorhombic phase (23) 183

(9) Preparation of $[Mn_2(bpym)_4(\mu\text{-}F)(\eta^1\text{-}BF_4)(BF_4)_2(MeCN)$ $\bullet 2MeCN]_\infty$ (25). 183
(10) $[Et_4N]Cl\bullet[Fe_2Cl_4(MeOH)_4(\mu\text{-}2,2'\text{-}bpym)]$ (26). 184
(a) Bulk preparation. 184
(b) Single crystal growth. 184
B. Structural Studies. 184
(1) Structure of $[Mn_5Cl_{10}(THF)_8]_\infty$ (16). 184
(2) Structure of $[MnBr_2(THF)_2]_\infty$ (17). 185
(3) $[MnCl_2(MeOH)_2]_\infty$ (18) 186
(4) $Fe_2Cl_4(bpy)_2$ (19). 187
(5) $[Fe_2Cl_4(bpy)]_\infty$ (20). 187
(6) Structure of $[ppn]_2[Co_2Cl_6]$ (21) 190
(7) $[ppn]_2[Mn_2Cl_6]$ (22). 192
(8) Structure of $[ppn]_2NiCl_4$ orthorhombic phase (23). 193
(9) Composite phases of $[ppn]_2NiCl_4$ with orthorhombic and triclinic forms (23b, 24). 194
(10) $[Et_4N]Cl\bullet[Fe_2Cl_4(MeOH)_4(\mu\text{-}2,2'\text{-}bpym)]$ (26) 197
3. Discussion 199
A. X-ray Structural Results and Discussion. 199
(1) Structure of $[Mn_5Cl_{10}(THF)_8]_\infty$ (16). 199
(2) Structure of $[MnBr_2(THF)_2]_\infty$ (17) 200
(3) Structure of $Fe_2Cl_4(bpy)_2$ (19). 206
(4) Structures of $[ppn]_2[Co_2Cl_6]$ (21) and $[ppn]_2[Mn_2Cl_6]$ (22) 209
(a) $[ppn]_2[Co_2Cl_6]$ (21). 214
(b) $[ppn]_2[Mn_2Cl_6$ (22) 214
(c) $[Et_4N]Cl\bullet[Fe_2Cl_4(MeOH)_4(\mu\text{-}2,2'\text{-}bpym)]$ (26) 215
B. Magnetic Studies 219

(1) Magnetic properties of $[ppn]_2[Co_2Cl_6]$ and $[ppn]_2[Mn_2Cl_6]$. 219
(2) Magnetic fitting of Mn(II) chains of (17). 224
(3) $[Mn_5Cl_{10}(THF)_8]_\infty$chain of (16) 224
(4) Magnetism of the Mn cluster (16) 224
4. Conclusion 232
References 233
CHAPTER V
THE USE OF THE CCD AREA DETECTOR X-RAY INSTRUMENT TO RESOLVE TWINNING PROBLEMS 236
1. Introduction 237
A. Background 238
(1) A brief history of diffractometers 238
(2) Modern area detectors and CCD techniques 240
B. The Advantages and Disadvantages of Area Detectors 241
C. New Problems in the CCD Era 241
(1) The problem of twinning 241
(a) Definition of twinning 241
D. Manipulation of Data for Twinned Crystals - Why not Grow a Better Crystal? 243
(1) Indexing of twinned crystals: 244
(a) Simple algorithm method. 244
(b) Difference vector and related methods. 245
E. Data Integration and Deconvolution. 246
(1) A rotational twin. 246
(2) A nearly perfect twin. 247
F. Structure solution and refinement. 247
2. Mastering the CCD Technique for Special Needs 247

A. Problematic Structures: Seven Case Studies. 248
(1) Example 1: Large cell, "small molecule" data set: of
{[$Mo_2(O_2CCMe_3)_3$(NC)2CC(CN)CONH] •$8CH_2Cl_2$ }$_\infty$ (3) 248
(2) Example 2: A Pseudo-Merohedral twin: [$Mn_2(\mu^4$-σ-TCNQ-
TCNQ)$_2$(μ-cis-TCNQ)$_2$(MeOH)$_2$]$_\infty$ (9) 249
(3) Example 3: A rotational twin:
[Et_4N]Cl·Fe_2Cl_4(MeOH)$_4$(bpym)$_3$ (26). 250
(a) A data set from a scintillation detector compared to a data
set from CCD detector. 250
(b) Using a rotational twinning matrix in the refinement 251
(4) Examples 4a and 4b: Nearly perfect twins: 254
(a) Mn_2(bpym)$_2$(μ-F)(η^1-BF_4)(BF_4)$_2$(MeCN)•2MeCN (25). 254
(b) Structure of Mn(η^1-TCNQ)$_2$(TCNQ)($HOCH_2CH_2OH$)$_3$
(28). 255
(i) Big box integration. 255
(ii) Small box integration 255
(5) Example 5: Crystal movement during data collection:
Structure of Rh_2(pynp)$_2$(O_2CCH_3)$_2$(BF_4)$_2$•C_7H_8 (27). 258
(6) Example 6: A quadruply twinned crystal:CuTCNQ phase II
(8) 261
(7) Example 7: A composite of two polymorphic crystals: Two
morphologies of [ppn]$_2$$NiCl_4$•$Me_2CO$, (23, 24). 264
B. Discussion 265
(1) Considerations before data collection. 265
(2) Data collection 266
(3) Data processing. 266
(4) Structure solution and refinement. 266

3. Conclusio

References .

APPENDICES

APPENDIX A

GENERAL PR

1. Data colle

diffracton

A. Crystal

B. Data co

C. Data in

D. Beam i

References ..

APPENDIX B

ATOM POSIT

3. Conclusions 269
References 270
APPENDICES 272
APPENDIX A
GENERAL PROCEDURES FOR DATA COLLECTION 273
1. Data collection procedure for Siemens CCD platform diffractometer 274
A. Crystal mounting and preliminary data collection 274
B. Data collection 274
C. Data integration. 275
D. Beam inhomogeneity, crystal decay and absorption correction. 275
References 276
APPENDIX B
ATOM POSITIONS TABLES 277

Table 1. St
C
[N
Table 2. Cr
{[
{[
Table 3. St
an
Table 4. Se
[N
Table 5. Ge
DC
Table 6. Se
Table 7. Co
tri
Table 8. Co
gr
Table 9. Str
lin
Table 10. Se
{[N
Table 11. (Co
Table 12. Lib
Table 13. Sur

LIST OF TABLES

page

Table 1. Structural parameters for $\{[Mo_2(O_2CCF_3)_4]_2(\mu^4\text{-TCNQ})\bullet 2m\text{-}C_8H_{10}\}_\infty\{[Mo_2(O_2CCF_3)_4]\bullet(m\text{-}C_8H_{10})_2\}_\infty$ (1) and $[Mo_2(O_2CCF_3)_4(DM\text{-}DCNQI)\bullet C_6H_6]_\infty$ (2)..... 38

Table 2. Crystal data and structure refinement for $\{[Mo_2(O_2CCMe_3)_3(NC)_2CC(CN)CONH]\bullet 8CH_2Cl_2\}_\infty$ (3) and $\{[Mo_2(O_2CCMe_3)_3(NC)_2CC(CN)CONH]\bullet 0.5C_6H_6\}_\infty$ (4)..... 41

Table 3. Structural parameters for $[Re_2Cl_4(dppm)_2]_2TCNQ\bullet 10THF$ (5) and $[Re_2Cl_4(dppm)_2]_2DMDCNQI\bullet 10THF$ (6)..... 44

Table 4. Selected bond distances (Å) and bond angles (°) for $[Mo_2(O_2CCF_3)_4(TCNQ)]_\infty$, (1)..... 52

Table 5. Geometric parameters for compounds that exhibit metal DM-DCNQI σ-bonding..... 58

Table 6. Selected bond distances [Å] and bond angles (°) for (2)..... 59

Table 7. Comparison of semi-empirical calculations for two 2,3,3-tricyanoacrylamide anion isomers..... 62

Table 8. Comparison of refinement results of (3) in different space groups..... 63

Table 9. Structural parameters for a $Mo_2^{II,II}$ core coordinated to non-linear nitriles..... 66

Table 10. Selected bond distances (Å) and bond angles (°) for $\{[Mo_2(O_2CCMe_3)_3(NC)_2C(CN)CCONH)]\bullet 8CH_2Cl_2\}_\infty$ (3)..... 67

Table 11. (Cont'd)..... 68

Table 12. Librational disorder refinement of the CN bond length in (5).... 72

Table 13. Summary of key crystallographic parameters for Cu(TCNQ)

p
Table 14. Cr
[N
[N
Table 15. Cr
ar
Table 16. Cr
TC
(1
Table 17. Cr
[N
Table 18. IR
Table 19. Ke
[N
[N
41
Table 20. Se
[N
Table 21. Bo
Table 22. Bo
Table 23. Sta
Table 24. Hy
for
Table 25. Hy
for
Table 26. Hy
for

phase I (7) and phase II (8). 93

Table 14. Crystal data and structure refinement parameters for $[Mn(TCNQ\text{-}TCNQ)_{0.5}(TCNQ)(MeOH)_2]_\infty$ (9) and $[Mn(TCNQ)_2(H_2O)_2]_\infty$.(10). 95

Table 15. Crystal data and structure refinement for $[^nBu_4N][TCNQ]$ (11) and $[^nBu_4N][TCNQF_4]$ (12). 99

Table 16. Crystal data and structure refinement for $\{[Zn(H_2O)_4](\eta^1\text{-}TCNQ)_2\bullet 2TCNQ\bullet 2MeCN\}_\infty$ (13) and $[Ni(DMSO)_6](TCNQ)_3$ (14). 101

Table 17. Crystal data and structure refinement for $[Ni(TCNQ)_2(H_2O)]_\infty$.(15) 104

Table 18. IR and XPS data for Cu(TCNQ) and Cu(DM-DCNQI) 113

Table 19. Key bond distances(Å) in the TCNQ unit(s) for $[Mn(TCNQ)(TCNQ\text{-}TCNQ)_{0.5}(MeOH)_2]_\infty$ (9) and $[Mn(TCNQ)_2(H_2O)_2]_\infty$ (10) according to diagram in Figure 41 137

Table 20. Selected bond lengths [Å] and angles [°] for $[Mn(TCNQ)_2(H_2O)_2]_\infty$ (10). 142

Table 21. Bond lengths [Å] and angles [°] for $[^nBu_4N][TCNQ]$ (11). 144

Table 22. Bond lengths [Å] and angles [°] for $[^nBu_4N][TCNQF_4]$ (12) 145

Table 23. Stacking interactions for $TCNQ^{-1}$ units in selected structures.. 158

Table 24. Hydrogen bonds (with esds except for fixed and riding atoms) for $[Mn(TCNQ)_2(H_2O)_2]_\infty$.(10). 159

Table 25. Hydrogen bonds (with esds except for fixed and riding atoms) for $[Mn(TCNQ)(TCNQ\text{-}TCNQ)_{0.5}(MeOH)_2]_\infty$ (9). 159

Table 26. Hydrogen bonds (with esds except for fixed and riding atoms) for $[Zn(H_2O)_4(\eta^1\text{-}TCNQ)_2\bullet TCNQ\bullet 2MeCN]_\infty$ (13). 159

Table 27. Crystal data and structure refinement for $[Mn_5Cl_{10}(THF)_8]_\infty$(16) and $[MnBr_2(THF)_2]_\infty$ (17). 188
Table 28. Crystal data and structure refinement for $[MnCl_2(MeOH)_2]_\infty$ (18). 189
Table 29. Crystal data and structure refinement for $Fe_2Cl_4(bpy)_2$ (19) and $[FeCl_2(bpy)]_\infty$(20). 191
Table 30. Crystal data and structure refinement for $[ppn]_2[Co_2Cl_6]$ (21) and for $[ppn]_2[Mn_2Cl_6]$ (22). 195
Table 31. Crystal data and structure refinement for $[ppn]_2NiCl_4 \bullet Me_2CO$ (23) and (24). 196
Table 32. Crystal data and structure refinement for $[Et_4N]Cl \bullet Fe_2Cl_4(bpym)(MeOH)_4$. (26) 198
Table 33. Bond lengths [Å] and angles [°] for $[FeCl_2(bpy)]_\infty$ (20). 210
Table 34. Selected bond distances (Å) and bond angles (°) for $[ppn]_2[Co_2Cl_6]$, (21). 216
Table 35. Selected bond distances (Å) and bond angles (°) for $[ppn]_2[Mn_2Cl_6]$, (22). 221
Table 36. Selected bond distances (Å) and bond angles (°) for $[Et_4N]Cl \bullet [Fe_2Cl_4(MeOH)_4(\mu\text{-}2,2'\text{-bpym})]$, (26). 226
Table 37. Rotational transformation of $[Et_4N]Cl \bullet Fe_2Cl_4(MeOH)_4(bpym)_3$ (26). from orientation A_1 to orientation A_2. 252
Table 38. Indexing result of rotationally twinned $[Et_4N]Cl \bullet Fe_2Cl_4(MeOH)_4(bpym)_3$ (26). 253
Table 39. Rotational transformation of $Mn_2(bpym)_2(\mu\text{-}F)(\eta^1\text{-}BF_4)(BF_4)_2(MeCN) \bullet 2MeCN$ (25) from orientation A_1 to orientation A_2... 256
Table 40. Rotational transformation of

$Mn(TCNQ)_2(TCNQ)(HOCH_2CH_2OH)_3$ (28) from orientation A_1 to orientation A_2 257

Table 41. Rotational transformation of $Rh_2(O_2CMe)_2(pynp)_2.(BF_4)_2 \bullet C_7H_8$ (27) from orientation A_1 to orientation A_2. 259

Table 42. Comparison of two TWINDX solutions of (27). 260

Table 43. Rotational transformation of $[ppn]_2[NiCl_4] \bullet Me_2CO$ (23b, 24) from orientation A_1 to orientation A_2. 267

Table 44. Comparison of indexing results of the two TWINDX solutions of $ppn]_2[NiCl_4] \bullet Me_2CO$ (23b, 24). 268

Table 45. Atomic coordinates (x 10^4) and equivalent isotropic displacement parameters ($Å^2$x 10^3) for $[Mo_2(O_2CCF_3)_4(TCNQ) \bullet 2m\text{-}C_8H_{10})]_\infty \bullet \cdot [\ Mo_2(O_2CCF_3)_4 \bullet 2m\text{-}C_8H_{10})]_\infty$ (1). 278

Table 46. Atomic coordinates (x 10^4) and equivalent isotropic displacement parameters ($Å^2$x 10^3) for $[Mo_2(O_2CCF_3)_4(DM\text{-}DCNQI) \bullet C_6H_6]_\infty$ (2). 282

Table 47. Atomic coordinates (x 10^4) and equivalent isotropic displacement parameters ($Å^2$x 10^3) for $\{[Mo_2(O_2C(CH_3)_3)_3((NC)_2C(CN)CCONH)] \cdot 6CH_2Cl_2\}_\infty$ (3).... 283

Table 48. Atomic coordinates (x 10^4) and equivalent isotropic displacement parameters ($Å^2$x 10^3) for $\{[Mo_2(O_2C(CH_3)_3)_3((NC)_2C(CN)CCONH)] \cdot 0.5C_6H_6\}_\infty$ (4). ... 289

Table 49. Atomic coordinates (x 10^4) and equivalent isotropic displacement parameters ($Å^2$x 10^3) for $[Re_2Cl_4(dppm)_2]_2(TCNQ)$ (5). 291

Table 50. Atomic coordinates (x 10^4) and equivalent isotropic

displacement parameters ($Å^2$x 10^3) for $[Re_2Cl_4(dppm)_2]_2$(DMDCNQI) (6).....295

Table 51. Atomic coordinates (x 10^4) and equivalent isotropic displacement parameters ($Å^2$x 10^3) for Cu(TCNQ) phase I (7).299

Table 52. Atomic coordinates (x 10^4) and equivalent isotropic displacement parameters ($Å^2$x 10^3) for Cu(TCNQ) phase II (8).....301

Table 53. Atomic coordinates (x 10^4) and equivalent isotropic displacement parameters ($Å^2$x 10^3) [Mn(TCNQ-TCNQ)$_{0.5}$(TCNQ)$(MeOH)_2]_\infty$ (9).....302

Table 54. Atomic coordinates (x 10^4) and equivalent isotropic displacement parameters ($Å^2$x 10^3) $[Mn(TCNQ)_2(H_2O)_2]_\infty$ (10).....304

Table 55. Atomic coordinates (x 10^4) and equivalent isotropic displacement parameters ($Å^2$x 10^3) $[Bu_4N][TCNQ]$ (11).....305

Table 56. Atomic coordinates (x 10^4) and equivalent isotropic displacement parameters ($Å^2$x 10^3) $[Bu_4N][TCNQF_4]$ (12).....307

Table 57. Atomic coordinates (x 10^4) and equivalent isotropic displacement parameters ($Å^2$x 10^3) for $[Zn(TCNQ)_2(H_2O)_4(TCNQ)_2(MeCN)_4]_\infty$ (13).....310

Table 58. Atomic coordinates (x 10^4) and equivalent isotropic displacement parameters ($Å^2$x 10^3) $[Ni(DMSO)_6][TCNQ]_3$ (14).....312

Table 59. Atomic coordinates (x 10^4) and equivalent isotropic displacement parameters ($Å^2$x 10^3) for $[Mn_5Cl_{10}(THF)_8]_\infty$ (16).....314

Table 60. Atomic coordinates (x 10^4) and equivalent isotropic

d

Table 61. At

d

Table 62. At

d

(

Table 63. At

d

[H

displacement parameters ($Å^2$x 10^3) for $[MnBr_2(THF)_2]_\infty$ (17). 316

Table 61. Atomic coordinates (x 10^4) and equivalent isotropic displacement parameters ($Å^2$x 10^3) $[Fe_2Cl_4(\mu\text{-}2,2'\text{-bpy})_2]$ (19).317

Table 62. Atomic coordinates (x 10^4) and equivalent isotropic displacement parameters ($Å^2$x 10^3) for $[FeCl_2(\mu\text{-}2,2'\text{-bpy})]_\infty$ (20).....318

Table 63. Atomic coordinates (x 10^4) and equivalent isotropic displacement parameters ($Å^2$x 10^3) for $[Et_4N]Cl\cdot[Fe_2Cl_4(MeOH)_4(\mu\text{-}2,2'\text{-bpym})]$ (26).....319

Figure 1. O
(J
=
=
Figure 2. S
Figure 3. In
Figure 4. In
Figure 5. O
re
Figure 6. Pr
Figure 7. M
Figure 8. Int
su
Figure 9. Int
bo
Figure 10. D
Figure 11. M
id
RH
Figure 12. Th
bo
by
Figure 13. Th
the

LIST OF FIGURES

page

Figure 1. Orbital interactions in $(NC)_5M\text{-}CN\text{-}M'(NC)_5$ dinuclear units: (a) Orthogonality between t_{2g} and e_g magnetic orbitals, *e.g.* M = Cr^{III}, M' = Ni^{II}. (b) Overlap between two t_{2g} orbitals, *e.g.* M = Cr^{III}, M'= V^{II}. 5

Figure 2. Simplified MO diagrams of metal-metal bonded units. 7

Figure 3. Interactions between an axial ligand and dimetal units. 8

Figure 4. Interactions between an equatorial ligand and dimetal unit. 9

Figure 5. Organonitrile acceptors that behave as ligands in their reduced forms. 11

Figure 6. Preparation of $[Mo_2(O_2CCF_3)_4$ DM-DCNQI·$C_6H_6]_\infty$ (2). 30

Figure 7. Metal-metal bonded orbitals diagrams. 45

Figure 8. Interactions from an axial ligand to metal-metal bonded units such as $Mo_2^{II,II}$. 46

Figure 9. Interactions between equatorial ligands and metal-metal bonded units such as $Re_2^{II,III}$. 48

Figure 10. Documented reactions involving the decomposition of TCNE.. 49

Figure 11. Metallocyclic rings of polynitriles with dimetal units and idealized angles: (a) $Mo_2(O_2CCF_3)_4$(TCNQ) (1), (b) $Rh_2(O_2CCF_3)_4$(TCNE). 54

Figure 12. Thermal ellipsoid representation of (1) showing one Mo_2 unit bonded with the TCNQ ligand and a second Mo_2 unit bonded by *m*-xylene 55

Figure 13. Thermal ellipsoid representation of (2) showing a portion of the chain with the disordered CF_3 group and benzene

m
Figure 14. P
fe
in
Figure 15. M
Figure 16. S
in
Figure 17. P
in
Figure 18. N
Figure 19. P
bo
Figure 20. E
Figure 21. T
Figure 22. T
(6
Figure 23. O
re
Figure 24. C
Figure 25. X
ph
Figure.26. X
[C
Figure 27. SE
Figure 28. SE
Cu
Figure 29. SE

molecule omitted.....56
Figure 14. Plotting diagram of *ab* plane of (2) showing the stacking feature of the DM-DCNQI ligand with the benzene molecule in the lattice.....57
Figure 15. Molybdenum TCNE modeled from the partial P3/V structure. .64
Figure 16. Simulation of dimolybdenum TCNE reaction product (3) indicates an overcrowded hyper μ^4-TCNE bonding mode.....65
Figure 17. Plot of $[Mo_2(O_2CCMe_3)_3((NC)_2C(CN)CCONH)\bullet 8CH_2Cl_2]$ (3) in space group P6cc 69
Figure 18. Nitrile bonding modes with a $Mo_2^{II,II}$ core.....70
Figure 19. Pluto representation of (4) clearly shows that the CN groups bonded to the Mo_2 unit are in an unusual bent mode. 71
Figure 20. Electron density map of nitrile region in (5). 73
Figure 21. Thermal ellipsoid representation of $Re_2(dppm)_2TCNQ$ (5).....74
Figure 22. Thermal ellipsoid representation of $Re_2(dppm)_2DMDCNQI$ (6).....75
Figure 23. Organonitrile acceptors that behave as ligands in their reduced forms. 83
Figure 24. Crystal growing setup for two Cu(TCNQ) phases. 90
Figure 25. XPS data in the Cu $2p_{3/2}$ and $2p_{1/2}$ regions for phase I (a) and phase II Cu(TCNQ) (b).....109
Figure.26. XPS data in the Cu $2p_{3/2}$ and $2p_{1/2}$ regions for $[Cu^{I}(MeCN)_4][BF_4]$ (a) and $[Cu^{II}(MeCN)_4][BF_4]_2$ (b).....110
Figure 27. SEM micrographs for solution-prepared Cu(TCNQ) crystals..115
Figure 28. SEM micrographs showing the progressive changes from Cu(TCNQ) phase I to phase II.....116
Figure 29. SEM of Cu(TCNQ) films grown on copper in MeCN for

1hour at different temperatures: (a) at 60°C, (b) at 80°C. 117

Figure 30. SEM micrographs of Cu(TCNQ) grown on copper in CH_3CN: (a) top and (b) side views of films grown for 1h at 40 °C (phase I) and (c) top and (d) side views of films grown for 1 h at 80 °C (phase II). The reference scale on all micrographs is 10 μm. 118

Figure 31. XRD powder patterns illustrating the conversion of Cu(TCNQ) phase I to phase II in CH_3CN. 121

Figure 32. XRD pattern for a Cu(TCNQ) sample grown on a Cu substrate for 1 h at 80°C in a CH_3CN solution of TCNQ..... 122

Figure 33. XRD pattern of $M(TCNQ)_2$, (M = Mn, Fe, Co, Ni). 123

Figure 34. $Mn(TCNQ)_2$ small particles in nanometer size could be seen from (a) SEM (1μm scale) and (b) TEM (0.1 μm scale) micrographs. 124

Figure 35. Pluto representation of Cu(TCNQ) phase I. 128

Figure 36. Thermol elipsoid representation of CuTCNQ phase II. 129

Figure 37. Interpenetrating networks of Cu(TCNQ) phase I features TCNQ stacking between different networks (solid bond -- network 1, holo bond – network 2)..... 131

Figure 38. Interpenetrating networks of Cu(TCNQ) phase II. Note that the TCNQ units between different networks are shifted and not π–stacked between different networks (solid bond: network 1, holo bond: network 2). 132

Figure 39. Schematic diagrams of Cu(TCNQ) phase I and phase II with an emphasis on the geometry of the Cu-N connection..... 134

Figure 40. Experimental XRD powder pattern for (a) Cu(TCNQ) phase I and (b) Ag(TCNQ)..... 135

Figure 41. V

Figure 42. T

Figure 43. T

Figure 44. T

Figure 45. F

Figure 46.

Figure 47. T

Figure 48. F

Figure 49. T

Figure 50.

Figure 51. T

Figure 52. P

Figure 53. S

Figure 54. P

Figure 55. E

Figure 41. Various bond lengths in TCNQ compounds (9), (10). 138
Figure 42. Thermal ellipsoid representation of [Mn(TCNQ)(TCNQ-TCNQ)$_{0.5}$(MeOH)$_2$]$_\infty$ (9). 139
Figure 43. Thermal ellipsoid representation of Mn(TCNQ)$_2$(H$_2$O)$_4$ (10).. 141
Figure 44. Thermal ellipsoid representation of [^{n}Bu$_4$N][TCNQ] (11)..... 146
Figure 45. Packing diagram of [^{n}Bu$_4$N][TCNQ] (11) along the *a* axis..... 147
Figure 46. (a)The dimer radical pair of $(TCNQ)_2]^{2-}$ packed in a nearly eclipsed pattern in (11). (b) The two dimer pairs of (12). 148
Figure 47. Thermal ellipsoid representation of [^{n}Bu$_4$N][TCNQF$_4$] (12). .. 149
Figure 48. Packing diagram of [Bu$_4$N][TCNQF$_4$] (12) viewed down *b* axis shows both the stacking TCNQF$_4$ dimer and the loosely packed dimer. 150
Figure 49. Thermal ellipsoid representation of {Zn(η^1-TCNQ)$_2$(H$_2$O)$_4$(TCNQ)•2MeCN}$_\infty$ (13•2MeCN). 151
Figure 50. Packing diagram of (13) along the [1 0 1] plane emphasizes the TCNQ stacking pattern. 152
Figure 51. Thermal ellipsoid representation of [Ni(DMSO)$_6$][TCNQ]$_3$ (14). 153
Figure 52. Packing diagram of (14) viewed down a axis showing TCNQ stacking column. 154
Figure 53. Superimposed thermal ellipsoid representations of [Ni(TCNQ)$_2$(H$_2$O)]$_\infty$ (15) depicting the disorder modeling of (15). 156
Figure 54. Pluto representation of the $[(TCNQ)_2]^{2-}$ unit in (9) and the hydrogen bonding scheme. 160
Figure 55. Extended hydrogen bonding networks in [Mn(TCNQ)$_2$(H$_2$O)$_4$]$_\infty$ (10) 161

Figure 56. H
T
Figure 57. V
V
(
Figure 58. V
z
(
Figure 59. V
Figure 60. P
(
Figure 61. T
Figure 62. (
n
Figure 63. P
Figure 64. T
c
Figure 65. T
[
Figure 66. T
Figure 67. P
Figure 68. T
Figure 69. P
d
Figure 70. S
Figure 71. P
Figure 72. T

Figure 56. Hydrogen bonding networks in [Zn(η^1-TCNQ)$_2$(H$_2$O)$_4$(TCNQ) •2MeCN]$_\infty$ (13). 162
Figure 57. Variable temperature susceptibility data for Cu(TCNQ) (a) χ versus T for phase I (7); (b) χ and μ_{eff} versus T for phase II (8). 164
Figure 58. Variable temperature susceptibility data for Cu(TCNQ) (c) zero-field cooled and field-cooled χ versus T for phase II (8); (d) hysteresis of phase II(8). 165
Figure 59. Magnetic data for Mn TCNQ compounds (9),(10)..... 167
Figure 60. Plot of conductivity σ (S cm^{-1}) versus temperature for bulk Cu(TCNQ) phase I and phase II measured on pressed pellets. 168
Figure 61. Thermal ellipsoid representation of {Mn$_5$Cl$_{10}$(THF)$_8$}$_\infty$(16)....201
Figure 62. Comparison of different types of Mn(II) sites in (16) with the metal sites in M$_4$Cl$_8$(THF)$_6$ clusters. 202
Figure 63. Packing view of [Mn$_5$Cl$_{10}$(THF)$_8$]$_\infty$ (16) down the *b* axis. 203
Figure 64. Thermal ellipsoid representation of a portion of the chain compound [MnBr$_2$(THF)$_2$]$_\infty$ (17). 204
Figure 65. Thermal ellipsoid representation of mononuclear [MnI$_2$(THF)$_3$]. 205
Figure 66. Thermal ellipsoid representation of [Fe$_2$Cl$_4$(bpy)$_2$]. (19) 207
Figure 67. Packing view of [Fe$_2$Cl$_4$(bpy)$_2$](19) down the *a* axis. 208
Figure 68. Thermal ellipsoid representation of [FeCl$_2$(bpy)]$_\infty$ (20.) 211
Figure 69. Packing diagram of [FeCl$_2$(bpy)]$_\infty$ (20) showing the one-dimensional chain along *c* axis. 212
Figure 70. Structures of [MCl$_2$(bidentateL)]$_2$ 213
Figure 71. Packing view of [ppn]$_2$Mn$_2$Cl$_6$ in the *ac* plane. 217
Figure 72. Thermal ellipsoid representation of (21). 218

Figure 73. Thermal ellipsoid representation of (22). 222

Figure 74. Packing view of $[ppn]_2Mn_2Cl_6$ in the *ac* plane. 223

Figure 75. Thermal ellipsoid representation of $[Et_4N]Cl{\cdot}[Fe_2Cl_4(MeOH)_4(\mu\text{-}2,2'\text{-bpym})]$ (26) illustrates the hydrogen bond between the iron dimer units and the chloride ion. 225

Figure 76. Thermal dependence of the susceptibility for the $[ppn]_2[Co_2Cl_6]$ dimer (filled circles) and the best fit to the experimental data obtained (solid line). Dashed-dotted lines represent the perpendicular (upper) and parallel (lower) susceptibility. The theoretical behavior of a fully isotropic antiferromagnetic Co(II) dimer is shown as dotted line. 227

Figure 77. Thermal dependence of the product χT for $[ppn]_2[Co_2Cl_6]$ (filled circles) and the best fit to the experimental data obtained (solid line). The theoretical behavior of a fully isotropic antiferromagnetic Co(II) dimer is shown as dotted line 228

Figure 78. Thermal dependence of the susceptibility for $[ppn][Mn_2Cl_6]$ (filled circles) and the best fit to the experimental data obtained (solid line). The theoretical behavior of a fully isotropic antiferromagnetic Mn(II) dimer is shown as dotted line 229

Figure 79. Polymeric chain of $MnCl_2$ units in (16). 230

Figure 80. Fitting with the cluster model of magnetic measurement data of (16). 230

Figure 81. Magnetic data fitting of $[MnBr_2(THF)_2]_\infty$ (17). 231

Figure 82. The Curie-Weiss behavior of $[MnCl_2(MeOH)_2]_\infty$ (18). Solid

Figure 83.

Figure 84.

line is the Curie-Weiss fit, dot is the $1/\chi$ and diamond dot is the μ_{eff} plot. 231

Figure 83. The experimental setup used by Laue, Friedrich and Knipping to measure X-ray diffraction intensities. This same general experimental setup is still currently used, although the source of X rays and the detection system are now much more sophisticated..... 239

Figure 84. Using local symmetry to reduce independently refined parameters..... 250

CHAPTER I

INTRODUCTION

1. History

Conductor

The

to remain

magnetic m

coordinatio

area of ino

arguments

metals and

solids, incl

with magne

A. Molecul

The

in 1954,[7]

temperatur

(TCNQ = 7

that opened

discoveries

donor TTF

namely [T

increases w

where a m

been devot

donors an

synthesized

In

1. History of Molecule-Based Materials (Molecular Magnets/Molecular Conductors)

The exploration of molecule-based materials is a topic that promises to remain at the forefront of the search for new conducting, optical and magnetic materials for years to come.[1] The use of soluble transition metal coordination complexes as precursors to materials is a rapidly expanding area of inorganic chemistry with many potential applications.[2] Topological arguments that take into consideration the geometrical preferences of the metals and ligands have allowed chemists to design new molecule-based solids, including porous,[3] magnetic,[4] conducting,[5] and conducting materials with magnetic centers.[6]

A. Molecule-based Conductors

The first report of electrical conductivity in an organic solid appeared in 1954,[7] namely, a perylene-bromine complex, which has a room-temperature conductivity of 0.1 S cm^{-1}. In 1960, the organic acceptor TCNQ (TCNQ = 7,7',8,8'-tetracyanoquinodimethane) was synthesized, a discovery that opened up a whole field of conducting charge-transfer materials.[8] These discoveries were followed in the 1970s with the synthesis of the organic donor TTF(TTF = tetrathiafulvalene)[9] which led to the first organic metal, namely [TTF-TCNQ]. Its room-temperature conductivity (500 Ω^{-1} cm^{-1}) increases with a decrease in temperature to a value of 6000 Ω^{-1} cm^{-1} at 60 K where a metal-insulator transition occurs.[10] Since then, great interest has been devoted to this type of material, and a great number of new organic donors and acceptors, as well as their charge-transfer salts, have been synthesized.

In 1979, Jerome *et al.* discovered a superconducting state in

(TMTSF)

improvem

symmetric

ones such

acceptor-b

discovered

reported is

B. Molecu

The

when Wic

diethyldith

ferromagne

based mag

Kahn who

chain of M

organic ba

tetracyanoe

developme

motif,[20] spi

temperatur

magnetic r

single-dom

combinatio

with intere

Inor

as TCNE a

$(TMTSF)_2PF_6$ at T_c =1.2 K under 10 kbar.[11] Since then, significant improvements in T_c have been obtained in other organic salts based on either symmetrical molecules such as BEDT-TTF (or "ET")[12] or unsymmetrical ones such as DMET-TTF[13] or MDT-TTF.[14] Later, another family of acceptor-based superconductors of the type $M(dmit)_2$, (M = Ni, Pd) were discovered, and these continue to be investigated.[15] The highest T_c to be reported is 12.8K in κ-$(ET)_2(CuN(CN)_2)Cl$.[16]

B. Molecule-based Magnets

The origin of *molecular* magnetism can be traced back to 30 years ago when Wickman *et al.*, reported that the complex $FeCl(L\text{-}L)_2$ (L-L = N,N-diethyldithiocarbamate) with an S = 3/2 ground state orders ferromagnetically with a T_c of 2.5K.[17] Since then, the study of molecule-based magnets has emerged as a new field, with notable breakthroughs by Kahn who reported the first inorganic-based molecular magnet ferrimagnetic chain of Mn(II)Cu(II)[18] centers and by Miller *et al.*, who discovered the first organic based molecular magnet, namely $[FeCp^*_2]^{+\bullet}[TCNE]^{-\bullet}$ (TCNE = tetracyanoethylene).[19] The rapid reports in the ten years since these developments include high T_c ferromagnets based on the Prussian-blue motif,[20] spin-crossover compounds that undergo abrupt transitions near room temperature,[4a,21] compounds that superconduct in the presence of localized magnetic moments,[22] and high spin clusters that mimic the properties of a single-domain magnet.[23] Our approach is to use organocyanide ligands in combination with inorganic open shell cations as to prepare new materials with interesting properties.

Inorganic chemists are interested in the fact that organocyanides such as TCNE and TCNQ can also bond to metals in a σ fashion to the lone-pair

electrons o

addition to

acceptors,

also been

species. R

bidentate c

extended π

molecule.

inorganic r

electron de

2. Interact

A. Orthog

To u

basic magn

types of r

paramagne

The last th

properties

fashion. I

kinds of s

constant J.

and is de

separation

coupling, J

containing

rule keeps

electrons on the nitrogen atoms, forming covalently linked materials.[24,25] In addition to metal-radical charge-transfer complexes with organocyanide π-acceptors, other π-acceptor radicals in the nitronyl nitroxide family[26] have also been used in establishing communication channels between metal species. Requirements for the organic ligands are (1) that they exhibit bidentate or multidentate binding properties and (2) that they possess an extended π-network to allow for electron delocalization throughout the molecule. Cyanide groups on organic molecules are able to bond to inorganic moieties through their nitrogen lone pair electrons and accept π-electron density from the metal donor complex lying π* orbital.

2. Interaction of Magnetic Spins

A. Orthogonality of Spins

To understand the factors involved in molecular magnet design, some basic magnetic phenomena must be understood. There are five important types of magnetic behavior observed in solids, namely diamagnetism, paramagnetism, ferromagnetism, antiferromagnetism, and ferrimagnetism. The last three properties are characterized by cooperative behavior (or bulk properties). In ferromagnets, the individual spins are oriented in a parallel fashion. In both antiferromagnets and ferrimagnets, there are at least two kinds of spins that are coupled antiparallel to each other. The coupling constant J, describes the isotropic interaction between two spins S_1 and S_2, and is defined by the spin Hamiltonian $H = -2J(S_1 \cdot S_2)$.[27a] The energy separation between the singlet and the triplet states is J. In ferromagnetic coupling, $J > 0$, while in antiferromagnetic coupling, $J < 0$. If the orbitals containing the unpaired electron(s) are orthogonal to each other,then Hund's rule keeps the spins parallel and ferromagnetic coupling between the two

Figure 1.
Orthogona
(b) Overla

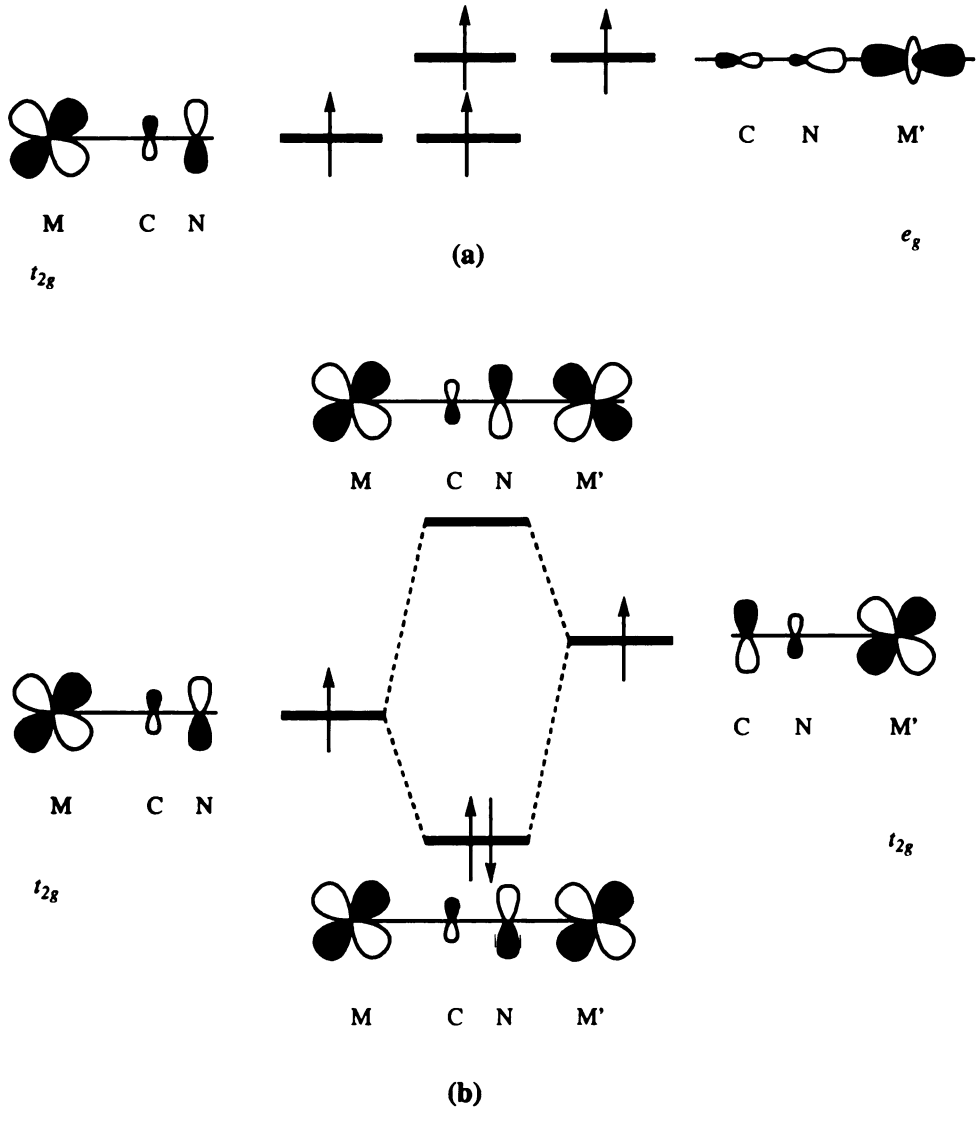


Figure 1. Orbital interactions in $(NC)_5M\text{-}CN\text{-}M'(NC)_5$ dinuclear units: (a) Orthogonality between t_{2g} and e_g magnetic orbitals, *e.g.* $M = Cr^{III}$, $M' = Ni^{II}$. (b) Overlap between two t_{2g} orbitals, *e.g.* $M = Cr^{III}$, $M' = V^{II}$.

spins occu

alignment

spins in o

required.[28]

equal magn

B. Orbital

Com

second and

configurati

separations

open-shell

examples o

are stabliz

HOMO/LU

spatial orie

and magne

3. Design

Precursor

In o

between c

we have di

a. Synthe

metal

b. Synthe

solvat

c. Correl

spins occurs. If there is direct overlap between the orbitals, the antiparallel alignment will be favored. In order to achieve a ferromagnetic interaction, spins in orthogonal orbitals in the same spatial region (adjacent sites) is required.[28] *Ferri*magnetism is achieved when the interacting spins are not of equal magnitude.

B. Orbital Interactions of Dimetal Complexes with Polynitrile Ligands.

Compared to the first row transition metal series (3d metals), the second and third row transition metals are less commonly found in high spin configurations with a single metal center due to their larger t_{2g} and e_g energy separations. Additionally, the formation of metal-metal bonds,[29] stablizes open-shell metal ions of the heavier elements. Nevertheless, there are some examples of M-M compounds with two and three unpaired electrons which are stablized due to degenerated or nearly degenerated HOMO or HOMO/LUMO orbitals. The frontier orbitals of the dimetal units and their spatial orientation with respect to the incoming ligand dictates their bonding and magnetic interactions (Figure. 2-4).

3. Design of Molecule-based Materials from Inorganic/Organic Precursors.

In order to better understand the basic principles of spin interactions between covalently linked dimetal moieties and their bridging π-acceptors, we have directed our research efforts towards the following goals:

a. Synthesis and characterization of molecular materials based on metal-metal building blocks and polynitrile ligands.
b. Synthesis and characterization of molecular materials based on inorganic solvated cations coordinated to polynitrile ligands.
c. Correlation of the structures of metal-TCNQ materials with their



properties.

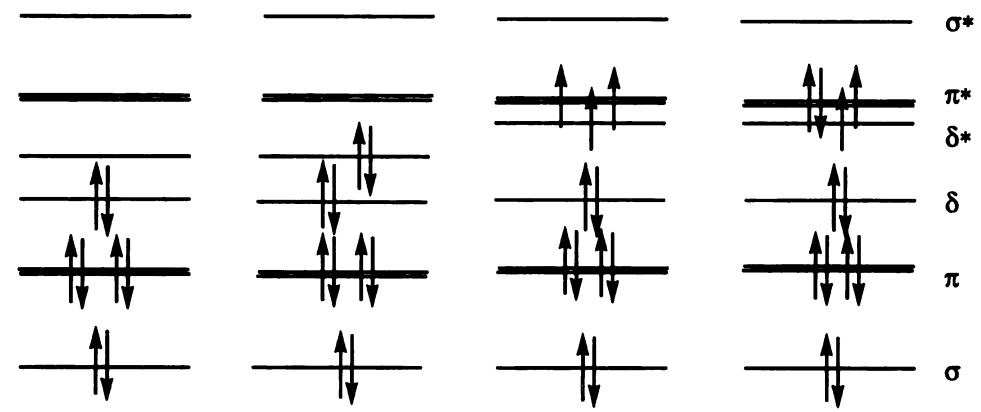


Figure 2. Simplified MO diagrams of metal-metal bonded units.

A. M(TCNQ) and M(TCNQ)$_2$ Materials.

(1) General background

A particularly intriguing approach to the design of molecular solids that exhibit cooperative behavior is to assemble open-shell metal centers and organic radicals into inorganic/organic "hybrid" structures.[30,31,32] An excellent illustration of this strategy is the design of highly conducting covalent solids with σ- as well as dπ-pπ interactions between the metal and organic constituents, for example the class of compounds Cu(R,R'-DCNQI)$_2$ (DCNQI = N,N'-dicyanoquinonediimine, R, R' = halide, alkyl group or alkoxide groups) with direct bonding of the nitriles to the Cu centers.[28] X-ray studies of the Cu(DCNQI)$_2$ compounds reveal that the structures adopt polymeric motifs consisting of partially reduced DCNQI molecules that

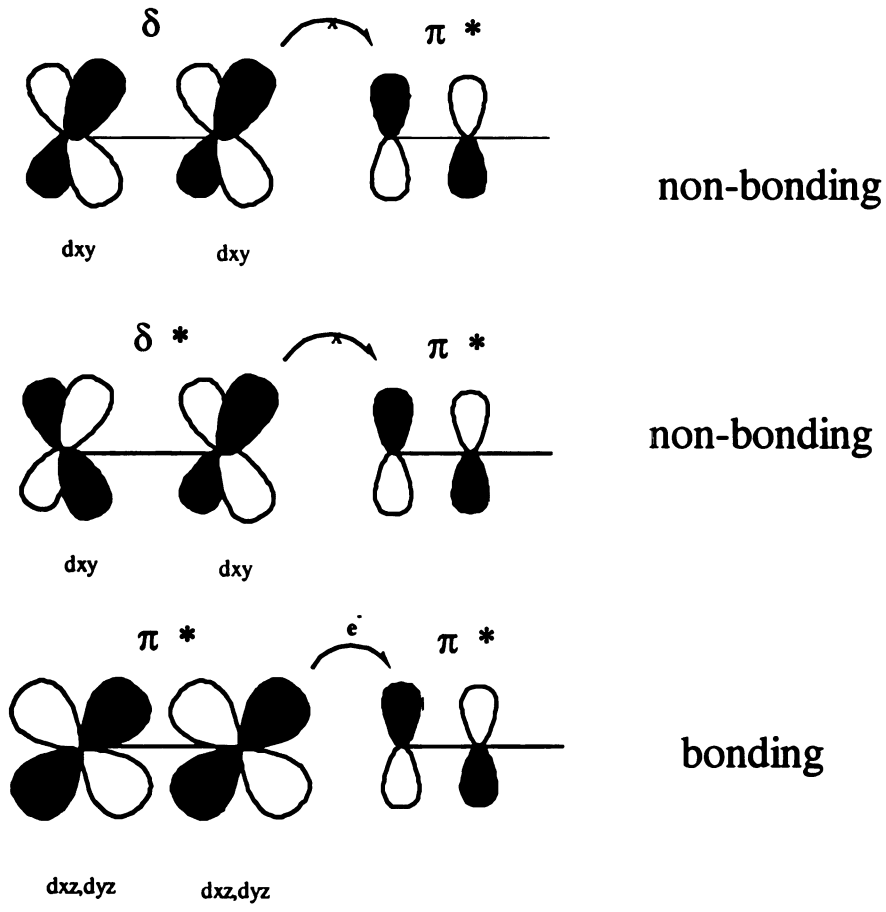


Figure 3. Interactions between an axial ligand and dimetal units.

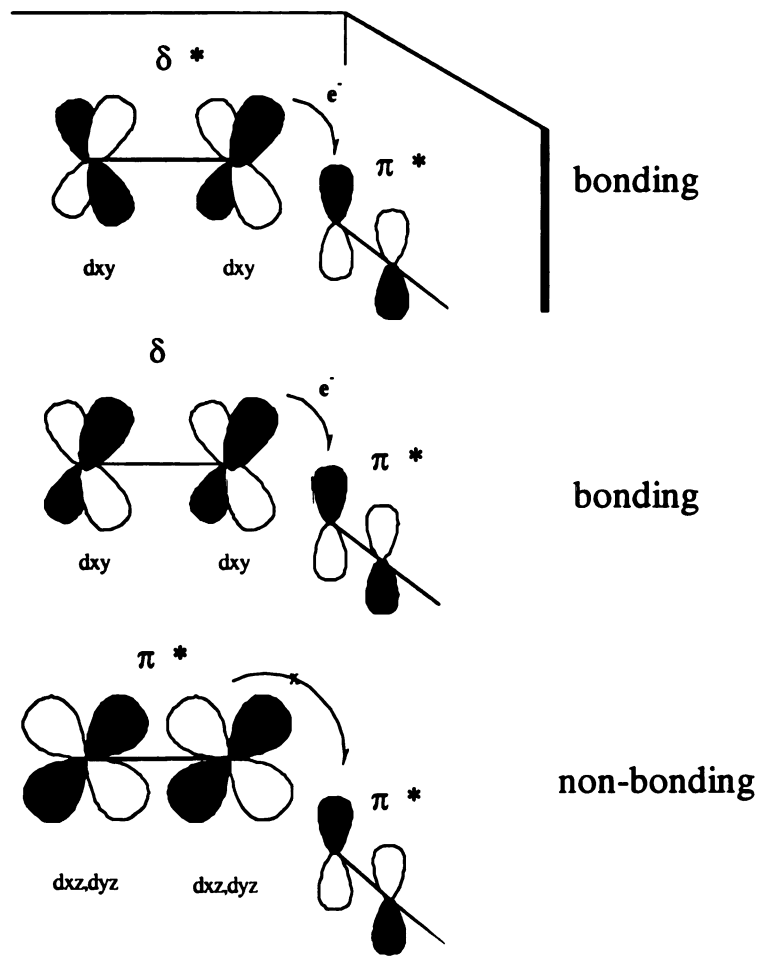


Figure 4. Interactions between an equatorial ligand and dimetal unit.

form one-di
mixed-valen
mainly to
delocalizatio
mixing is si
creating a "n
(2) Polymer

One c
organic radi
ions has a c
properties;
crystallize w
high electric
of donors ar
properties.

In lig
acceptor mo
molecules c
multidimens
component.
heightened t
anions that a

One s
and organic
anions suc
(tetracyanoe
In this man

form one-dimensional columns connected to each other by tetrahedral mixed-valence $Cu^{+/2+}$ cations. Although high conductivity is attributed mainly to DCNQI-DCNQI stacking, it has been suggested that the delocalization of metal electrons into the conduction band from dπ-pπ mixing is significant for removing the degeneracy of the pπ bands thereby creating a "multi-Fermi" surface that stabilizes the metallic state.[30]

(2) Polymeric metal-TCNQ materials

One of the main issues in low-dimensional salts composed of planar organic radicals is the mode of stacking. The solid-state arrangement of the ions has a dramatic effect on the resulting magnetic and charge-transport properties; for example charge-transfer salts such as [TTF][TCNQ] that crystallize with segregated stacks of donors and acceptors typically exhibit high electrical conductivity whereas those that assemble as alternating stacks of donors and acceptors tend to show interesting optical as well as magnetic properties.

In light of the promise for the use of tunable organic donor and acceptor molecules in materials applications, researchers are incorporating molecules of the types depicted in Figure 4 into complex solids with multidimensional frameworks that involve a paramagnetic inorganic component. Interest in hybrid organic/inorganic materials has been heightened by the recent reports of (BEDT-TTF) salts of paramagnetic metal anions that are highly conducting and even superconducting.[33]

One synthetic strategy to obtaining materials that contain both metals and organic acceptors is to combine metal cations with organic acceptor anions such as $TCNQ^{\cdot-}$ (7,7,8,8-tetracyanoquinodimethane), $TCNE^{\cdot-}$ (tetracyanoethylene) and $DCNQI^{\cdot-}$ (N,N'-dicyanoquinonediimine) (Figure 5). In this manner one can take advantage of the tendency for planar organic

radicals to

imparting n

Among the

metallic pol

and Ag with

TCNE. Not

of metals

dimensionali

of this type

research eff

however, tha

possible to

ions bridged

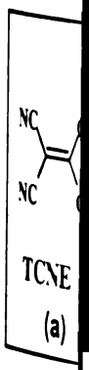


Figure 5.

As p

conducting

crystalline

effort to est

radicals to engage in π-stacking interactions, while at the same time imparting new properties based on the presence of metal-based electrons. Among the interesting materials that have emerged from these studies are metallic polymers of Cu with DCNQI, electrically bistable materials of Cu and Ag with TCNQ, and a room temperature bulk ferromagnet of V with TCNE. Notably, all of these materials are binary compounds composed only of metals and organic acceptors with no co-ligands to reduce the dimensionality of the extended arrays. Unfortunately, polymeric materials of this type are notoriously difficult to crystallize, a fact that has hampered research efforts aimed at magneto-structural correlation. We have found, however, that with the proper selection of starting materials and solvents it is possible to prepare crystalline, neutral framework compounds with metal ions bridged only by ligands derived from $TCNQ^{-1}$.

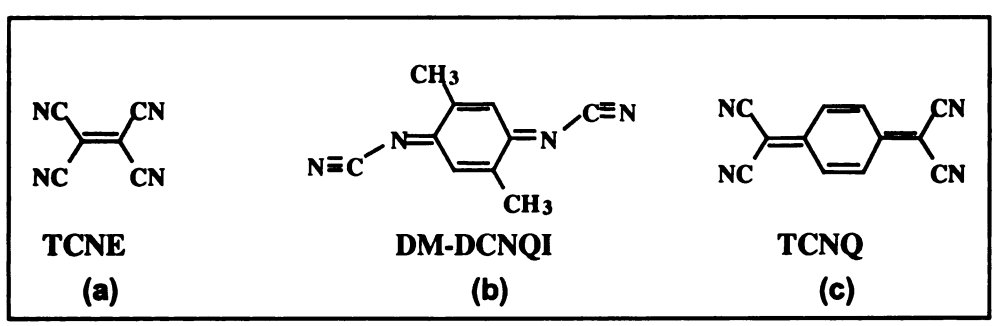


Figure 5. Organonitrile acceptors that behave as ligands in their reduced forms.

As part of a comprehensive investigation of the magnetic and conducting properties of M/TCNQ materials we have prepared several crystalline phases of general formulae M(TCNQ) and $M(TCNQ)_2$ in an effort to establish structure/property relationships. During the course of

these studie
water, aceto
of metal-TC
behavior of
Cu(TCNQ)
crystalline s
polymorphs
powder X-
spectroscopy
spectroscopy
involving M
presented.
data, infrare
light of the
detailed is
paramagneti
ferromagnet

B. Metal-M

Clearl
organic radi
building bl
population/d
intriguing p
there has b
blocks whe
physical pro

these studies, we became aware of the role of the solvent (e.g., methanol, water, acetonitrile) in determining the structures, and, therefore, properties of metal-TCNQ materials. In addition, new insight into the electrical behavior of Cu(TCNQ) was gained by our discovery that two polymorphs of Cu(TCNQ) could be accessed by solution routes and readily isolated as pure crystalline solids. Specifically we report the discovery of two distinct polymorphs of Cu(TCNQ) and characterization of these two phases by powder X-ray diffraction, single crystal crystallography, infrared spectroscopy, conductivity, magnetic susceptibility, and X-ray photoelectron spectroscopy. The syntheses and characterization of products from reactions involving Mn(II), Fe(II), Co(II), Ni(II) and Zn(II) ions with and $TCNQ^{-1}$ are presented. Representative single-crystal X-ray structures, powder X-ray data, infrared spectral properties and magnetic properties are discussed in light of the TCNQ packing motif that is adopted in the solid-state. Also detailed is the solid-state conversion of $Mn(TCNQ)_2(MeOH)_2$ from a paramagnetic crystalline phase to an ordered phase that displays ferromagnetic behavior.

B. Metal-Metal Bonded Precursors in Molecule-Based Materials.

Clearly, the combination of mononuclear metal complexes and π-organic radicals gives rise to interesting behavior,[34] but dinuclear metal building blocks with open-shell electron configurations based on the population/depopulation of low lying π^* and δ/δ^* orbitals also present intriguing possibilities for the elaboration of extended arrays.[29,35] Recently, there has been a trend towards building larger molecules with building blocks where interaction between the metal-metal moieties leads to tunable physical properties.[36,37] For example, it has been noted that rhodium(II)

trifluoroace
metal-metal
structures c
acceptors ha
pivalate di
trifluoroace
and co-wor
tetrapropion
co-workers.

Attem
moieties link
been investi
laboratories
complexes,
the first din
Finally, a
complex link

The w
compounds
design and
organic moi
with organo
materials. In
Mo_2^{4+} dimet
DCNQI and
of $Re_2Cl_4(dp$

trifluoroacetate is efficient for propogating spin interactions through its metal-metal bonded framework.[38] A few polymeric and oligomeric crystal structures of dinuclear metal moieties covalently linked by conjugated π-acceptors have recently been synthesized. An infinite chain of rhodium (II) pivalate dimers linked by 1,4-benzoquinone and molybdenum (II) trifluoroacetate units joined by 9,10-anthraquinone were reported by Handa and co-workers.[39,40] In addition, an infinite chain consisting of ruthenium tetrapropionate bridged by phenazine was recently reported by Cotton and co-workers.[41]

Attempts to model macromolecular systems of metal dinuclear moieties linked by π-electron acceptors with oligomeric sub-units have also been investigated. Eexamples of tetrameric structures discovered in our laboratories are $[Re_2Cl_4(dppm)_2]_2$·μ-TCNQ, and its analogous DMDCNQI complexes, synthesized by Stuart Bartley several years ago.[42,43] These are the first dinuclear metal complex bridged by an organocyanide π-acceptor. Finally, a tetrakis(μ-6-chloro-2-hydroxypyridinato)diruthenium (II,III) complex linked by pyrazine, was reported by Cotton and co-workers.[44.]

The wide availability of redox active metal-metal bonded dinuclear compounds that can be tailored electronically and sterically allows one to design and modify hybrid macromolecules that contain both inorganic and organic moieties. Dinuclear metal carboxylates in alternating frameworks with organocyanides are targeted in this project for the synthesis of new materials. In this thesis, syntheses and structural studies of compounds with Mo_2^{4+} dimetalcarboxylates coordinated to the polynitriles TCNQ, 2,5-DM-DCNQI and chemically transformed TCNE are presented. Structural studies of $Re_2Cl_4(dppm)_2$ with TCNQ and DM-DCNQI are also discussed.

C. Soluble

High

their magne

With respec

polynuclear

ferric syste

substantial

interesting p

magnetic da

A nu

between anH

trimethoxyp

and formati

This serendi

or other sta

lower insolu

interest in p

spin halide

arrays. In th

with 2,2'-bi

attention in

magnetic in

characteriza

= Mn, and C

and Co) and

$Fe_4Cl_8(THF$

of $FeCl_2(2,$

C. Soluble Transition Metal Coordination Complexes as Precursors.

High spin polynuclear transition metal compounds are of interest for their magnetic properties in biological as well as materials chemistry.[45] With respect to iron compounds, the magnetic behavior of dinuclear and polynuclear ferrous systems has not been well investigated compared to ferric systems. This is due, in part, to the large zero-field splittings and substantial anisotropies of the magnetic hyperfine interactions, which lend interesting properties to the compounds but which render it difficult to fit the magnetic data due to the large number of parameters involved.

A number of years ago, Dunbar and Quillevéré reported a reaction between anhydrous ferric chloride and the highly basic phosphine tris(2,4,6-trimethoxyphenyl)phosphine (TMPP) that led to the reduction of Fe^{III} to Fe^{II} and formation of $[Fe_2Cl_6]^{2-}$, a hitherto unknown binary ferrous chloride.[46] This serendipitous discovery led us to investigate whether the $[Fe_2Cl_6]^{2-}$ unit or other stable polynuclear species would be readily accessible from the lower insoluble halides of the type MCl_2 (M = Mn, Fe, Co, Ni). Our main interest in preparing these salts was to access discrete, soluble forms of high spin halide complexes for use as building blocks in larger molecules or arrays. In this vein, we have investigated reactions of several $[Fe_2Cl_6]^{2-}$ salts with 2,2'-bipyrimidine, a bis-chelating ligand that has received much attention in the literature due to its ability to transmit electronic and magnetic information between metal centers. The syntheses, structural characterization, and magnetic studies of the dinuclear anions $[M_2Cl_6]^{2-}$ (M = Mn, and Co), polynuclear metal halide clusters of $M_4Cl_8(THF)_6$ (M = Fe and Co) and $Mn_5Cl_{10}(THF)_8$, and two bipyridine reaction products with the $Fe_4Cl_8(THF)_6$ cluster, $Fe_2Cl_4(2,2'\text{-bpy})_2$ (bpy = bipyridine) and the structure of $FeCl_2(2,2'\text{-bpy})$, and the bpym (bpym = bipyrimidine) complex,

[Et4N]Cl•[F

4. Handling

Cryst
and biology
to the techn
improved s
Coupled De
has been ca
new structu
with the nu
new entries
total entries

In spi
solution and
introduction
with a CCD
year. As ma
other proble
processing.
data collecti
and other pr

$[Et_4N]Cl•[Fe_2Cl_4(MeOH)_4(\mu\text{-}2,2'\text{-bpym})]$, are presented.

4. Handling Crystallographic Problems with a CCD Detector.

Crystallography has become an essential component of both chemistry and biology. New structures are emerging at an ever-increasing rate owing to the technical advances in radiation sources, detectors, computing and improved structural methods. The introduction of the CCD (Charge Coupled Device) detector in the last few years has added to the trend of what has been called a "structural explosion".[47] On average, every 40 minutes, a new structure is deposited in the CSD (Cambridge Structure Data Base)[48] with the number published by CSD on their website.[49,50] The number of new entries added to CSD reached 14,799 in 1997 and 15,645 in 1998. The total entries in the database reached 195,798 by the end of 1998.

In spite of the obvious advantages, problems such as data collection, solution and refinement for twinned crystals have also emerged with the introduction of CCD area detector. A typical crystallography lab equipped with a CCD area detector may collect three to four hundred data sets per year. As many as 10% of these may be problematic, exhibiting twinning or other problems,[51] which require special handling during data collection and processing. In this thesis, strategies for handling problematic crystal data, data collection and processing, as well as solution and refinement of twinned and other problematic crystals will be presented and discussed.

References

1. (a) *Molecular Magnetism: From Molecular Assembies to the Devices* Coronado, E.; Delhaès, P.; Gatteschi, D.; Miller, J.S.Eds.; Kluwer Academic Publishers: Dordrecht, Netherlands **1996**. (b) *Molecular Engineering for Advanced Materials* Becher, J.; Schaumburg, K. Eds.; Kluwer Academic Publishers: Dordrecht, Netherlands **1995.** (c) Kaszynski, P.; Frieli, A.C.; Michl, J. *J. Am. Chem. Soc.* **1992**, *114*, 601. (d) Mallouk, T.E.; Lee, H. *J. Chem. Ed.***1990**, *67(10)*, 2704.

2. (a) Chen, C.-T.; Suslick, K. S. *Coord. Chem. Rev.*, **1993**, *128*, 293-322; see also references therein. (b) Archer, R. D.; Lauterbach, A.; Ochaya, V. O. *Polyhedron,* **1994,** *13*, 2043-2048.

3. (a) Gardner, G. B.; Venkataraman, D.; Moore, J. S.; Lee, S. *Nature,* **1995**, *374*, 792-795. (b) Venkataraman, D.; Gardner, G. B.; Lee, S.; Moore, J. S. *J. Am. Chem. Soc.*, **1995,** *117,* 11600-11601. (c) Yaghi, O. M.; Li, H. *J. Am. Chem. Soc.*, **1995**, *117,* 10401.

4. (a) Manriquez, J. M.; Yee, G. T.; McLean, S.; Epstein, A. J.; Miller, J. S. *Science* **1991**, *252*, 1415-1417. (b) Tamaki, H.; Zhuang, Z. J.; Matsumoto, N.; Kida, S.; Koikawa, M.; Achiwa, Hashimoto, Y.; Okawa, H. *J. Am. Chem. Soc.*, **1992**, *114*, 6974. (c) Stumpf, H. O.; Pei, Y.; Kahn, O.; Sletten, J.; Renard, J. P. *J. Am. Chem. Soc.*, **1993**, *115*, 6738. (d) Inoue, K.; Iwamura, H. *J. Am. Chem. Soc.*, **1994**, *116*, 3173. (e) Ohba, M.; Maruono, N.; Okawa, H.; Enoki, T.; Latour, J.-M. *J. Am. Chem. Soc.*, **1994**, *116*, 11566-11567. (f) Kahn, O. in *Molecular Magnetism: From Molecular Assemblies to the Devices: NATO ASI Series.* Eds., Coronado, E.; Delhaes, Gatteschi, D.; Miller, J. S. Kluwer Academic, Dordrecht, **1996,** *321*, pp. 243-288. (g) Decurtins, S.; Schmalle, H. W.; Schneuwly, P.; Zheng, Li-M.; Ensling, J.; Hauser, A. *Inorg. Chem.*, **1995**, *34*, 5501. (h) Miyasaka, H.; Matsumoto, N.; Okawa, H.; Re, N.; Gallo, E.; Floriani, C. *Angew. Chem. Int. Ed. Engl.* **1995**, *34*, 1446-1448. (i) Ohba, M.; Okawa, H.; Ito, T.; Ohto, A. *J. Chem. Soc. Chem. Commun.*, **1995**, 1545-1546. (j) Michaut, C.; Ouahab, L.; Bergerat, P.; Kahn, O.; Bousseksou, A. *J. Am. Chem. Soc.*, **1996**, *118*, 3610. (k) de Munno, G. ; Poerio, T.; Viau, G.; Julve, M.; Lloret, F.; Journaux, Y.; Riviere, E. *Chem.*

Commun., **1996**, 2587.

5. (a) Lacroix, P.; Kahn, O.; Gliezes, A.; Valade, L.; Cassoux, P. *Nouv. J. de Chimie*, **1985**, 643-651. (b) Gross, R.; Kaim, W. *Angew. Chem. Int. Ed. Engl.* **1987**, *26*, 251. (c) Bartley, S. L.; Dunbar, K. R. *Angew. Chem. Int. Ed. Eng.* **1991**, *30*, 448. (d) Ballester, L.; Barral, M.; Gutiérrez, A.; Jiménez-Aparicio, R.; Martinez-Muyo, J.; Perpiñan, M.; Monge, M.; Ruiz-Valero, C. *J. Chem. Soc. Chem. Commun.* **1991**, 1396-1397. (e) Humphrey, D.G.; Fallon, G.D.; Murray, K.S. *J. Chem. Soc., Chem. Commun.* **1988**, 1356. (f) Cornelissen, J.P.; van Diemen, J. H.; Groeneveld, L. R.; Haasnoot, J. G.; Spek, A. L.; Reedijk, J. *Inorg. Chem.* **1992**, *31*, 198-202. (g) Oshio, H.; Ino, E.; Mogi, I,; Ito, T. *Inorg. Chem.*, **1993**, *32*, 5697-5703. (h) Ballester, L.; Barral, M.; Gutiérrez, A.; Monge, A.; Perpiñan, M. F.; Ruiz-Valero, C.; Sánchez-Pélaez, A. *Inorg. Chem.* **1994**, *33*, 2142-2146. (i) Dunbar, K. R.; Ouyang, X. *Mol. Crys. Liq. Crys.*, **1995**, *273*, 21-28. (j) Oshio, H.; Ino, E.; Ito, T.; Maeda, Y. *Bull. Chem. Soc. Jpn.*, **1995**, *68*, 889. (k) Dunbar, K. R. *Angew Chem.*, **1996**, *35*, 1659. (l) Decurtins, S.; Dunbar, K. R. ; Gomez-Garcia, C. J.; Mallah, T.; Raptis, R. G.; Talham, D.; Veciana, J. in *Molecular Magnetism: From Molecular Assemblies to the Devices*. (Eds.: E. Coronado, P. Delhaès, D. Gatteschi, J. S. Miller) NATO ASI Series vol. E321 Kluwer, **1996**, 571-582. (m) Dunbar, K. R.; Ouyang, X. *Chem. Commun.*, **1996**, 2427. (n) Zhao, H.; Heintz, R. A.; Rogers, R. D.; Dunbar, K. R. *J. Am. Chem. Soc.*, **1996**, *118*, 12844. (o) Dunbar, K. R.; Ouyang, X. *Inorg. Chem.*, **1996**, *35*, 7188. (p) Azcondo, M. T.; Ballester, L.; Gutiérrez, A.; Perpiñán, F.; Amador, U.; Ruiz-Valero, C.; Bellitto, C. *J. Chem. Soc., Dalton Trans.* **1996**, 3015.

6. (a) Aumüller, A.; Erk, P.; Klebe, G.; Hünig, S.; von Schütz, J.; Werner, H. *Angew. Chem. Int. Ed. Engl.* **1986**, *25*, 740-741. (b) Aumüller, A.; Erk, P.; Hünig, S. *Mol. Cryst. Liq. Cryst. Inc. Nonlin. Opt.* **1988**, *156*, 215-221. (c) Erk, P.; Gross, H.-J.; Hünig, U. L.; Meixner, H.; Werner, H.-P.; von Schütz, J. U.; Wolf, H. C. *Angew. Chem. Int. Ed. Engl.* **1989**, *28*, 1245-1246. (d) Kato, R.; Kobayashi, H.; Kobayashi, A. *J. Am. Chem. Soc.*, **1989**, *111*, 5224-5232. (e) Aumüller, A.; Erk, P.; Hünig, S.; Hädicke, E.; Peters, K.; von Schnering, H. G. *Chem Ber.* **1991**, *124*, 2001.(f) Sinzger, K.; Hünig,

S.; Jopp, M.; Bauer, D.; Bietsch, W.; von Schütz, J. U.; Wolf, H. C; Kremer, R. K.; Metzenthin, T.; Bau, R.; Khan, S. I.; Lindbaum, A.; Lengauer, C. L.; Tillmanns, E. *J. Am. Chem. Soc.* **1993**, *115*, 7696. (g) Kato, R.; Kobayashi, H.; Kobayashi, A. *J. Am. Chem. Soc.* **1989**, *111*, 5224.

7. (a) Akamatu, H.; Inokuchi, H.; Matsunaga, Y. *Nature (London)* **1954**, *173*, 168. (b) Akamatu, H.; Inokuchi, H.; Matsunaga, Y. *Bull. Chem. Soc. Jpn.* **1956**, *29*, 213.

8. Melby, L. R.; Harder, F. J.; Hertler, W. F.; Mahler, W.; Benson, F. E.; Mochel, W. E. *J. Am Chem. Soc.* **1962**, *84*, 3374.

9. Wudl, F.; Smith, G. M.; Hufnagel, E. J. *J. Chem. Soc., Chem. Commun.* **1970**, 1453.

10. (a) Ferraris, J.; Cowan, D. O.; Walatka, V.; Perlstein, J. H. *J. Am. Chem. Soc.* **1973**, *95*, 498. (b) Coleman, L. B.; Cohen, M. J.; Sandman, D. J.; Yanagishi, F. G.; Garito, A. F.; Heeger, A. J. *Solid State Commun.* **1973**, *12*, 1125.

11. (a) Jerome, D.; Mazaud, A.; Ribault, M.; Bechgaard, K. *J. Phys. Lett.* **1980**, *41*, L95. (b) Bechgaard, K.; Jacobsen, S.; Mortensen, K; Pedersen, H. J.; Thorup, N. *Solid State Commun.* **1980**, *33*, 1119.

12. Mizuno, M.; Cava, M. P. *J. Org. Chem.* **1978**, *43*, 416.

13. Kikuchi, K.; Kikuchi, M.; Namiki, T.; Saito, K.; Ikemoto, I.; Murata, K.; Ishiguro, T.; Kobayashi, K. *Chem. Lett.* **1987**, 931.

14. Papavassillou, G. C.; Mousdis, G. A.; Zamboni, J. S.; Terzis, A.; Hountas, A.; Hilti, B.; Mayer, C. W.; Pfeiffer, J. *Synth. Met.* **1988**, *27*, B379.

15. Bossard, L.; Ribault, M.; Brousseau, M.; Valade, L.; Cassoux, P. C. R. *Acad. Sci. Paris* **1986**, *Ser. 2, 302*, 205.

16. Williams, J. M.; Kini, A. M.; Wang, H. H.; Carlson, K. D.; Geiser, U.;

Mon
Bory
Over
3272

17. (a) V
and
G. C
Am.

18. Pei,
1986

19. Mille
H.; R

20. (a) K
Day.
I.; Bo
M. S
S.; E
Mole
(e)Bu
Epste
(f) F
Inorg

21. (a) N
Zhan
Gord
1385.
A. J.;

22. (a) Ku
B.; Ca
Guior
Tume
Physi

Montgomery, L. K.; Pyrka, G. J.; Watkins, D. M.; Kommers, J. M.; Boryschuk, S. J.; Crouch, A. V. S.; Kwok, W. K.; Schirber, J. E.; Overmyer, D. L.; Jung, D.; Whangbo, M. H. *Inorg. Chem.* **1990**, *29*, 3272.

17. (a) Wickman, H. H.; Trozzolo, A. M.; Williams, H. J.; Hull, G. W.; and Merritt, F. R. *The Physical Review,* **1967**, *155*, 563. (b) DeFotis, G. C.; Palacio, F.; O'Connor, C. J.; Bhatia, S. N.; Carling, R. L. *J. Am. Chem. Soc.*, **1977**, *99*, 8314.

18. Pei, Y.; Verdaguer, M; Sletten, J; Renard, J. P. *J. Am. Chem. Soc.* **1986**, *108*, 7428.

19. Miller, J. S.; Calabresse, J. C.; Epstein, A. J.; Bigelow, W.; Zhang, J. H.; Reiff, W. M. *J. Chem. Soc., Chem. Commun.* **1986**, 1026.

20. (a) Keggin, J. F.; Miles, F. D. *Nature* **1936,** *137,* 577. (b) Mayoh, B.; Day, P. *J. C. S. Dalton* **1976,** 1483. (b) Gadet, V.; Mallah, T.; Castro, I.; Berdaguer, M. *J. Am. Chem. Soc.* **1992,** *114,* 9213. (c) Verdaguer, M. *Science,* **1996,** *272,* 698, and references therein. (d) Girolami, G. S.; Entley, W. R.; Treadway, C. R.; Holmes, S. M. *VIth Int'l Conf. On Molecule-Based Magnets,* Seignosse, France, Sept. 12-17, **1998.** (e)Bushmann, W. E.; Paulson, S. C.; Wynn, C. M.; Girtu, M. A.; Epstein, A. J.; White, H. S.; Miller, J. S. *Chem. Mat.,* **1998,** *10,* 1386. (f) Ferlay, S.; Mallah, T.; Ouahès, R.; Veillet, P,; Verdaguer, M. *Inorg. Chem.,* **1999,** *38,* 229.

21. (a) Miller, J. S.; Epstein, A. J. *Chem. Commun.,* **1998**, 1319. (b) Zhang, J.; Liable-Sands, L. M.; Rheingold, A. L.; Del Sesto, R. E.; Gordon, D. C.; Burkhart, B. M.; Miller, J. S. *Chem. Commun.,* **1998**, 1385. (c)Zhang, J.; Ensling, J.; Ksenofontov, V.; Gütlich, P.; Epstein, A. J.; Miller, J. S. *Angew. Chem. Int. Ed.,* **1998,** *37,* 637.

22. (a) Kurmoo, M.; Graham, A. W.; Day, P.; Coles, S. J.; Hursthouse, M. B.; Caulfield, J. L.; Singleton, J.; Pratt, S. J.; Hayes, W.; Ducasse, L.; Guionneau, P. *J. Am. Chem. Soc.* **1995,** *117,* 12209. (b) Martin, L.; Turner, S. S.; Day, P. *Chem. Commun.* **1997,** *15,* 1367. (c) Day, P. *Physica Scripta,* **1993,** *T49,* 726.

23. (a)
113
G.;
Squ
199
L.;

24. Sun
Ino

25. Mill
199

26. (a) I
Che

27. Ther
mag
Mag
198
New
the

28. (a)
Ang

29. Mill

30. Mar
Scie

31. (a)
Wer
Aun
Non
Meix
Cher

23. (a) Caneschi, A.; Gatteschi, D.; Sessoli, R. *J. Am. Chem. Soc.*, **1991,** *113,* 5873. (b) Aromi, G.; Aubin, S. M. J.; Bolcar, M. A.; Christou, G.; Eppley, H. J.; Folting, K.; Hendrickson, D. N.; Huffman, J. C.; Squire, R. C.; Tsai, H. L.; Wang, S.; Wemple, M. W. *Polyhedron,* **1998,** *17,* 3005. (c) Barra, A. L.; Brunel, L. C.; Gatteschi, D.; Pardi, L.; Sessoli, R. *Acct. Chem. Res.,* **1998,** *31,* 460.

24. Summerville, D. A.; Cape, T. W.; Johnson, E. D.; and Basolo, F. *Inorg. Chem* **1978**, *17*, 3297.

25. Miller, J. S.; Calabrese, J. C.; Mclean, R. S; Epstein, A. J. *Adv. Mat.* **1992,** *4*, 498

26. (a) Lacroix, P.; Kahn, O.; Gleizes, A.; Valade, L.; Cassoux, P. *New J. Chem.* **1984**, *8*, 643. (b) Rey Paul *Acc. Chem. Res.* **1989**, *22*, 392.

27. There are different conventions being used in the description of magnetic interactions. See, for example, (a) Carlin R. L. *Magnetochemistry*; Springer-Verlag: Berlin Heidelberg, Chapter 5, **1986**. (b) Mattis D. C. *The Theory of Magnetism;* Springer-Verlag: New York, **1981**; Vol. I. The convention used in this thesis follows the convention used in reference (a).

28. (a) Kahn, O. *Structure and Bonding*, **1987,** *68*, 89. (b) Kahn, O. *Angew. Chem., Int. Ed.* **1985**, *24*, 834.

29. Miller, J. S.; Esptein, A. J. *Prog. Inorg. Chem.* **1976** Vol *20* p1.

30. Manriquez, J. M.; Yee, G. T.; Mclean, S.; Epstein, A. J.: Miller, J. S. *Science* **1991**, *252*, 1415.

31. (a) Aumüller, A.; Erk, P.; Klebe, G.; Hünig, S.; von Schütz, J. U. and Werner, H.-P. *Angew. Chem. Int. Ed. Engl.* **1986**, *25*, 740. (b) Aumüller, A.; Erk P. and Hünig, S. *Mol. Cryst. Liq. Cryst. Inc. Nonlin. Opt.* **1988**, *156*, 215. (c) Erk, P.; Gross, H.-J.; Hünig,; Meixner, H.; Werner, H.-P.; von Schütz, J. U. and Wolf, H. C. *Angew. Chem. Int. Ed. Engl.* **1989**, *28*, 1245. (d) Kato, R.; Kobayashi, H.;

Kob

32. (a) I
103,
Ang
Chis
262
199
Lob
C.; *Met*
Paff
J. D
Synt
Bein
C.;
(i) D
Ouy

33. Trik
C.; D

34. (a)
(b)
199
199
Apa
Vale

35. (a)
(b)
Kot

Kobayashi, A. *J. Am. Chem. Soc.* **1989**, *111*, 5224.

32. (a) Bartley, S. L.; Dunbar, K. R. *Angew. Chem. Int. Ed. Engl.* **1991**, *103*, 447. (b) Cayton, R. H.; Chisholm, M. H.; Darrington, F. D. *Angew. Chem. Int. Ed Engl.*, **1990**, *29*, 1481-1483. (c) Cayton, R. H.; Chisholm, M. H.; Putilina, E. F.; Folting, K. *Polyhedron*, **1993**, *12*, 2627. (d) Stoner, T. C.; Dallinger, R. F.; Hopkins, *J. Am. Chem. Soc.*, **1990**, *112*, 5651. (e) Cayton, R. H.; Chisholm, M. H.; J. Huffman, C.; Lobkovsky, E. B. *J. Am. Chem. Soc.*, **1991**, *113*, 8709. (f) Huckett, S. C.; Arrington, C. A.; Burns, C. J.; Clark, D. L.; Swanson, B. I. *Synt. Met.* **1991**, *41-43*, 2769. (g) Li, D.; Huckett, S. C.; Frankcom, T.; Paffett, M. T.; Farr, J. D.; Hawley, M. E.; Gottesfeld, S.; Thompson, J. D.; Burns, C. J.; Swanson, B. I. in *Supramolecular Architecture: Synthetic Control in Thin Films and Solids ACS Symp. Ser. 499*, (Ed: Bein, T.) *American Chemical Society*, **1992**, Ch. 4, 33. (h) Stoner, T. C.; Geib, S. J.; Hopkins, M. D. *J. Am. Chem. Soc.*, **1992**, *114*, 4201. (i) Dunbar, K. R.; *J. Cluster Science* **1994**, *5*, 125. (j) Dunbar, K. R.; Ouyang, X. *Mol. Cryst. Liq. Cryst.* **1995**, *273*, 21.

33. Triki, S.; Ouahab, L.; Grandjean, D.; Amiell, J.; Garrigou-Lagrange, C.; Delahes, P.; Fabre, J. M. *Synth. Met.* **1991**, *41-43*, 2589.

34. (a) Gross, R.; Kaim, W. *Angew. Chem. Int. Ed. Engl.*, **1987**, *26*, 251. (b) Gross-Lannert, R.; Kaim, W.; Olbrich-Deussner, B. *Inorg. Chem.*, **1990**, *29*, 5046. (c) Kaim, W.; Moscherosch, M. *Coord. Chem. Rev.*, **1994**, *129*, 157. (d) Ballester, L.; Barral, M.; Gutiérrez, A.; Jiménez-Aparicio, R.; Martinez-Muyo, J.; Perpiñan, M.; Monge, M.; Ruiz-Valero, C. *J. Chem. Soc. Chem. Commun.*, **1991**, 1396.

35. (a) Cotton, F. A. and Norman, J. G. Jr. *J. Coord. Chem.*, **1971**, *1*, 161. (b) Handa, M.; Yamada, K.; Nakao, T.; Kasuga, K.; Mikuriya, M. and Kotera, T. *Chem. Lett.*, **1993**, 1969. (c) Dunbar, K. R. and Ouyang, X. *Chem. Commun.*, **1996**, 2427.

36. Cayton, R. H.; Chisholm, M. H.; Huffman, J. C.; and Lobkovsky, E. B. *J. Am. Chem. Soc.* **1991**, *113*, 8709.

37. Cayton, R. H.; Chisholm, M. H.; Putilina, E. F.; Flting, K.; Huffman,

J. C.

38. Cog
111,

39. Han
Kote

40. Han
Iken

41. Cott

42. Bart
448.

43. Bart

44. Cott

45. (a) H
Chem
Mou
4703
9629
Gran
L.; P
Zang
Inorg
Wan
1994
Com
Gold
1995

46. (a) D
31, 1
(c) D

J. C.; and Moodley, K. G. *Inorg. Chem.* **1992**, *31*, 2928.

38. Cogne, A.; Grand, A.; Rey, P.; and Subra, R. *J. Am. Chem. Soc.* **1989**, *111*, 3230.

39. Handa, M.; Takata, A; Nkao, T.; Kasuga, K.; Mikuriya, M.; and Kotera,T. *Chem. Letter.* **1992**, 2085.

40. Handa, M.; Sono, H.; Kasamatsu, K.; Kasuga, K.; Mikuriya, M.; Ikenoue, S. *Chem. Lett.* **1992**, 453.

41. Cotton, F. A.; Kim, Y.; Ren, T. *Inorg. Chem.* **1992**, *31*, 2723.

42. Bartley, S. L.; Dunbar, K. R. *Angew. Chem. Int. Ed. Engl.* **1991**, *30*, 448.

43. Bartley, S. L.; Dunbar, K. R. unpublished results.

44. Cotton, F. A.; Kim, Y.; Ren, T., *Inorg. Chem.* **1992**, *31*, 2608.

45. (a) Holm, R. H. *Acc. Chem. Res.* **1977**, *10*, 427. (b) Holm, R. H. *Chem. Soc. Rev.* **1981**, *10*, 455. (c) Papaefthymiou,V.; Girerd, J.J.; Moura, I.; Moura, J.J.G.; Münck, E. *J. Am. Chem. Soc.* **1987**, *109*, 4703. (d) Taft, K. L.; Lippard, S. J. *J. Am. Chem. Soc.* **1990**, *112*, 9629.(e) Ménage, S.; Vincent, J. M.; Lambeaux, C.; Chottard, G.; Grand, A.; Fontecave, M. *Inorg. Chem.* **1993**, *32*, 4766. (f) Taft, K. L.; Papaefthymiou, G. C.; Lippard, S. J. *Science* **1993**, *259*, 1302. (g) Zang, Y.; Jang, H. G.; Chiou, Y. M.; Hendrich, M. P.; Que, L. Jr. *Inorg. Chim. Acta* **1993**, *213*, 41. (h) Hendrich, M. P.; Day, E. P.; Wang, C. -P.; Synder, B. S.; Holm, R. H.; Münck, E. *Inorg. Chem.* **1994**, *33*, 2848 and references therein. (i) Powell, A. K.; Heath, S. L. Comments *Inorg. Chem.* **1994**, *15*, 255 and references therein. (j) Goldberg, D. P.; Tesler, J.; Bastos, C. M.; Lippard, S. J. *Inorg. Chem.*, **1995**, *34*, 3011.

46. (a) Dunbar, K. R.; Quillevéré, A. *Angew. Chem., Int. Ed. Engl.* **1992**, *31*, 1360. (b) Dunbar, K. R.; Quillevéré, A. *Polyhedron* **1993**, *12*, 807. (c) Dunbar, K. R.; Sun, J.-S. *Mol. Cryst. Liq. Cryst.* **1995**, *274*, 51.

47. Baker, T. *IUCr Newslett.* **1997**, *5*, 1.

48. (a) CAMBRIDGE DATABASE -Allen, F. H.; Kennard, O.; Taylor, R. *Acc. Chem. Res.* **1983**, *16*, 655. (b) Allen, F. H. and Kennard, O. *Chemical Design Automation News*, **1993**, *8*, 31.

49. "CCDC Annual Report 1997", Hartley, D and Allen, F. H. May, 1998 http://www.ccdc.cam.ac.uk/news/annrep/AnnRep97.html.

50. "CCDC Annual Report 1998", Hartley, D and Allen, F. H. Jun. 23, 1999 http://www.ccdc.cam.ac.uk/annrep/report98.html.

51. Young, V. G. Jr. *New Strategies in the Refinement of Rotationally Twinned Materials*, Poster presentation in ACA 1998 Annual Meeting, St. Louis, MO.

CHAPTER II

SYNTHESES AND CHARACTERIZATION OF EXTENDED ARRAYS WITH METAL-METAL BONDED COMPLEXES AND POLYNITRILE ACCEPTOR LIGANDS

1. Introdu

The

centers ha

compound

the commu

by simple

synthesize

with the M

group on t

ground sta

the magne

by Cotton

spins). No

was obser

Ru_2 units

displays a

closed-she

reported

$\{[Ru_2(chp)$

pyrazine a

involving

dicyanoqui

have been

magnetic s

ferromagne

(R = Tol)

1. Introduction

The synthesis and reactivity of compounds containing dinuclear metal centers has been extensively studied for nearly 30 years.[1] Numerous compounds reported over the years have contributed to the understanding of the communication pathway between metal-metal bonded M_2 units bridged by simple inorganic atoms or organic ligands. $Ru_2(O_2CR)_4Cl$, first synthesized by Wilkinson,[2] exists as a polymeric zigzag chain compound with the M-Cl-M angles ranging from 120° to 180°, depending on the R group on the carboxylate ligand. These Ru_2^{5+} compounds possess an S = 3/2 ground state based on the $\sigma^2\pi^4\delta^2(\pi^*\delta^*)^3$ electronic configuration. However, the magnetic study of the $Ru_2(O_2C_3H_7)_4Cl$ compound reported independently by Cotton[3] and by Drago[4] shows only paramagnetic behavior (isolated spins). No interaction between the dimetal units through the chlorine bridge was observed. A paper by Cotton describes an infinite chain structure where Ru_2 units are connected by linear cholride bridges. This material actually displays antiferromagnetic behavior.[5] Diruthenium carboxylates bridged by closed-shell organic conjugated π-species such as phenazine[6] were also reported to exhibit antiferromagnetic coupling, while the compound $\{[Ru_2(chp)_4]_2(pyz)\}(BF_4)_2$ (where chp = 6-chloro-2-hydroxypyridinato) with pyrazine as the π bridging unit exhibits no appreciable coupling.[7] Studies involving polynitrile ligands such as DM-DCNQI (2,5-dimethyl-N,N'-dicyanoquinonediimine) with a series of diruthenium carboxylate complexes have been reported by Swanson *et al.*[8] When acetate ligands were used, the magnetic study revealed both antiferromagnetic behavior for T(K) > 150 and ferromagnetic-like behavior for T(K) < 150, while $[Ru_2(O_2CR)_4]$DMDCNQI (R = Tol) shows only antiferromagnetic coupling. However no structural

informatic

In t

co-worker

can be c

dichloroet

order has

$\sigma^2\pi^4\delta^1$, wi

reaction b

reported t

oxidized

([Mo_2(R_2C

showed th

organonitr

channel to

Interesting

interaction

weakened

of Mo_2^{4+}

Mo_2(O_2CC

namely 1,

strong con

axially or

characteriz

due to the

acceptors

successfull

Meta

information is available to address the interaction mechanism.

In terms of dimolybdenum redox-active compounds, McCarley and co-workers have reported[9] that $Mo_2(O_2CR)_4$ (R = C_2H_5, $C(CH_3)_3$, or C_6H_5) can be oxidized by I_2 in a non-coordinating solvent such as 1,2-dichloroethane to form I_3^- salts of the cation $[Mo_2(O_2CR)_4]^{\bullet+}$. The bond order has been reduced to B.O. = 3.5 and the electron configuration is $\sigma^2\pi^4\delta^1$, with a single electron residing in the δ orbital. Evidence of a redox reaction between TCNE and a quadruply bonded dimolybdenum unit was reported by Giraudon *et al.*[10,11] The $Mo_2(R_2C_{22}H_{20}N_4)_2$ molecule was oxidized by TCNE to form a diradical species ($[Mo_2(R_2C_{22}H_{20}N_4)_2]^{\bullet+}TCNE^{\bullet-}$). Research reported by Felthouse *et al*[12] showed that when $Mo_2(O_2CCF_3)_4$ is used as a bridging unit to connect two organonitronyl radicals, that the quadruply-bonded unit is not an efficient channel to propagate spin interactions of the organic radicals TEMPO. Interestingly, the analogous dirhodium complex exhibits antiferromagnetic interactions with J = -200 K through its metal-metal bond,[13] which should be weakened by the introduction of axial ligands. There is promise for the use of Mo_2^{4+} units in this chemistry, however, as Handa has reported that $Mo_2(O_2CCF_3)_4$ forms an infinite one-dimensional chain with a π-acceptor, namely 1,4-benzoquinone, as the bridging unit[14]. Oligomers that exhibit strong communication between paramagnetic M-M bonded units through axially or equatorially bound bridging ligands have been structurally characterized,[25] but there is a general lack of X-ray data for polymeric arrays due to the difficulties in obtaining single crystals. Of the polynitrile acceptors TCNQ, TCNE and DM-DCNQI,[15] only TCNE has been successfully incorporated into infinite arrays with a dimetal unit.[16]

Metal-metal bonded compounds offer a diverse selection of oxidation

state, ligat

issues that

the applic

main goal

polymeric

crystallogr

compound

"$Ru_2(O_2C$

ferrimagne

characteriz

structural

contain th

addition, t

presented.

2. Experin

A. Startin

Mo_2

$Mo(CO)_6$

prepared b

trifluoroace

purchased

DCNQI w

bis(trimeth

was prepar

and freshly

argon or N_2

state, ligand and metal ion choices for molecule-based materials. The main issues that must be addressed are the isolation of pure crystalline phases and the application of various methods to characterize polymeric products. The main goal of the studies in this chapter is to synthesize pure oligomeric or polymeric compounds whose structures could be determined by X-ray crystallography. In this way we hope to model the structures of other related compound of interests for their magnetic properties, for example "$Ru_2(O_2CR)_4$(DM-DCNQI)"[17] which has been reported to form ferrimagnetic chains with DM-DCNQI, e.g., $Ru_2^{4+/5+}$ (S = 1 or 2), but whose characterization by X-ray techniques has eluded researchers. In this chapter, structural studies of $Mo_2(O_2CCF_3)_4$ and $Re_2Cl_4(dppm)_2$ complexes that contain the polynitrile ligands DM-DCNQI and TCNQ are described. In addition, the products of dimolybdenum pivalate reactions with TCNE are presented.

2. Experimental Section

A. Starting Materials and Reaction Procedures

$Mo_2(O_2CMe)_4$ and $Mo_2(O_2CCMe_3)_4$ were prepared by the reaction of $Mo(CO)_6$ with the corresponding carboxylic acid.[18] $Mo_2(O_2CCF_3)_4$ was prepared by the reaction of $Mo_2(O_2CMe)_4$ with trifluoroacetic acid and trifluoroacetic anhydride under reflux conditions.[19] TCNQ and TCNE were purchased from Aldrich and purified by sublimation before use. DM-DCNQI was prepared by the reaction of the 2,5-dimethylquinone with bis(trimethylsilyl)carbodiimide in the presence of $TiCl_4$.[20] $Re_2Cl_4(dppm)_2$ was prepared by the literature method.[21] All solvents were deoxygenated and freshly distilled before use, and all reactions were carried out in an argon or N_2 atmosphere unless otherwise noted.

B. Synthe

(1) Prepa

(a) 2:1 Re

Mo

were load

THF. The

THF was

with 3 x 5

NMR spec

2264(m), 2

1020(w), 8

(b) 2:1 Re

Mo_2

were loade

toluene. T

orange sol

had forme

diffractom

problem.

1228(s br)

503(m), 47

(c) 2:1 Rea

Quar

g. 0.01 m

degassed x

h in an oil

B. Synthesis

(1) Preparation of $Mo_2(O_2CCF_3)_4$(TCNQ) (1).

(a) 2:1 Reaction of $Mo_2(O_2CCF_3)_4$ with TCNQ in THF.

$Mo_2(O_2CCF_3)_4$ (0.095 g, 0.02 mmol) and TCNQ (0.020 g, 0.01 mmol) were loaded into a Schlenk tube and dissolved in 20 mL of freshly distilled THF. The yellow-green mixture was stirred for 12 h after which time the THF was removed by vacuum. The resulting dark green residue was washed with 3 x 5 mL of diethyl ether. The product was examined by infrared and NMR spectroscopies. IR (KBr pellet, cm^{-1}): 3435(vs), 2924(m), 2882(m), 2264(m), 2226(w), 1730(s), 1639(m), 1510(w), 1415(w), 1192(vs), 1170(w), 1020(w), 856(w), 825(w), 731(w).

(b) 2:1 Reaction of $Mo_2(O_2CCF_3)_4$ with TCNQ in toluene.

$Mo_2(O_2CCF_3)_4$ (0.095 g, 0.02 mmol) and TCNQ (0.020 g, 0.01 mmol) were loaded into a Schlenk tube and dissolved in 20 mL of freshly distilled toluene. The orange mixture was refluxed for 12 hours, and the resulting orange solution was stored in the freezer (~ –12 °C) until red needle crystals had formed. A few crystals was screened on the Nicolet (Siemens) P3/V diffractometer but they were unable to be indexed due to a severe twinning problem. IR (Nujol, cm^{-1}): 2243(w), 2218(m), 1603(s), 1589(vs), 1545(m), 1228(s br), 1190(vs br), 1157(vs br), 858(m), 850(m), 781(m), 731(vs), 503(m), 474(m).

(c) 2:1 Reaction of $Mo_2(O_2CCF_3)_4$ with TCNQ in xylenes.

Quantities of $Mo_2(O_2CCF_3)_4$ (0.095 g, 0.02 mmol) and TCNQ (0.020 g, 0.01 mmol) were loaded into a Schlenk tube along with 20 mL of degassed xylenes (b.p. 138.2-141.7°C). The red mixture was refluxed for 12 h in an oil bath and slowly cooled to room temperature. IR (Nujol, cm^{-1}):

2243(w),
1190(vs
474(w).
hours. (R
a dark red
(2) Prepa
(a) 1:1
benzene/(
Mo
benzene in
benzene w
undisturbe
crop of re
washed w
pressure
2232(w),
1234(s), 1
(b) Growt
Sing
reaction.
5 mL of C
solution of
carefully l
tube was f
week. Bro
light yello
study.

2243(w), 2220(m), 1603(s), 1589(vs), 1570(m sh), 1545(m), 1228(vs br), 1190(vs br), 1159(vs br), 858(s), 781(m), 733(vs), 518(w sh), 503(m), 474(w). Dark red, rectangular platelet crystals formed over the course of 24 hours. (Reaction in degassed *m*-xylene led to the immediate precipitation of a dark red product but no crystals.)

(2) Preparation of $Mo_2(O_2CCF_3)_4$(DM-DCNQI) (2).

(a) 1:1 Reaction of $Mo_2(O_2CCF_3)_4$ with DM-DCNQI in benzene/CH_2Cl_2.

$Mo_2(O_2CCF_3)_4$ (0.045 g, 0.1 mmol) was dissolved in 10 mL of benzene in a Schlenk tube and DM-DCNQI (0.018 g, 0.1 mmol) in 15 mL of benzene was slowly added. The yellow brown mixture was allowed to stand undisturbed for 24 hours, after which time the solvent was decanted and a crop of red-brown needle-like crystals was collected. The crystals were washed with 3 x 5 mL of freshly distilled benzene and dried under reduced pressure (yield 0.035 g, 56%). IR (Nujol, cm^{-1}): 3497(m), 3365(m, br), 2232(w), 1726(w), 1701(w, sh), 1603(s), 1537(s, br), 1410(w), 1354(m, sh), 1234(s), 1194(vs, br), 1167(vs), 858(m), 781(m), 733(s), 476(w).

(b) Growth of single crystals by slow diffusion reaction.

Single crystals of (2) were grown in a sealed tube by a slow diffusion reaction. A 2 mL CH_2Cl_2 solution of $Mo_2(O_2CCF_3)_4$ (0.047 g, 0.01 mmol) in 5 mL of CH_2Cl_2 was transferred to a 1 mm diameter Pyrex tube, and a 2 mL solution of 2,5-DM-DCNQI (0.018 g, 0.01 mmol in 10 mL of benzene) was carefully layered on top of the $Mo_2(O_2CCF_3)_4$ solution via a syringe. The tube was flame-sealed under a slight vacuum and allowed to stand for one week. Brown needle crystals were observed to form at the interface of the light yellow solution. The crystals were harvested for a crystallographic study.



Figu

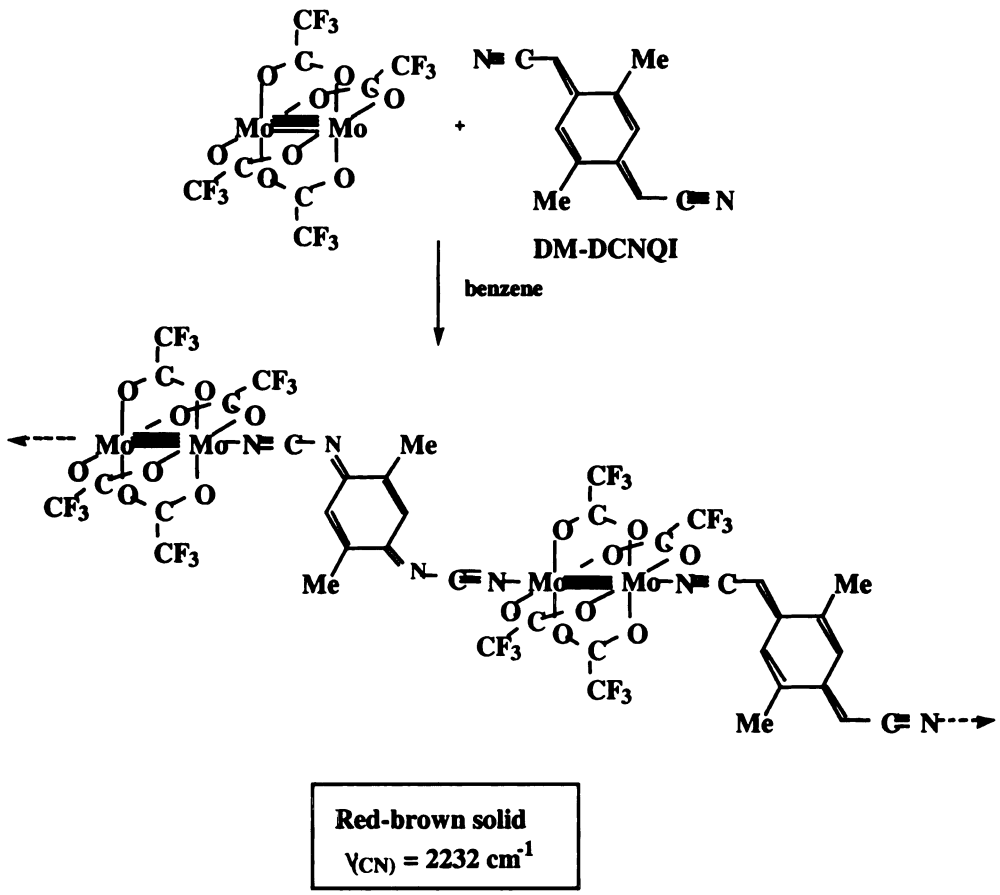


Figure 6. Preparation of $[Mo_2(O_2CCF_3)_4$ DM-DCNQI·$C_6H_6]_\infty$ (2).

(3) Preparation of {[$Mo_2(O_2CCMe_3)_3$(NC)2CC(CN)CONH] •8CH_2Cl_2 }$_\infty$ (3).

(a) Reaction of $Mo_2(O_2CCMe_3)_4$ with TCNE in CH_2Cl_2 at –78 °C.

$Mo_2(O_2CCMe_3)_4$ (0.120 g, 0.02 mmol) was loaded into a 100 mL Schlenk flask and dissolved in 20 mL of freshly distilled CH_2Cl_2. TCNE (0.026 g, 0.02 mmol) in 30 mL of CH_2Cl_2 was added drop-wise through a cannula to the Schlenk flask which was cooled in an isopropanol/CO_2(s) bath (–78 °C) over a period of 1 h. The Schlenk flask was then kept in the low temperature bath. No visible color change in the dark green solution was observed after one week. The solution was warmed up to room temperature, and stirred for 10 h, after which time the solution was stored in a freezer for three weeks. During this time tiny amounts of red crystalline product were observed to have formed.

(b) Reaction of $Mo_2(O_2CCMe_3)_4$ with TCNE in CH_2Cl_2 at room temperature.

$Mo_2(O_2CCMe_3)_4$ (0.120 g, 0.02 mmol) was dissolved in 20 mL of freshly distilled CH_2Cl_2, and TCNE (0.026 g, 0.02 mmol) in 30 mL of CH_2Cl_2 was added drop-wise through a cannula over the period of 1 h. The mixture was stirred at r.t. for 12 h, during which time the solution changed from dark green to dark brown. A small amount of black solid was observed on the side of the flask. Red hexagonal platelet crystals grew after the solution was stored at low temperature (-10 to -40°C) for 5 days. The crystals continued to grow over the period of one month. The crystals are soft and thin, and the larger ones have the tendency to be twinned. When removed from the mother liquid, the crystals quickly lose dichloromethane which leads to rapid loss of crystallinity. IR (Crushed crystals between KBr plates, cm^{-1}): 3440(vs, br), 3260(s, sh), 2980(m), 2204(s), 2160(m, sh),

1633(vs,
1020(w),
(c) Singl
conditio
(i) Ethyle
A
glycol/C
microcry
days.
(ii) Freez
A
for three
of ~ 0.2 r
(iii) Low
A
Cryogen
between
red hexa
observed
time to t
but they
flask wa
remove t
between
1560(w,
1020(vs,

1633(vs, br), 1458(s, br), 1290(w), 1267(m), 1221(s), 1130(w), 1036(w), 1020(w), 1010(w), 895(m), 796(m, sh), 717(s), 696(m, sh), 610(m), 455(w).

(c) Single crystal growth of (3) under various low temperature conditions.

(i) Ethylene glycol/CO_2(s) bath.

A reaction flask containing (3) was cooled in an ethylene glycol/CO_2(s) bath at -12°C for one week. A finely divided red microcrystalline product was observed to be present in the solution after 4 days.

(ii) Freezer storage.

A reaction flask containing (3) was stored in the freezer at ~ –12°C for three to four weeks, during which time small hexagonal platelet crystals of ~ 0.2 mm diameter and ~ 0.05 mm thickness had formed.

(iii) Low temperature circulating bath.

A reaction solution containing (3) was placed in a programmable Cryogen II-80 low temperature bath. The temperature was set to circulate between –10 to –40°C with a gradient of $\pm$ 1°C per hour. After ~ 1 week, red hexagonal crystals in the size range of 0.2 – 0.4 mm diameter were observed. Within two weeks, the crystals were in the mm size range. From time to time, colorless needles were observed at the surface of the solution, but they melted immediately and dissolved in the CH_2Cl_2 solution when the flask was disturbed or removed from the bath. Attempts were made to remove the melted crystals by pipette for characterization. IR (liquid drops between KBr plates, cm^{-1}): 2261(w), 2202(w), 1684(vs br), 1606(m, br), 1560(w, sh), 1550(w, sh), 1471(w), 1402(m, br), 1259(vs), 1089(vs, br), 1020(vs, br).

(iv) Solv

Th

30 mL o

diffusion

ethylene

of red cr

(4) Prep

{[Mo

(a) Room

Qu

g, 0.1 mn

room tem

and wash

br), 3330

2261(vw)

1460(w),

sh), 1091

(b) Benze

The

dark brov

CH_2Cl_2 w

mL) was

transferre

temperatu

crystals f

1155(m),

503(m).

(iv) Solvent diffusion in a fritted H-tube at ~ -12°C.

The reaction mixture was transferred to an H-tube via a cannula, and 30 mL of hexane was added to the other side of the H-tube to allow for slow diffusion crystallization. The H-tube was maintained in an ethyleneglycol/CO_2(s) bath (~ -10 to ~ -40°C) for 10 days. A small quantity of red crystals was obtained by this method.

(4) Preparation of

{[$Mo_2(O_2CCMe_3)_3$(NC)2CC(CN)CONH]•0.5C_6H_6}$_\infty$ (4).

(a) Room temperature reaction.

Quantities of $Mo_2(O_2CCMe_3)_4$ (0.060 g, 0.1 mmol) and TCNE (0.013 g, 0.1 mmol) were dissolved in 10 mL of benzene and stirred for two days at room temperature. A yellow brown precipitate was collected by filtration and washed with 3x5 mL of diethyl ether. IR (KBr pellet, cm^{-1}): 3420(vs, br), 3330(s, br), 3204(s, br), 2967(m), 2928(m), 2878(vw, sh), 2854(vw, sh 2261(vw), 2216(vw), 2157(w), 1686(vs), 1626(m), 1520(m), 1485(s), 1460(w), 1425(s), 1402(s, sh), 1381(s, sh), 1365(m, sh), 1228(m), 1196(w, sh), 1091(vw), 976(s), 734(s, br), 614(w), 488(w, br).

(b) Benzene extraction from the CH_2Cl_2 reaction product (4).

The reaction proceeded at room temperature as described in (4). The dark brown solution was kept in a low temperature bath (~ -20 °C) while CH_2Cl_2 was removed by a dynamic vacuum. Freshly distilled benzene (20 mL) was added to the resulting residue, and the dark green solution was transferred to a Schlenk flask by a cannula. The solution was stored at room temperature for one week, during which time, tiny red hexagonal platelet crystals formed. IR (Nujol, cm^{-1}): 2216(w), 1684(m, br) 1221(m, br) 1155(m), 1093(w), 1022(w), 970(w), 800(w), 721(m), 638(w), 555(w), 503(m).

(5) Preparation of $[Re_2Cl_4(dppm)_2]_2TCNQ•10THF$ (5).

$Re_2Cl_4(dppm)_2$ (0.100 g 0.04 mmol) in 3 mL of THF was layered with a THF solution of TCNQ (0.007 g 0.04 mmol) in a 1 mm Pyrex tube. The tube was sealed under vacuum and stored at low temperature (~ 2 °C) for three days during which time small brown blocks had grown. Removal of the crystals from the THF solvent led to rapid loss of crystallinity.

(6) Preparation of $[Re_2Cl_4(dppm)_2]_2$DM-DCNQI•10THF (6).

$Re_2Cl_4(dppm)_2$ (0.100 g, 0.04 mmol) in THF was layered with a THF solution of DM-DCNQI (0.007 g, 0.04mmol) in a 1 mm Pyrex tube. The tube was sealed and stored at low temperature (~ 2°C) for three days to yield a small quantity of tiny brown crystals.

C. X-ray Crystallographic Studies

General data collection procedures are described in appendix A.

(1) $[Mo_2(O_2CCF_3)_4]_2(TCNQ)•2(m\text{-}C_8H_{10})$

$•[Mo_2(O_2CCF_3)_4]•2(m\text{-}C_8H_{10})$ (1).

Single crystals of (1) used for crystallographic study were grown from the reaction of $Mo_2(O_2CCF_3)_4$ and TCNQ in xylenes (b.p. 138-141°C). A rectangular platelet crystal of approximate size 0.73 x 0.55 x 0.14 mm was secured on the tip of a glass fiber with Dow Corning silicone grease. The crystal was mounted on a Nicolet (Siemens) P3/V diffractometer equipped with a low temperature device at -108±1°C. Least-squares refinement using 20 well centered reflections in the range $15° \leq 2\theta \leq 25°$ indicated a triclinic system with a = 11.712(2) Å, b = 12.831(3) Å, c = 15.882(3) Å, α= 73.88(3)°, β= 73.87(3)°, γ= 87.87(3)°, V = 2200.8(8) Å^3. The data were collected at -108±1°C by the ω-2θ scan technique in the range $4° \leq 2\theta \leq 50°$. The total number of reflections measured were 6908, of which 6536

reflectio
refined b
package
the diso
anisotrop
occupanc
occupanc
molecule
disordere
residuals
R1= 0.0€
and with
(2) $Mo_2($

Sir
solution
$Mo_2(O_2C$
approxim
fiber wit
1K CCD
was bath
cooling
carried o
Å) powe
exposure
hemisphe
in ω and
generated

reflections are unique. The structure was solved by direct methods and refined by full-matrix least squares on F^2 using the Siemens SHEXTL v5.03 package on a Silicon Graphics Workstation. All non-hydrogen atoms except the disordered -CF_3 group and the *m*-xylene molecules were refined anisotropically. The disorder in the -CF_3 groups was modeled at 50% occupancy over two conformers for one –CF_3 group, and at ~ 33% occupancy over three conformers for a second –CF_3 group. The *m*-xylene molecules were modeled at 50% occupancy each for two orientations. All disordered atoms were refined isotropically. The structure was refined to residuals of *R1* = 0.0478 (*wR2* = 0.119) for 5385 reflections with $I > 2\sigma$ and *R1*= 0.0616 (*wR2*= 0.130) for all 6532 reflections against 625 parameters and with a goodness of fit = 1.232.

(2) $Mo_2(O_2CCF_3)_4$ DM-DCNQI•C_6H_6 (2).

Single crystals of (2) were grown by slow diffusion of a benzene solution of 2,5-DM-DCNQI into a methylene chloride solution of $Mo_2(O_2CCF_3)_4$ in a 1 mm diameter sealed Pyrex tube. A crystal of approximate size 0.20 x 0.20 x 0.35 mm was secured on the tip of a glass fiber with Dow Corning silicone grease and mounted on a Siemens SMART 1K CCD platform diffractometer at a detector distance of 6 cm. The crystal was bathed in a cold nitrogen stream at -140(2)°C with a Siemens LT2 cooling device. Preliminary examination and final data collection were carried out with graphite-monochromated Mo Kα radiation (λ_α = 0.71073 Å) powered at 50 KV and 40 mA. An indexing of 45 frames of data with exposure times of 10 sec/frame indicated a monoclinic crystal system. A hemisphere of data with 1321 frames was collected with a scan with of 0.3° in ω and an exposure time of 30 sec/frame. Final unit cell parameters were generated from the refinement of the XYZ centroids of the reflections with

I > 10c

(3) Å, c

related

an azi

Xprep,

and 1.

monoc

The str

squares

Graphi

half o

anisotr

atoms

(2) is l

(3) {[N

(a) Da

0.1 mm

The c

equipp

refiner

indica

22.86

confir

collec

intens

partial

$I > 10\sigma(I)$ from a total of 6044 reflections with a =20.755 (4) Å, b = 13.794 (3) Å, c = 13.924 (3) Å, β = 130.92 (3) °, and V = 3012.1(11) Å^3. Symmetry related and multiply measured reflections were averaged. Crystal decay and an azimuthal absorption correction were accounted for by the program Xprep,[22] which led to R_{int} = 0.0415, and transmission factors between 0.789 and 1.0. Systematic absences indicated that the crystal belongs to the monoclinic space group C2/c (#15), with R_{int} = 0.0476 and R_{sigma} = 0.0349. The structure was solved by direct methods and refined by full-matrix least squares on F^2 using the Siemens SHEXTL v5.03[22] package on a Silicon Graphics Workstation. A trifluoromethyl group disorder was modeled at half occupancy for each of the two conformers. All atoms were anisotropically refined except for the disordered $-CF_3$ group. Hydrogen atoms were fixed to ideal positions. A summary of crystallographic data for (2) is listed in Table 1.

(3) $\{[Mo_2(O_2CCMe_3)_3(NC)2CC(CN)CONH]\bullet 8CH_2Cl_2\}_\infty$ (3).

(a) Data collected on a Siemens P3/V diffractometer.

A thin hexagonal platelet of (3) of approximate dimensions 0.5 x 0.5 x 0.1 mm was secured on the tip of a glass fiber with Dow Corning grease. The crystal was mounted on a Nicolet (Siemens) P3/V diffractometer equipped with a low temperature device at -110(2)°C. Least-squares refinement using 20 well-centered reflections in the range $15° \leq 2\theta \leq 25°$ indicated a trigonal/hexagonal system with $a = b$ = 27.1010(38) Å, c = 22.8610(46) Å, $\alpha = \beta = 90°$, $\gamma = 120°$, V = 14,000(8) Å^3. Axial photographs confirmed that the Laue symmetry of the crystal is 6/mmm. Data were collected at -110(2)°C for 3692 reflections of which only 16% had intensities of $I > 4\sigma(F)$. Due to the low number of observed data, only a partial solution was obtained with the program SHELXS86 and DIRDIF[23] of

the TE

refinen

(b) Da

diffrac

secure

mount

detect

at -14

and fi

Kα ra

total c

indica

frame

30 sec

of the

was f

22.80

and c

progr

XPRE

hexag

straig

error

(#163

in P6

the TEXSAN[24] v5.0 package in the space group P6/mcc (#192). No refinement was attempted.

(b) Data collected on a Siemens SMART CCD 1K platform diffractometer.

A crystal of approximate dimensions 0.46 x 0.40 x 0.20 mm was secured on the tip of a glass fiber with Dow Corning silicone grease and mounted on a Siemens SMART 1K CCD platform diffractometer at a detector distance of 6 cm. The crystal was bathed in a cold nitrogen stream at -140(2)°C with a Siemens LT2 cooling device. Preliminary examination and final data collection were carried on with graphite-monochromated Mo Kα radiation (λ_α = 0.71073 Å) powered at 50 KV and 40 mA. Indexing a total of 45 frames of preliminary data with exposure time of 10 sec/frame indicated a monoclinic crystal system. A hemisphere of data with 1321 frames was collected with a scan with of 0.3° in ω and an exposure time of 30 sec/frame. Final unit cell parameters were generated from the refinement of the XYZ centroids of 8192 reflections with $I/\sigma > 10$. The crystal system was found to be trigonal/hexagonal with $a = b = 46.9356(12)$ Å, $c = 22.8009(6)$ Å, $\beta = 120.0\ (3)$ °, $V = 43324.33(11)$ Å^3. Beam inhomogeneity and crystal absorption and decay were corrected for by application of the program SADABS.[25] Data merging was performed with the program XPREP. Systematic absences indicated that the crystal belonged to the hexagonal system, but space group determination failed to be straightforward due to violations. Structure solution proceeded by a trial and error method, with the best results being achieved in space group P-31c (#163) with a merohedral twinning matrix (0 -1 0, -1 0 0 ,0 0 -1) or in P6cc (#184) with the merohedral twinning matrix (1 0 0, 0 1 0, 0 0 -1).

Table

Struct
Formu
Cryst
Space
a, Å
b, Å
c, Å
α, deg
β, deg
γ, deg
V, Å^3
T, K
Radia
Z
ρcalc,
μ, mm
F(000
Colle
Param
$R1$ (w
GoF
Scan
Note:
goodn
reflec

Table 1. Structural parameters for $\{[Mo_2(O_2CCF_3)_4]_2(\mu^4\text{-TCNQ})\bullet 2m\text{-}C_8H_{10}\}_\infty\{[Mo_2(O_2CCF_3)_4]\bullet(m\text{-}C_8H_{10})_2\}_\infty$ (1) and $[Mo_2(O_2CCF_3)_4(DM\text{-}DCNQI)\bullet C_6H_6]_\infty$ (2).

Structure	(1)	(2)
Formula	$C_{34}H_{22}F_{18}Mo_3N_2O_{12}$	$C_{24}H_{14}F_{12}Mo_2N_4O_8$
Crystal system	Triclinic	Monoclinic
Space group	*P*-1	*C*2/c
a, Å	11.712(2)	20.755(4)
b, Å	12.831(3)	13.794(3)
c, Å	15.882(3)	13.924(3)
α, deg	73.88(3)	90
β, deg	73.87(3)	130.92(3)
γ, deg	87.87(3)	90
V, Å^3	2200.8(8)	3012.1(11)
T, K	165(2)	133(2)
Radiation source	Mo Kα (λ_α = 0.71073 Å)	
Z	2	4
ρcalc, g/cm^3	1.932	1.998
μ, mm^{-1}	0.978	0.962
F(000)	1248	1768
Collected /unique Data	6908 / 6536	5917 / 2151
Parameters / restraints	625/0	251/72
R1 (*wR2*) (F^2, $I > 2\sigma$)	0.0478 (0.119)	0.0695(0.1767)
GoF	1.232	1.098
Scan type	ω-2θ	ω

Note: $R1 = \Sigma \| |F_o| - |F_c| \| / \Sigma |F_o|$, $wR2 = \{\Sigma [w(F_o^2 - F_c^2)^2] / \Sigma [w(F_o^2)^2]\}^{1/2}$, goodness-of-fit = $S = \{[w(F_o^2 - F_c^2)^2] / (n - p)\}^{1/2}$, n is the total number of reflections and p is the total parameters refined.

The stru
Subsequ
refinem
disorder
atoms v
idealize
(4) {[M
S
benzene
dimensi
with Do
CCD pl
stream
device.
with a g
and 40
distance
generate
The unit
b = 11.1
from the
$10\sigma(I)$ f
beam in
SADAB
17,791 r
were in
and mul

The structure solutions were obtained by direct methods in the XS program. Subsequent atoms were located from difference maps generated during refinement cycles. Least-squares refinement and *t*-butyl group and solvent disorder modeling were performed with the refinement program XL. All atoms were anisotropically refined, and hydrogen atoms were fixed in idealized positions.

(4) $\{[Mo_2(O_2CCMe_3)_3(NC)_2CC(CN)CONH]\bullet 0.5C_6H_6\}_\infty$ (4).

Single crystals of (4) were grown from the slow evaporation of a benzene extraction of (3). A red, hexagonal platelet crystal of approximate dimensions 0.052 x 0.052 x 0.078 mm was secured on the tip of a glass fiber with Dow Corning silicone grease and mounted on a Siemens SMART 1K CCD platform diffractometer. The crystal was bathed in a cold nitrogen stream at −100(2)°C with the Oxford Cryosystem Cryostream cooling device. Preliminary examination and final data collection were carried out with a graphite-monochromated Mo Kα radiation source powered at 50 KV and 40 mA. Intensity data were collected with 0.3° ω–scans at a detector distance of 5 cm. Initial cell parameters and an orientation matrix were generated from 60 preliminary data frames with a 15 sec exposure time. The unit cell was found to be monoclinic, C-centered with a = 30.8937(9) Å, b = 11.1253(2) Å, c = 17.9818(6) Å, β = 105.123(1)°, V = 5966.34(38) Å^3 from the refinement of the XYZ centroids of 2651 strong reflections with $I > 10\sigma(I)$ from a total of 17,791 reflections. The intensities were corrected for beam inhomogeneity, crystal decay and absorption with the program SADABS which led to R_{int}= 0.0530, T_{min} = 0.67, T_{max} = 1.0. A total of 17,791 reflections were measured at a maximum 2θ = 56.59, of which 6,297 were in the category of $I > 2\sigma(I)$, and 7274 were unique. Symmetry related and multiply measured reflections were averaged with the program Xprep.

Systen
C2/c (
achiev
the ful
sum of
(5) Cr

TCNQ
days.
mm w
and
diffrac
100(2
Prelim
graph
KV a
detec

60 pr
found
expos
centro
reflec
72.82
The i
absor
0.78,

Systematic absences indicated that the crystal belongs to the space group C2/c (#15), with R_{int} = 0.11 and R_{sigma} = 0.22. Structure solution was achieved from direct methods for all non-hydrogen atoms. Amide group and the fully rotationally t-butyl group disorder were modeled by refining the sum of the occupancies of the different disordered groups to be unity.

(5) Crystallographic study of $[Re_2Cl_4(dppm)_2]_2TCNQ•10THF$ (5).

Single crystals of (5) were grown by diffusion of a THF solution of TCNQ into a THF solution of $Re_2Cl_4(dppm)_2$ at 0°C over the course of three days. A dark brown crystal of approximate dimension 0.39 x 0.26 x 0.09 mm was secured on the tip of a glass fiber with Dow Corning silicone grease and mounted on a Bruker (Siemens) SMART 1K CCD platform diffractometer. The crystal was bathed in a cold nitrogen stream at -100(2)°C with the Oxford Cryosystem Cryostream cooling device. Preliminary examination and final data collection were carried on with graphite-monochromated Mo Kα radiation (λ_α = 0.71073 Å) powered at 50 KV and 40 mA. Intensity data were collected with 0.3° ω–scans at a detector distance of 5 cm.

Initial cell parameters and an orientation matrix were generated from 60 preliminary data frames with 10 sec/frame exposure times. The cell was found to be triclinic. A full sphere of data was collected with 30 sec/frame exposure times. The final unit cell obtained from the refinement of the XYZ centroids of 8,192 reflections with $I > 10\sigma(I)$ from a total of 39,411 reflections, is a = 12.1888(3) Å, b = 14.2908(3) Å, c = 23.3125(6) Å, α = 72.8220(10)°, β = 81.9380(10)°, γ = 75.7760(10)° and V = 3752.06(16) Å. The intensities were corrected for beam inhomogeneity, crystal decay and absorption with the program SADABS which led to $R1$ = 0.0399, T_{min} = 0.78, T_{max} = 1.0. A total of 17,791 reflections was measured with the

Table 2.

{[Mo_2(O_2C(

{[Mo_2(O_2C(

Identificatio
Empirical fo
Formula we
Temperature
Wavelength
Crystal syst
Space group
Unit cell dir
Volume
Z
Density (ca
Absorption
F(000)
Crystal size
Reflections
Refinement
Data / restr
parameters
GoF
R1(*wR2*) [*I*

Note: R_1 =
goodness-o
bP]

Table 2. Crystal data and structure refinement for $\{[Mo_2(O_2CCMe_3)_3(NC)_2CC(CN)CONH]\bullet 8CH_2Cl_2\}_\infty$ (3) and $\{[Mo_2(O_2CCMe_3)_3(NC)_2CC(CN)CONH]\bullet 0.5C_6H_6\}_\infty$ (4).

Identification code	(3)	(4)
Empirical formula	$C_{78}H_{111}Cl_{33}Mo_6N_{12}O_{21}$	$C_{50}H_{66}C_{14}Mo_4N_8O_{14}$
Formula weight	3281.62	1528.67
Temperature	133(2) K	133(2) K
Wavelength	0.71073 Å	0.71073 Å
Crystal system	Hexagonal	Monoclinic
Space group	P6cc	C2/c
Unit cell dimensions	a = 46.8862(4) Å	a = 30.855(4) Å
	b = 46.8862(4) Å	b = 11.1126(13) Å
	c = 22.7568(4) Å	c = 17.964(2) Å
	α= 90°.	α= 90°.
	β= 90°.	β= 105.111(2)°.
	γ= 120°.	γ= 90°.
Volume	43324.3(9) $Å^3$	5946.5(13) $Å^3$
Z	12	4
Density (calculated)	1.509 Mg/m^3	1.708 Mg/m^3
Absorption coefficient	1.164 mm^{-1}	1.072 mm^{-1}
F(000)	19626	3080
Crystal size	0.46 x 0.40 x 0.20 mm^3	0.052 x 0.052 x 0.078 mm^3
Reflections collected	10711	13892
Refinement method	Full-matrix on F^2	Full-matrix on F^2
Data / restraints / parameters	10707 / 1734 / 815	5023 / 32 / 236
GoF	1.367	1.062
R1(*wR2*) [F^2, $I>2\sigma(I)$]	0.1762/0.3880	0.1101/0.2117

Note: $R_1 = \Sigma \, ||F_o| - |F_c|| \, / \, \Sigma \, |F_o|$, $wR_2 = \{\Sigma \, [w(F_o^2 - F_c^2)^2] \, / \, \Sigma \, [w(F_o^2)^2]\}^{1/2}$, goodness-of-fit = $S = \{[w(F_o^2 - F_c^2)^2] \, / \, (n - p)\}^{1/2}$, $w = 1 \, / \, [\sigma^2(F_o^2) + (aP)^2 + bP]$

maxim

reflecti

S

with th

was tri

solutio

SHEX

Hydrog

hydrog

metho

were r

summa

(6) Cr

S

of DM

course

0.35 x

silicon

diffrac

Cryosy

data

MoKα

Intensi

cm.

60 data

collect

maximum $2\theta = 56.59$, of which 26,832 were of the type $I > 2\sigma(I)$ and 16,984 reflections were unique.

Symmetry related and multiply measured reflections were averaged with the program XPREP. Systematic absences confirmed that the crystal was triclinic P -1 (#2), with $R_{int} = 0.0493$ and $R_{sigma} = 0.0805$. Structure solution was achieved by application of the direct methods program in SHEXTL v5.04 with subsequent atoms being located from difference maps. Hydrogen atoms were calculated and fixed during refinement. All non-hydrogen atoms were refined anisotropically by full matrix least-squares methods. Disordered solvent molecules situated around the inversion center were modeled by refining two individual fragments as half occupied. A summary of refinement details is listed in Table 3.

(6) Crystallographic study of $[Re_2Cl_4(dppm)_2]_2$DM-DCNQI•10THF (6).

Single crystals of (6) were grown by slow diffusion of a THF solution of DM-DCNQI into a THF solution of $Re_2Cl_4(dppm)_2$ at -12°C over the course of a week. A dark brown crystal of approximate dimensions 0.50 x 0.35 x 0.20 mm was secured on the tip of a glass fiber with Dow Corning silicone grease and mounted on a Siemens SMART 1K CCD platform diffractometer in a cold nitrogen stream at -100(2) °C with the Oxford Cryosystem Cryostream cooling device. Preliminary examination and final data collection were carried out with a graphite-monochromated MoKα ($\lambda_\alpha = 0.71073$ Å) radiation source powered at 50 KV and 40 mA. Intensity data were collected with 0.3° ω–scans at a detector distance of 5 cm.

Initial cell parameters and an orientation matrix were generated from 60 data frames with 10 sec/frame exposure times. A full sphere of data was collected for a total of 2,474 frames and an exposure time of 22 sec/frame.

The fi

c = 23

V = 3

7242

The ir

absorp

0.662,

maxim

17,05

with t

triclin

soluti

V5.0-

differ

fixed

F^2. A

molec

by re

refine

3. Re

comp

mater

are il

The final unit cell was triclinic with a = 12.1264(2) Å, b = 14.25319(10) Å, c = 23.0826(3) Å, α = 74.5780(10)°, β = 83.1510(10)°, γ = 75.4330(10)° and V = 3716.42(8) Å^3 obtained from the refinement of the XYZ centroids of 7242 strong reflections with $I > 10\sigma(I)$ from a total of 41,616 reflections. The intensities were corrected for beam inhomogeneity, crystal decay and absorption with the program SADABS which led to $R1$ = 0.0560, T_{min} = 0.662, T_{max} = 1.0. A total of 41,123 reflections was measured with the maximum angle 2θ = 56.63, of which 25,260 were of the type $I > 2\sigma(I)$ and 17,059 reflections were unique.

Symmetry related and multiply measured reflections were averaged with the program XPREP. Systematic absences confirmed that the system is triclinic P -1 (#2), with R_{int} = 0.071 and R_{sigma} = 0.12. Initial structure solution was achieved by application of the direct methods in SHEXTL V5.04, with subsequent atoms being located from a series of alternating difference maps. Hydrogen atoms were placed in idealized positions and fixed during refinement. Full-matrix least-square refinement was carried out F^2. All non-hydrogen atoms were refined anisotropically. Disordered THF molecules which occupy positions around the inversion center were modeled by refining two fragments at half occupancy each. A summary of refinement details is printed in Table 3.

3. Results and Discussion

One of the interests in the current work is that metal-metal bonded compounds with unpaired spins are interesting building blocks for magnetic materials. The qualitative orbital interactions in metal-metal bonded species are illustrated in the simplified diagram in Figure 7.

The HOMOs for the different metal-metal bonded units in this study

Table 3.

and [Re_2Cl

Structure
Crystal sys
Space grou
a, Å
b, Å
c, Å
α, degree
β, degree
γ, degree
V, Å^3
Z
Dcalc, g/cr
μ, mm^{-1}
F(000)
Radiation
Data colle
R(int.)[a] /
Parameter
$R1$ ($wR2$)
GoF[d]
Collecting
Scan type

Note: [a] R
$= \Sigma \| |F_o| -$
of-fit = S

Table 3. Structural parameters for $[Re_2Cl_4(dppm)_2]_2TCNQ•10THF$ (5) and $[Re_2Cl_4(dppm)_2]_2DMDCNQI•10THF$ (6).

Structure	(5)	(6)
Crystal system	Triclinic	Triclinic
Space group	P-1	P-1
a, Å	12.1888(3)	12.1264(2)
b, Å	14.2908(3)	14.25319(10)
c, Å	23.3125(6)	23.0826(3)
α, degree	72.8220(10)	74.5780(10)
β, degree	81.9380(10)	83.1510(10)
γ, degree	75.7760(10)	75.4330(100
V, Å^3	3752.06(16)	3716.42(8)
Z	2	2
*D*calc, g/cm^3	1.546	1.551
μ, mm^{-1}	3.501	3.534
F(000)	1750	1740
Radiation Source	Mo Kα (λ_α = 0.71073 Å)	
Data collected / unique	39411/16984	41616/17152
R(int.) [a] / *R*(sigma) [b]	0.0493/0.085	0.0710/0.012
Parameters / constrains	787/100	745/150
R1 (*wR2*) (F^2, $I > 2\ \sigma$) [c]	0.0529 (0.1172)	0.0648 (0.1526)
GoF [d]	0.985	0.836
Collecting Temperature,°C	-100(2)	-100(2)
Scan type	ω	ω

Note: [a] $R_{int} = \Sigma\ |F_o^2 - F_c^2(\text{mean})| / \Sigma\ [F_o^2]$, [b] $R_{sigma} = \Sigma\ [\sigma(F_o^2) / \Sigma\ [F_o^2]$, [c] $R1 = \Sigma\ ||F_o| - |F_c|| / \Sigma\ |F_o|$, $wR2 = \{\Sigma\ [w(F_o^2 - F_c^2)^2] / \Sigma\ [w(F_o^2)^2]\ \}^{1/2}$, [d] Goodness-of-fit = $S = \{\ [w(F_o^2 - F_c^2)^2] / (n - p)\ \}^{1/2}$, $w = 1 / [\sigma^2(F_o^2) + (aP)^2 + bP]$

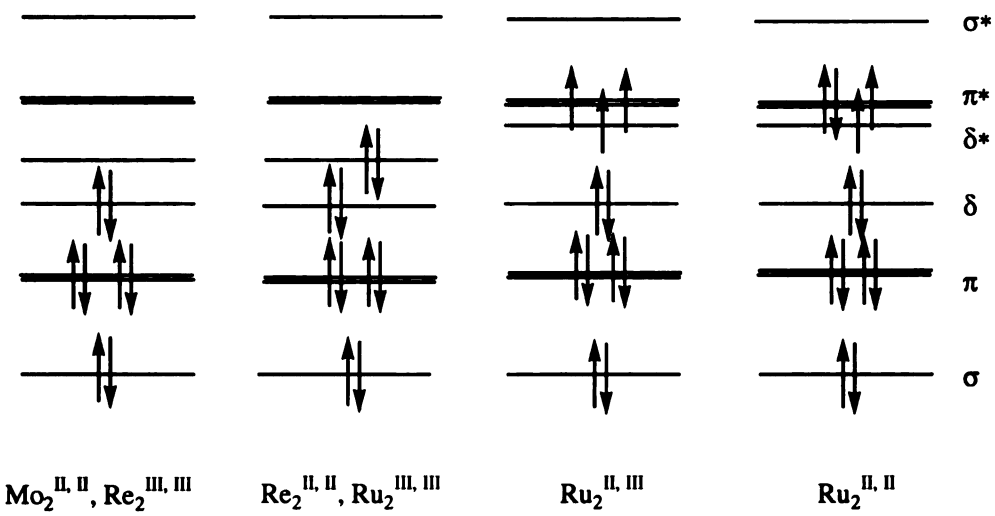


Figure 7. Metal-metal bonded orbitals diagrams.

are δ, δ*, δ*π* or the π* orbitals (Figure 7). Ligands with unpaired spins such as $TCNQ^{-1\bullet}$, $TCNE^{-1\bullet}$ or $DMDCNQI^{-1\bullet}$ may interact with the unpaired electrons residing on the metal-metal bonded unit. When the HOMO of an axial ligand is π*, which is the case for nitrile or carbonyl groups, there is no interaction between the unpaired electron in the ligand with the HOMO of Mo_2^{5+} and Re_2^{5+} unit with unpaired electrons in the δ or δ* (d_{xy}-based) orbitals of the metal-metal bond. There will be no direct overlap of the orthogonal M-L orbitals (Figure 8), therefore, one would expect a ferromagnetic interaction pathway. When unpaired spins from an axial ligand residing in π* orbitals interact with a metal-metal bonded unit such as Ru_2^{4+} and Ru_2^{5+}, however, the π* orbital of axial ligands overlaps with the HOMO (Figure 8), therefore providing a direct antiferromagnetic pathway.

When a ligand with an unpaired spin bonds to the equatorial position of a metal-meal bonded unit such as Re_2^{5+}, the interaction is quite different. The δ/δ* levels will then have the correct symmetry to overlap with the π*

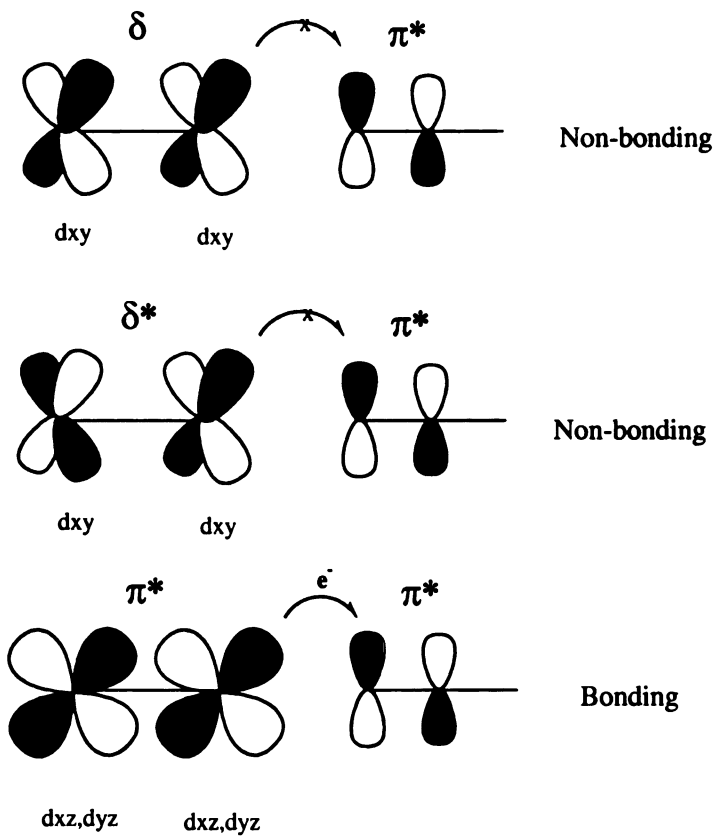


Figure 8. Interactions from an axial ligand to metal-metal bonded units such as $Mo_2^{II,II}$.

orbital of t
antiferroma
The
used to bu
compounds
particular t
regard. De
S = 3/2 gr
when bridg
anions. W
TCNE$^{\bullet-}$, T
(II, III),
antiferrom

A. Prepar

(1) Synthe

TCN
and magne
the compo
of the unf
highly rea
the preser
drawbacks
arrays suc

TCN
common h
base is pre

orbital of the ligand, and there should be good direct communication or an antiferromagnetic interaction (Figure 9).

The tetracarboxylate complexes of Ru_2^{5+}, Mo_2^{5+}, and Re_2^{5+} can be used to build low-dimensional arrays with multidentate ligands. Such compounds are of potential interest for their magnetic properties. In particular the diruthenium complexes have attracted high interest in this regard. Depending on the bridging ligand, the diruthenium complex, with an S = 3/2 ground state, has been found to exhibit antiferromagnetic coupling when bridged by closed shell organic bidentate ligands or simple inorganic anions. When bonded to an S = 1/2 organic π-acceptor radical such as $TCNE^{\bullet-}$, $TCNQ^{\bullet-}$, or $DMDCNQI^{\bullet-}$, in the case of tetrakispivilatodiruthenium (II, III), the complex behaves like a ferrimagnet due to local antiferromagnetic coupling but without cancellation of spins.

A. Preparation and Characterization

(1) Synthesis of the TCNE product of $Mo_2(O_2CCMe_3)_4$.

TCNE has been used extensively as a building block in conducting and magnetic materials. One of the most surprising examples of its use is in the compound $V(TCNE)_x$ that shows high T_c ferromagnetic ordering.[26] One of the unfortunate facts of the chemistry of TCNE, however, is that it is highly reactive toward hydrolysis, condensation and cleavage, especially in the presence of metal ions that enhance its reactivity.[27] In spite of its drawbacks, it has been noted that TCNE can be incorporated into a 3-D arrays such as $Rh_2(O_2CCF_3)_4TCNE{\bullet}C_6H_6$.[28]

TCNE hydrolysis reactions have been reported in the literature.[27] The common hydrolysis routes involve the release of an HCN molecule when a base is present, to form a cleavage products as shown in Figure 10. TCNE

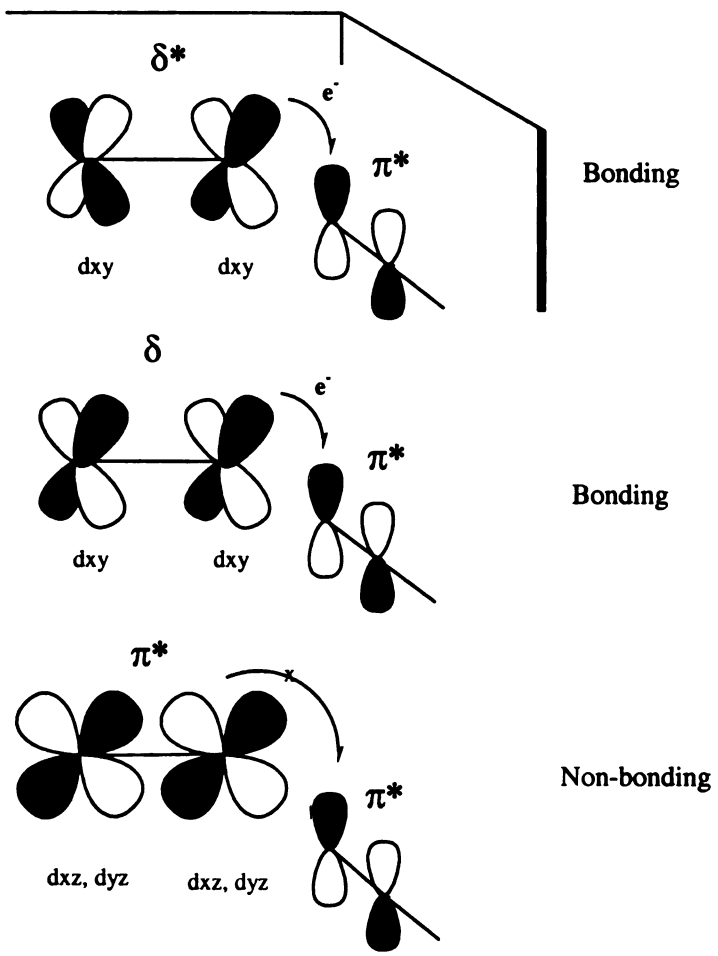


Figure 9. Interactions between equatorial ligands and metal-metal bonded units such as $Re_2^{II,III}$.

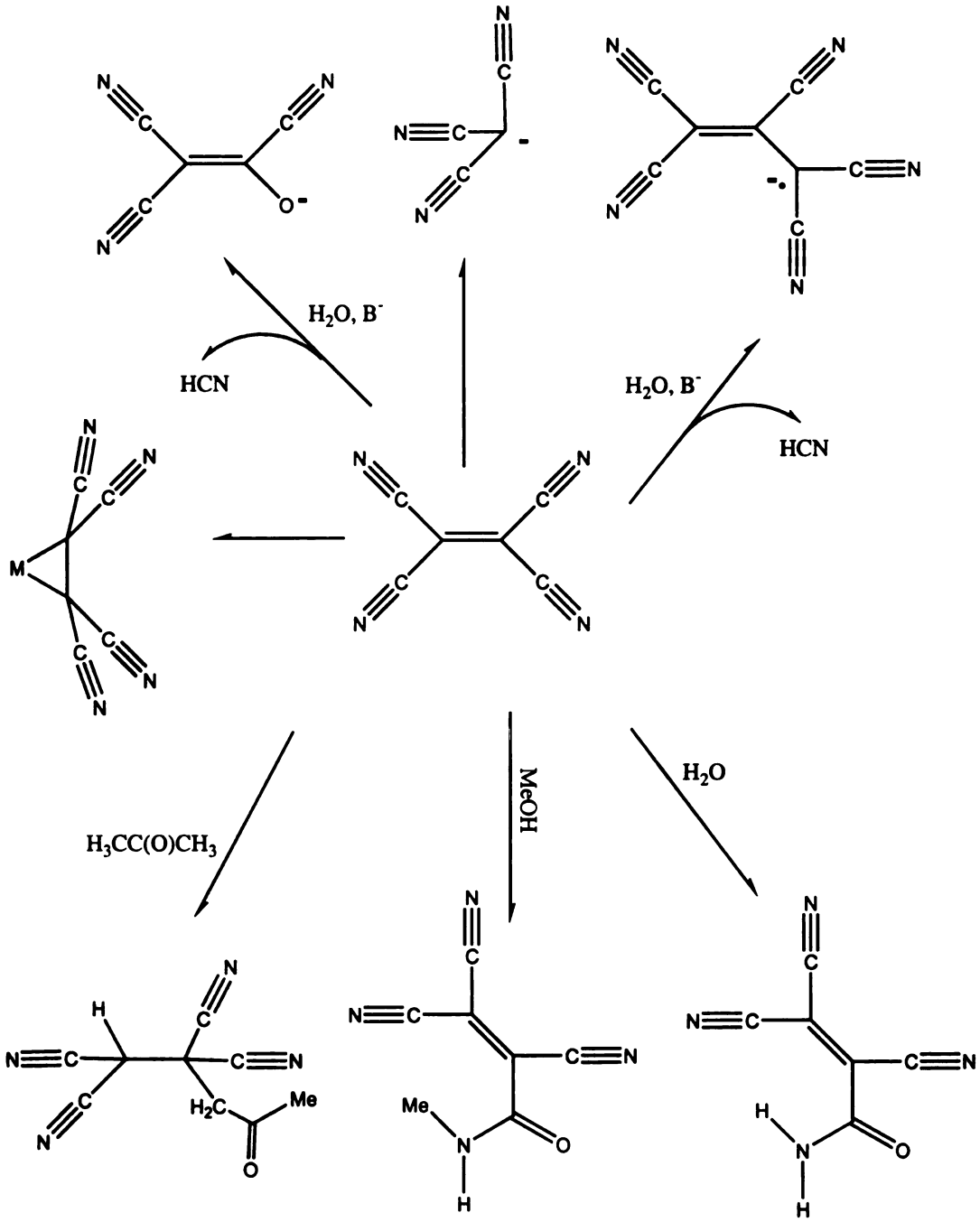


Figure 10. Documented reactions involving the decomposition of TCNE.

also form
acetone.[27]
polynitrile
relevance
route has b
high pressu
no CN cle
believed to
tricyanoacr
precedence
unusual rel
compound

Fron
the nitroge
non- coor
energy tha

B. Crystal

(1) Mo_2(O

An
composed
to four ind
A second
xylene lig
midpoint
μ^4-TCNQ
representa

also form adducts with small molecules such as water, methanol and acetone.[27] TCNE can also further react with the intermediate to form other polynitrile anions or act as an olefin in organometallic reactions. Of direct relevance to the present work is the fact that a very uncommon hydrolysis route has been reported in which TCNE is hydrolyzed under the condition of high pressure.[27] The product is an addition product of H_2O and TCNE with no CN cleavage. Structure (3) from our reaction with $Mo_2(O_2CBu^t)_4$ is believed to be the only example wherein the hydrolysis of TCNE to give the tricyanoacrylamide anion has occurred under mild conditions. As precedence for this work, we note that Cotton and Haefner observed the unusual related hydrolysis reaction of acetonitrile in the presence of a Mo_2^{4+} compound and a base.[29]

From the crystallographic data, one cannot determine the location of the nitrogen versus the oxygen atom. A semi-empirical calculations on the non- coordinated anion ligand suggest that conformer (1) is of a lower energy than conformer (2).

B. Crystallographic Studies.

(1) $Mo_2(O_2CCF_3)_4$ TCNQ

An X-ray crystallographic study revealed that compound (1) is composed, in part, of a chain of μ^4-TCNQ ligands bound in axial positions to four independent $Mo_2(O_2CCF_3)_4$ molecules to give a 1-D polymeric motif. A second type of $Mo_2(O_2CCF_3)_4$ molecule is situated in a cavity with two *m*-xylene ligands perpendicularly oriented near the axial positions. The midpoint of the Mo-Mo bond in the unique Mo_2 unit and the center of the μ^4-TCNQ rings reside on inversion centers. A thermal ellipsoid representation of (1) is depicted in Figure 12 and selected bond lengths and

bond angl

The

2.1131(11

statistical

the M-M

Mo-N(TC

distances

other axial

Å, L = D

L = 4,4'-

stretching

ν(C≡N) =

Mo-Mo u

involved

molecules

3.43(2) Å

structure,

xylenes u

but only

toluene

observat

of this r

arenes

$Mo_2(O$

Calcul

indica

bond angles are listed in Table 4.

The Mo-Mo bond length of 2.1126(8) Å in the polymeric chain and 2.1131(11) Å in the molecule of $Mo_2(O_2CCF_3)_4$(*m*-xylene)$_2$ in (1) are not statistically different from each other, but they are longer by ~0.023 Å than the M-M bond in $Mo_2(O_2CCF_3)_4$ (2.090(4) Å) without axial ligands.[30] The Mo-N(TCNQ) bond length of 2.627(5)Å is longer than the corresponding distances reported for polymeric $Mo_2(O_2CCF_3)_4L_2$ complexes containing other axial nitrogen donor ligands (Mo-Mo = 2.127(2) Å, Mo-N = 2.531(8) Å, L = DM-DCNQI (2); Mo-Mo = 2.128(1) Å, Mo-N = 2.557(8) Å, L = 4,4'-bpy).[31] These observations taken together with the ν(C≡N) stretching frequencies of 2243 and 2220 cm^{-1} for (1) (neutral TCNQ ν(C≡N) = 2230 cm^{-1}) imply that the interactions between the nitrile and the Mo-Mo unit in (1) are weak π-interactions. The TCNQ ligand is also involved in π-stacking interactions with interstitial *m*-xylene solvent molecules, with the shortest distance from the *m*-xylene to TCNQ being 3.43(2) Å. The presence of these π-interactions helps to stabilize the structure, and, indeed, crystals will not grow in the absence of xylenes. The xylenes used in the reaction is a mixture of isomers (b.p. 138.2-141.7 °C), but only *m*-xylene is incorporated! Furthermore, neither benzene nor toluene is suitable as solvents for crystal growth. These collective observations point to the selective enclathration of *m*-xylene in the formation of this rather unusual inclusion compound.

Metal-metal bonded complexes involved in axial coordination to arenes are rare. In fact only two examples, $Cr_2(O_2CCF_3)_4 \cdot C_6H_6$[32] and $Mo_2(O_2CP(Bu^t)_2)_4 \cdot 2C_6H_6$,[33] have been reported for Group 6 metals. Calculations performed on $Cr_2(O_2CCF_3)_4 \cdot C_6H_6$ by the Xα-SW-SCF method indicate that the e_{1u} orbital of the benzene molecules donate electron

Table 4.

A	
Mo1	N
Mo1	(
Mo1	(
Mo1	(
Mo1	N
Mo1	(
C17	(
C13	(

A	
Mo2	
C13	
N1	

Table 4. Selected bond distances (Å) and bond angles (°) for $[Mo_2(O_2CCF_3)_4(TCNQ)]_\infty$, (1).

Bond Distances

A	B	A-B (Å)	A	B	A-B (Å)	A	B	A-B (Å)
Mo1	Mo2	2.1126(8)	Mo2	O7	2.108(4)	Mo3	O10	2.107(4)
Mo1	O4	2.118(4)	Mo2	O2	2.109(4)	Mo3	O9	2.108(4)
Mo1	O5	2.124(4)	Mo2	O3	2.110(4)	Mo3	O11	2.109(4)
Mo1	O1	2.127(4)	Mo2	O6	2.134(4)	Mo3	Mo3*	2.113(1)
Mo1	N1*	2.630(6)	Mo2	N2	2.623(5)	Mo3	O12	2.122(4)
Mo1	O(8)	2.105(4)	N1	C13	1.148(8)	N2	C15	1.126(8)
C17	C18	1.337(9)	C17	C16	1.451(8)	C18	C16*	1.440(8)
C13	C14	1.431(9)	C14	C16	1.363(8)	C14	C15	1.453(8)

Bond Angles

A	B	C	A-B-C(°)	A	B	C	A-B-C(°)
Mo2	Mo1	N1*	175.50(13)	Mo1	Mo2	N2	171.15(12)
C13	N1	Mo1*	147.5(5)	C15	N2	Mo2	163.5(5)
N1	C13	C14	176.8(6)	N2	C15	C14	178.5(7)

density to
interaction
with the p
distance f
2.99(1) Å
Å. These
earlier exa
2.090(4) Å
presence o

This
units in po
in (1) is
adopts wi
nitrile to
e.g., the s
a 2-D mo
and four
11(a)).
and 163
ligands
polynitr
adjacen
dimolyl
(2) [M

monoc
residi

density to the π^* orbital of the Cr_2 units.[32] As was observed for the interactions involving benzene, the *m*-xylene molecules in (1) are oriented with the planes of the rings perpendicular to the Mo-Mo axis. The average distance from the least squares plane of the xylene ring to the Mo atom is 2.99(1) Å and the shortest Mo-C distance is essentially the same, *viz.*, 3.00 Å. These values are much less than the corresponding M-C distances in the earlier examples.[32] Furthermore, a lengthening of the Mo-Mo bond from 2.090(4) Å in $Mo_2(O_2CCF_3)_4$ to 2.1131(11) Å in (1) is in accord with the presence of axial interactions to the arene groups.[32]

This study supports the feasibility of using TCNQ to connect dimetal units in polymeric arrays. The 24-membered metallocyclic ring that forms in (1) is a consequence of the angle that the TCNQ nitrile functionality adopts with the Mo_2 units. These angles are expected to vary from one nitrile to another, thereby giving rise to different metallocyclic ring sizes, *e.g.*, the structure of $Rh_2(O_2CCF_3)_4TCNE$[34] involves a 30-membered ring in a 2-D motif. In the dirhodium compound, the Rh-N-C angle is close to 180° and four polynitrile ligands are used in the formation of the ring (Figure 11(a)). In compound (1), the two independent Mo-N-C angles of 147.5 ° and 163.5° are closer to 150°, which permits ring closure with only two ligands (Figure 11(b)). This situation gives rise to a one-dimensional μ^4-polynitrile polymer. In addition, the large cavities created by the packing of adjacent chains in (1) allow for the inclusion of a separate *m*-xylene bonded dimolybdenum complex.

(2) $[Mo_2(O_2CCF_3)_4(DM\text{-}DCNQI)\cdot C_6H_6]_\infty$ (2)

$[Mo_2(O_2CCF_3)_4(DM\text{-}DCNQI)\cdot C_6H_6]_\infty$ (2) crystallizes in the monoclinic space group C2/c, with the midpoint of the Mo-Mo bond residing on an inversion center. The structure consists of alternating

Figure 11.

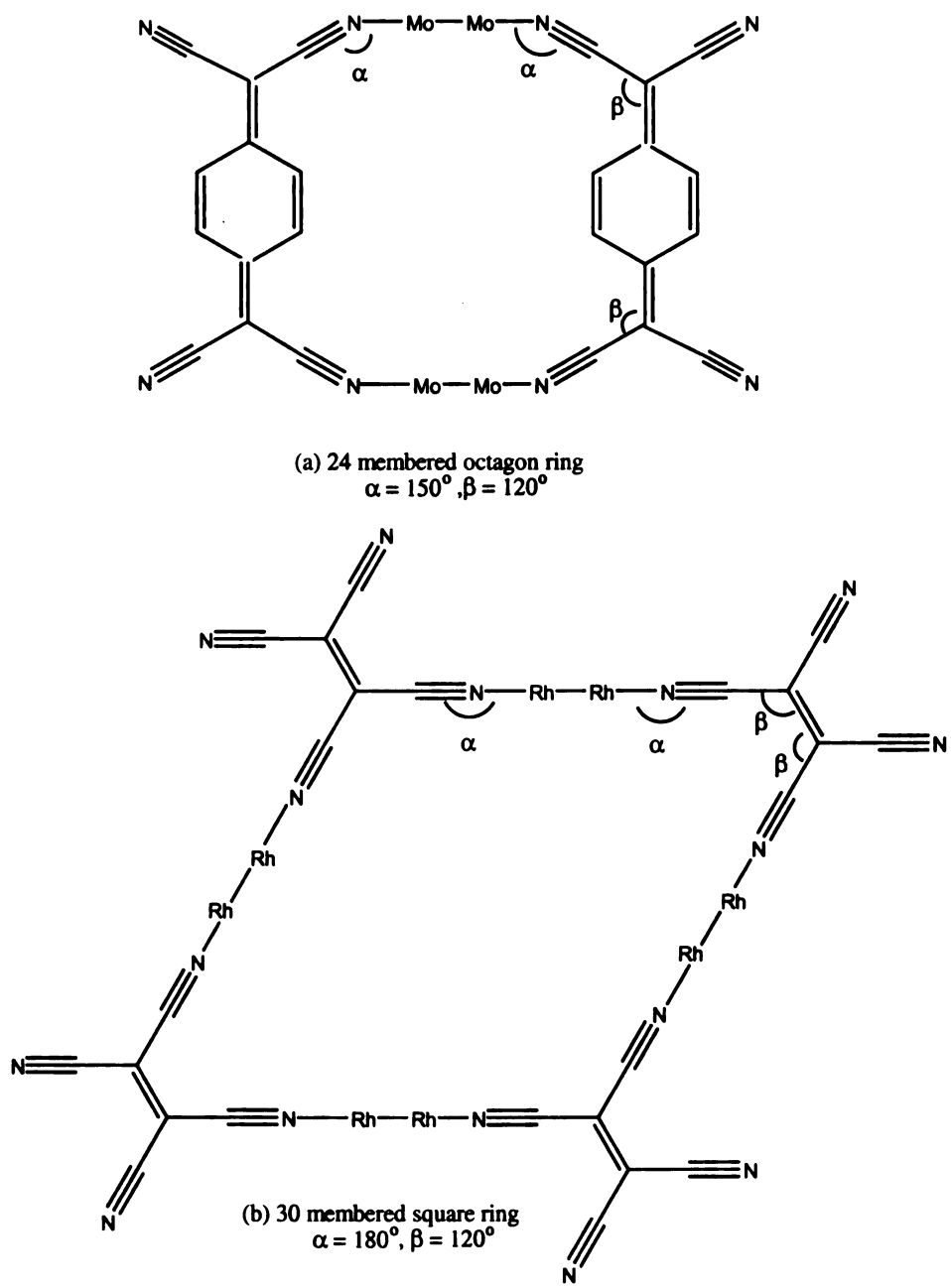


Figure 11. Metallocyclic rings of polynitriles with dimetal units and idealized angles: (a) $Mo_2(O_2CCF_3)_4(TCNQ)$ (1), (b) $Rh_2(O_2CCF_3)_4(TCNE)$.

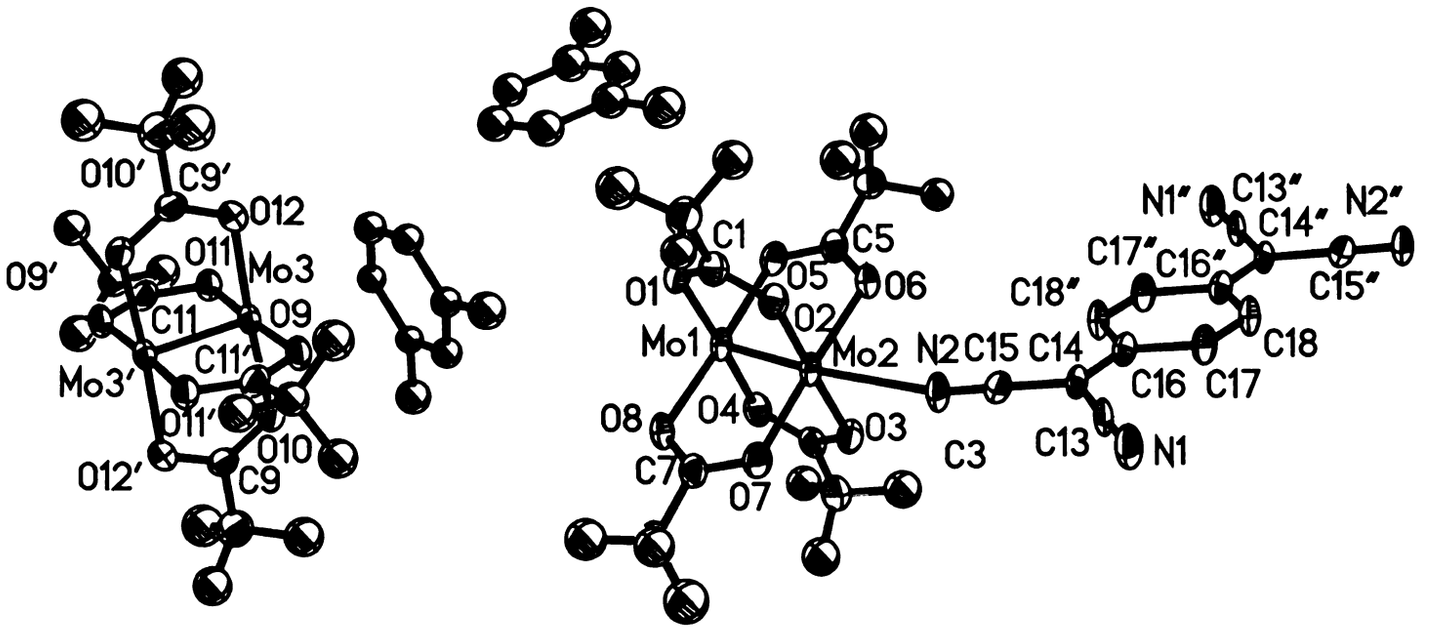


Figure 12. Thermal ellipsoid representation of (1) showing one Mo_2 unit bonded with the TCNQ ligand and a second Mo_2 unit bonded by *m*-xylene.

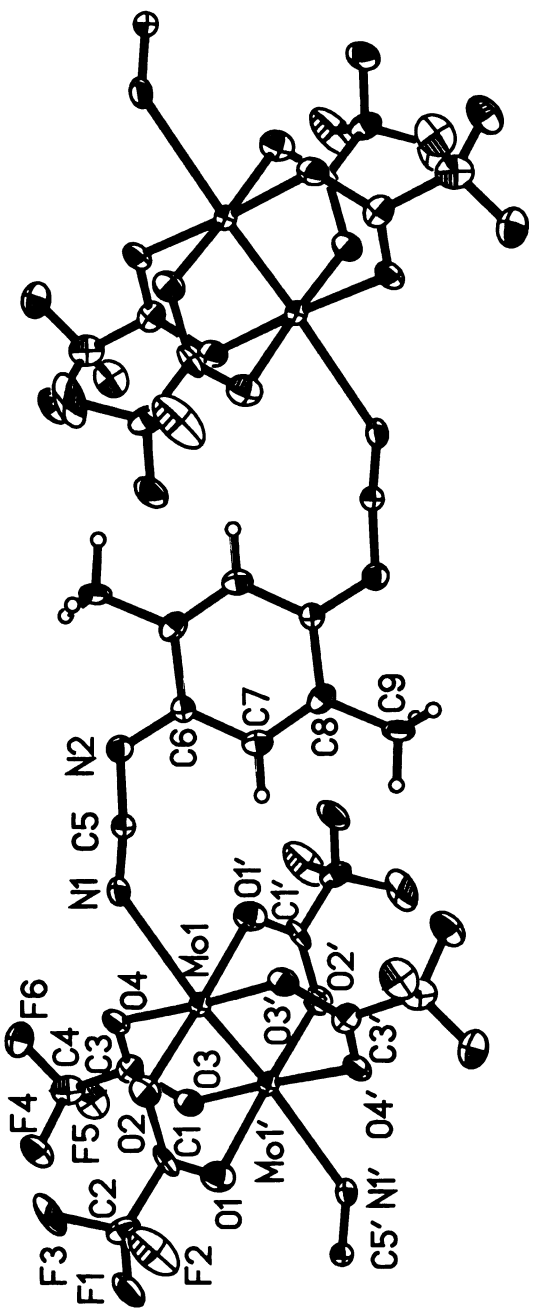


Figure 13. Thermal ellipsoid representation of (2) showing a portion of the chain with the disordered CF_3 group and benzene molecule omitted.

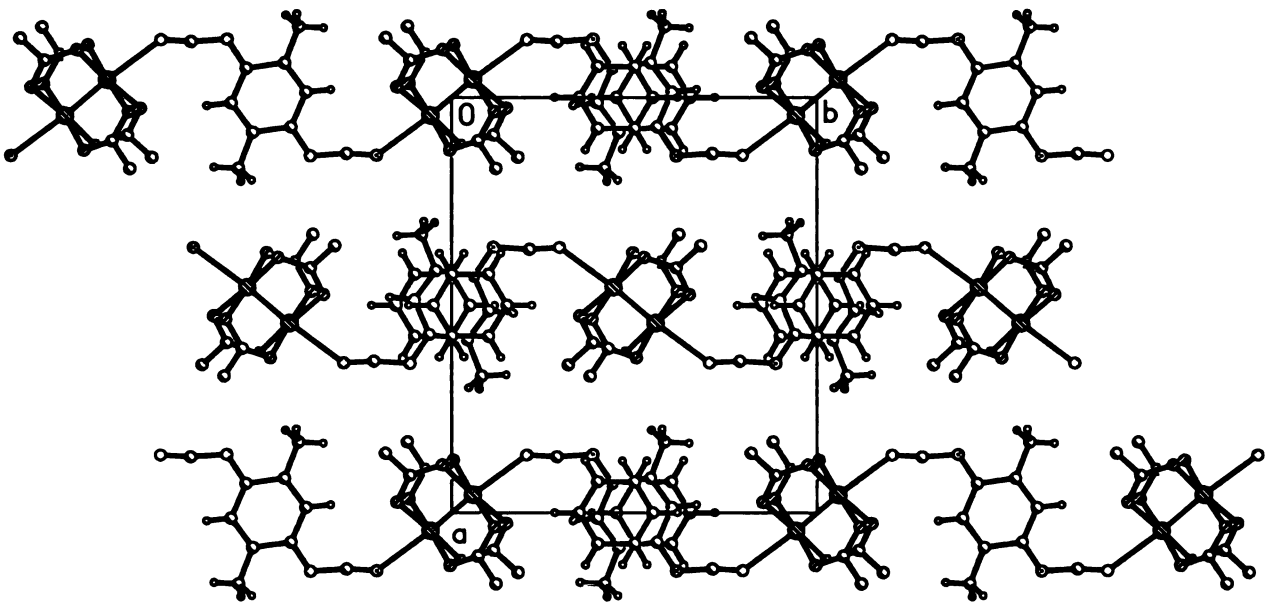


Figure 14. Plotting diagram of *ab* plane of (2) showing the stacking feature of the DM-DCNQI ligand with the benzene molecule in the lattice.

Table 5. *Geometric parameters for compounds that exhibit metal DM-DCNQI σ-bonding.*

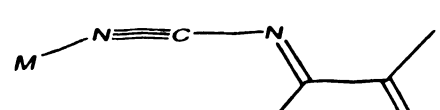
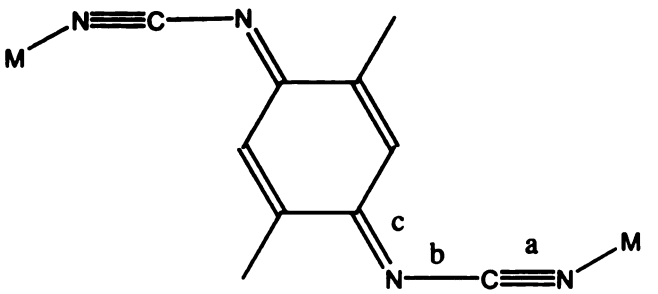


Table 5. Geometric parameters for compounds that exhibit metal DM-DCNQI σ-bonding.



M-σ- DM-DCNQI	charge	a	b	c	<MNC	<NCN	Ref.
$Cu(DM\text{-}DCNQI)_2$	μ^2, -1/2	1.159(6)	1.314(6)	1.342(6)	170.6(4)	172.8(2)	36c
$CuL(DM\text{-}DCNQI)_3$	η^1, -2/3	1.145(4)	1.330(4)	1.334(4)	153.9(3)	171.2(5)	36b
$CuL(DM\text{-}DCNQI)_2$	η^1, -1	1.149(5)	1.313(5)	1.405(5)	137.7(4)	174.0(5)	36b
$(RuL)_2DM\text{-}DCNQI$	μ^2, -2	1.155(19)	1.298(19)	1.376(17)	175.1(10)	171.5(15)	36d
$(RuL)_2DM\text{-}DCNQI$	μ^2, -2	1.188(24)	1.28(3)	1.468(23)	149.8(12)	169.6(18)	36d
$[Mo_2](DM\text{-}DCNQI)$	μ^2, 0	1.148(12)	1.365(13)	1.314(12)	140.3(7)	173.1(9)	(2)
DCNQI	0	1.150(2)	1.334(2)	1.303(2)		172.8(2)	36c

Table 6.

A
Mo1
Mo1
Mo1

A
Mo1'
Mo1'

Table 6. Selected bond distances [Å] and bond angles (°) for (2).

Bond Distances

A	B	A-B (Å)	A	B	A-B (Å)	A	B	A-B (Å)
Mo1	Mo1'	2.127(2)	Mo1	O2	2.114(6)	N1	C5	1.146(12)
Mo1	O4	2.118(6)	Mo1	O1'	2.131(7)	C5	N2	1.368(12)
Mo1	O3'	2.105(6)	Mo1	N1	2.531(8)			

Bond Angles

A	B	C	A-B-C(°)	A	B	C	A-B-C(°)
Mo1'	Mo1	N1	166.7(2)	Mo1	N1	C5	140.1(6)
Mo1'	Mo1	O1	90.4(2)	N1	C5	N2	173.1(9)

$Mo_2(O_2C$
positions
ellipsoid
stacking
be seen f
14). Sele
the more
Mo-N≡C
through
structure
DCNQI]
structure
larger th
suggesti
C≡N bo
than for
neutral,
2.531(8)
interacti
such as
bipyridi
shorter
$[Mo_2(O_2$
(2.622(5
compou
to electr

T

$Mo_2(O_2CCF_3)_4$ and DM-DCNQI molecules bonded through trans axial positions of the dimetal unit to give a zig-zag polymeric chain. A Thermal ellipsoid plot of a segment of the chain is depicted in Figure 13. The stacking feature of the DM-DCNQI molecule with the benzene molecule can be seen from the plotting diagram of the *ab* plane of the molecule (Figure. 14). Selected bond distances and bond angles are listed in Figure 6. One of the more striking features of the structure is the 140.1(6)° bond angle for the Mo-N≡C bond which is a low value for an sp hybridized N atom interacting through its lone pair. An inspection of related metric parameters for structures in which the σ-coordinated DM-DCNQI is formulated as [DM-DCNQI]$^{2-}$ and [DM-DCNQI]$_3^{2-}$, reveals that the M-N≡C angles in these structures also deviate from 180°, although, with one exception, they are all larger than 140° (Table 5).[36] While the M-N≡C bond angle of 140° is suggestive of an sp^2 hybridized N atom, it should be pointed out that the C≡N bond distance of 1.146(12)Å, which one would expect to be longer than for an sp nitrogen, is essentially the same as the corresponding value for neutral, free DM-DCNQI (1.148(5) Å).[37] The axial Mo-N distances of 2.531(8) Å and the Mo-Mo distance of 2.127(2)Å are typical of analogous interactions in other $Mo_2(O_2CCF_3)_4$ complexes with nonpolymeric N-donors such as pyridine (Mo-N 2.548(5)Å, Mo-Mo 2.129(2)Å)[38] and 4,4'-bipyridine (Mo-N 2.530(9)Å, Mo-Mo 2.124(1)Å)[39]. The Mo-N distance is shorter than those structures with polymeric interactions such as $[Mo_2(O_2CCF_3)_4(4,4'\text{-bpy})_2]_\infty$ (2.557(8)Å) and $[Mo_2(O_2CCF_3)_4\ (TCNQ)_{0.5}]_\infty$ (2.622(5)Å) (1). The slightly lengthened C≡N single bond (1.368(12)Å) in compound (2) compared to the neutral ligand (1.350(5)Å) can be attributed to electronic effects.

The structural characterization of a one-dimensional polymeric metal

complex
knowled
the polyr
stacked c
at a sepa
polymeri
(3) Struc

Mo_2(

(a) Data

Th
(only 10
fragment
the prog
hexagon
promisin
techniqu
obtained
order to
the SPA

O
just a he
that the
conclude
the man
impossib
Mo_2 uni
into an

complex/DM-DCNQI compound has not been previously reported to our knowledge. The stability of the present structure and the ease with which the polymer crystallizes from benzene is rationalized on the basis of the π-stacked columns formed by the DCNQI ligands and the benzene molecules at a separation of 3.4 Å. These additional interactions serve to "stitch" the polymeric chains together hence stabilizing the structure in two-dimensions

(3) Structural characterization of transformed TCNE with $Mo_2(O_2CCMe_3)_4$

(a) Data from a P3/V instrument partially solved by DIRDIF.

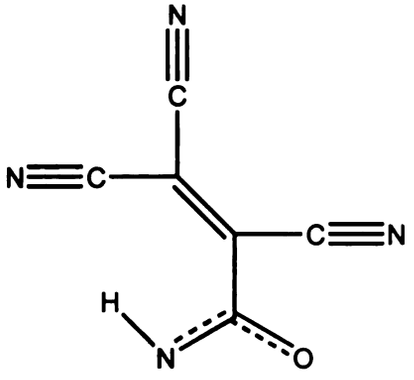
The data obtained on the Nicolet P3/V instrument were very weak (only 10% of reflections were of the type $F > 3\sigma$). Nevertheless, a structure fragment was solved (Hexagonal system, space group P6/mcc (#192)) with the program SHEXS86, and DIRDIF, which allowed for the detection of a hexagonal ring of six Mo-Mo units linked by cis-μ-TCNE. This was a very promising result that encouraged us to keep trying different crystallization techniques in order to obtain a better data set. From the structure fragment obtained, it was not possible to know if this was a polymeric structure. In order to assist in prediction of the structure, a simulation was performed with the SPARTAN[35] program based on the partial structure.

Our main question was whether the product is a polymeric sheet or just a hexamer. From the simulation in Figures 15 and 16, one can ascertain that the center of the structure contains a 10 Å hole. It is also possible to conclude that it is too crowded to link four Mo_2 units to one TCNE ligand, in the manner that four Rh_2 units were linked by a TCNE ligand.[28] It is impossible then for a polymeric structure to have formed without altering the Mo_2 unit or the TCNE ligand. The possibilities that TCNE has decomposed into another cyanocarbon molecule is not remote, given that many

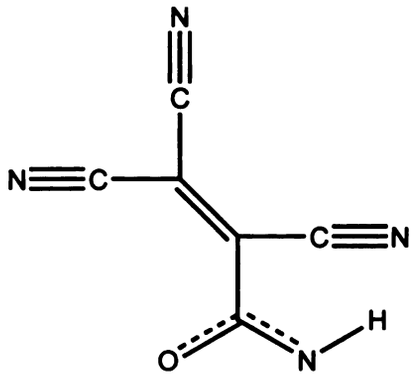
Table 7

Heat (Kcal/mo
Amide H neighbor
N-H bond
C-N bond
C-O bond

Table 7. Comparison of semi-empirical calculations for two 2,3,3-tricyanoacrylamide anion isomers.



(1)



(2)

	(1)	(2)
Heat of Formation (Kcal/mole)	66.02	64.86
Amide H to the nearest neighbor, Å	2.304	2.405
N-H bond length, Å	0.991	0.993
C-N bond length, Å	1.332	1.335
C-O bond length, Å	1.249	1.247

tran

(b)

SM

(i) [

circ

with

P3/

drop

were

be ir

90°,

Wisc

area

a hex

90°,

volur

The e

high

severa

Table

Space
Uniqu
R_{int} / R
RI (wR
GOF

transformations of the molecule have been reported (Figure 10).

(b) Structure solution and refinement of data from a Siemens SMART CCD.

(i) $[Mo_2(O_2CCMe_3)_3(NC)_2CC(CN)CONH)]\cdot 8CH_2Cl_2$ (3)

A new batch of crystals of (3) was grown using the low temperature circulation control bath as described in the experimental section. A crystal with dimensions of 0.70 x 0.70 x 0.40 was mounted on a Nicolet/Siemens P3/V. It was found that the crystal diffracted strongly, but the intensity dropped off rapidly at high angles due to extreme solvent disorder. The data were not solved due to possible twinning as well, although the crystal could be indexed to a trigonal/hexagonal cell with $a \approx b \approx 27$ Å, $c \approx 23$ Å, $\alpha \approx \beta \approx 90°$, $\gamma \approx 120°$ $V \approx 14000$ Å^3. Another crystal of (3) was taken to Siemens in Wisconsin in dry ice and the crystal was mounted on a SMART CCD 1K area detector diffractometer. A pre-data collection routine of 45 frames gave a hexagonal system, with cell parameters of $a \approx b \approx 47$ Å, $c \approx 23$ Å, $\alpha \approx \beta \approx 90°$, $\gamma \approx 120°$ $V \approx 46000$ Å^3. This cell is approximately three times the volume of the cell originally indexed from the data collected on the P3/V. The exact space group was not able to be discerned due to twinning and the high disorder in solvent molecules. The structure was therefore solved in several space groups. Among them, solutions from space groups P-3c1

Table 8. Comparison of refinement results of (3) in different space groups.

Space group	P-3c1 (#147)	P6cc (#184)
Unique data	20021(26480)	17481(25328)
$R_{(int.)}/R_{(sigma)}$	0.048(0.091)	0.130(0.104)
R1(*wR2*)	0.1636(0.375)	0.160(0.363)
GOF	2.12	2.08

Figure 1

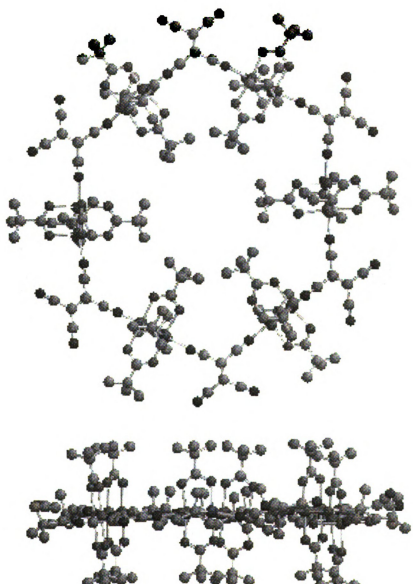


Figure 15. Molybdenum TCNE modeled from the partial P3/V structure.

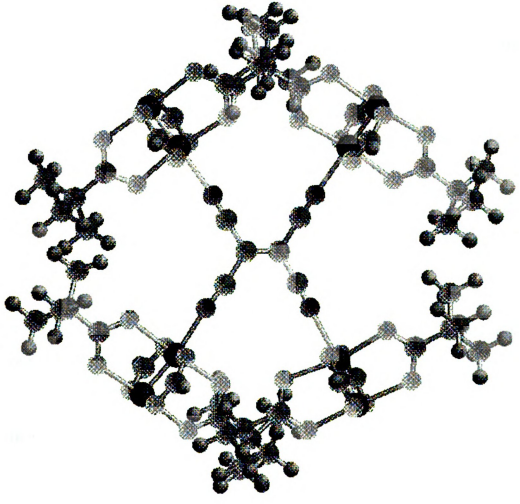


Figure 16. Simulation of dimolybdenum TCNE reaction product (3) indicates an overcrowded hyper μ^4-TCNE bonding mode.

(#147) a

refineme

space gr

(ii) [Mo

In

electrons

axial pos

involved

dangling

This is

involves

making

those wit

19 and a

in Table

Th

which is

compoun

Table 9.

Compd.	
(1)	
(2)	
(3)	
(4)	

(#147) and P6cc (#184) produced the best refinements. A comparison of refinement results is produced in Table 8. A plotting diagram of (3) in P6cc space group is shown in (Figure 17).

(ii) $[Mo_2(O_2CCMe_3)_3(NC)_2C(CN)CCONH)]\bullet 0.5C_6H_6$ (4)

In this structure, it can be easily discovered that the lone pair of electrons on two of the three unperturbed CN groups act as σ donors to the axial positions of another Mo_2 unit. The bond length of the nitrile groups involved in a weak σ-bond with Mo_2 are 1.141(17) Å, 1.138(13) Å while the dangling nitrile group is 1.13(2) Å, slightly shorter than the bonding group. This is easily understood by the fact that the bonding of the CN group involves a degree of π-backbonding which weakens the C≡N bond, thus making it longer. The Mo-Mo bond length of 2.131(2) Å is longer than those without an axial ligand. A plotting diagram of (4) is depicted in Figure 19 and a comparison of Mo-Mo bond lengths for related structures is listed in Table 9.

The bonding in this structure involves a highly bent nitrile group which is unusual. This is the smallest angle within the four dimolybdenum compounds that we have characterized with polynitrile ligands. Other nitrile

Table 9. Structural parameters for a $Mo_2^{II,II}$ core coordinated to non-linear nitriles.

Compd.	Mo-N distance Å	Mo-Mo distance Å	<Mo-N-C (°)	<Mo-Mo-N(°)
(1)	2.630(6)	2.113(1)	147.5(5),163.5(5)	175.50(13)
(2)	2.531(8)	2.127(2)	140.1(6)	166.6(2)
(3)	2.54(7)	2.142(13)	155.8(59)	174.1(16)
(4)	2.559(13)	2.131(2)	122.1(12)	168.7(3)

Table 10. Selected bond distances (Å) and bond angles (°) for $\{[Mo_2(O_2CCMe_3)_3(NC)_2C(CN)CCONH)]\bullet 8CH_2Cl_2\}_\infty$ (3).

Bond Distances

A	B	A-B (Å)	A	B	A-B (Å)
Mo1	Mo2	2.14(1)	Mo1	N1	2.54(7)
Mo1	N7	1.99(7)	Mo2	O3	2.03(9)
Mo1	O4	2.00(10)	Mo2	O2	2.06(6)
Mo1	O1	2.12(6)	Mo2	O5	2.12(8)
Mo1	O6	2.16(7)	Mo2	O7	2.16(7)
Mo2	N6	2.53(8)	O10	C5	1.45(10)
N1	C1	1.23(11)	C1	C2	1.28(14)
N2	C3	1.11(12)	C2	C3	1.59(14)
N3	C5	1.32(10)	C2	C4	1.53(15)
N4	C6	1.13(14)	C4	C5	1.35(13)

Table 1

A
Mo2
O2
O3
O5
Mo1
N7
O4
Mo2
N7
O4
O3
O5

Table 11. (Cont'd)

Bond Angles

A	B	C	A-B-C (°)	A	B	C	A-B-C (°)
Mo2	Mo1	N1	174.1(16)	C1	N1	Mo1	155.8(59)
O2	Mo2	Mo1	92.0(18)	C2	C1	N1	165.1(93)
O3	Mo2	Mo1	89.4(27)	Mo3	N4	C6	158.0(90)
O5	Mo2	Mo1	89.7(22)	N4	C6	C4	157.4(100)
Mo1	Mo2	O7	91.7(19)	N2	C3	C2	173.9(100)
N7	Mo1	Mo2	92.9(20)	C1	C2	C3	116.8(90)
O4	Mo1	Mo2	93.0(29)	C3	C2	C4	111.1(84)
Mo2	Mo1	O6	90.1(17)	C1	C2	C4	129.8(98)
N7	Mo1	O1	174.3(26)	C5	C4	C2	114.4(89)
O4	Mo1	O6	174.1(34)	C5	C4	C6	124.6(96)
O3	Mo2	O2	177.6(34)	N3	C5	C4	124.6(80)
O5	Mo2	O7	173.4(30)	C4	C5	O10	117.8(75)

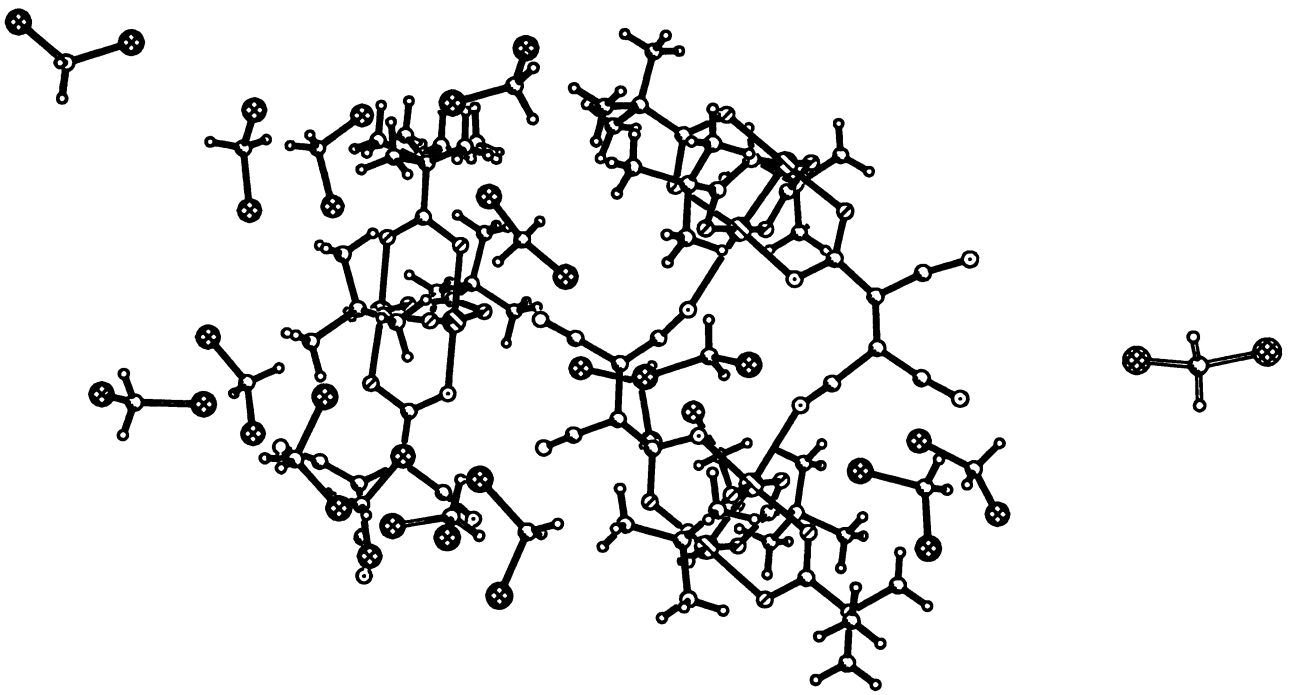
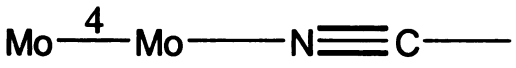
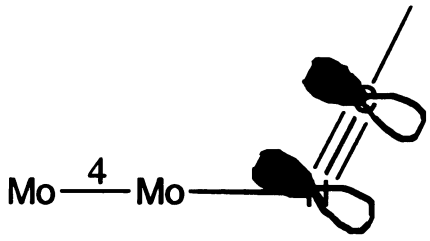


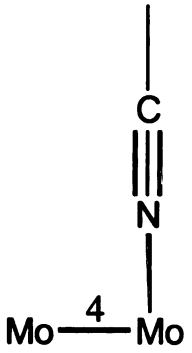
Figure 17. Plot of $[Mo_2(O_2CCMe_3)_3((NC)_2C(CN)CCONH)\bullet 8CH_2Cl_2]$ (3) in space group P6cc .

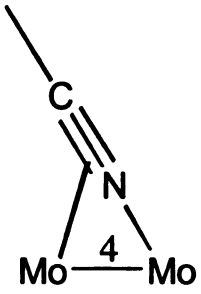


Nitrile bonding mode in (3)



Nitrile bonding mode in (4)





Other nitrile bonding modes with $Mo_2^{II, II}$ cores

Figure 18. Nitrile bonding modes with a $Mo_2^{II, II}$ core.

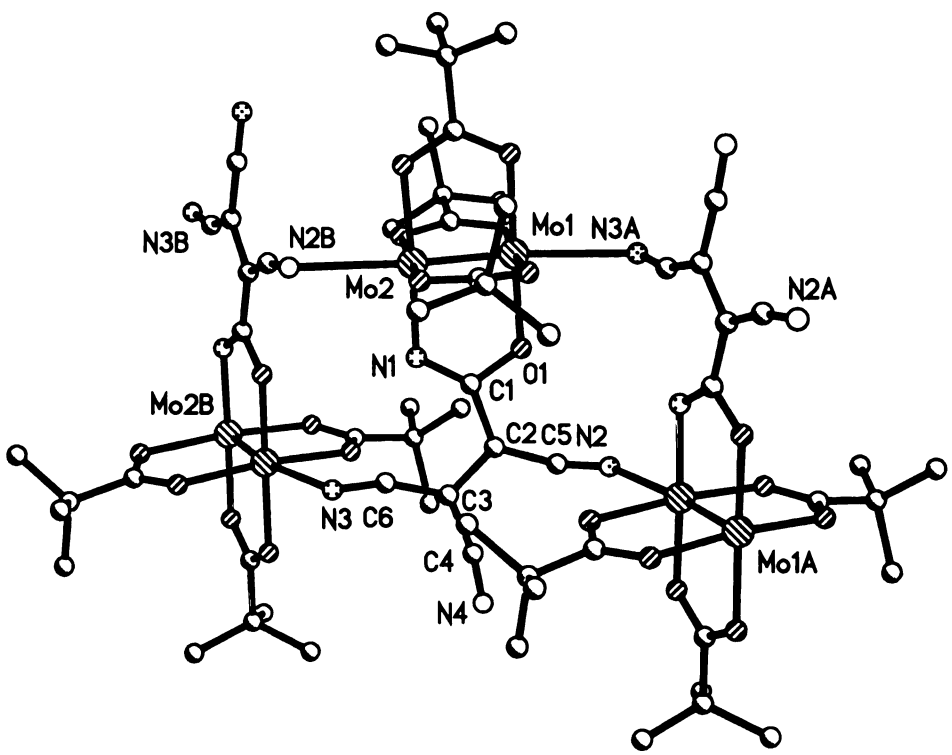


Figure 19. Pluto representation of (4) clearly shows that the CN groups bonded to the Mo_2 unit are in an unusual bent mode.

ligand bonding modes involving axial interactions exhibit a tilt such as the one shown in Figure 18. The Mo-N distance of 2.53 Å is comparable to other Mo-N bond lengths involving Mo-Mo bond. The structure shows disorder in the transformed TCNE (amide) group.

(4) Structural features of $[Re_2Cl_4(dppm)_2]_2TCNQ\cdot 10THF$(5) and $[Re_2Cl_4(dppm)_2]_2DMDCNQI\cdot 10THF$ (6).

Due to librational disorder, the –CN bond length of the nitrile bonded directly to the Re-Re core cannot accurately be refined. Normal –CN bond lengths are in the range of 1.10 – 1.15 Å. The CN bond length in compound (5) is 1.05 Å. An electron density map clearly shows that the CN bond should be longer, which we attribute to a phenomenon called librational disorder.[40] This typically occurs when a light atom involved in a multiple bond which is attached to a heavy atom, or ,in general, when the normal spherical model for electron density is not correct. Figure 20 shows the electron density map of the nitrile group involved in the coordination bonding with the refined position of the -CN group in the absence of a libration correction. Refinement was carried out first without bond length constraints, then with soft constraints to match the CN bond length indicated by the E-map. A comparison of the refined bond length with bond length constraints, the distance between peaks centers of the –CN group in the electron density map, and the result of refinement with librational disorder correction are listed in Table 12.

Table 12. Librational disorder refinement of the CN bond length in (5).

Refined bond length	length from E-map	libration correction
1.05	1.105	1.05

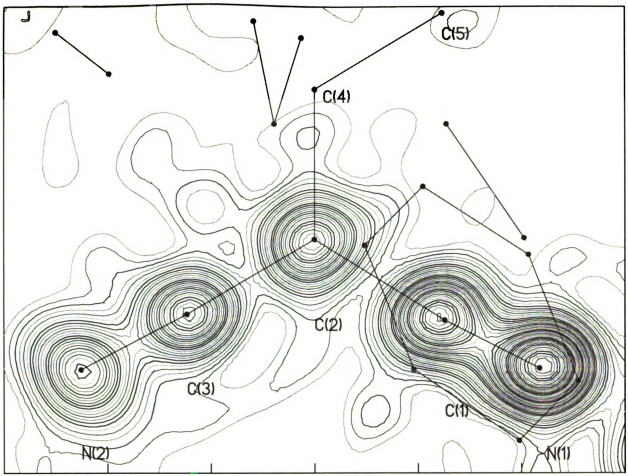


Figure 20. Electron density map of nitrile region in (5).

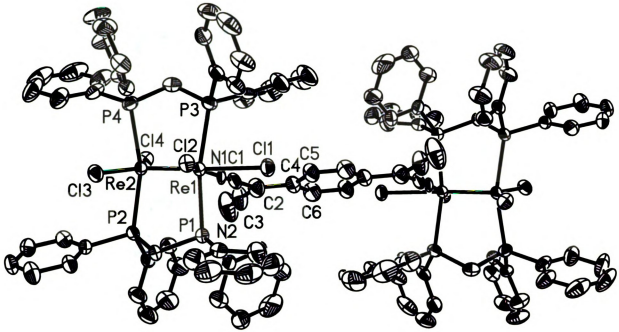


Figure 21. Thermal ellipsoid representation of $Re_2(dppm)_2TCNQ$ (5).

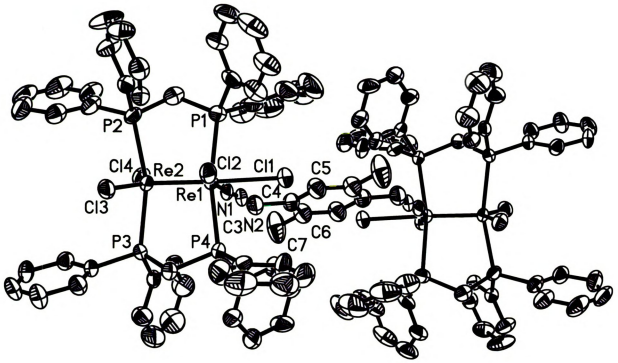


Figure 22. Thermal ellipsoid representation of $Re_2(dppm)_2DMDCNQI$ (6).

C

ris

sy

D_4

ex

a l

ho

onl

ene

has

of (

TC

tem

inde

com

are

two

TCN

first

the

for t

dihe

core

as Re

$[Re_2]$

C. Charge Transfer and Infrared Spectral Data.

Neutral TCNQ shows only one CN stretching band but $TCNQ^{-1}$ gives rise to an A_g and a B_u mode when interactions are present that lower the symmetry. Also when the molecule engages in a trans-μ bonding mode, the D_{4h} symmetry is broken and there are two modes. The dangling CN group exhibits a higher frequency, while the σ-bonding CN group typically shows a lower frequency due to backbonding from the metal. It should be noted, however, that when TCNQ bonds to metal centers with no backbonding and only σ-donation, the stretching frequency of the CN bond shifts to higher energies due to electron donation from the lone pair of electrons on N which has antibonding character with respect to the C≡N bond. The IR spectrum of (5) shows that the TCNQ moiety in the rhenium structure is not a typical $TCNQ^{(1-)}$ anion radical, but the SQUID measurement shows that, at room temperature the moment is 3.2 B.M., After subtracting a temperature independent paramagnetic (TIP) contribution, the moment is about 2.3 B.M. comparable to the value of 2.47 for two non-interacting S = 1/2 spins. There are two possibilities for this scenario: (1) a doubly reduced $TCNQ^{2-}$ linking two one-electron oxidized Re_2^{5+} units and (2) a one electron reduced $TCNQ^{-1\bullet}$ anion radical linking mixed valence Re_2^{5+} and Re_2^{4+} species. In the first case, the unpaired spins in the dirhenium centers would be isolated by the diamagnetic $TCNQ^{2-}$ bridge. If this is true, then the average oxidation for the Re_2 core is +5, this may be reasonable considering the fact that the dihedral angle of the P-Re—Re-P is about 14° large than the 3° in the Re_2^{5+} core found in $Re_2Cl_5(dppm)_2$, but smaller than the 30° of a Re_2^{4+} core, such as $Re_2(dppm)_2Cl_3(CNR)_2^+$. It could be considered as a $[Re_2](+)$-TCNQ(1-)-$[Re_2](0)$ and $[Re_2](+)$-TCNQ(2-)-$[Re_2](+)$equilibrium, in which the

TCNQ(1-) bridge provides an AF interaction pathway, while TCNQ(2-) with a higher LUMO would most likely isolate the two Re_2^{5+} units.

4. Summary

Metal-metal bonded building blocks are capable of being used to build extended arrays with polynitrile ligands which provide a different architecture than products with 3d transition metal cations. Such structural possibilities provide a different approach for building supramolecular structures as compared to the more strict limitations of 3d transition metals. In addition, their rich redox chemistry makes them good candidates for the design of electronic and optical devices for energy storage and conversion.

References

1. Cotton, F. A.; Walton, R. A. *Multiple Bonds between Metal Atoms; 2nd ed.* **1993**; Oxford University Press, New York.

2. Stephenson, T. A.; Wilkinson G. J. *Inorg. Nucl. Chem.* **1966**, *28*, 2285

3. Cotton, F. A.; Pedersen, E. *Inorg. Chem.* **1975**, *14*, 388

4. Telser, J.; Drago R. S. *Inorg. Chem.* **1984**, *23*, 3114

5. Cotton, F. A.; Kim, Y.; Ren, T. *Polyhedron* **1993**, 12 607

6. Cotton, F. A.; Kim, Y.; Ren, T. *Inorg. Chem.* **1992**, *31*, 2723.

7. Cotton, F. A.; Kim, Y.; Ren, T., *Inorg. Chem.* **1992**, *31*, 2608.

8. Li, D.-Q.; Huckett, S. C.; Frankcom, T.; Paffett, M. T.; Farr, J. D.; Hawley, M. E.; Gottesfeld, S.; Thompson, J. D.; Burns, C. J.; and Swanson, B. I. in "Supramolecular Architecture : Synthetic Comtrol in Thin Films and Solids" *ACS Symp. Ser. 499*, Ed., Bein, T. *American Chemistry Society,* **1992**, Ch. 4, pp33-45

9. McCarley, R. E.; Templeton, J. L.; Clburn, T. J.; Katovic, V. and Hoxmeier, R. J. in "*Inorganic Compounds with Unusual Properties*". *Adv. Chem.Ser.* **1975**, *150,* 318

10. Mandon, D.; Giraudon, J. M.; Toupet, L.; Sala-pala, J.; Guerchais, J. E. *J. Am. Chem. Soc.* **1987**, *109*, 3490

11. Giraudon, J. M.; Sala-Pal, J.; Guerchais, J. E.; and Toupet, L. *Inorg. Chem.*, **1991**, *30*, 891

12. Felthouse, T. R.; Dong, T.-Y.; Hendrickson, D. N.; Shieh, H.-S. and Thompson, M. *J. Am. Chem. Soc* **1986**, *108*, 8201

13. Cogne A.; Grand A.; Rey P.; and Subra R. *J. Am. Chem. Soc.* **1989**, *111*, 3230

14. Handa, M.; Sono, H.; Kasamatsu, K.; Kasuga, K.; Mikuriya, M.; Ikenoue, S. *Chem. Lett.* **1992**, 453.

15. TCNQ = 7,7',8,8'-Tetracyano-quinodimethane, TCNE = tetracyanoethylene, DCNQI = *N,N'*-dicyanoquinonediimine, DM-DCNQI = 2,5-dimethyl-*N,N'*-dicyanoquinone-diimine.

16. (a) Cotton, F. A.; Kim, Y. *J. Am. Chem. Soc.* **1993**, *115*, 8511. (b) Cotton, F. A.; Kim,Y.; Lu, J. *Inorg. Chim. Acta* **1994**, *221*, 1.

17. (a) Huckett, S. C.; Arrington, C. A.; Burns, C. J.; Clark, D. L.; Swanson, B. I. *Synt. Met.* **1991**, *41-43*, 2769. (b) Li, D.; Huckett, S. C.; Frankcom, T.; Paffett, M. T.; Farr, J. D.; Hawley, M. E.; Gottesfeld, S.; Thompson, J. D.; Burns, C. J.; Swanson, B. I. in *Supramolecular Architecture: Synthetic Control in Thin Films and Solids ACS Symp. Ser. 499*, (Ed: Bein, T.) *American Chemical Society*, **1992**, Ch. 4, 33.

18. Stephenson, T. A.; Bannister, C.; Wilkinson, G., *J. Chem. Soc.*, **1964**, 2538.

19. Cotton, F. A. and Norman, J. G. *J. Coord. Chem.*, **1971**, *1*, 161.

20. Aumüller, A.; Hünig, S. *Liebigs Ann. Chem.* **1986**, 142.

21. Barder, T. J.; Cotton, F. A.; Dunbar, K. R.; Powell, G. L.; Schwotzer, W. and Walton, R. A. *Inorg. Chem.*, **1985**, *24*, 2550.

22. SHELXTL 5.0 suites (XPREP, XS, XL and XP) Structure solution and refinement package, Siemens Energy & Automation, Inc. Analytical Instrumentation.

23. **DIRDIF**84 – Beurskens, P.T. – Direct Methods for Difference Structures; Technical Report **1984**/1, Crystallography Laboratory, Toernooiveld, 6525 Ed Nijmegen, Netherlands.

24. **TEXSAN**-TEXRAY Structure Analysis Package, Molecular Structure

Corporation, 1985

25. **SADABS** – Sheldrick, G. M. – Area Detector Absorption (and other) Correction Program. **1998**. University of Gttingen, Germany.

26. Manriquez, J. M.; Yee, G. T.; McLean, S.; Epstein, A. J.; Miller, J. S. *Science* **1991**, *252*, 1415

27. Prince, M. and Hornyak, J. *Chem. Comm.* **1966**, *14*, 455.

28. Cotton, F. A. and Kim, Y. *J. Am. Chem. Soc.* **1993**, *115*, 8511.

29. Cotton, F. A. and Haefner S., Personal communication.

30. Cotton, F. A. and Norman, J. G. Jr., *J. Coord. Chem.*, **1971**, *1*, 161.

31. Handa, M.; Yamada, K.; Nakao, T.; Kasuga, K.; Mikuriya, M. and Kotera, T., *Chem. Lett.*, **1993**, 1969.

32. Cotton, F. A.; Feng, X., Kibala, P. and Matusz, *J* M. *Am. Chem. Soc.*, **1988**, *110*, 2807.

33. Buhro, W. E.; Chisholm, M. H. J.; Martin, D.; Huffman, J. C.; Folting, K. and Sterib, W. E. *J. Am. Chem. Soc.*, **1989**, *111*, 8149.

34. Cotton, F, A.; Kim, Y.; Lu, J., *Inorg. Chim. Acta* **1994**, *221*, 1.

35. SPARTAN V4.0, Wavefunction, Inc

36. (a) Aumüller, A.; Erk, P.; Klebe, G.; Hünig, S.; von Schütz, J. U.; and Werner, H.-P. *Angew. Chem. Int. Ed. Engl.* **1986**, *25*, 740. (b) Oshio, H. *Inorg. Chem.* **1993**, *32*, 4123. (c) Kato, R.; Kobayashi, H.; Kobayashi, A. *J. Am. Chem. Soc.*, **1989**, *111*, 5224. (d) M. A. S. Aquino, F. L. Lee, E. J. Gabe, C. Bensimon, J. E. Greedan, and R. J. Crutchley, J. Am. Chem. Soc., 1992, 114, 5130.

37. Aumüller, A.; Erk, P.; Hünig, S.; Hadicke, K.; Peters, H.; von Schütz, J. U. *Chem. Ber.* **1991,** *124,* 2001.

38. Cotton, F. A. and Norman, J. G. Jr. *J. Coord. Chem.*, **1971,** *1,* 161.

39. Handa, M.; Yamada, K.; Nakao, T.; Kasuga, K.; Mikuriya, M. and Kotera, T. *Chem. Lett.*, **1993,** 1969.

40. Braga, D. and Koetzle, T. F. *Chem. Commun.*, **1987,** 144.

CHAPTER III

PREPARATION, STRUCTURAL CHARACTERIZATION AND PROPERTIES OF BINARY TRANSITION METAL TCNQ MATERIALS

1. Introduction

The use of soluble transition metal coordination complexes as precursors to materials is a rapidly expanding area of inorganic chemistry, rich in structural diversity and potential applications.[1-4] Topological arguments that take into consideration the geometrical preferences of the metal and ligand building blocks have allowed chemists to design new molecular solids, including novel porous,[2] magnetic[3] and conducting[5] materials. Among the compounds in the latter category are charge-transfer solids composed of metal complexes and the radical forms of the organonitrile acceptors depicted in Figure 23.[4,5] The most well-investigated of these hybrid inorganic/organic materials are the binary, mixed-valence compounds $Cu(2,5\text{-}R_2\text{-}DCNQI)_2$(DCNQI = dicyanoquinodiimine) (Figure 23).[5,6] These metallopolymers exhibit unusually high, anisotropic conductivities that are attributed, not only to the columns of stacked DCNQI radicals formed by interpenetrating networks, but to the interaction of the *d* orbitals of the metal with the *p* orbitals of the diimine bridge.

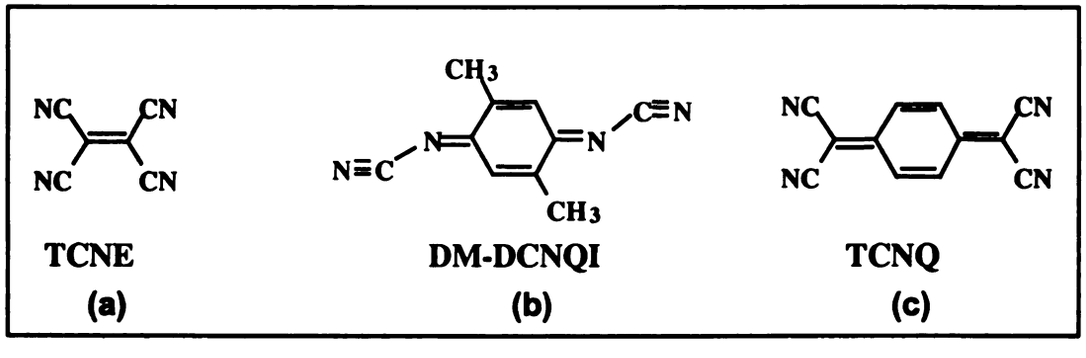


Figure 23. Organonitrile acceptors that behave as ligands in their reduced forms.

In considering the remarkable properties exhibited by copper DCNQI polymers, we were reminded of a class of intriguing metal complexes of 7,7-8,8-tetracyanoquinodimethane (TCNQ) first reported in 1962. From the perspective of metal complexation, the main difference between DCNQI and TCNQ is that TCNQ is capable of behaving as a tetradentate as well as a bidentate bridging ligand which allows it to form products with both 1:1 and 1:2 metal/TCNQ ratios.[4,6,7] The 1:1 materials of Ag and Cu are the subject of intense interest due to the fact that crystalline films of these compounds undergo electric-field induced bi-stable switching under certain conditions.[8-22] In spite of extensive efforts to understand these materials, however, this phenomenon continues to be the source of debate in the literature. One of the crucial issues to be resolved is the source of conflicting data regarding the electrical behavior of Cu(TCNQ). Independent findings of several groups suggest that the physical appearance of the crystalline films is highly dependent on film preparation conditions.[15,19,20-22]

In light of the high interest in such materials, we find it to be curious that no X-ray data for Cu(TCNQ) or related binary materials with 3d elements have been determined. In fact, no full-scale investigation of binary metal compounds of TCNQ has been undertaken, although materials formulated as $M(TCNQ)_2(H_2O)_2$ were recognized as being easily prepared, tractable solids as early as 1962.[6,23] As part of a comprehensive investigation of the magnetic and conducting properties of M/TCNQ materials and in an effort to establish structural/property relationships, we have prepared a variety of crystalline phases of general formulae M(TCNQ) and $M(TCNQ)_2$. One synthetic strategy to such materials is the combination of metal cations with organic acceptor anions such as $TCNQ^{\cdot-}$ (7,7,8,8-tetracyanoquinodimethane),[5] $TCNE^{\cdot-}$ (tetracyanoethylene)[6] and $DCNQI^{\cdot-}$

(N,N'-dicyanoquinonediimine).[7] Unfortunately, polymeric materials of this type are notoriously difficult to crystallize, a fact that has hampered research efforts aimed at structure/property correlations. We have found, however, that with the proper selection of starting materials and solvents, it is possible to prepare crystalline, neutral framework compounds with metal ions bridged only by ligands derived from $TCNQ^{-1}$. During the course of these studies, we became aware of the role of the solvent (*e.g.*, methanol, water, acetonitrile) in determining the structures and therefore physical properties of metal/TCNQ materials.

In this chapter the syntheses and characterization of TCNQ compounds with the metal ions Mn(II), Ni(II), Zn(II) and Cu(I) are discribed. Representative single-crystal X-ray structures, powder X-ray data, infrared spectral properties and properties are discussed in light of the TCNQ packing motif that is adopted in the solid-state. The structures of $[^{n}Bu_4N][TCNQ]$ and $[^{n}Bu_4N][TCNQF_4]$ as well as the salt $[Ni(DMSO)_6][TCNQ]_3$ (all with outersphere $TCNQ^{-1}$ anions) are also presented as a comparison to the compounds in which $TCNQ^{-1}$ acts as a ligand. Structural studies on $Ni(TCNQ)_2(H_2O)$, which bears a strong resemblance to other 3d metal TCNQ hydrate compounds such as $Mn(TCNQ)_2(H_2O)_2$, is also discussed.

2. Experimental Section

A. Synthesis

(1) Starting materials and reaction procedures.

All reactions were carried out under an argon atmosphere by the use of standard Schlenk-line techniques. Methanol was pre-dried over 4 Å molecular sieves and freshly distilled under a nitrogen atmosphere from

$Mg(OCH_3)_2$. Acetonitrile was dried over 3 Å molecular sieves and freshly distilled under an atmosphere of N_2 prior to use. TCNQ was purchased from TCI Chemical Company. The salt $[^nBu_4N][TCNQ]$[23a] was prepared by metathesis of LiTCNQ with $^nBu_4NI$ in boiling water followed by recrystallization from CH_2Cl_2.[24a,b] Crystalline LiTCNQ was prepared by combining TCNQ and 3 equivalents of LiI in hot acetonitrile and allowing the mixture to cool for 12 hours. MnX_2 (X = Cl, Br) and CuI starting materials were obtained from commercial sources and used without further purification. $[Cu(MeCN)_4][BF_4]$,[25] $[Mn(MeCN)_4][BF_4]_2$ and $Ni(MeCN)_4(BF_4)_2$[26] were prepared as described in the literature.

(2) Bulk syntheses of Cu(TCNQ) phase I (7).

(a) Method A.

CuI (0.95 g, 5 mmol) was added to 150 mL of a hot acetonitrile solution of TCNQ and stirred for 3 minutes.[23a] The dark blue microcrystalline product that formed was separated from a brown solution by filtration, washed with copious amounts of acetonitrile and dried *in vacuo*; yield 1.22 g, 91%. *Anal.* Calcd for $C_{12}H_4N_4Cu$: C, 53.83; H, 1.51; N, 20.93. Found: C, 53.46; H, 1.39; N, 20.57. Characteristic IR data (Nujol mull, KBr plates, cm^{-1}): ν(CN), 2199s,br; 2172sh; δ(C-H) 825s.

(b) Method B.

A quantity of $[^nBu_4N][TCNQ]$ (0.500 g, 1.12 mmol) was dissolved in 50 mL of acetonitrile to give a green solution which was added to a solution of $[Cu(MeCN)_4][BF_4]$ (0.352 g, 1.12 mmol) dissolved in 20 mL of acetonitrile. Upon mixing, a color change to dark blue occurred with the deposition of a dark blue microcrystalline solid. The solid was collected by filtration, washed with acetonitrile and dried *in vacuo* to give 0.265 g (88% yield) of a dark blue solid whose X-ray pattern is identical to the product

obtained in method A.

(3) Bulk synthesis of Cu(TCNQ) phase II (8).

A quantity of acetonitrile (20 mL) was added to 0.300 g of phase I. The resulting suspension and light green solution was stirred at room temperature for 4 days after which time the solvent was evaporated to yield a dark blue solid. If the solution is refluxed for 3 hours, the conversion process occurs much faster (within 30 minutes). Both methods lead to virtually quantitative conversion of phase I to phase II as judged by X-ray powder diffraction and infrared spectroscopy. *Anal.* Calcd for $C_{12}H_4N_4Cu$: C, 53.83; H, 1.51; N, 20.93. Found: C, 53.68; H, 1.33; N, 20.85. Characteristic IR data (Nujol mull, KBr plates, cm^{-1}): ν(CN), 2211s; 2172s; δ(C-H) 825s.

(4) Thin films of Cu(TCNQ) .

Cu(TCNQ) thin films were prepared by a method similar to those described in the literature.[8] Rectangular pieces of copper foil were cleaned mechanically and then chemically with a dilute H_2SO_4 solution and washed with water followed by acetone in an N_2 atmosphere. The dipping experiments were conducted in an N_2 purged glove bag in a two-compartment, fritted reaction vessel that contained a saturated CH_3CN solution of TCNQ. To avoid contaminating the Cu(TCNQ) films with solid TCNQ, the copper pieces were placed in a glass thimble with a coarse glass frit at one end and carefully arranged such that copper surfaces did not touch. The thimble was lowered into the TCNQ saturated solution and the reaction vessel was sealed with a ground glass stopper. Upon contact with the solution, black-purple films were observed to appear on the exposed copper surfaces. At periodic, timed intervals the reaction vessel was opened to retrieve one of the copper pieces which was then washed with acetonitrile,

dried and placed in a vial under anaerobic conditions for later analysis.

(5) Bulk synthesis of $Mn(TCNQ)_2(MeOH)_2$ (9).

A MeOH solution (20 mL) of [^{n}Bu$_4$N][TCNQ] (0.447 g, 1.00 mmol) was slowly added to a MeOH solution (10 mL) of $[Mn(MeCN)_4][BF_4]_2$ (0.197 g, 0.5 mmol). The resulting reaction solution was stirred for 20 min to give a blue precipitate that was collected by filtration, washed with methanol followed by diethyl ether and dried *in vacuo*. Yield: 0.187 g, 71%. Analytical data: Mn (x = 2) Calcd for $C_{26}H_{16}MnN_8O_2$: C, 59.21; H, 3.06; N, 21.25. Found: C, 59.53; H, 2.41; N, 21.71. Thermogravimetric measurements indicate that the samples are stable with approximately two equivalents of coordinated MeOH.

(6) Bulk synthesis of $Mn(TCNQ)_2(H_2O)_2$ (10).

An aqueous solution (20 mL) of LiTCNQ (0.211 g, 1.0 mmol) was added to an aqueous solution (20 mL) of $MnCl_2$ (0.063 g, 0.5 mmol), and stirred at room temperature for 30 min. The resulting blue precipitate was collected by filtration, washed with water followed by ethanol and diethyl ether, and finally dried *in vacuo*. Yield: 0.242 g, 94%. Elemental analyses: Calcd for $C_{24}H_{12}MnN_8O_2$: C, 57.73; H, 2.40; N, 22.44. Found: C, 57.76; H, 2.20; N, 22.47.

B. Single Crystal Growth.

(1) Cu(TCNQ) phase I and phase II (7), (8).

Tiny crystals of both Cu(TCNQ) phases were grown by a technique that involves the use of a three-compartment fritted cell. In the outer two compartments, small Soxhlet thimbles containing the starting materials CuI and TCNQ were suspended on a wire and immersed in the solution (Figure 24). The entire cell was placed in a water bath and gently heated to 60 °C

for 3-5 days to expedite mixing of the reactants in the center compartment. Within days, the solution gradually turned green signifying the production of $TCNQ^{-1}$, and tiny needles, admixed with platelets, began to form in the middle compartment. The needles (phase I) were harvested immediately because they eventually re-dissolve to produce crystals of phase II (the platelet habit).

(2) $[Mn(TCNQ)(TCNQ\text{-}TCNQ)_{0.5}(MeOH)_2]_\infty$ (9).

Purple needles of $[Mn(TCNQ)(TCNQ\text{-}TCNQ)_{0.5}(MeOH)_2]_\infty$ (9) were grown by slow diffusion of a methanolic solution of $[Mn(MeCN)_4][BF_4]_2$ into a mixture of MeCN/MeOH (2:1) containing $[^nBu_4N][TCNQ]$ in a 3 mm diameter sealed pyrex tube.

(3) $[Mn(TCNQ)_2(H_2O)_2]_\infty$ (10).

Red-purple monoclinic prisms of $[Mn(TCNQ)_2(H_2O)_2]_\infty$ (10) were grown by slow diffusion of aqueous solutions of $MnBr_2$ and LiTCNQ in 3 mm diameter sealed pyrex tube.

(4) $[^nBu_4N][TCNQ]$ (11).

Purple prismatic crystals of $[^nBu_4N][TCNQ]$ were grown by slow evaporation of a saturated methanol solution of $[^nBu_4N][TCNQ]$.

(5) $[^nBu_4N][TCNQF_4]$ (12).

Blue green platelet-shaped crystals of $[^nBu_4][TCNQF_4]$ were grown by slow diffusion of water into a methanol solution of $[^nBu_4N][TCNQF_4]$.

(6) $[Zn(H_2O)_4(\eta^1\text{-}TCNQ)_2\bullet TCNQ\bullet 2MeCN]_\infty$ (13).

Purple prisms of $[Zn(H_2O)_4(\eta^1\text{-}TCNQ)_2\bullet TCNQ\bullet 2MeCN]_\infty$ were grown by a slow reaction of Zn metal pellets with a 1:1 acetonitrile/water solution of TCNQ.

(7) $[Ni(DMSO)_6][TCNQ]_3$ (14).

Purple platelets of $[Ni(DMSO)_6][TCNQ]_3$ were grown by the

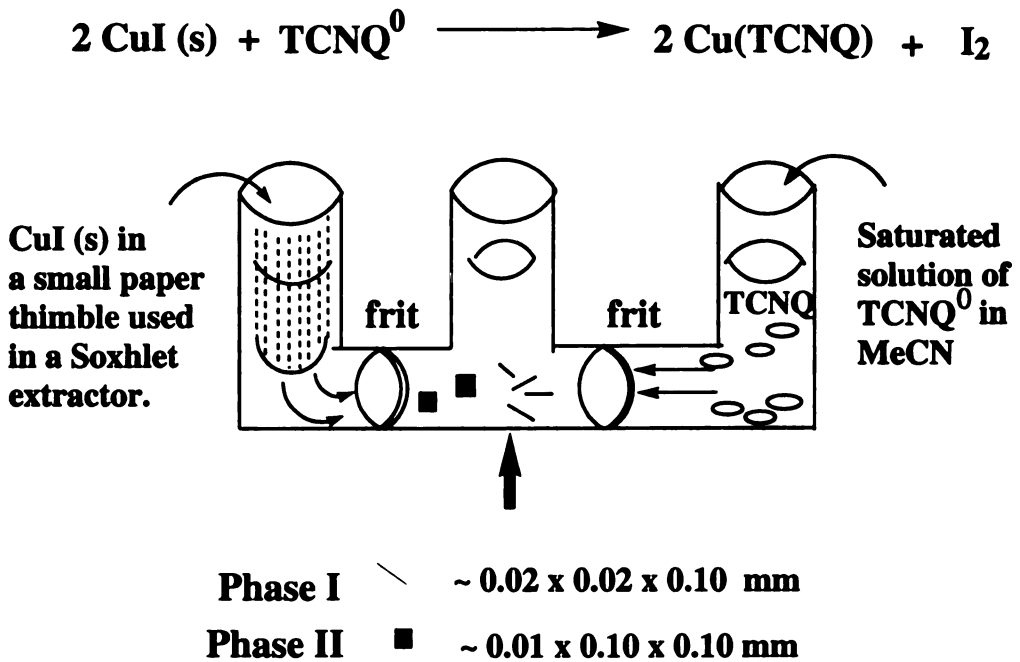


Figure 24. Crystal growing setup for two Cu(TCNQ) phases.

diffusion of acetonitrile into a 1:1 DMSO/H_2O solution of $Ni(TCNQ)_2$. The solid $Ni(TCNQ)_2$ was prepared from the reaction of $[Ni(MeCN)_6][BF_4]_2$ with 2 equivalents of $[^nBu_4N][TCNQ]$.

(8) $[Ni(TCNQ)_2(H_2O)]_\infty$ (15).

Purple prismatic crystals of $[Ni(TCNQ)_2(H_2O)]_\infty$ were grown by layering an aqueous solution of $[Ni(MeCN)_6][BF_4]_2$ with an aqueous solution of LiTCNQ. A small amount of acetonitrile was used as a buffer solution to separate the reactant layers.

C. Physical Measurements.

Single crystal X-ray data were obtained on a Siemens (Bruker) SMART 1K CCD area detector instrument or a Nicolet P3/V diffractometer. Both are equipped with sealed tube Mo anodes. Powder X-ray data were collected using a Rigaku RU200B X-ray powder diffractometer with Cu Kα radiation. The variable temperature magnetic susceptibility data were collected in the range 5-300 K using a Quantum Design, Model MPMS-5 SQUID magnetometer housed in the Physics & Astronomy Department at Michigan State University. Infrared spectra were recorded in Nujol on KBr plates using a Nicolet IR/42 FT-IR spectrometer. X-ray Photoelectron Spectral (XPS) data were obtained on a PHI 5400 instrument with a Mg source in the Composite Materials and Structures Center at Michigan State University. Thermogravimetric analyses were performed between 25-1000 °C on a SHIMADZU, TGA-50. Scanning electron microscopy measurements were performed on a JEOL 6400V instrument with a LaB_6 gun housed in the Center for Electron Optics at Michigan State University.

(1) X-ray crystallography.

(a) Cu(TCNQ) phase I (7).

A dark purple needle crystal of dimensions $0.25 \times 0.02 \times 0.02$ mm was mounted on the end of a glass fiber with silicone grease. A hemisphere of data was collected at -100(2) °C on a Siemens SMART 1K CCD area detector diffractometer by Dr. Victor Young at the University of Minnesota. The frame scan-width was 0.3 in ω, and the exposure time was 60 sec/frame. No cell information was available before data collection due to the weak diffraction. Post data collection processing results suggested that the crystal belongs to the tetragonal 4/m Laue group. The data were integrated with the cell parameters $a = b = 11.266(2)$ Å, $c = 3.8878(8)$ Å, $\alpha = \beta = \gamma = 90°$, $V = 493.47(17)$ Å^3. After numerous failures to solve the structure in the 4/m or mmm crystal symmetry group, the structure was ultimately solved in the lower symmetry monoclinic space group *P*n with the cell parameters $a = 3.8878(8)$ Å, $b = 11.266(2)$ Å, $c = 11.266(2)$ Å, $\beta = 90.00(3)°$. The structural model was refined as disordered and pseudo-merohedrally twinned. The 3x3 twinning matrix [1 0 0, 0 0 1, 0 -1 0] was used to model the pseudo 4-fold rotation. A summary of data collection and refinement results is listed in Table 13.

(b) Cu(TCNQ) phase II (8).

A tiny, square platelet crystal of dimensions $0.13 \times 0.13 \times 0.01$ mm was mounted on the tip of a glass fiber with the use of silicone grease. A full sphere of data was collected at -100±(2) °C on a Bruker (Siemens) SMART 1K CCD area detector diffractometer. Due to the small size of the crystal and twinning problems, cell parameters were not refined before data collection. Data were collected in 0.3° ω-scans with an exposure time of 90 sec/frame (total time 69 hours). Strong reflections (253) were extracted with

Table 13. Summary of key crystallographic parameters for Cu(TCNQ) phase I (7) and phase II (8).

Compound Name	(7)	(8)
Formula	$CuN_4C_{12}H_4$	$CuN_4C_{12}H_4$
Morphology	Needle	Square Platelet
Crystal size (mm^3)	$0.25 \times 0.02 \times 0.02$	$0.13 \times 0.13 \times 0.01$
Crystal system	Monoclinic	Monoclinic
Space group	*P* n	*P* 2/n
a, Å	3.8878(8)	5.3337(8)
b, Å	11.266(2)	5.3312(8)
c, Å	11.266(2)	18.875(3)
α, deg	90	90
β, deg	90.00(3)	94.036(3)
γ, deg	90	90
V, $Å^3$	493.5(2)	535.38(14)
Z	2	2
T, K	173	173
Radiation [a]	Mo Kα	Mo Kα
ρcalc, g/cm^3	1.802	1.661
μ, mm^{-1}	2.188	2.017
Collected/ unique data	1995/1111	4456/955
Indexing method	SMART	TWINDX
Solution and refinement method	Pseudo merohedral twinning and disordered, isotropically refined.	Quadruplet rotational twinning, anisotropically refined.
R1(*wR2*)[c]	0.234(0.485)	0.159(0.335)
GOF[d]	2.576	1.060

[a]Graphite monochromated. [b]$I > 2\sigma(I)$. [c]$R1 = \Sigma||F_o|-|F_c||/\Sigma|F_o|$; $wR2 = [\Sigma[w(F_o^2-F_c^2)^2]/\Sigma[w(F_o^2)^2]]^{1/2}$. [d]Goodnees-of Fit (*GOF*) = S = $[\Sigma[w(F_o^2-F_c^2)^2]/(n-p)]^{1/2}$, n is the total number of reflections and p is the total parameters refined.

the SMART index routine, but this failed to give a reasonable cell. The indexing solution was obtained by the use of programs in the TWINNING package written by R. Sparks.[27] (The indexing process is discussed in detail in Chapter V). Four monoclinic cells were indexed with a = 5.3337(8) Å, b = 5.3312(8) Å, c = 18.875(3) Å, β = 94.036(3)° and V = 535.38(14) Å^3. The twinning law matrix [0 –1 0, 1 0 0, 0.25 0.25 1] transforms the component A to the other three components by successive rotations along (0 0 1) axis. Because the TWHKL module in the TWINNING package only handles two component twins, a revised version of TWHKL was used to process the four component twin data. The refinement is not stable because of the severity of the twinning. The data for solving the structure in the space group P2/n were integrated with one component only. The final residuals for this treatment were $R1$= 0.159 and $wR2$= 0.345 for 4456 reflections with $I > 2\sigma(I)$. A summary of data collection parameters is listed in Table 13.

(c) [Mn(TCNQ)(TCNQ-TCNQ)$_{0.5}$(MeOH)$_2$]$_n$ (9).

A long needle crystal of approximate size 0.40 × 0.04 × 0.04 mm was mounted on a glass fiber and secured with silicone grease. A hemisphere of data was collected on a Siemens SMART CCD area detector instrument at -140(1)°C by Dr. D. Powell in University of Wisconsin. (This was prior to the time that Michigan State Univeristy had a CCD instrument). A summary of data collection parameters for the compound is given in Table 9. The data were solved and refined in SHELXTL V.5.0 by full-matrix least-squares on F^2. The original cell and systematic absences suggested an orthorhombic C-centered crystal system, but the structure was ultimately solved as a 33.2/66.8 twin in C2/c (twinning law [1 0 0, 0 1 0, 0 0 –1]). The disordered MeOH group was modeled in two orientations with occupancies of 0.535 (C2M') and 0.465 (C2M"). All non-hydrogen atoms were located and

Table 14. Crystal data and structure refinement parameters for $[Mn(TCNQ\text{-}TCNQ)_{0.5}(TCNQ)(MeOH)_2]_\infty$ (9) and $[Mn(TCNQ)_2(H_2O)_2]_\infty$.(10).

Identification code	(9)	(10)
Empirical formula	$C_{26}H_{16}N_8O_2Mn$	$C_{24}H_{12}MnN_8O_2$
Formula weight	527.41	499.36
Temperature	133(2) K	133(2) K
Wavelength	0.71073 Å	0.71073 Å
Crystal system	Monoclinic	Monoclinic
Space group	C2/c	C2/c
Unit cell dimensions	a = 14.4910(6) Å	a = 17.8904(6) Å
	b = 27.4207(10) Å	b = 13.7183(4) Å
	C = 13.1146(5) Å	c = 12.6348(4) Å
	α = 90°	α = 90°
	β = 90.0049(8)°	β = 131.7610(10)°
	γ = 90°	γ = 90°
Volume, Å^3	5211.1(3)	2313.06(13)
Z	8	4
rcalc, Mg/m^3	1.344	1.434
Absorption coefficient, mm^{-1}	0.545	0.610
F(000)	2152	1012
Crystal size, mm^3	0.40 × 0.04 × 0.04	0.40 × 0.36 × 0.30
Reflections collected	10510	6944
Absorption correction	ψ-Scan	Multi-scan, SADABS
Refinement method	Full-matrix on F^2	Full-matrix on F^2
Data/restraints/parameters	4523 / 0 / 337	2710 / 0 / 184
Goodness-of-fit on F^2	1.137	1.048
R indices [$I>2\sigma(I)$], $R1(wR2)$	0.0359 (0.0742)	0.0386 (0.0872)
Largest diff. peak and hole	0.395 and -0.345 e/Å^3	0.257 and -0.427 e/Å^3

Note: $R1 = \Sigma \| |F_o| - |F_c| \| / \Sigma |F_o|$, $wR2 = \{\Sigma [w(F_o^2 - F_c^2)^2] / \Sigma [w(F_o^2)^2]\}^{1/2}$, goodness-of-fit = $S = \{[w(F_o^2 - F_c^2)^2] / (n - p)\}^{1/2}$, $w = 1 / [\sigma^2(F_o^2) + (aP)^2 + bP]$

refined with anisotropic thermal parameters, and hydrogen atoms were located from difference Fourier maps and refined with isotropic thermal parameters. Hydrogen atoms were assigned to ideal positions. The final refinement gave $R1$= 0.0361 ($wR2$= 0.0772) for 4149 reflections with $I > 2\sigma$ and $R1$= 0.0414 ($wR2$= 0.0847) for 4532 data and a GOF value of 1.146.

(d) $[Mn(TCNQ)_2(H_2O)_2]_\infty$ (10).

A blue crystal of approximate dimensions 0.40 × 0.36 × 0.30 mm was mounted on a glass fiber and secured with Dow corning grease. Diffraction data were collected on a Siemens SMART CCD area detector instrument at –140(2)°C. Preliminary cell parameters indicated a monoclinic system from the refinement of 26 reflections taken from 45 frames with 10 second exposure times. The initial cell parameters were a = 17.839(10) Å, b = 13.692(7) Å, c = 12.597(7) Å, β= 131.740(10)°, V = 2296(4) Å^3. The final cell parameters were obtained from the refinement of the XYZ centroids of 3816 reflections with I > 10σ from a total of 7,094 integrated reflections. Systematic absences indicate that the crystal belongs to a monoclinic system, space group C2/c (#15), with a = 17.8904(6) Å, b = 13.7183(4) Å, c = 12.6348(4) Å, α= 90°, β= 131.7610(10)°, γ= 90°, V = 2313.06(13) Å^3. A summary of data collection parameters is given in Table 14. The data were solved and refined in SHELXTL V. 5.0 by full-matrix least-squares on F^2. All non-hydrogen atoms were located and refined with anisotropic thermal parameters, and hydrogen atoms were located from difference Fourier maps and refined with isotropic thermal parameters.

(e) [^{n}Bu$_4$N][TCNQ] (11).

A purple needle crystal of approximate dimensions 0.21 × 0.16 × 0.10 mm was mounted on a glass fiber and secured with

grease. Diffraction data were collected on a Siemens SMART CCD area detector instrument at –100(2)°C. Preliminary cell parameters were obtained from the refinement of 63 reflections from 60 frames with 10 second exposure times. Initial unit cell parameters were a = 9.300(2) Å, b = 19.343(5) Å, c = 15.385(5) Å, β = 100.990(18) °, V = 2716.74(132) Å^3. A hemisphere of data was collected at a scan-width of 0.3° in ω at 30 sec/frame. Final cell parameters and an orientation matrix were obtained from the refinement of the XYZ centroids of 3296 reflections with I > 10σ with a = 9.3028(7) Å, b = 19.3520(14) Å, c = 15.3880(11) Å, β = 100.979(1)°, V = 2719.57(59) Å^3. A summary of data collection parameters for compound (11) is given in Table 10. The data were solved and refined in SHELXTL V. 5.04 by full-matrix least-squares on F^2. All non-hydrogen atoms were located and refined with anisotropic thermal parameters, and hydrogen atoms were fixed in the idealized positions. The refinement led to $R1$= 0.0638 ($wR2$= 0.111) for 3259 reflections with $I > 2\sigma$ and $R1$= 0.1497 ($wR2$= 0.1357) for all 6327 data against 298 parameters with a goodness-of-fit of 0.973. The highest residual peak in the electron difference map is 0.18 e/Å^3.

(f) [^{n}Bu$_4$N][TCNQF$_4$] (12).

A thin, blue green platelet crystal of approximate dimensions 0.20 × 0.08 × 0.01 mm was mounted on a glass fiber and secured with Dow Corning grease. Diffraction data were collected on a Siemens SMART CCD platform diffractometer at –100(2)°C. Preliminary 10 sec/frames indicated a triclinic system with a = 9.630 Å, b = 14.934 Å, c = 21.305 Å, α = 107.445°, β = 93.422°, γ = 104.716°, V = 2800 Å^3. A hemisphere of data was collected at a scan width of 0.3° in ω. Final cell parameters and an orientation matrix were obtained from the refinement of XYZ centroids of 2,850 strong

reflections with $I/\sigma > 10$ from a total of 15,276 reflections with a = 9.6335(3) Å, b = 14.9574(3) Å, c = 21.3615(5) Å, α = 107.440(1)°, β = 93.436(2)°, γ= 104.785(1)°, V = 2808.07(17) Å^3. Absorption was corrected for with program SADABS which lead to a transmission factor between 0.56 and 1. Data were further merged and truncated with XPREP to .85Å resolution to reduce the high *R*sigma. The structure was solved in space group *P-1* by direct method with subsequent atoms being located from difference maps and refined in SHELXTL V. 5.10 package by full-matrix least-squares on F^2. All non-hydrogen atoms were located and refined anisotropically, and hydrogen atoms were fixed in idealized positions. The final refinement was based on 668 parameters and 13369 reflections, of which 8918 were unique. The refinement led to *R*1= 0.0621 and *wR*2= 0.1221 and a goodness-of –fit 1.075 for reflections with $I > 2\sigma$ and *R1*= 0.1568 (*wR2*= 0.1582) for all data. The highest peak in the final difference map was 0.204 e-/Å^3. A summary of data collection parameters for compound (12) is given in Table 15.

(g) {[Zn(H$_2$O)$_4$](η^1-TCNQ)$_2$•2TCNQ•2MeCN}$_\infty$ (13).

Single crystals of (13) were grown from the reaction of Zn pellets with TCNQ in a 1:1 MeCN/H$_2$O solution. A brown needle crystal of approximate dimensions 0.40 × 0.10 × 0.08 mm was secured on the tip of a glass fiber with Dow Corning silicone grease and mounted on a Siemens SMART 1K CCD platform diffractometer. Preliminary examination indicated that the unit cell was triclinic with a = 10.7624(4) Å, b = 11.0007(3) Å, c = 12.1897(4) Å, α = 70.147(1)°, β = 88.086(1)°, γ = 89.784(2)°, V = 1356.61(8) Å^3 reflections with $I > 10\sigma(I)$ from 8,554 reflections. The final unit cell was a = 10.7624(4) Å, b = 11.0007(3) Å, c = 12.1897(4) Å, α = 70.1470(10)°, β = 88.0860(10)°, γ = 89.784(2)°,

Table 15. Crystal data and structure refinement for [^{n}Bu$_4$N][TCNQ] (11) and [^{n}Bu$_4$N][TCNQF$_4$] (12).

Identification code	(11)	(12)
Empirical formula	$C_{56}H_{80}N_{10}$	$C_{60}H_{72}F_8N_{10}$
Formula weight	893.30	1085.28
Temperature	173(2) K	173(2) K
Wavelength	0.71073 Å	0.71073 Å
Crystal system	Monoclinic	Triclinic
Space group	P2(1)/n	P $\bar{1}$
Unit cell dimensions	a = 9.3028(7) Å	a = 9.6335(3) Å
	b = 19.3520(14) Å	b = 14.9574(3) Å
	c = 15.3880(11) Å	c = 21.3615(5) Å
	α = 90°	α = 107.4400(10)°
	β = 100.979(2)°	β = 93.437(2)°
	γ = 90°	γ = 104.785(2)°
Volume Å^3	2719.6(3)	2808.07(12)
Z	2	2
Density (calculated)	1.091 Mg/m^3	1.284 Mg/m^3
Absorption coefficient mm^{-1}	0.065	0.096
F(000)	972	1148
Crystal size, mm^3	0.21 × 0.16 × 0.10	0.20 × 0.08x 0.01
Reflections collected	16240	13369
Absorption correction	Multi-scan, SADABS	Multi-scan, SADABS
Refinement method	Full-matrix on F^2	Full-matrix on F^2
Data / restraints / parameters	6327 / 0 / 298	8918 / 0 / 667
Goodness-of-fit on F2	0.973	0.950
$R1$ ($wR2$) [F^2, I>2σ(I)],	0.0638 (0.1111)	0.0755 (0.1694)
Largest diff. peak and hole	0.178 and -0.242 e/Å^3	0.486 and -0.409 e/Å^3

Note: $R1 = \Sigma \| |F_o| - |F_c| \| / \Sigma |F_o|$, $wR2 = \{\Sigma [w(F_o^2 - F_c^2)^2] / \Sigma [w(F_o^2)^2]\}^{1/2}$, goodness-of-fit = $S = \{[w(F_o^2 - F_c^2)^2] / (n - p)\}^{1/2}$, $w = 1 / [\sigma^2(F_o^2) + (aP)^2 + bP]$

V = 1356.61(8) Å^3. The intensities were corrected for beam inhomogeneity, crystal decay and absorption with the program SADABS which led to R_{int} = 0.0258 and transmission factors T_{min} = 0.704, T_{max} = 1.0. A total of 8,554 reflections was measured with the maximum 2θ = 56.36°, of which 4230 were in the category I > 2σ(I) and 5,669 reflections were unique.

Systematic absences indicated that the system belongs to the space group P-1 (#2). Symmetry and multiply measured reflections were then averaged with SHELXTL to give values of R_{int} = 0.0303 and R_{sig} = 0.0887. The structure was solved by direct methods. All non-hydrogen atoms were refined anisotropically by a full matrix least-squares refinement on F^2. Hydrogen atoms were fixed in idealized position and were not refined. The final residuals were *R1*= 0.0642 (*wR2*= 0.1339) for 4230 (I > 2σ(I)) reflections and *R1*= 0.0991 (*wR2*= 0.1492) for all 5969 reflections and 408 parameters. A heavy residual of 2.264 e$^-$/Å^3 was observed to reside at an inversion center, which was modeled as a disordered Zn atom (3.3%) bonding to the –CN group *trans* to the original position in the framework dominated by the TCNQ stacks. A summary of the data collection and refinement results is listed in Table 16.

(h) Structure of [Ni(DMSO)$_6$][TCNQ]$_3$ (14).

A square platelet crystal of approximate dimensions 0.52 × 0.52 × 0.18 mm was secured on the tip of a glass fiber with Dow Corning silicone grease. The crystal was mounted on a Nicolet (Siemens) P3/V diffractometer equipped with a low temperature device at –108(1)°C. Least-squares refinement using 20 well centered reflections in the range 15° ≤ 2θ ≤ 25° indicated a triclinic system with a = 7.927(2) Å, b = 10.057(2) Å, c = 17.141(3) Å, α= 84.59(3)°, β= 82.67(3)°, γ= 82.26(3)°, V = 1338.8(5) Å^3. The data were collected at –108(1)°C by the ω-2θ scan

Table 16. Crystal data and structure refinement for $\{[Zn(H_2O)_4](\eta^1\text{-}TCNQ)_2\bullet 2TCNQ\bullet 2MeCN\}_\infty$ (13) and $[Ni(DMSO)_6](TCNQ)_3$ (14).

Identification code	(13)	(14)
Empirical formula	$C_{28}\ H_{18}\ N_{10}\ O_2\ Zn_{0.5}$	$C_{24}\ H_{24}\ N_6\ Ni_{0.5}\ O_3\ S_3$
Formula weight	559.21	570.03
Temperature	173(2) K	165(2) K
Wavelength	0.71073 Å	0.71073 Å
Crystal system	Triclinic	Triclinic
Space group	P-1	P- 1
Unit cell dimensions	a = 10.7624(4) Å	a = 7.9267(16) Å
	b = 11.0007(3) Å	b = 10.057(2) Å
	c = 12.1897(4) Å	c = 17.141(3) Å
	α= 70.1470(10)°	α= 84.59(3)°
	β= 88.0860(10)°	β= 82.67(3)°
	γ= 89.784(2)°	γ= 82.26(3)°
Volume Å^3	1356.61(8)	1338.8(5)
Z	2	2
Density (calculated)	1.369 Mg/m^3	1.414 Mg/m^3
Absorption coefficient	0.520 mm^{-1}	0.655 mm^{-1}
F(000)	574	592
Crystal size mm^3	0.40 × 0.10 × 0.08	0.52 × 0.52 × 0.15
Reflections collected	8554	5110
Refinement method	Full-matrix on F^2	Full-matrix on F^2
Data / restraints / parameters	5969 / 6 / 409	4738 / 22 / 358
Absorption correction	Multi-scan, SADABS	ψ-Scan
Goodness-of-fit on F^2	0.992	1.088
$R1(wR2)$ [F^2, $I>2\sigma(I)$]	0.0642(0.1375)	0.0683(0.1281)
Largest diff. peak and hole	2.276 and -1.003 e/Å^3	0.523 and -1.122 e/Å^3

Note: $R1 = \Sigma\ ||F_o| - |F_c|| / \Sigma\ |F_o|$, $wR2 = \{\Sigma\ [w(F_o^2 - F_c^2)^2] / \Sigma\ [w(F_o^2)^2]\}^{1/2}$, goodness-of-fit = $S = \{[w(F_o^2 - F_c^2)^2] / (n - p)\}^{1/2}$, $w = 1 / [\sigma^2(F_o^2) + (aP)^2 + bP]$.

technique in the range $4° \leq 2\theta \leq 50°$. A total of 5,110 reflections was measured, of which 4,738 are unique. The structure was solved by direct methods and refined by full-matrix least squares on F^2. All non-hydrogen atoms except the disordered SMe_2 groups were refined anisotropically. The disorder in the SMe_2 groups was modeled at ~33% occupancy distributed among three conformers. The structure was refined to residuals of *R1* = 0.0683 (*wR2*= 0.128) for 3048 reflections ($I > 2\sigma$) and a goodness-of-fit = 1.088.

A summary of key data collection and refinement parameters is provided in Table 16.

(i) Crystal structure of $[Ni(TCNQ)_2(H_2O)]_\infty$ (15).

Single crystals of (15) were grown by layering an acetonitrile solution of $[Ni(MeCN)_6][(BF_4)_2]$ with LiTCNQ in H_2O. A small purple cube crystal of dimensions 0.080 × 0.060 × 0.060 mm was secured on the tip of a glass fiber with epoxy. The data were collected at –60(1)°C on a Siemens P4-CCD four circle diffractometer equipped with Mo rotating anode source by Dr. Jim Britton at McMaster University, in Ontario, Canada. Preliminary examination indicated that the crystal system belongs to the tetragonal system, but the crystal diffracted so weakly. A combination of ψ-ω scan with scan-widths of 0.3° and 60 sec/frames led to 1,750 data frames with the maximum 2θ = 52.96° and a resolution of 0.8Å.

The final cell parameters and an orientation matrix were obtained from the refinement of XYZ centroids of 1290 reflections with $I > 20\sigma(I)$ from a total of 6,634 reflections. Data integration with tetragonal cell constraints led to a = 12.2420(12) Å, b = 12.2420(15) Å, c = 3.9067(5) Å, α = 90.0000(23)°, β = 90.0000(35)°, γ = 90.0000(25)°, V = 585.480(194) Å^3 and a total of 6,634 reflections of which 2,158 were in the category $I > 2\sigma(I)$

and 1,474 were unique. The intensities were corrected for beam inhomogeneity, crystal decay and absorption with the program SADABS, which led to $R_{int} = 0.0454$, and transmission factors $T_{min} = 0.742$, $T_{max} = 1.0$.

After many failures to solve the structure in the 4/m or mmm crystal symmetry group, the structure was ultimately solved in the lower symmetry monoclinic space group *P*c with the cell parameters $a = 3.9169(5)$ Å, $b = 12.2945(12)$, $c = 12.3005(15)$ Å, $\beta = 90.130(2)°$, due to probable twining. The structural model was refined as disordered and pseudo-merohedrally twinned. The 3x3 twinning matrix [1 0 0, 0 -1 0, 0 0 -1] was used to model a two-fold rotational twinning. This modeling led to *R1*= 0.0829, and *wR2*= 0.1789 for 1106 ($I > 2\sigma(I)$) unique reflections for 151 parameter, and *R1*= 0.1781, *wR2*= 0.2386 for all 1184 data and a goodness-of-fit of 1.050. Absolute configuration testing leads to a Flack constant of 0.00 which indicates the solution is a correct configuration. The largest difference peak and hole in the residual difference map is 0.301 and -0.262 e/Å^3 respectively. A summary of data collection and refinement results is listed in Table 17.

(2) Powder X-ray diffraction studies.

Powder XRD methods were used to probe the formation and conversion of the two phases of Cu(TCNQ). XRD was used to probe the relationship of $M(TCNQ)_2L$ (M = Fe, Co, Ni; L = MeOH, H_2O) products to the more crystalline Mn phase for which several single crystal phases were obtained. The binary metal TCNQ phase formulated as $M(TCNQ)_2$ (M = Mn, Fe, Co, Ni) were also subjected to powder XRD studies. All samples were measured from 5 to 50° in 2θ with a diffractometer power of 45 kV and 100 mA.

Table 17. Crystal data and structure refinement for $[Ni(TCNQ)_2(H_2O)]_\infty$.(15).

Identification code	(15)
Empirical formula	$C_{12}\ H_6\ N_4\ Ni_{0.50}\ O$
Formula weight	251.56
Temperature	213(2) K
Wavelength	1.54178 Å
Crystal system	Monoclinic
Space group	*Pc*
Unit cell dimensions	a = 3.9169(5) Å
	b = 12.2945(12) Å
	c = 12.3005(15) Å
	α = 90°
	β = 90.130(2)°
	γ = 90°
Volume Å^3	592.35(12)
Z	2
Density (calculated)	1.410 Mg/m^3
Absorption coefficient mm^{-1}	0.857
F(000)	256
Crystal size, mm^3	0.08 × 0.06 × 0.06
Reflections collected	4874
Independent reflections	2264 [$R_{(int)}$ = 0.0619]
Absorption correction	Multi-scan, SADABS
Max. and min. transmission	1.00 and 0.69
Refinement method	Full-matrix on F^2
Data / restraints / parameters	2264 / 46 / 151
Goodness-of-fit on F^2	1.050
Final R indices [$I>2\sigma(I)$]	$R1$ = 0.0829, $wR2$ = 0.1789
Absolute structure parameter	0.00
Largest diff. peak and hole	0.301 and -0.262 e/Å^3

Note: $R1 = \Sigma \| |F_o| - |F_c| \| / \Sigma |F_o|$, $wR2 = \{\Sigma [w(F_o^2 - F_c^2)^2] / \Sigma [w(F_o^2)^2]\}^{1/2}$, goodness-of-fit = $S = \{[w(F_o^2 - F_c^2)^2] / (n - p)\}^{1/2}$, $w = 1 / [\sigma^2(F_o^2) + (aP)^2 + bP]$

3. Results and Discussion

A. Synthetic Methods and Powder X-ray Characterization of Cu(TCNQ).

(1) Bulk synthesis of phase I.

Two methods were used to prepare bulk samples of Cu(TCNQ), (7), and the products were compared to the well-investigated phase first reported by Melby *et al.* in 1962 (Eq 2).[23a] In Melby's method, TCNQ is reduced *in situ* by CuI which leads to the immediate formation of Cu(TCNQ) as blue-black microcrystals and I_2 as a by-product (Eq 2). The I_2 is trapped by excess CuI to form I_3^-, thus avoiding any side-reaction with I_2. The second method, which is new, follows from our interest in the use of acetonitrile solvated transition metal cations as useful starting materials in non-aqueous substitution reactions.[28] In the reaction depicted in Eq. 3, acetonitrile solutions of $[^nBu_4N][TCNQ]$ and $[Cu(CH_3CN)_4][(BF_4)$ are combined to give Cu(TCNQ) as a dark blue precipitate with $[^nBu_4N][BF_4]$ as the by-product (Eq 2).

$$3\ CuI + 2\ TCNQ \rightarrow 2\ Cu(TCNQ) + CuI_3 \quad \text{(Eq. 2)}$$

$$[Cu(MeCN)_4][BF_4] + [^nBu_4N][TCNQ] \rightarrow Cu(TCNQ) + [^nBu_4N][(BF_4] \quad \text{(Eq. 3)}$$

A variety of characterization tools including X-ray powder diffraction support the conclusion that the products of the reactions in Eqs. 2 and 3 (hereafter referred to as phase I) are the same material, except that the product of the CuI reaction is typically more crystalline as judged by the intensity of the powder patterns and by SEM. We were curious as to whether a different product could be obtained by the use of the Cu(II)

starting material $[Cu^{II}(CH_3CN)_4][(BF_4)_2]$. As depicted in Eq 4 the products are $Cu^{I}(TCNQ)$ and neutral TCNQ and not $Cu^{II}(TCNQ)_2$ as one might have predicted.

$$[Cu(MeCN)_4][BF_4]_2 + 2\ [^nBu_4N][TCNQ] \rightarrow Cu(TCNQ) + TCNQ + [^nBu_4N][BF_4] \quad \text{(Eq.4)}$$

This is in accord with results reported for the reaction of $Cu^{II}SO_4$ with LiTCNQ in H_2O which gives an unstable green powder that is occasionally written as $Cu(TCNQ)_2$,[23a] but which is actually $Cu^{I}(TCNQ^{-1})(TCNQ^{0})$ with trapped $TCNQ^0$ as established by Raman, XPS and IR spectroscopies.[23b-d] Our results from the reaction performed in CH_3CN indicate that $Cu^{II}(TCNQ)_2$ is also unstable under non-aqueous conditions. An important difference between the aqueous versus non-aqueous reaction is that the Cu(TCNQ) material retains the neutral TCNQ molecule as part of the formula due to the insolubility of neutral TCNQ in H_2O. TCNQ is soluble in CH_3CN, however, and therefore it remains in solution after the reaction in Eq. 4. The characteristic yellow color of the acetonitrile filtrate and the $\nu(C\equiv N)$ stretch at 2222 cm^{-1} are convincing evidence that the by-product is neutral TCNQ.[29]

(2) Conversion of phase I to phase II Cu(TCNQ) in acetonitrile.

In the course of preparing Cu(TCNQ) by the reactions given in Equations 2 and 3, we made an unexpected observation. We discovered that if suspensions of phase I are stirred in CH_3CN at room temperature for several days, or if the reaction solution is refluxed for several hours, a second phase, (8), is produced in essentially quantitative yields. This was quite surprising to us as we had observed that phase I can be heated in the solid-state at 150 °C for two days in air or exposed to air and ambient light

for weeks with no change as evidenced by X-ray powder diffraction and IR spectroscopy. Clearly, acetonitrile is capable of dissolving phase I into its constituents, i.e., Cu(I) and $TCNQ^{-1}$ ions which then recombine to give a different phase as judged by physical changes that can be monitored.[19,20a,22] This conversion produces a form of Cu(TCNQ) (Eq 5) that is stable with respect to further changes under forcing thermal conditions in the solid-state or in solution.

$$\underset{\text{phase I}}{\text{Cu(TCNQ) suspended in } CH_3CN} \rightarrow \underset{\text{phase II}}{\text{Cu(TCNQ)}} \qquad \text{(Eq 5)}$$

B. Syntheses of the $Mn(TCNQ)_2(solvent)_2$ phases.

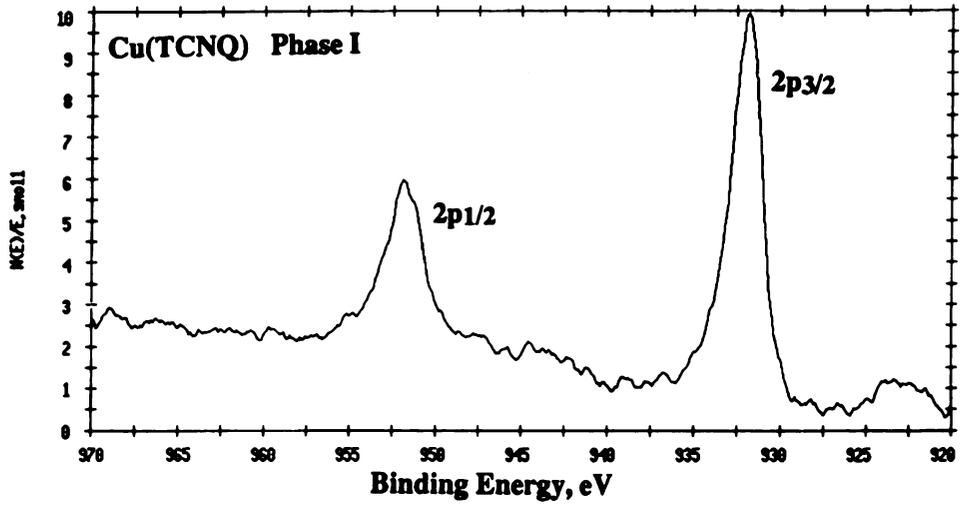
Reactions of $[Mn(MeCN)_4][BF_4]_2$ with $[^nBu_4N][BF_4]$ in MeOH or LiTCNQ in H_2O lead to the rapid formation of dark blue-purple crystalline solids. These materials are robust under ambient conditions upon exposure to air, moisture and light, with no decomposition being detected after several months. Elemental analyses for the water compounds fit the empirical formula $M(TCNQ)_2(H_2O)_2$ rather than $M(TCNQ)_2(H_2O)_3$ which had been previously reported.[24b,30] Presumably, handling and storage conditions affect the quantity of water that these materials retain, which is an important point because degree of hydration is known to influence the magnetic properties of these aqueous-derived materials.[30a]

No prior reports of binary metal/TCNQ compounds prepared in alcohols have appeared in the literature to our knowledge. Analytical data for the bulk methanol product support the formulation of $Mn(TCNQ)_2(MeOH)_2$ as do the TGA measurements.

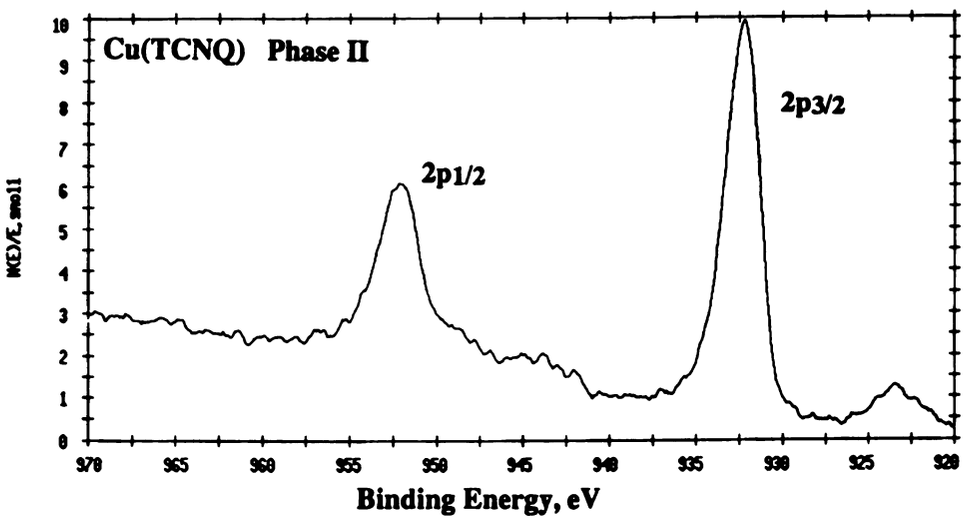
C. Spectroscopic Studies.

(1) X-ray photoelectron spectroscopy.

The 1:1 ratio of Cu to TCNQ in the material does not necessarily mean that complete charge transfer between the metal and the acceptor has occurred, thus it is important to probe the oxidation state of the metal in the Cu(TCNQ) phases, One method that is useful in this regard is X-ray Photoelectron Spectroscopy (XPS). In earlier reports, XPS data of Cu(TCNQ) prepared from CuI revealed characteristic binding energies for Cu(I) $2p_{1/2}$ and $2p_{3/2}$ for Cu(I),[9,b,d;31] with no evidence for shoulders or higher binding energy satellites that can be attributed to Cu(II).[32] Likewise, XPS data for compounds (7) and (8) prepared in our laboratories gave essentially identical results in accord with Cu(I). Data from this work as well as from earlier papers are presented in Table 18. The $2p_{3/2}$ and $2p_{1/2}$ signals are depicted in Figure 25. Both phases exhibit essentially identical binding energies for the Cu 2p orbitals, with no evidence for shoulders or satellites due to Cu(II). Likewise, the N1s orbitals appear as a single feature at 398.7 eV in both phases which is indicative of one type of TCNQ. Mixtures of $TCNQ^{-1}$ and TCNQ can be readily discerned in this region.[31] The ease with which Cu(II) can be observed in *bona fide* mixed-valence Cu^{I}/Cu^{II} compounds and materials is illustrated by a comparison of the data for chemically prepared Cu(TCNQ) with electrochemically prepared $Cu(DCNQI)_2$ materials. For example, the mixed-valence metallic compound $Cu(DM\text{-}DCNQI)_2$ shows two sets of Cu $2p_{1/2}$ and $2p_{3/2}$ (931.6, 933.6 eV) signals and a more obvious second set of satellite features at 943 and 962 eV that are characteristic of paramagnetic Cu(II).[33a] As further support for the lack of Cu(II) in our TCNQ samples we undertook XPS (Figure 25 and 26)

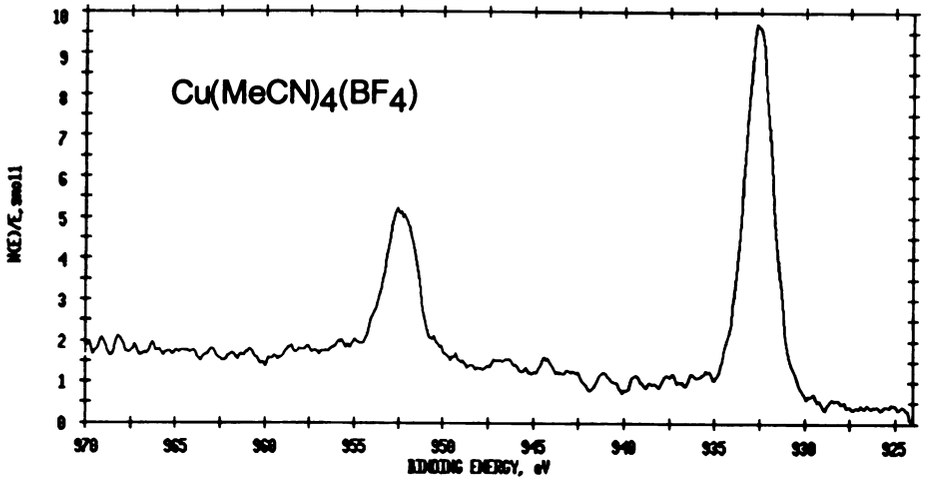


(a)

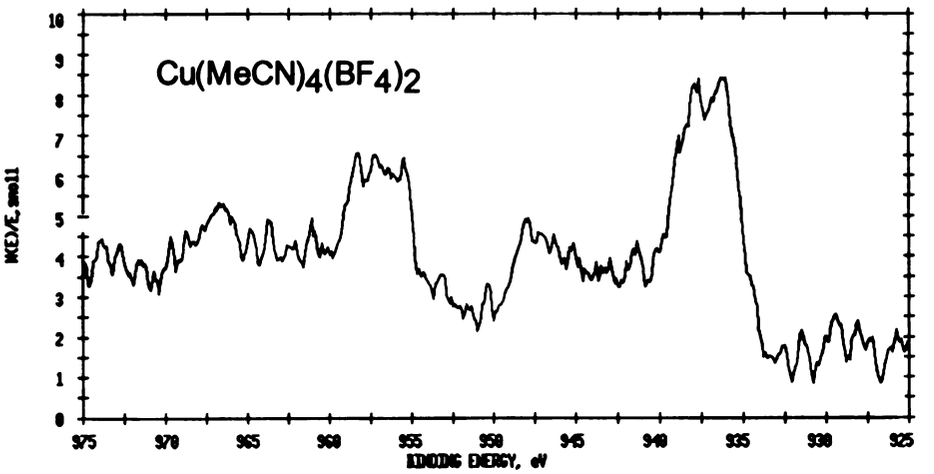


(b)

Figure 25. XPS data in the Cu $2p_{3/2}$ and $2p_{1/2}$ regions for phase I (a) and phase II Cu(TCNQ) (b).



(a)



(b)

Figure.26. XPS data in the Cu $2p_{3/2}$ and $2p_{1/2}$ regions for $[Cu^{I}(MeCN)_4][BF_4]$ (a) and $[Cu^{II}(MeCN)_4][BF_4]_2$ (b).

measurements of the nitrile salts $[Cu^{I}(CH_3CN)_4][BF_4]$ and $[Cu^{II}(CH_3CN)_4][BF_4]_2$ as references. Although they were rather unstable under the vacuum conditions of the experiment, it was possible to observe important differences. The Cu(II) salt exhibits four different signals in the Cu 2p region whereas the Cu(I) analog exhibits only two features. We take these data as convincing evidence that Cu(II) is not present in our samples to any appreciable degree. This conclusion is in contrast to data obtained for electrochemically prepared samples reported by Willett and co-workers which point to the presence of both Cu(I) and Cu(II) species.[33b]

(2) Infrared spectroscopic studies.

Infrared spectroscopy in the ν(C≡N) region is very useful for assigning charge as well as predicting stacking modes in $TCNQ^{n-}$ salts.[4d,6,34] Unfortunately, analysis of IR data for metal-bound TCNQ ligands is complicated by the fact that ν(C≡N) stretches can shift to higher energies if the TCNQ molecules acts primarily as a σ-donor, or to lower energies if there is significant metal to TCNQ π-backbonding.[6] A more informative infrared active mode is the δ(C-H) bend of TCNQ. We have discovered that this ring bending mode is a fingerprint for the presence of the σ-dimer $[TCNQ\text{-}TCNQ]^{2-}$ versus normal $TCNQ^{-1}$ in the materials. The spectrum for $[Mn(TCNQ)(TCNQ\text{-}TCNQ)_{0.5}(MeOH)_2]_\infty$ contains a feature at ~825 cm^{-1} in addition to one at 802 cm^{-1} which are indications of both $[TCNQ]^{\cdot-}$ and $[TCNQ\text{-}TCNQ]^{2-}$ being present as verified in the X-ray structure (see single crystal section). The spectrum of $[Mn(TCNQ)_2(H_2O)_2]_\infty$ on the other hand exhibits only one δ(C-H) feature at ~823 cm^{-1} due to the *syn*-μ^2-$[TCNQ]^-$ ligand.[4h]

Infrared spectra of the two phases of Cu(TCNQ) are quite similar as would be expected on the basis of their formulations as compounds of

$TCNQ^{-1}$. No peaks associated with acetonitrile were observed in either phase.[4f] Compound (7) shows a strong, broad ν(C≡N) absorption at 2199 cm^{-1} with a shoulder at 2172 cm^{-1} whereas (8) exhibits two strong, sharp stretches at 2211 cm^{-1} and 2172 cm^{-1}. Perhaps even more indicative of the similarity of the TCNQ unit in the two phases is the δ(C-H) mode at 825 cm^{-1} which is very sensitive to changes in oxidation state. These data are consistent with the presence of $TCNQ^{-1}$ and not TCNQ, $TCNQ^{2-}$, or mixed-valence stacks of $TCNQ^{-1}$ and TCNQ.[33] Furthermore, they are in accord with previously reported IR data for samples of Cu(TCNQ) prepared by the original CuI method.[10,33a] Since the existence of a second phase was unknown until the present work, there are no data with which to compare phase II.

(3) SEM studies of Cu(TCNQ).

Scanning electron microscopy was used to discern morphologies of the bulk Cu(TCNQ) samples in this study, and the results were compared to films of the material. It is evident from the micrographs depicted in Figure 27 (a) and (b) that the two bulk phases are physically quite different. Phase I is composed of regular needles whereas phase II consists of crystallites with a platelet morphology. The same two crystallite types have been reported to appear during the growth of Cu(TCNQ) films from acetonitrile solutions.[19,20a,22] If one compares these observations to Cu(TCNQ) grown asfilms on Cu substrates, it is obvious that the phase with densely packed needles oriented perpendicular to the Cu surface appears immediately and survives only during short dipping times at 60 °C (Figure 28 (a)).[19,20a] Within 20 minutes, the needles become visibly pitted (Figure 28 (b)) and after 1 h (Figure 28 (c)), the film consists of regular-shaped blocks. A further

Table 18. IR and XPS data for Cu(TCNQ) and Cu(DM-DCNQI).

	IR ν(C≡N) cm^{-1}	IR δ(C-H) cm^{-1}	XPS B.E. (eV): Cu $2p_{3/2}$, $2p_{1/2}$; N1s	XPS references
Cu(TCNQ)[a] phase I needles	2199s,br; 2172s	825s	932.0, 951.9; 398.7	this work
Cu(TCNQ)[b] phase II platelets	2211s, 2172s	825s	932.1, 952.0; 398.7	this work
Cu(TCNQ)[a]	2200s, 2170s[c]	826s	931.2, 951.0; 398.1	ref 28
$Cu(DM\text{-}DCNQI)_2$	2139w	-----	931.6, 933.6 943, 962	ref 30

[a] CuI + TCNQ synthesis method of Melby et al., ref 23a.

[b] Synthesis method in the experimental section B. (b).

[c] Data from ref 31.

illustration of the importance of reaction conditions in dictating the composition of the films is the comparison of SEM micrographs of films grown at 80 °C and 60 °C for 1 h (Figure 29). At 80 °C, the film consists of a single type of crystallite that is identical to bulk phase II as judged by powder XRD. In contrast, the 60 °C film shows regions of both polymorphs. At higher resolutions, one can observe from the micrographs in Figure 30a-d, that the needle morphology is dominant at 40 °C even after one hour (Figure 30 a,b) and that the platelets are present at 80 °C on Cu foil under the same conditions as indicated in Figure 30c,d. These results are compelling evidence for the high degree of variability in films prepared under different conditions, a fact that helps to explain the lack of reproducibility in the electrical switching studies reported by various groups.

(4) Powder X-ray studies of Cu(TCNQ) bulk phases.

The most convincing evidence that two distinctly different forms of Cu(TCNQ) exist can be found in the diffraction studies of microcrystalline samples prepared by bulk solution routes. A number of crystal structures containing copper and other ligands in addition to TCNQ have been reported,[4] but there are no published structural data for a binary phase containing only copper and TCNQ. Powder patterns of phase I prepared at room temperature from CuI and TCNQ and a suspension of phase I that had been refluxed in MeCN for three hours to convert it to phase II are depicted in Figure 31. Powder diffraction patterns from a Rigaku RU200B X-ray powder diffractometer were used for indexing by the programs Dicvol91 and Treor90. This led to the tetragonal cell $a = b = 11.252$ Å, $c = 3.950$ Å, $V = 500.16$ Å^3 for phase I and the monoclinic cell $a = 5.325$ Å, $b = 5.343$ Å, $c = 18.955$ Å, $\beta = 93.570°$, $V = 538.3$ Å^3 for phase II.

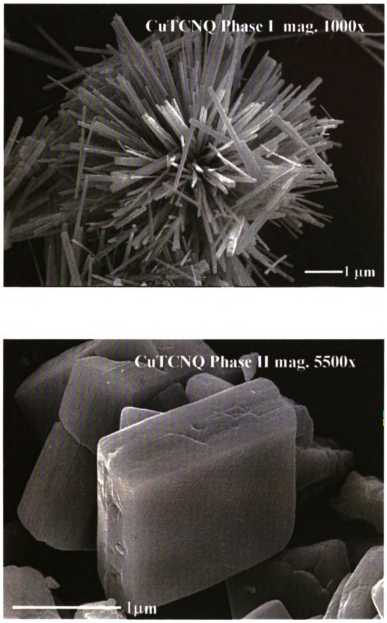
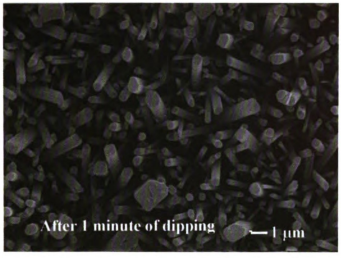


Figure 27. SEM micrographs for solution-prepared Cu(TCNQ) crystals.



(a)
Phase I



(b)
Phase I
dissolving

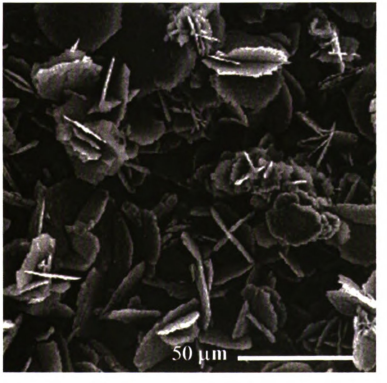


(c)
Phase II

Figure 28. SEM micrographs showing the progressive changes from Cu(TCNQ) phase I to phase II.



(a)



(b)

Figure 29. SEM of Cu(TCNQ) films grown on copper in MeCN for 1hour at different temperatures: (a) at 60°C, (b) at 80°C.

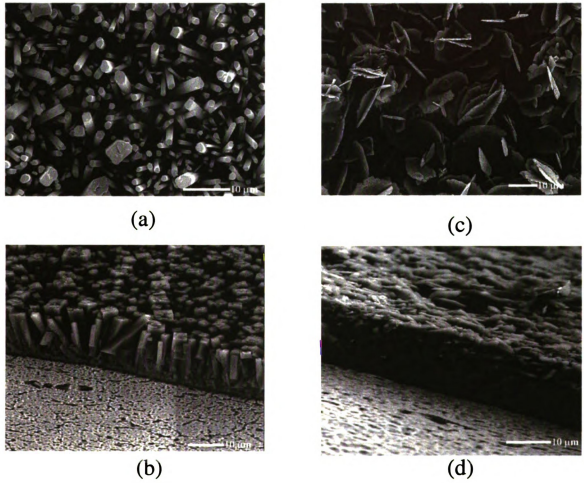


Figure 30. SEM micrographs of Cu(TCNQ) grown on copper in CH_3CN: (a) top and (b) side views of films grown for 1h at 40 °C (phase I) and (c) top and (d) side views of films grown for 1 h at 80 °C (phase II). The reference scale on all micrographs is 10 μm.

(5) Powder X-ray studies of Cu(TCNQ) films.

(a) At room temperature.

It has been reported that Cu(TCNQ) films grown on Cu foil surfaces at short reaction times are spectroscopically identical to the bulk material prepared from CuI.[10] Since our discovery that a second phase exists, however, it is important to investigate changes in film composition as a function of reaction time. Consequently, XRD patterns of the Cu(TCNQ) films were monitored periodically by removing one of the pieces of copper sheet from the TCNQ solution and collecting an X-ray powder pattern on the resulting material. Representative data are provided in Figure 31 with the top and bottom powder pattern being provided as references for pure phase I and II respectively. The powder pattern collected after 6 hours is dominated by the features of phase I, but within 46 hours it is evident that the second phase is being formed at the expense of the first phase; by 76 hours phase II is the major species (Figure 31). We noted that the color of the films remained constant during the reaction and that there were no other visible changes in the film with the exception of the thickness. The progressive powder X-ray monitoring of Cu film reactions with TCNQ acetonitrile solution is shown in Figure 31.

(b) At elevated temperatures

Since the Cu(TCNQ) films in devices are required to be at least 5 μm thick, CH_3CN solutions of TCNQ are typically heated to ~80 °C to accelerate the rate of growth on the Cu foil.[15,19] Clearly it is important to know the composition of these films prepared at elevated temperatures. Accordingly, a piece of Cu foil was dipped as described in the experimental section at 80 °C in CH_3CN and the resulting film was analyzed by X-ray powder diffraction. Figure 32 shows the resulting XRD pattern obtained on

the sample with the underlying Cu substrate. These data strongly support the conclusion that phase II is the main component of the films used for the switching experiments. There is a very low concentration of phase I for films prepared under the conditions cited in the literature for the fabrication of devices.

(6) XRD and SEM studies of $M(TCNQ)_2$ and $M(TCNQ)_2L$

Powder patterns of binary metal TCNQ samples indicate that the $M(TCNQ)_2$ (M = Mn, Fe, Co, Ni) binary phases are isomorphous. Indexing results for $Mn(TCNQ)_2$ and $Ni(TCNQ)_2$ indicate that both compounds belong to the tetragonal crystal system. Comparison of the powder patterns of $M(TCNQ)_2L$ (L = MeOH, H_2O) to a simulated pattern obtained from a structural model of the single crystal $Ni(TCNQ)_2(H_2O)$ reveal that bulk prepared samples of $Mn(TCNQ)_2(MeOH)_2$ and $Mn(TCNQ)_2(H_2O)_2$ should exhibit similar structural features, which are different from the known $Mn(TCNQ)_2(MeOH)_n$ (n = 2, 4) and the $Mn(TCNQ)_2(H_2O)_2$ phase.

(a) Powder patterns of $M(TCNQ)_2$.

The bulk prepared compounds samples of $M(TCNQ)_2$ (M = Mn, Fe, Co, Ni) from acetonitrile all exhibit essentially the same powder pattern, which indicates that these products are isostructural. Unfortunately, the samples suffer from having a small particle size, which hinders their structural determination by powder techniques. The SEM and TEM micrographs (Figure 34) of the $Mn(TCNQ)_2$ sample indicated that it consists of nano-crystals of approximate size 0.05 x 0.02 x 0.02 μm which leads to severe peak broadening in the powder pattern. Indexing results on the $Mn(TCNQ)_2$ compound, the most crystalline sample of the group, indicate a tetragonal crystal system with a = 12.272(2)Å, b = 12.272(2)Å c = 8.713(5)Å, $\alpha = \beta = \gamma = 90°$. V = 1312.12Å^3 The four strongest peaks

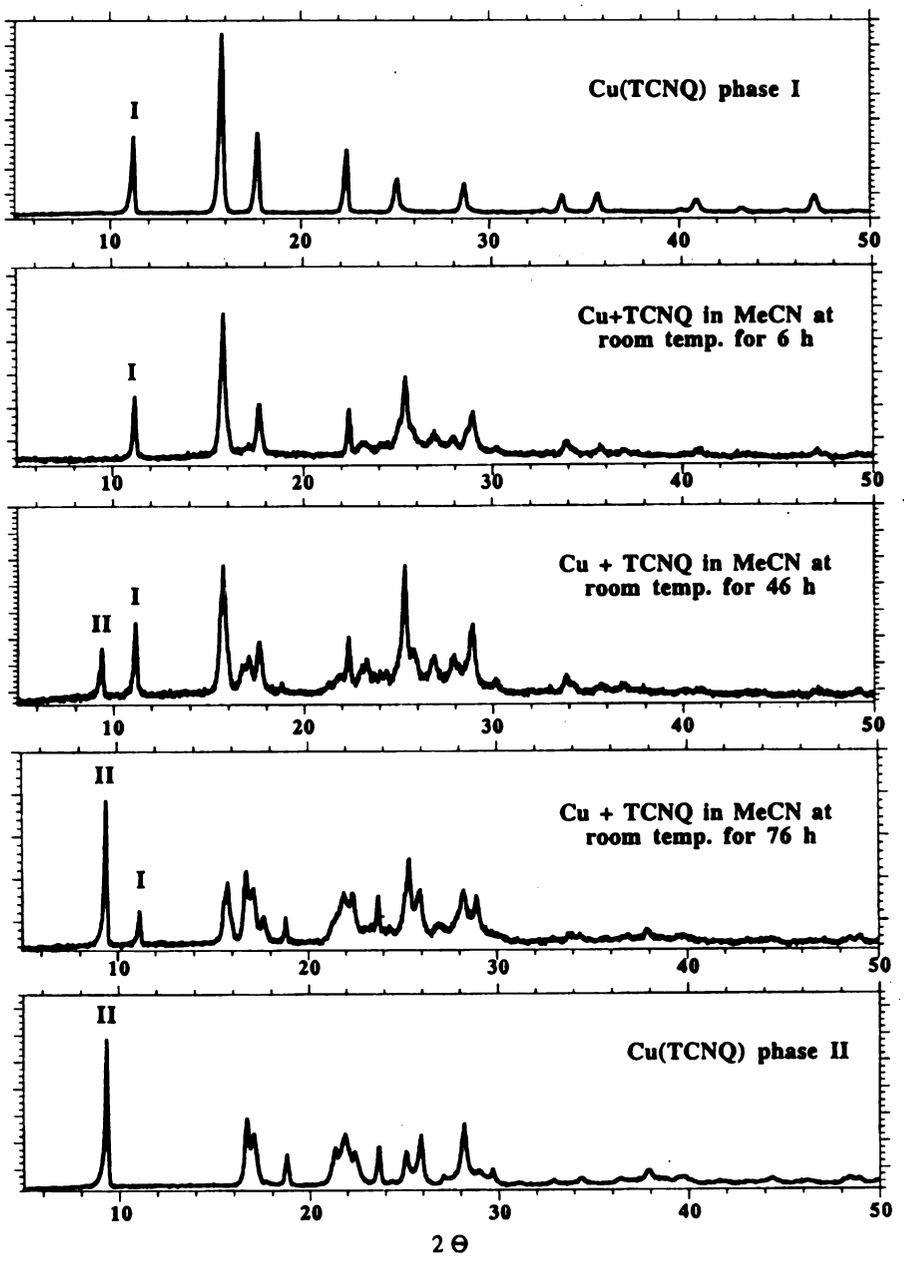


Figure 31. XRD powder patterns illustrating the conversion of Cu(TCNQ) phase I to phase II in CH_3CN.

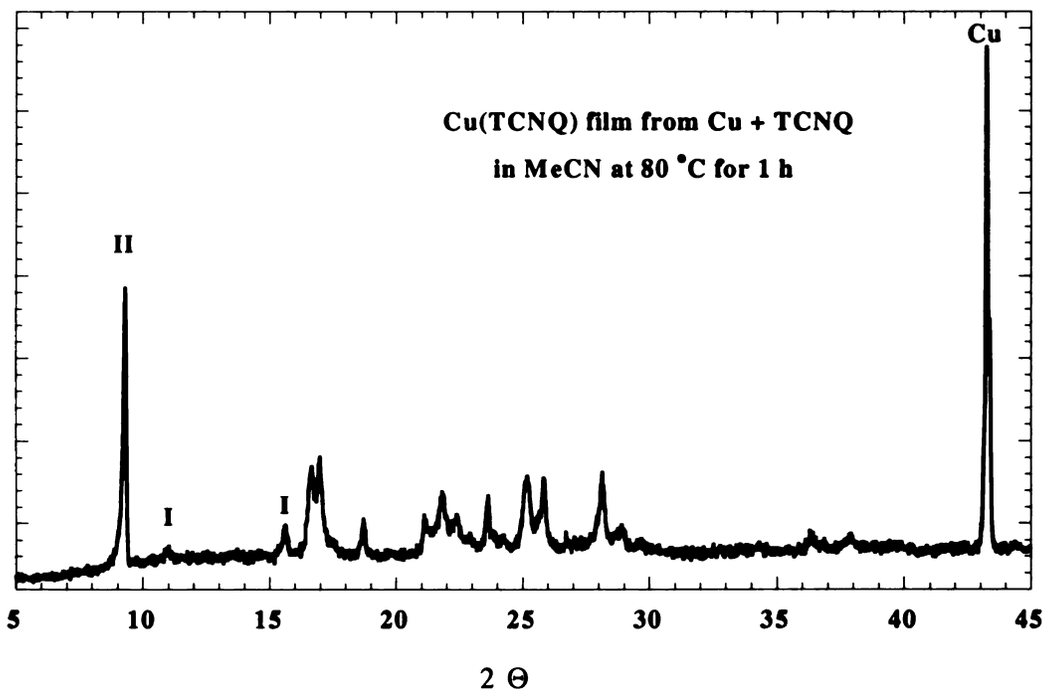


Figure 32. XRD pattern for a Cu(TCNQ) sample grown on a Cu substrate for 1 h at 80°C in a CH_3CN solution of TCNQ.

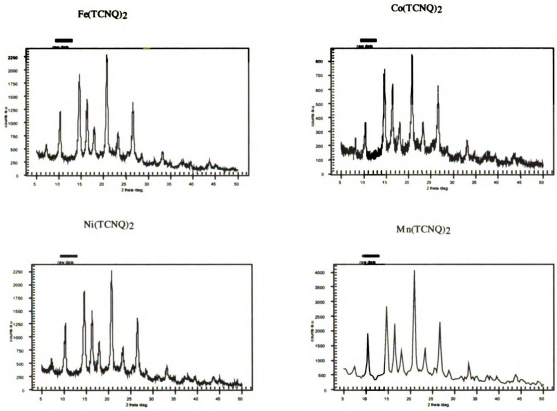
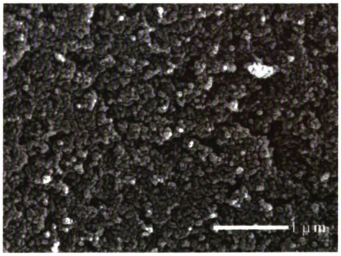
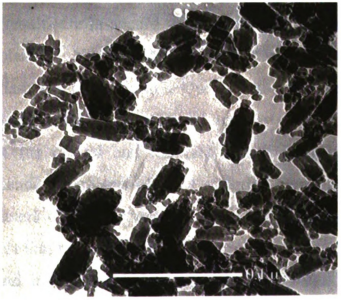


Figure 33. XRD pattern of $M(TCNQ)_2$, (M = Mn, Fe, Co, Ni).



$Mn(TCNQ)_2$

(a)



$Mn(TCNQ)_2$

(b)

Figure 34. $Mn(TCNQ)_2$ small particles in nanometer size could be seen from (a) SEM (1μm scale) and (b) TEM (0.1 μm scale) micrographs.

correspond to d spacings of 6.136, 5.488, 4.339 and 3.404 Å respectively. All four metal TCNQ (Mn, Fe, Co and Ni) have similar pattern.(Figure. 33) It is important to point out that the strong peak in the powder pattern with a d pacing of 3.4 Å points to well stacked TCNQ columns in the structure.

D. Single Crystal Diffraction Studies.

(1) Details of collection and refinement for Cu(TCNQ).

A tiny needle of Cu(TCNQ) phase I and a very thin platelet of Cu(TCNQ) phase II were each mounted on the end of a glass fiber and X-ray data were collected on a Siemens (Bruker) SMART 1K CCD area detector. In both instances, the crystals were exceedingly small, such that they tested the limits of the instrument. The weak data problems notwithstanding, the major features of the structures can readily be discerned. The results are in accord with the powder patterns, furthermore they help to explain the observed properties in a qualitative manner. The refinement of phase I is poor due to a low data-to-parameter ratio and to a merohedral twinning problem, but phase II actually refines quite well given the tiny size of the crystal and the fact that it is quadruply twinned. Numerous independent data sets of these materials have been collected on CCD diffractometers over the course of nearly two years, and the present results are the best that we have obtained. Since Cu(TCNQ) is the subject of much interest and its structural determination has eluded researchers for decades, these data sets, albeit marginal, are important to report. In keeping with the lower resolution of these structures, however, we have limited our discussion to the most important differences in phase I and II; no attempts to base conclusions on fine points of the structures are made.

(a) Cu(TCNQ) phase I.

The structure was partially solved by direct methods and refined in SHELXTL V5.10. The presence of twinning rendered the space group choice very difficult. Solutions were attempted in numerous tetragonal, orthorhombic and monoclinic space groups, but the only reasonable solution was obtained in monoclinic Pn. The pseudo-merohedral twinning matrix [1 0 0, 0 0 1, 0 –1 0] was used in the refinement to represent the pseudo-four-fold symmetry. The structural solution gave two independent Cu(TCNQ) orientations in a ratio of ~50% each. A total of 1111 unique data were refined isotropically on F^2 to *R1* (*wR2*) = 0.232(0.481) but, not surprisingly, the lack of data and other complications led to a slightly unstable refinement. Nevertheless, important features of the relationships within the structure can be gleaned from this very weak data set. The Cu atoms in the structure are coordinated to four nitrogen atoms in a highly distorted tetrahedral environment as evidenced by the N-Cu-N angles of 92° and 142° (Figure 35 and 37). The quinoid rings of the TCNQ units are engaged in interplanar stacking at a distance of 3.24 Å which is less than the van der Waals distance of 3.4 Å for carbon atoms. Adjacent TCNQ stacks are rotated by 90° with respect to each other which is a standard feature in most binary metal/TCNQ salts.[7,34] Powder simulations based on the raw reflection data and on the structure solution are very similar to the experimental powder pattern for the bulk phase I.

(b) Cu(TCNQ) phase II.

Cu(TCNQ) phase II features a new binary metal/TCNQ bonding mode. Other known TCNQ bonding modes including pseudo-tetragonal stacks with alkali metal TCNQ products, Cu(TCNQ) phase I, and Ag(TCNQ). The crystal was found to be a quadruplet twin; this was

resolved by deconvolution methods, and the data were refined in the space group P2/n. A thermal ellipsoid diagram of the asymmetric unit is provided in Figure 36. The N-Cu-N angles around the Cu atom are between 103° to 114.7°, and the average Cu-N bond length is 1.95 Å. The metal geometry is close to tetrahedral, unlike the highly distorted Cu(TCNQ) phase I. Adjacent TCNQ ligands are parallel to each another with the shortest face-to-face contact between nearest neighbors in the same network being 6.8 Å (Figure 38). This arrangement of $TCNQ^{-1}$ ions is unprecedented; typically they are situated around a metal ion as four TCNQ units related by a pseudo-four fold rotational axis such as that found in Ag(TCNQ) and alkali metal TCNQ salts.[7,32]

(c) Comparison of the Cu(TCNQ) polymorphs.

Schematic views of the two structures are depicted in Figure 39. Both phases exhibit polymeric motifs based on the repeat pattern of a four-coordinate Cu ion ligated to nitriles of independent TCNQ molecules. There are two important differences in the structures, however, that lead to entirely different spatial arrangements for the TCNQ units in the two structures. The first difference is the relative orientation of TCNQ moieties around the Cu atoms. In phase I and in all other structures of 1:1 M(TCNQ) compounds including that of Ag and alkali metal salts,[7,35] neighboring TCNQ molecules are rotated 90° with respect to one another as illustrated in Figure 37. Phase II represents a new structural archetype for this type of solid in which infinite arrays of co-planar TCNQ molecules are oriented in the same direction, but in two perpendicular planes as depicted in Figure 38. The second major difference in the two phases is the type of interpenetration that they exhibit. In phase I, the two independent networks bring the TCNQ molecules together to give a columnar stack with the closest distance being

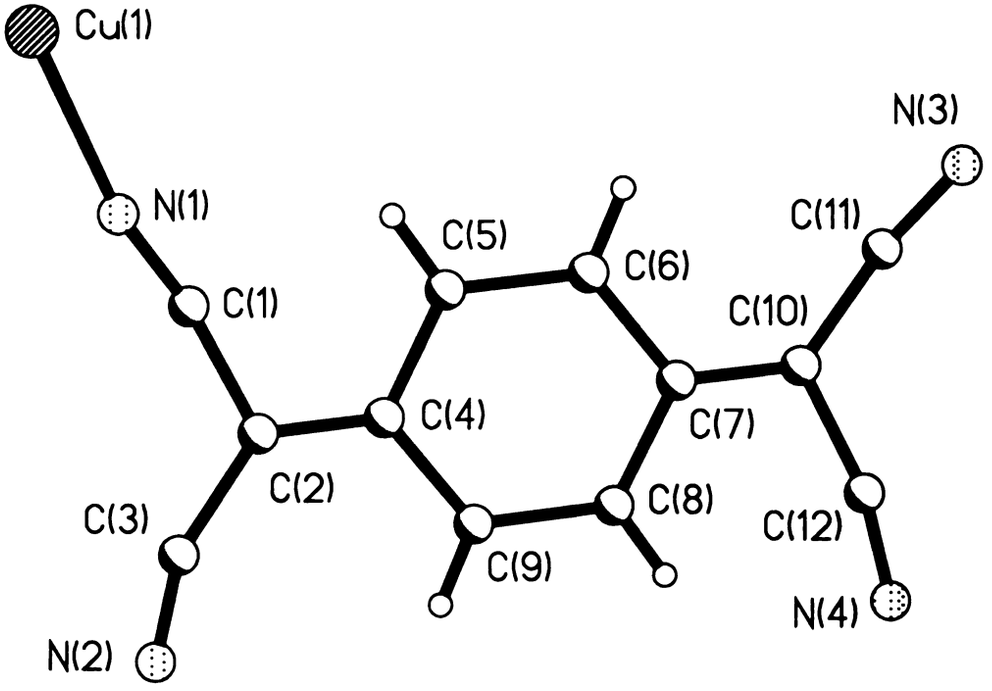


Figure 35. Pluto representation of Cu(TCNQ) phase I.

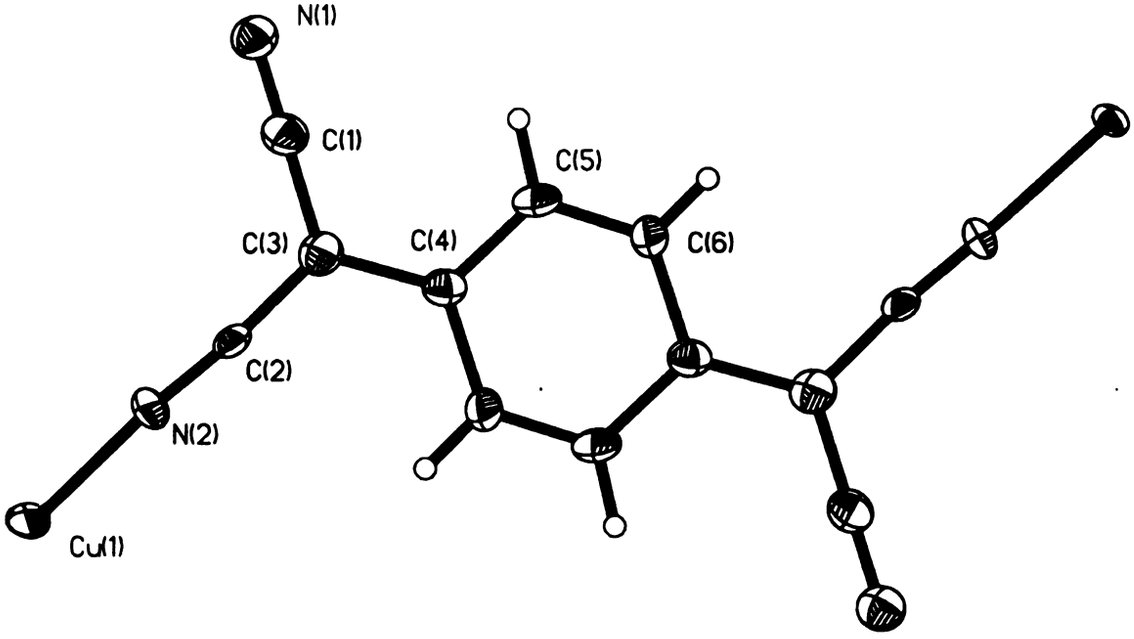


Figure 36. Thermol elipsoid representation of CuTCNQ phase II.

3.24 Å (Figure 37). In sharp contrast, the interpenetration in phase II does not bring the two independent networks together, rather the TCNQ rings are "slipped" and no π-stacking occurs (Figure 38). The closest distance between parallel TCNQ units in the same network is 6.8 Å.

(d) Further structural analysis of Cu(TCNQ) and a comparison to Ag(TCNQ).

At this point, it is instructive to return to the powder patterns for the two Cu(TCNQ) phases and also for the Ag(TCNQ) material that was structurally characterized by Shields.[7] An experimental powder pattern of Cu(TCNQ) phase I is given in (Figure 40) from which it can be observed that there are very few intense features in the high angle region. This is an indication that we are not observing much information about order in the third dimension. The fact that the sample is composed of very thin platelets leads to a preferred orientation which limits the amount of observed data. Since the Cu(TCNQ) phase I exhibits a connectivity reminiscent of Ag(TCNQ), it is important to comment on the fact that their powder patterns are very different. Ag(TCNQ) crystallizes in the orthorhombic space group Pnnm, with a = 6.975(1) Å, b = 16.689(1) Å, c = 17.455(1) Å, V = 2031.5 Å^3.[7] The powder pattern of Ag(TCNQ) simulated from the X-ray data of Shields shown in (Figure 40) is clearly different from that of Cu(TCNQ) phase I. Bulk samples of the Ag(TCNQ) phase (Figure 40) prepared from the reaction between Ag[BF_4] and [^{n}Bu$_4$N][TCNQ] in CH_3CN were found to be identical to the sample used for the X-ray simulation. Interestingly, if the reaction is stopped after only two minutes instead of 3 hours, the higher symmetry phase in Figure 40 is obtained. This new Ag(TCNQ) phase is similar to Cu(TCNQ) phase I in the low angle region; this implies a pseudo-tetragonal cell and a similar connectivity. From its short lifetime, however,

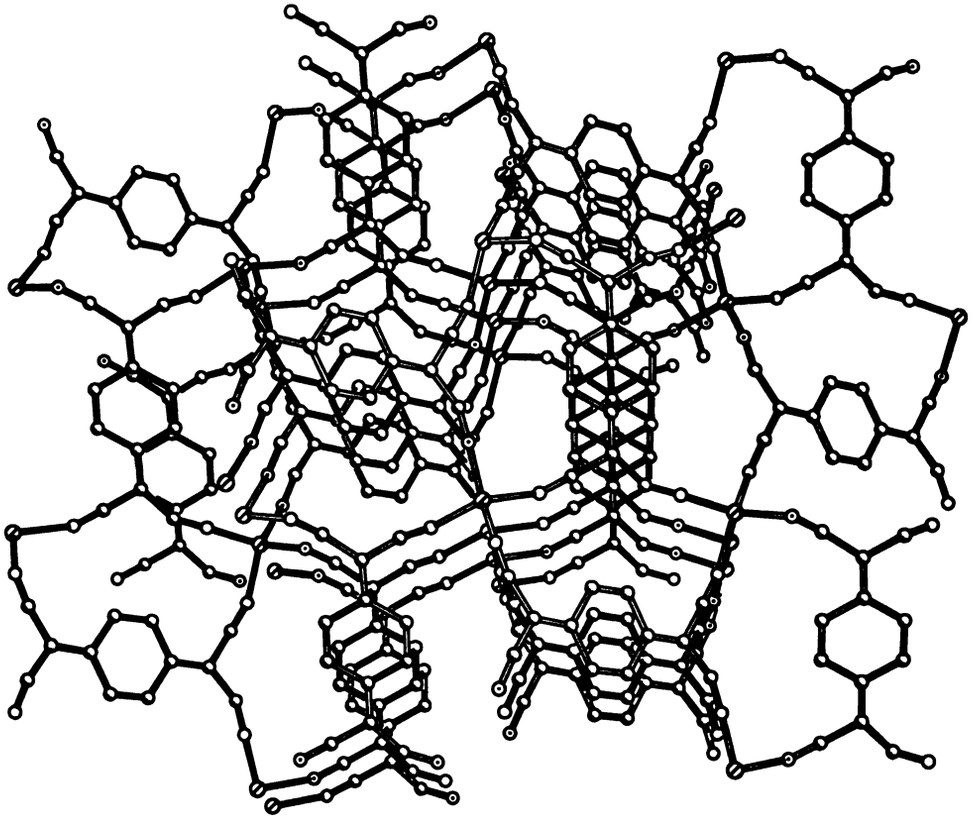


Figure 37. Interpenetrating networks of Cu(TCNQ) phase I features TCNQ stacking between different networks (solid bond -- network 1, holo bond – network 2).

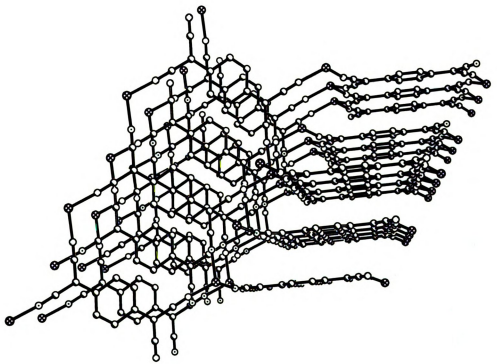


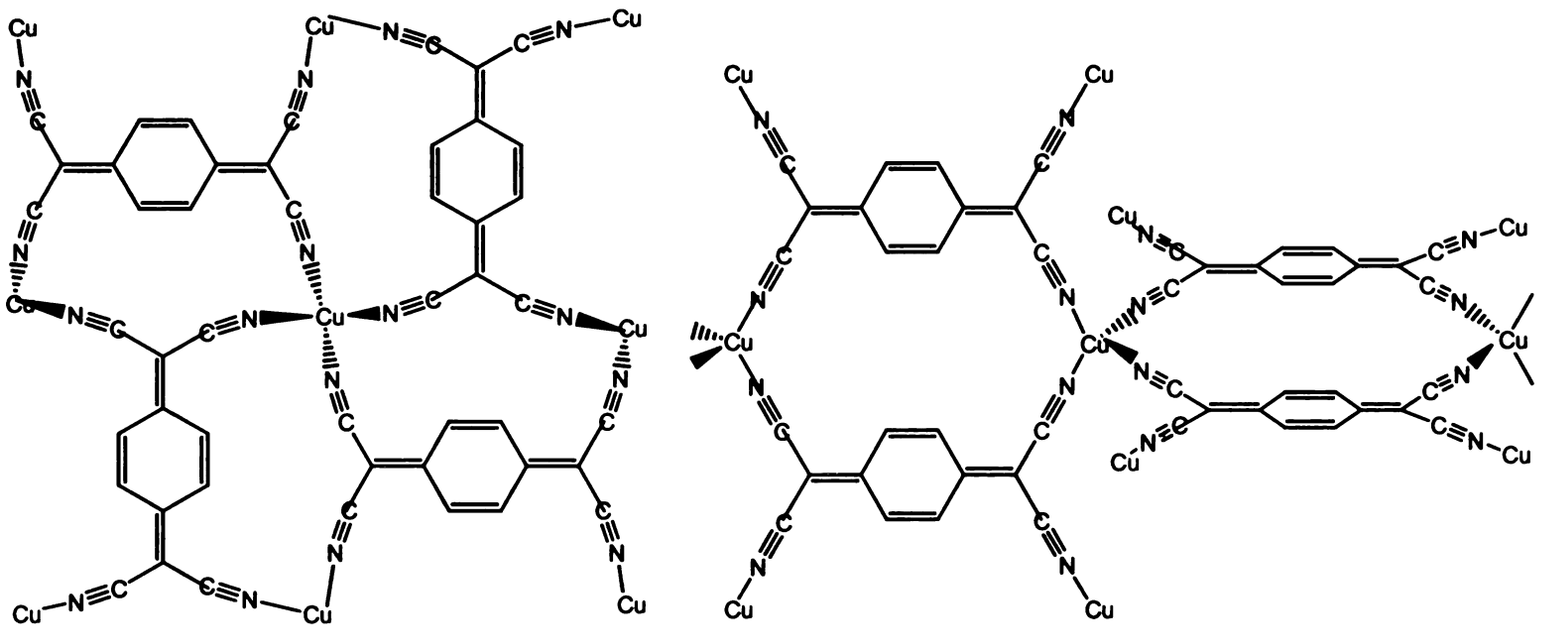
Figure 38. Interpenetrating networks of Cu(TCNQ) phase II. Note that the TCNQ units between different networks are shifted and not π–stacked between different networks (solid bond: network 1, holo bond: network 2).

it is doubtful that it will be possible to obtain this phase of Ag(TCNQ) as larger crystals for single crystal analysis. Interestingly, if one simulates the Ag(TCNQ) powder pattern with the artificially imposed average cell edges $a = b = 17.06$ Å, the lines collapse to a pattern that resembles both the Ag(TCNQ) and Cu(TCNQ) phase I structures (Figures 40).

(2) Crystallographic studies of $M(TCNQ)_2L_x$ phase (x=solvent).

(a) $[Mn(TCNQ)(TCNQ\text{-}TCNQ)_{0.5}(MeOH)_2]_\infty$.

Crystals of this compound exhibit a 2-D zig-zag network of Mn(II) ions coordinated to two different types of TCNQ ligands (Figure 41). The Mn(II) ions are surrounded by four nitrogen and two oxygen atoms from tetradentate μ_4-[TCNQ-TCNQ]$^{2-}$, bidentate *cis*-[μ-TCNQ]$^{-}$ and axial MeOH ligands. The [TCNQ-TCNQ]$^{2-}$ entity has been documented only three previous times, and in these instances, it behaves solely as an outer- sphere anion.[35] In the compound [EtP](TCNQ)$_2$ (EtP = N-ethylphenazinium),[35a] the σ-[(TCNQ-TCNQ]$^{2-}$ dimer contains a long C-C bond of 1.631(5) Å that joins the two rings, whereas in [Pt(bpy)$_2$][TCNQ-TCNQ][35b] and [Cu(DMP)$_2$]$_2$[TCNQ-TCNQ] (DMP = 2,9-dimethyl-1,10-phenanthroline)[35c] the corresponding distances are 1.65(2) Å and 1.630(13) Å. A schematic of the σ-dimerized [(TCNQ)$_2$]$^{2-}$ unit is depicted in Figure 41. These C-C bonds (g1-g1' in Figure 41.) including the one in the current compound of 1.630(13) Å are long, but obviously significant, since the C atoms involved are essentially tetrahedral. The uniformity of the distances in the rings (summarized in Table 19), and the significant lengthening of the C=C bond in the planar exocyclic C=C(C≡N)$_2$ groups in the [TCNQ-TCNQ]$^{2-}$ moiety are indications that there is a main contribution from the aromatic resonance structure depicted in Figure 41. Distances and angles within (TCNQ-TCNQ)$^{2-}$ (Table 19) are similar to those found in another



Cu(TCNQ) Phase I

Cu(TCNQ) Phase II

Figure 39. Schematic diagrams of Cu(TCNQ) phase I and phase II with an emphasis on the geometry of the Cu-N connection.

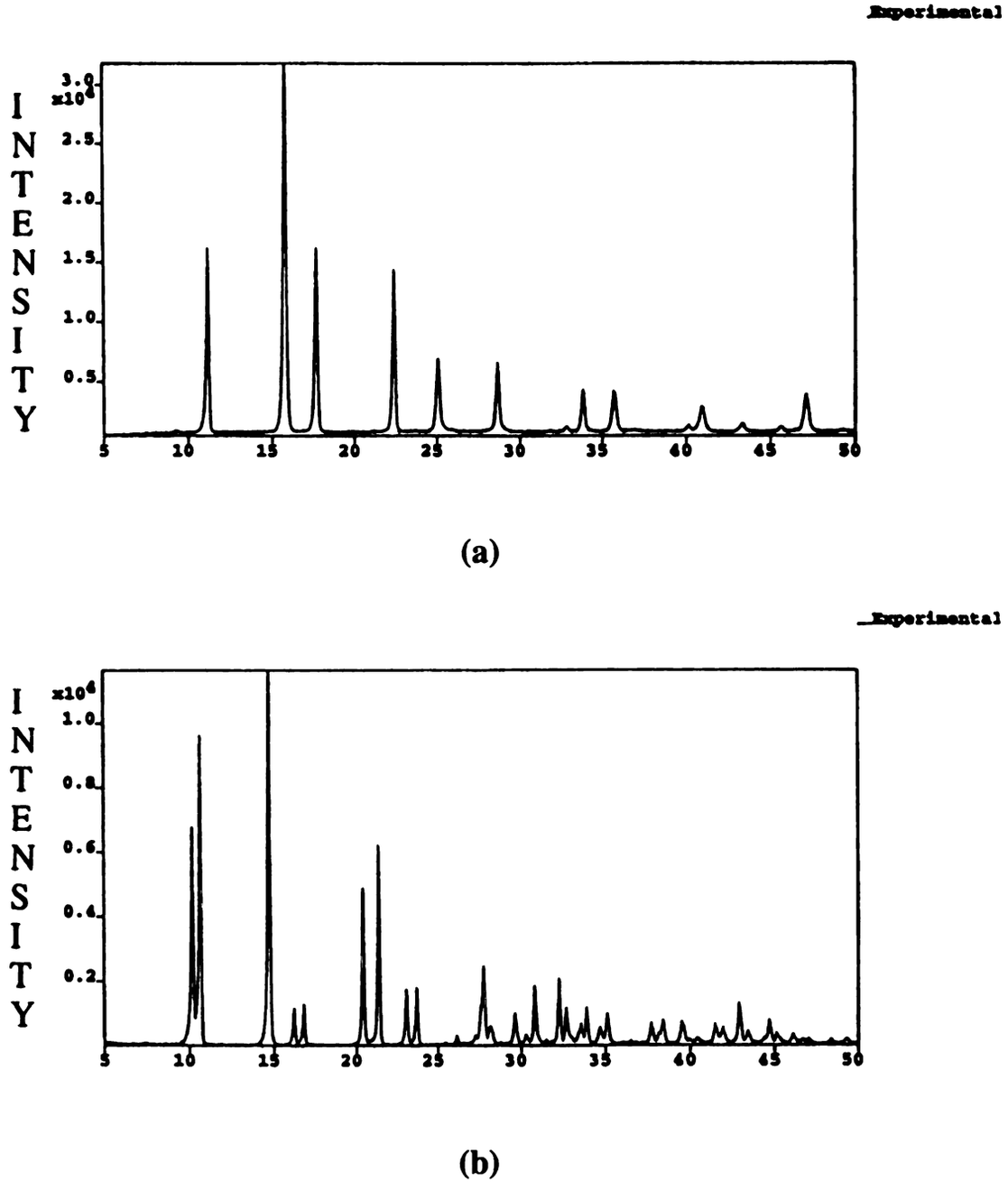


Figure 40. Experimental XRD powder pattern for (a) Cu(TCNQ) phase I and (b) Ag(TCNQ).

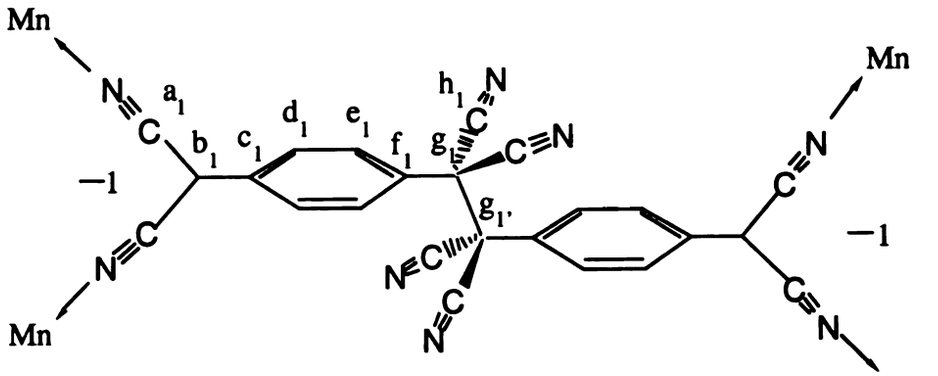
compound recently crystallized in our laboratories, namely [Mn(TCNQ-TCNQ)(MeOH)$_4$]$_\infty$, which also contains a σ-TCNQ dimer with a C-C bond joining the TCNQ units of 1.659(10) Å. The *cis*-[μ-TCNQ]$^-$ molecules act as bridging ligands via 1,2-dicyano positions with the two unligated N≡C-groups pointing outward from the edges of the zig-zag layers towards axial MeOH ligands in adjacent layers to form hydrogen bonds (N3---O2A = 2.834(8) Å and N4---O1A = 2.846(8) Å), Figure 41. The metrical parameters within the bidentate TCNQ^{-1} ligand (Table 19) are in accord with data reported for other structures that contain [TCNQ]$^{\cdot-}$.[4,7] In addition to participating in hydrogen bonding, the *cis*-[μ-TCNQ]$^-$ ligands are engaged in π-stacking interactions of 3.295 Å that serve to stabilize a densely packed, interdigitated arrangement of layers (Figure 41).

(b) [Mn(TCNQ)$_2$(H$_2$O)$_2$]$_\infty$ (10).

Compound (10) represents a new type of TCNQ bonding mode, i.e. syn-μ-TCNQ, which has not been reported before. A thermal ellipsoid diagram of the asymmetric unit in [Mn(TCNQ)$_2$(H$_2$O)$_2$]$_\infty$ is provided in Figure 43, and packing diagrams in the *ab* and *bc* planes are depicted in Figure 54 (b) and (c) respectively. The manganese ions are in a pseudo-octahedral environment consisting of four nitrogen atoms from two *syn*-[μ-TCNQ]$^{\cdot-}$ ligands and two axial H$_2$O molecules. The Mn-N distance of 2.225(2) Å is similar to the corresponding distances observed for the coordinated TCNQ ligands in [Mn(TCNQ)(TCNQ-TCNQ)$_{0.5}$(MeOH)$_2$]$_\infty$, but there are some notable differences (Table 19). The distances within the TCNQ rings are indicative of the resonance structure in Figure 41c. [Mn(TCNQ)$_2$(H$_2$O)$_2$]$_\infty$ contains alternating single and double bonds in the quinoid ring of the TCNQ, whereas in the MeOH containing structure, the bonding in the ring is uniform with charge being localized on the exocyclic

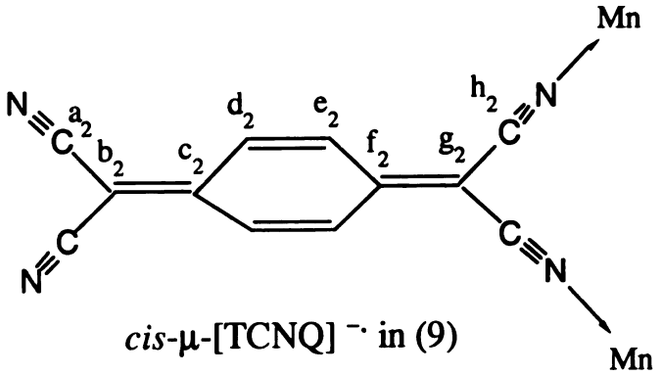
Table 19. Key bond distances(Å) in the TCNQ unit(s) for $[Mn(TCNQ)(TCNQ\text{-}TCNQ)_{0.5}(MeOH)_2]_\infty$ (9) and $[Mn(TCNQ)_2(H_2O)_2]_\infty$ (10) according to diagram in Figure 41.

(9)		(10)	
a1-b1	1.390(10)	a3-b3	1.415(2)
b1-c1	1.459(7)	b3-c3	1.419(2)
c1-d1	1.39(1)	c3-d3	1.429(2)
d1-e1	1.385(8)	d3-e3	1.365(2)
e1-f1	1.38(2)	e3-f3	1.430(2)
f1-g1	1.528(7)	f3-g3	1.419(2)
g1-g1'	1.635(10)	g3-h3	1.417(2)
g1-h1	1.48(2)		
a2-b2	1.401(10)		
b2-c2	1.404(8)		
c2-d2	1.43(2)		
d2-e2	1.365(8)		
e2-f2	1.43(1)		
f2-g2	1.421(7)		
g2-h2	1.407(10)		



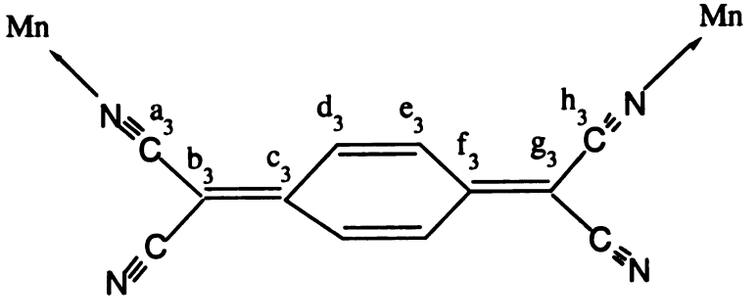
μ^4-[TCNQ-TCNQ] $^{2-}$ σ-dimer in (9)

(a)



cis-μ-[TCNQ] $^{-\cdot}$ in (9)

(b)



syn-μ-[TCNQ] $^{-\cdot}$ in (10)

(c)

Figure 41. Various bond lengths in TCNQ compounds (9), (10).

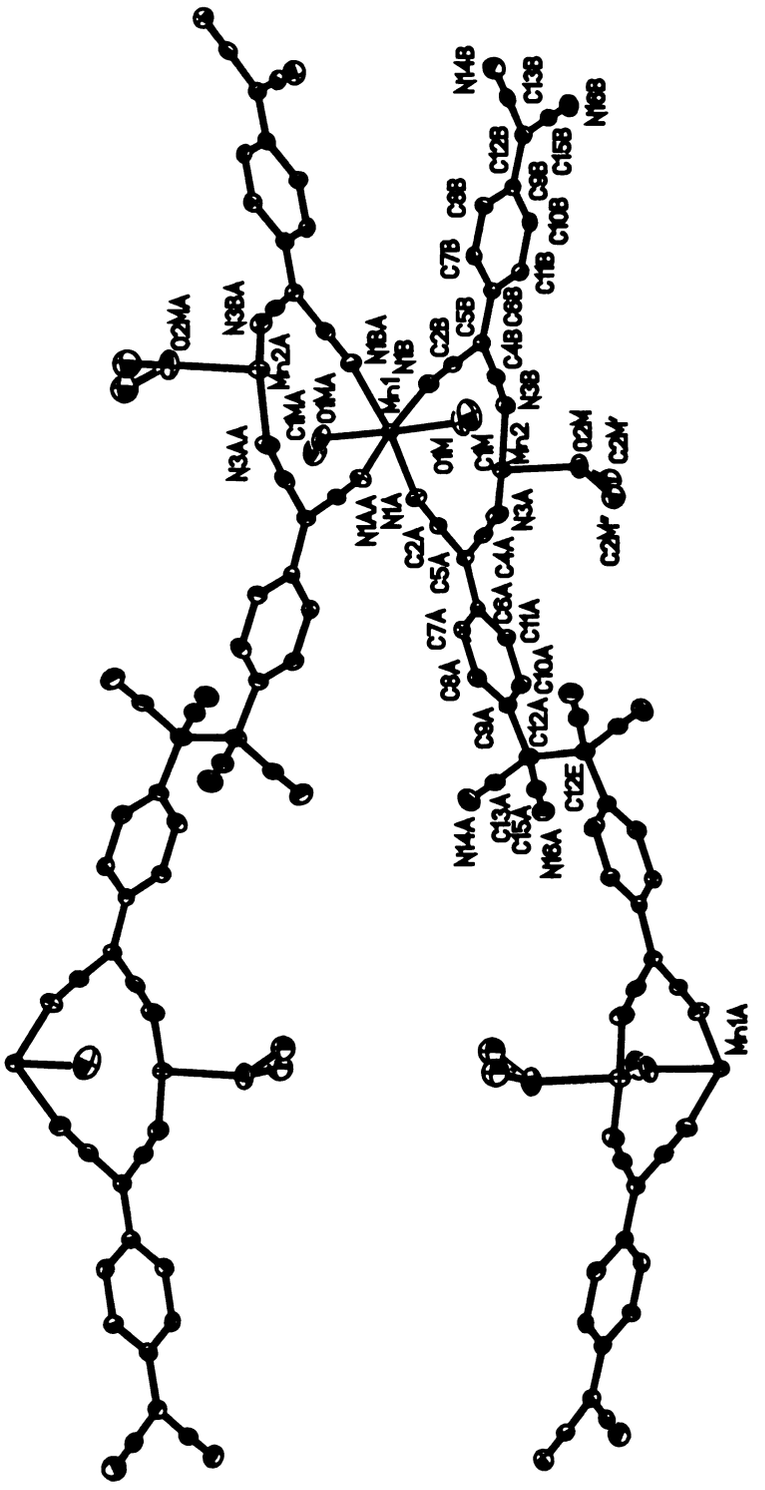


Figure 42. Thermal ellipsoid representation of $[Mn(TCNQ)(TCNQ\text{-}TCNQ)_{0.5}(MeOH)_2]_\infty$ (9).

carbon atom. The extended structure is a 2-D polymeric layered structure with extensive *intra*-layer (3.048(2) Å) and *inter*-layer (~3.3 Å) π-stacking of the $[TCNQ]^{\cdot-}$ radicals. While the latter value is fairly long to be a significant interaction, the 3.048 Å separation between the $[TCNQ]^{-1}$ ligands within the layers is a sign of very strongly coupled π-dimers. Typical ranges for π-$[TCNQ]_2^{2-}$ interactions for selected compounds are provided in Table 19.

(c) Structures of $[^nBu_4N][TCNQ]$ (11) and $[^nBu_4N][TCNQF_4]$ (12) salts.

The structure of (11) is dominated by the packing of the tetrabutylammonium cation rather than the TCNQ anion radical. Two TCNQ anion radicals are related by an inversion center, and form a dimerized divalent anion, which are stacked to a nearly eclipsed pattern (Figure 46). Refinement of the least-squares plane of the dimer revealed the inter-planar distance of the dimer is 3.218(2) Å, which is shorter than the van de Waals distance between aromatic rings. The dimerization of the TCNQ anion radical stabilizes the reactive radical. Important bond lengths and angles are listed in Table 21.

There are two independent $TCNQF_4$ moieties in the asymmetric positions of structure (12). Only one of them is packed in a stacked dimer radical form with the inter-planar distance of 3.206(5) Å. The other pair of $TCNQF_4$ anion are packed together loosely with the inter-planar distance of 3.265(9) Å. The angle between the least-square planes of the two unique dimer pairs is about 70°. Important bond lengths and bond angles of (12) are listed in Table 22.

(d) $\{Zn(H_2O)_4(TCNQ)_3 \cdot 2MeCN\}_\infty$ (13).

The structure of (13) features a Zn(II) cation coordinated to four H_2O

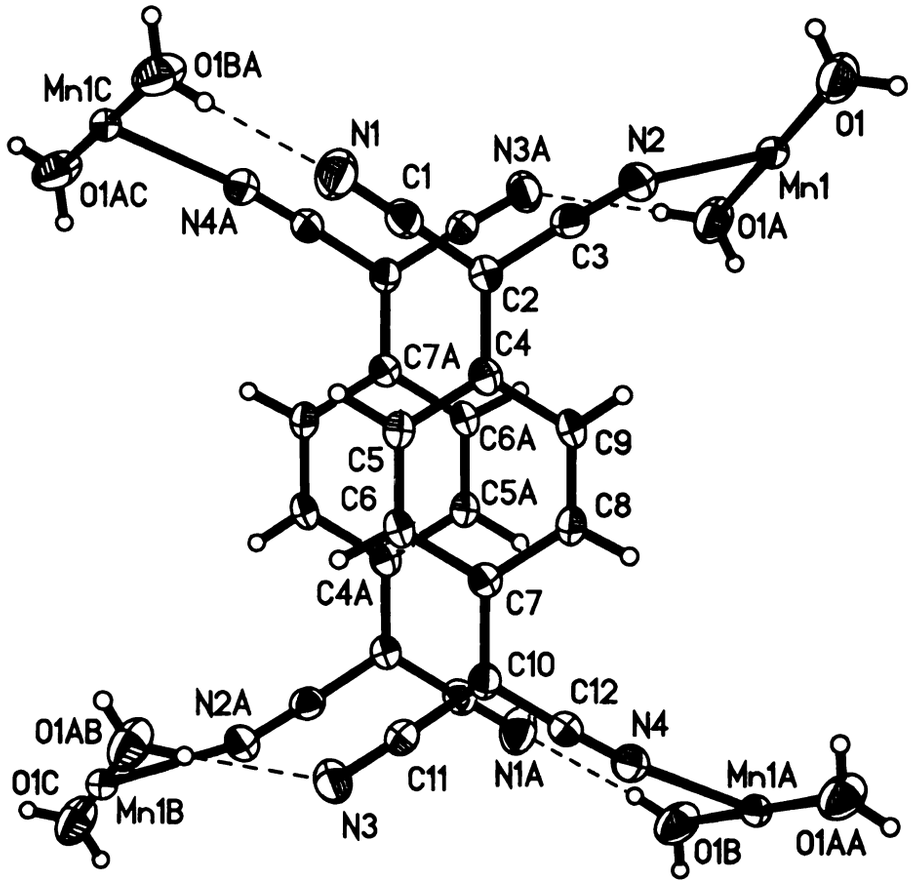


Figure 43. Thermal ellipsoid representation of $Mn(TCNQ)_2(H_2O)_4$ (10).

Ta
[M

O(1)-
N(2)-
O(1)-
N(2)-
C(3
Symm
#1 -x,-
#4 -x+

Table 20. Selected bond lengths [Å] and angles [°] for $[Mn(TCNQ)_2(H_2O)_2]_\infty$ (10).

A-B	Å	A-B	Å
Mn(1)-O(1)	2.1481(18)	C(7)-C(10)	1.419(2)
Mn(1)-N(2)	2.2237(16)	C(2)-C(4)	1.420(3)
Mn(1)-N(4)#2	2.2270(17)	C(5)-C(6)	1.369(2)
N(4)-Mn(1)#4	2.2270(17)	C(8)-C(9)	1.362(3)
N(1)-C(1)	1.148(3)	C(4)-C(5)	1.419(2)
N(2)-C(3)	1.151(2)	C(6)-C(7)	1.419(2)
N(4)-C(12)	1.148(2)	C(4)-C(9)	1.427(3)
N(3)-C(11)	1.151(2)	C(7)-C(8)	1.431(2)
C(10)-C(11)	1.423(2)		
C(10)-C(12)	1.412(3)		
C(1)-C(2)	1.417(3)		
C(2)-C(3)	1.419(3)		

A-B-C	°	A-B-C	°
O(1)-Mn(1)-N(4)#2	88.22(7)	O(1)-Mn(1)-N(2)	90.70(7)
N(2)-Mn(1)-N(4)#2	89.02(6)	O(1)-Mn(1)-N(2)#1	89.30(7)
O(1)-Mn(1)-N(4)#3	91.78(7)	N(1)-C(1)-C(2)	178.2(2)
N(2)-Mn(1)-N(4)#3	90.98(6)	C(1)-C(2)-C(3)	116.57(17)
C(3)-N(2)-Mn(1)	161.59(15)		

Symmetry transformations used to generate equivalent atoms:
#1 -x,-y,-z #2 x-1/2,-y-1/2,z-1/2 #3 -x+1/2,y+1/2,-z+1/2
#4 -x+1/2,y-1/2,-z+1/2

molecules and two η^1-TCNQ molecules in trans-positions. The Zn atom resides on an inversion center. There is one unique TCNQ molecule and two half TCNQ fragments in the asymmetric unit. Both TCNQ fragments are near inversion centers and are stacked in columns. There are two acetonitrile molecules in the interstices. These are hydrogen-bonded to the water molecules. The least-square refinement of the inter-plane distances between TCNQ molecules is ~3.28 Å, (the plane is slightly tilted by ~1.3°). There is one heavy residual peak in the difference map (~ $2e^-/Å^3$) which is located on an inversion center. This peak was modeled as a disordered position of the Zn atom with its coordinated water molecules as a group; the refinement led to a 96.6/3.4 ratio over the two positions. This treatment brought the residual *R1* down to 5.85% from 6.42% for 4230 reflections with $I > 2\sigma$ and the heaviest residual peak in the difference map down from 2.28 to $0.4e^-/Å^3$. A thermal ellipsoid representation of compound (13) is depicted in Figure 49. A packing diagram that shows the TCNQ stacking pattern is depicted in Figure 50.

(e) $[Ni(DMSO)_6][TCNQ]_3$ (14).

Compound (14) is a salt of the DMSO solvated nickel (II) cation with $TCNQ^{-1}$ anion radicals stacked along with neutral TCNQ. The cell volume is close to that of $\{Zn(\eta^1\text{-}TCNQ)_2(H_2O)_4(TCNQ)\bullet 2MeCN\}$ in which columns of $[TCNQ]_3^{2-}$ are dominant the structural framework. The nickel atom, which resides on an inversion center, is bonded to six DMSO ligands. There are one and one-half unique TCNQ moieties in the asymmetric unit. The stacks of TCNQ columns are arranged along the b axis at an inter-planar distance of ~ 3.32 Å, which is essentially the same as the 3.4 Å van der Waal distance for aromatic rings. A PLUTO drawing featuring the TCNQ stacks is shown in Figure 52. The SMe_2 group on one of the DMSO

N

N

C

C

C(

C(

C(

C(

C(6

C(7

C(7

C(8

C(10

C(10

C(13

C(14

Table 21. Bond lengths [Å] and angles [°] for [$^{n}Bu_4N$][TCNQ] (11).

N(1)-C(1)	1.155(3)	C(17)-N(5)-C(13)	108.53(16)
N(2)-C(3)	1.151(3)	C(17)-N(5)-C(25)	111.35(16)
N(3)-C(11)	1.154(3)	C(13)-N(5)-C(25)	108.57(16)
N(4)-C(12)	1.154(3)	C(17)-N(5)-C(21)	108.65(16)
N(5)-C(17)	1.524(3)	C(13)-N(5)-C(21)	112.02(16)
N(5)-C(13)	1.517(3)	C(25)-N(5)-C(21)	107.75(16)
N(5)-C(25)	1.525(3)	N(1)-C(1)-C(2)	177.8(3)
N(5)-C(21)	1.528(3)	C(4)-C(2)-C(1)	122.3(2)
C(1)-C(2)	1.419(3)	C(4)-C(2)-C(3)	120.9(2)
C(2)-C(4)	1.418(3)	C(1)-C(2)-C(3)	116.33(19)
C(2)-C(3)	1.424(3)	N(2)-C(3)-C(2)	179.9(3)
C(4)-C(9)	1.419(3)	C(9)-C(4)-C(2)	121.43(19)
C(4)-C(5)	1.419(3)	C(9)-C(4)-C(5)	116.8(2)
C(5)-C(6)	1.363(3)	C(2)-C(4)-C(5)	121.8(2)
C(6)-C(7)	1.412(3)	C(6)-C(5)-C(4)	121.4(2)
C(7)-C(10)	1.420(3)	C(5)-C(6)-C(7)	121.9(2)
C(7)-C(8)	1.422(3)	C(6)-C(7)-C(10)	121.7(2)
C(8)-C(9)	1.363(3)	C(6)-C(7)-C(8)	116.93(19)
C(10)-C(11)	1.415(3)	C(10)-C(7)-C(8)	121.3(2)
C(10)-C(12)	1.419(3)	C(9)-C(8)-C(7)	121.3(2)
C(13)-C(14)	1.519(3)	C(8)-C(9)-C(4)	121.7(2)
C(14)-C(15)	1.524(3)	C(11)-C(10)-C(7)	121.7(2)

Ta

F(4

F(2

F(3

F(1

N(1

C(3

C(1

C(1

C(8

C(8

F(4)

F(4)-

F(1)-

F(1)-

F(3)-

F(3)-(

F(2)-(

C(9)-(

C(9)-(

C(9)-(

Table 22. Bond lengths [Å] and angles [°] for [^{n}Bu$_4$N][TCNQF$_4$] (12).

Bond length			
F(4)-C(8)	1.345(4)	C(4)-C(9)	1.409(5)
F(2)-C(6)	1.358(4)	C(4)-C(2)	1.416(5)
F(3)-C(9)	1.351(4)	C(4)-C(5)	1.418(5)
F(1)-C(5)	1.340(4)	C(7)-C(6)	1.407(5)
N(1)-C(1)	1.155(5)	C(7)-C(10)	1.416(5)
C(3)-N(2)	1.155(5)	F(5)-C(17)	1.340(4)
C(11)-N(3)	1.144(4)	F(6)-C(18)	1.346(4)
C(12)-N(4)	1.144(5)	F(7)-C(21)	1.354(5)
C(8)-C(9)	1.356(5)	F(8)-C(20)	1.358(5)
C(8)-C(7)	1.421(5)		
Bond angle			
F(4)-C(8)-C(9)	118.1(3)	N(2)-C(3)-C(2)	176.8(4)
F(4)-C(8)-C(7)	118.3(3)	N(1)-C(1)-C(2)	176.8(4)
F(1)-C(5)-C(6)	118.0(3)	N(4)-C(12)-C(10)	174.6(4)
F(1)-C(5)-C(4)	118.6(3)	C(2)-C(4)-C(5)	123.2(3)
F(3)-C(9)-C(8)	117.3(3)	C(6)-C(7)-C(10)	124.0(3)
F(3)-C(9)-C(4)	119.0(3)	C(8)-C(9)-C(4)	123.7(3)
F(2)-C(6)-C(7)	118.8(3)	C(6)-C(7)-C(8)	112.3(3)
C(9)-C(8)-C(7)	123.6(3)	C(10)-C(7)-C(8)	123.7(3)
C(9)-C(4)-C(2)	124.1(3)	C(6)-C(5)-C(4)	123.4(3)
C(9)-C(4)-C(5)	112.7(3)		

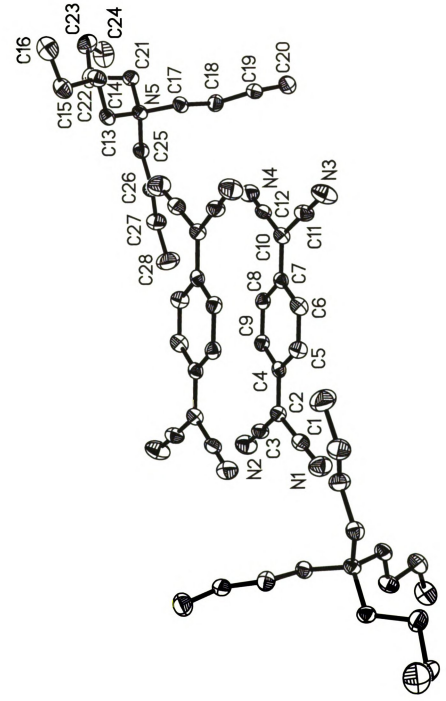


Figure 44. Thermal ellipsoid representation of [^{n}Bu$_4$N][TCNQ] (11).



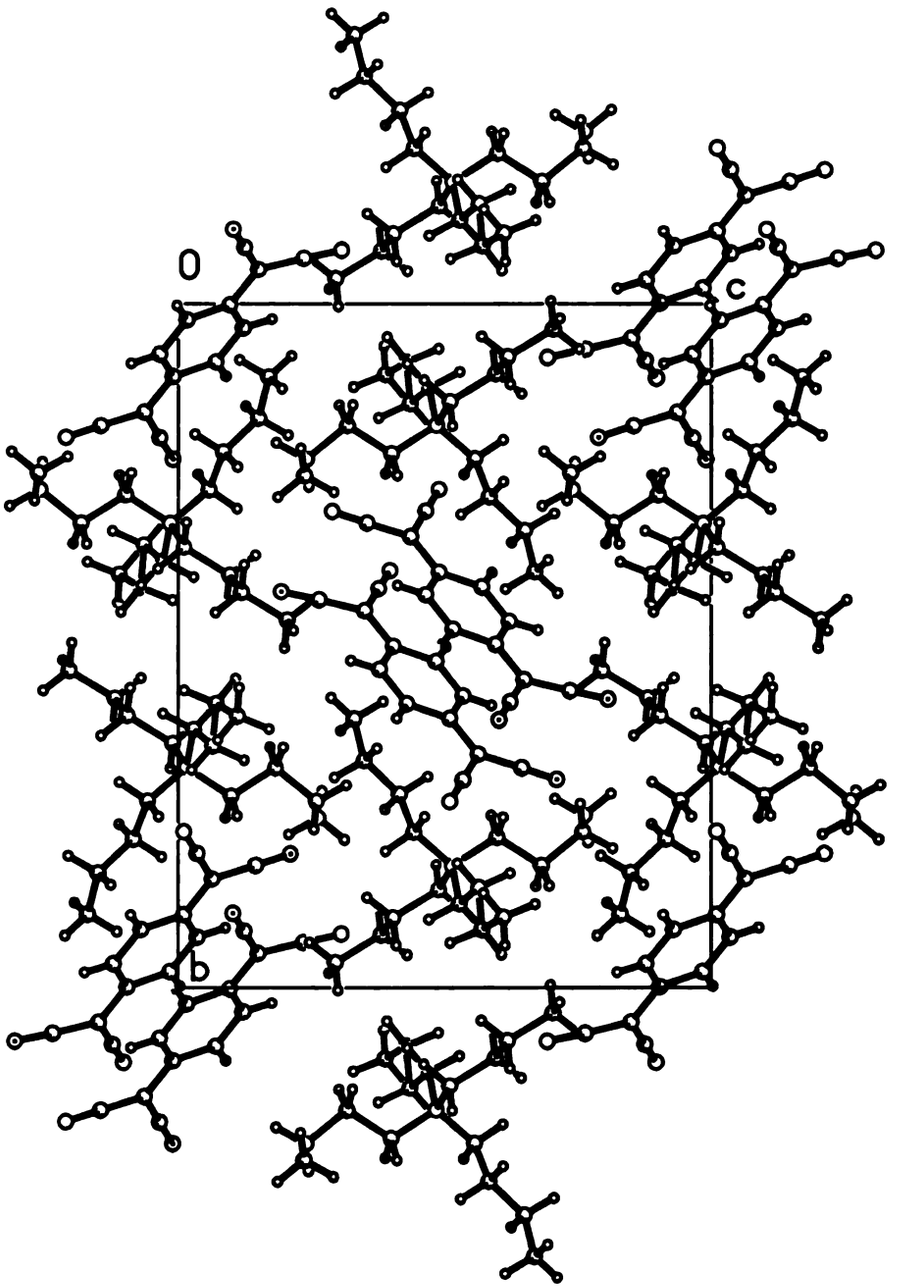
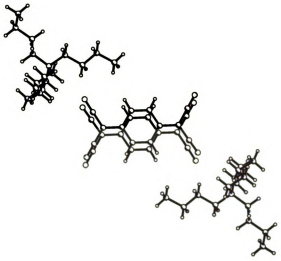
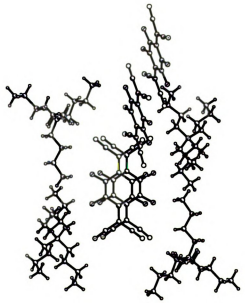


Figure 45. Packing diagram of [^{n}Bu$_4$N][TCNQ] (11) along the *a* axis.

Figur
eclips



(a)



(b)

Figure 46. (a)The dimer radical pair of $(TCNQ)_2]^{2-}$packed in a nearly eclipsed pattern in (11). (b) The two dimer pairs of (12).

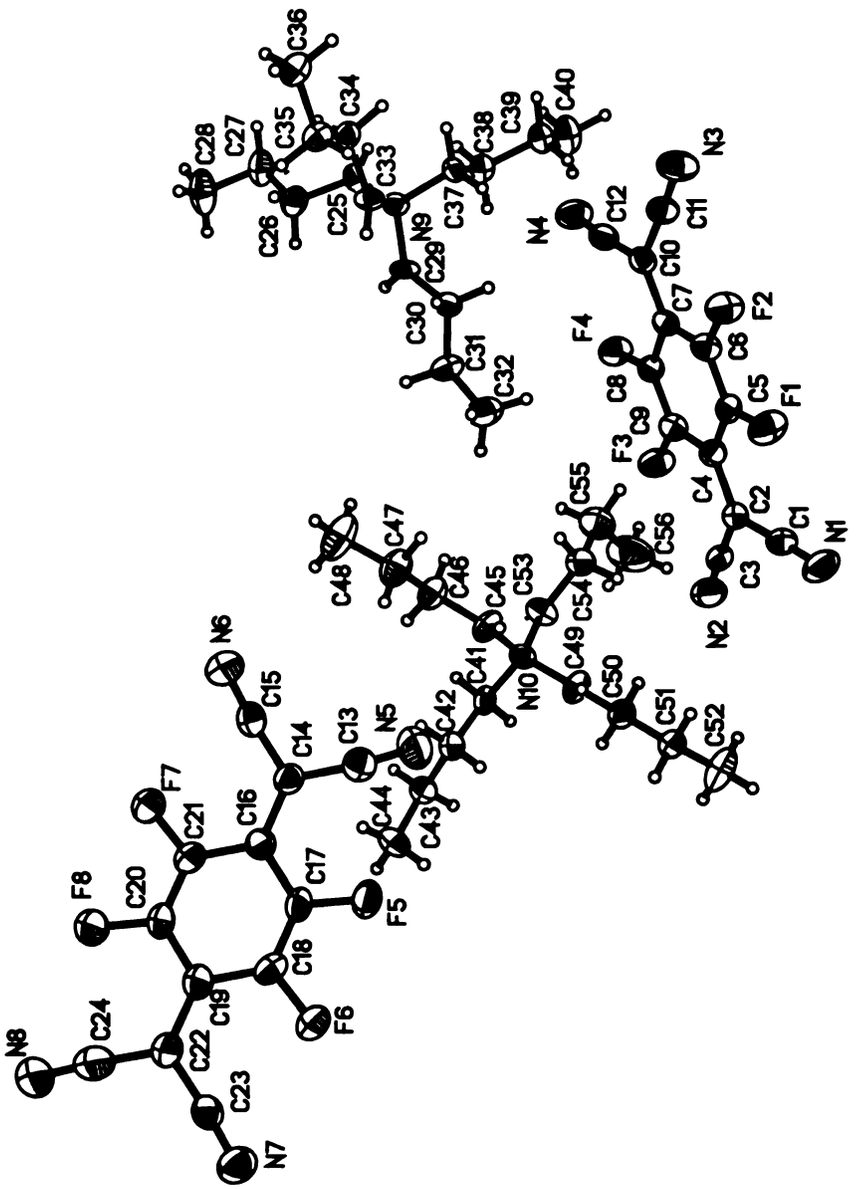


Figure 47. Thermal ellipsoid representation of [^{n}Bu$_4$N][TCNQF$_4$] (12).

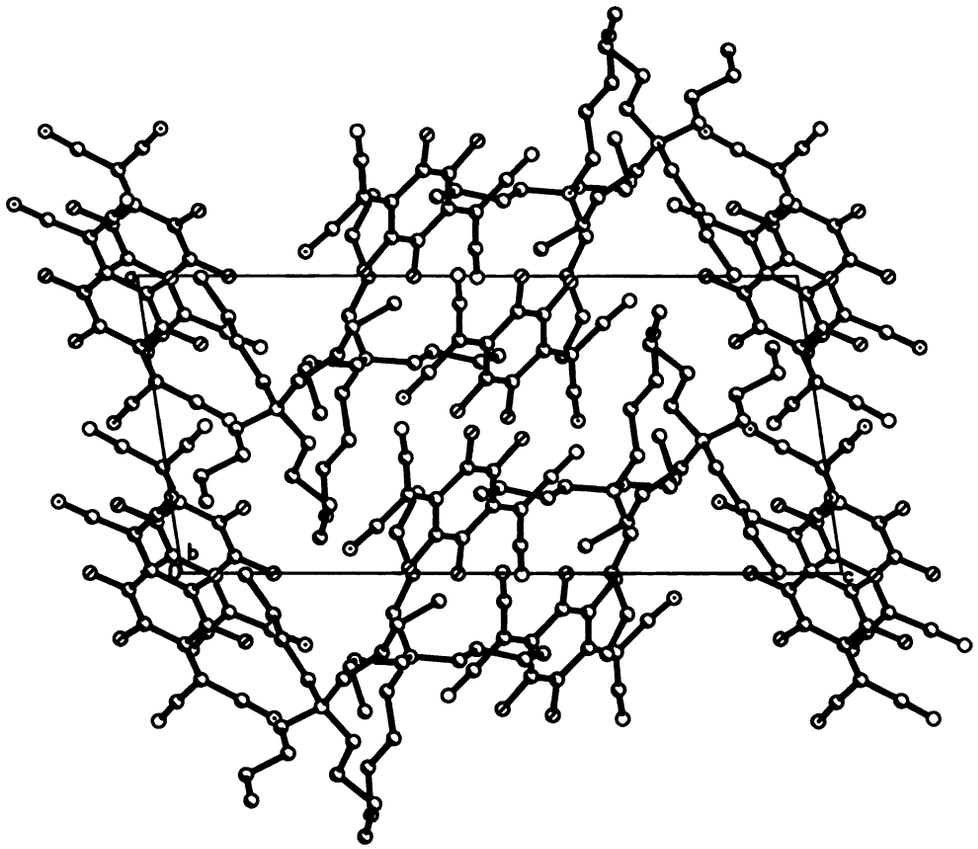


Figure 48. Packing diagram of $[Bu_4N][TCNQF_4]$ (12) viewed down *b* axis shows both the stacking $TCNQF_4$ dimer and the loosely packed dimer.

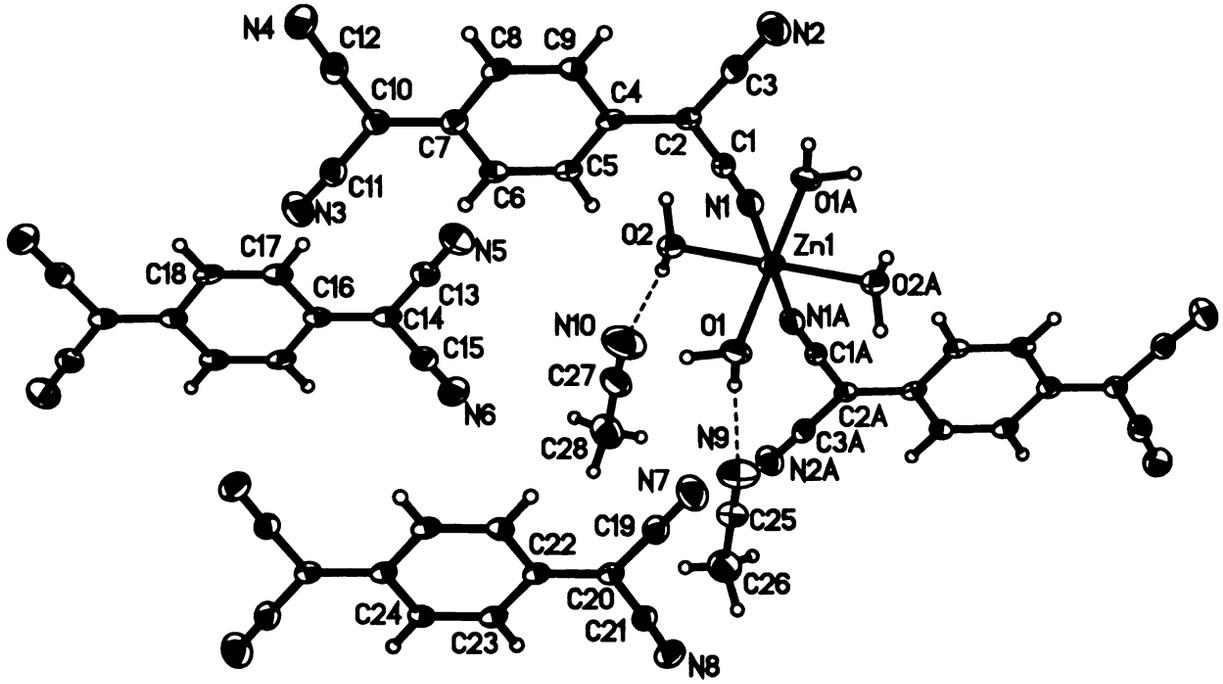


Figure 49. Thermal ellipsoid representation of $\{Zn(\eta^1\text{-TCNQ})_2(H_2O)_4(TCNQ)\bullet 2MeCN\}_\infty$ (13•2MeCN).

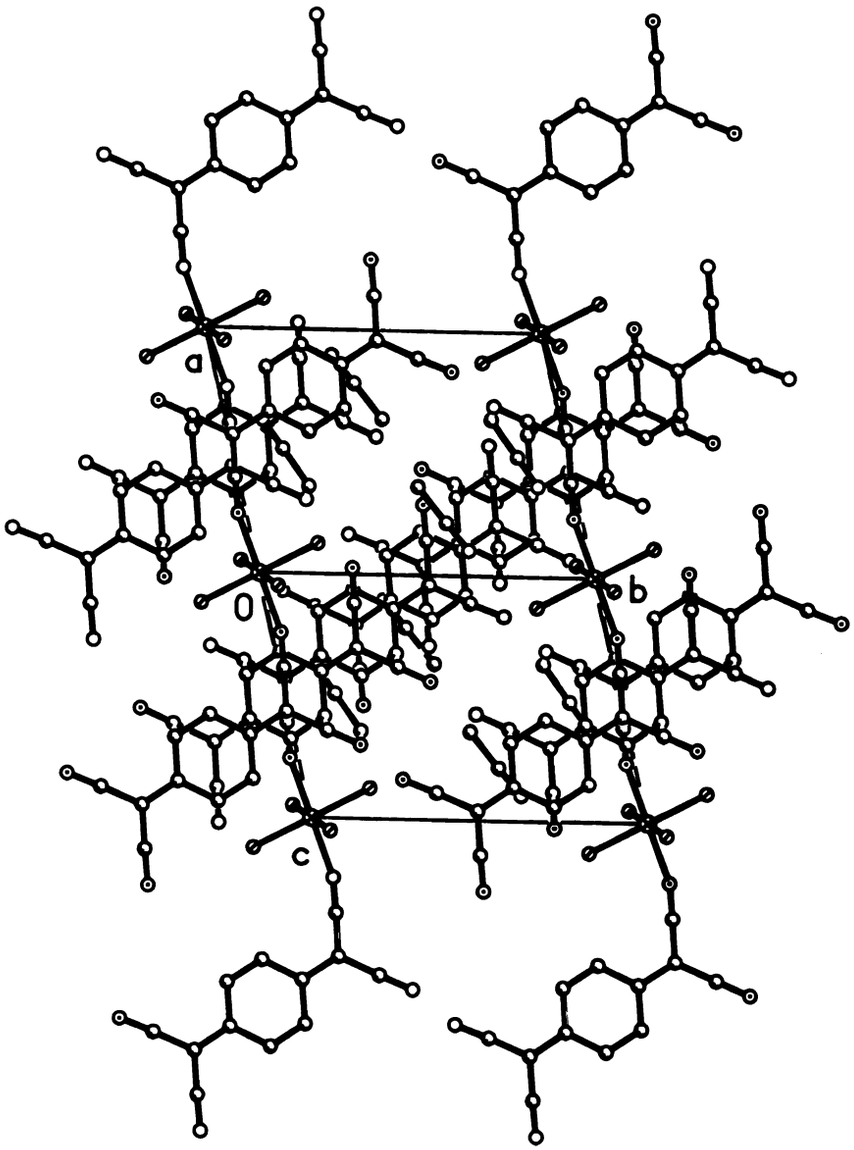


Figure 50. Packing diagram of (13) along the [1 0 1] plane emphasizes the TCNQ stacking pattern.

Figu

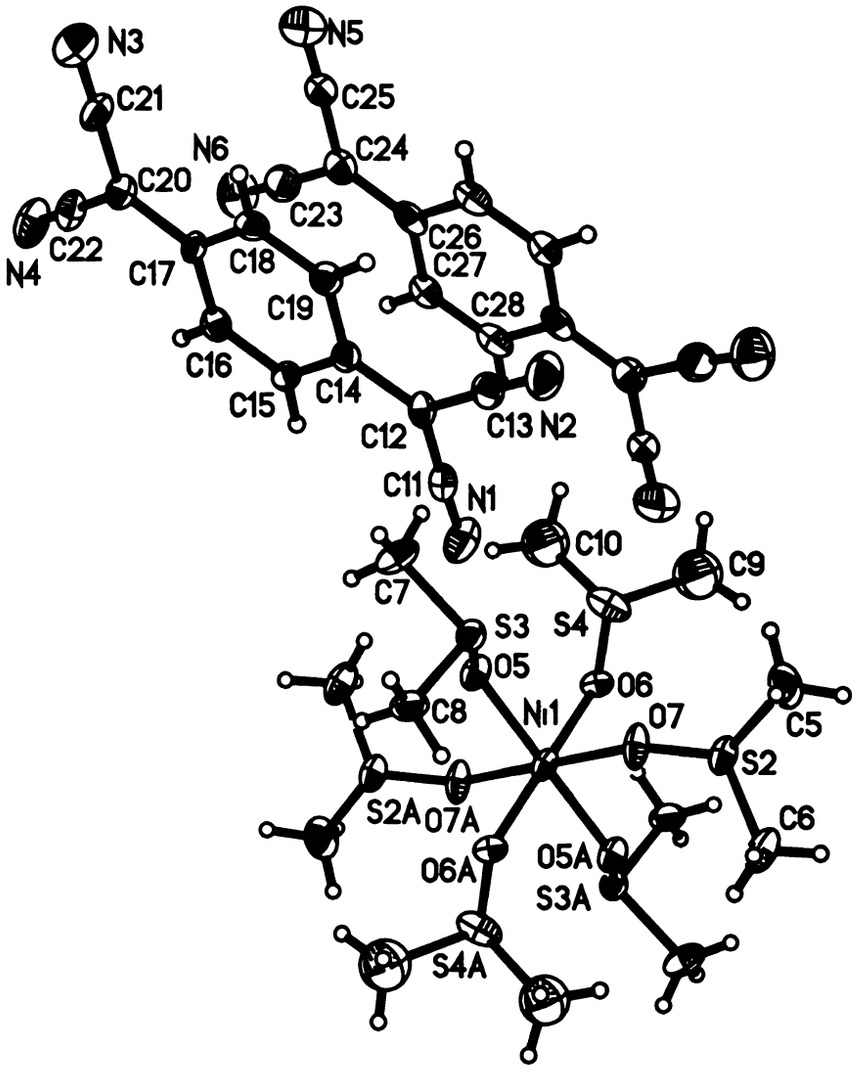


Figure 51. Thermal ellipsoid representation of $[Ni(DMSO)_6][TCNQ]_3$ (14).

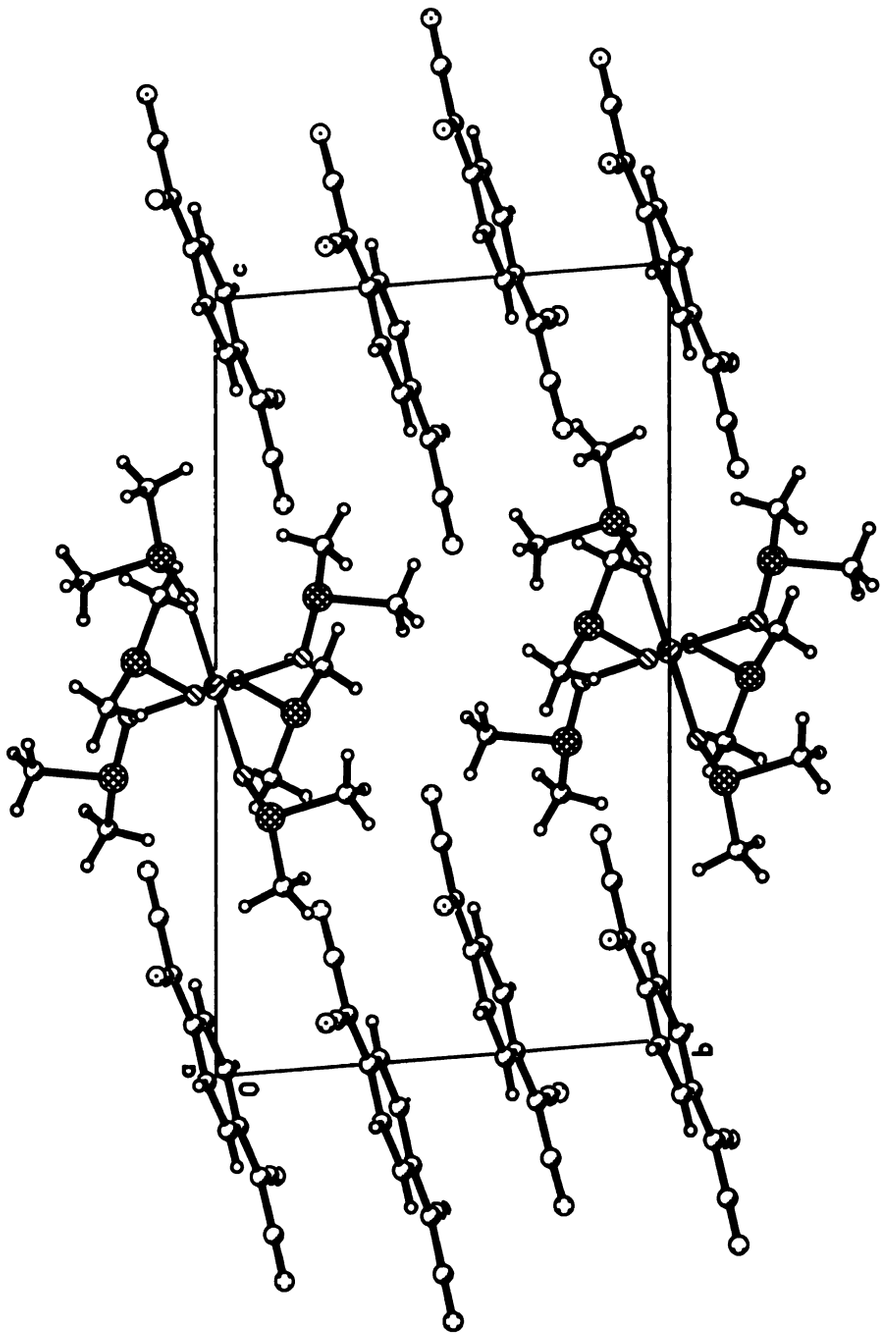


Figure 52. Packing diagram of (14) viewed down a axis showing TCNQ stacking column.

mc

iso

dra

(f)

dep

nic

this

ato

nic

sup

in t

faul

elec

(3)

(a)

term

radi

the

tran

bon

than

quin

TCN

carb

molecules is disordered over three positions, which were modeled and isotropically refined to a ratio of 65.7/22.8/11.2. A thermal ellipsoid drawing of (14) is depicted in Figure 51.

(f) $Ni(TCNQ)_2(H_2O)$ (15).

Compound (15) was solved by a disorder model. A plot of (15) is depicted in Figure 53. The residual *R1* is relatively low, given that only the nickel atom is refined anisotropically, but there are still major problems with this model. The elongated ellipsoid of nickel atom indicates that the nickel atom probably posited at the average position of the real solution, which nickel atoms could be disordered. The other possibility is that there is a superlattice problem. We suspect that there is a lack of long range ordering in the *c* direction (TCNQ-stacking direction) which is known a stacking fault. Further studies are needed to address these issues, for example electron diffraction could be very useful in helping to identify the problem.

(3) TCNQ bonding modes in various TCNQ containing compounds.

(a) Ring interactions and physical properties.

TCNQ exhibits several types of bonding and stacking modes.[36] In terms of the stacking and connection style of the quinoid structure, TCNQ radical anions can stack as π-dimers, σ-dimers or as π-columns. In terms of the linkage of the TCNQ ligand to metal centers can be η^1-σ-bonded (14), σ-trans-μ-bonded (5), σ-cis-μ-bonded (9), σ-syn-μ-bonded (10) and σ-μ^4-bonded (7), (8). When the π-stacking distance of the TCNQ rings is shorter than the 3.4 Å van der Waal distance for aromatic rings, the two TCNQ quinoid rings are considered to be strongly interacting. The σ-dimer of TCNQ is the extreme case of an interaction in which two the quinoid carbon atoms are actually linked by a weak σ-bond. When the π-stacking

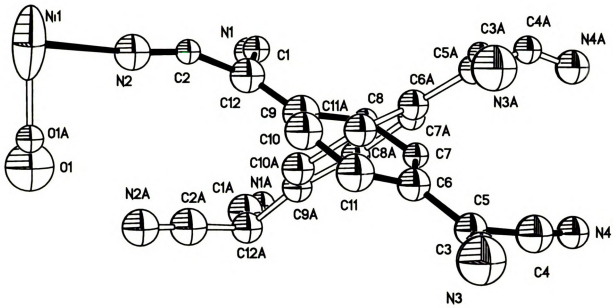


Figure 53. Superimposed thermal ellipsoid representations of $[Ni(TCNQ)_2(H_2O)]_\infty$ (15) depicting the disorder modeling of (15).

distance is longer than 3.4 Å, the interaction between TCNQ rings is weak, and, although this weak stacking is crucial for holding the structure together, it is not significant for enhancing magnetic interactions or engendering electrical conductivity.

(b) Hydrogen bonding and weak interactions.

Hydrogen bonding networks are an important feature of many supramoleculear architectures. In binary metal TCNQ coordination polymers crystallized from protonic solvents, hydrogen bonding also plays an important role in the packing. Figure 55 shows the hydrogen network found in compound (9) in which hydrogen bonding from the methanol ligand helps to stabilize the $(\pi\text{-TCNQ})_2^{2-}$ dimer anion.

(c) Bond length relationship and the degree of charge transfer in the TCNQ ligand.

The bond lengths in the TCNQ quinoid ring are sensitive to the degree of charge transfer between the cations and the TCNQ anions. Several methods have been used in the literature to correlate the degree of charge transfer to the bond lengths in outer-sphere TCNQ molecules. These are not especially helpful, however when TCNQ is acting as a ligand, as different binding modes also contribute to the bond length differences in the quinoid rings. Table 19 summarizes examples of different kinds of TCNQ ligands in the Mn/TCNQ MeOH and H_2O structures.

E. Magnetic Measurements.

(1) Cu(TCNQ) phases.

The discovery that Cu(TCNQ) exists as two different structural types is actually not surprising, as numerous TCNQ materials are known to exhibit several different phases with the same chemical composition.[6,37] What is

Table 23. *Stacking interactions for $TCNQ^{-1}$ units in selected structures*

Table 23. Stacking interactions for $TCNQ^{-1}$ units in selected structures.

Compound	Inter-planar distance(Å)	binding mode	stacking mode
$[^nBu_4N][TCNQ]$	3.218(2)	uncoordinated	eclipsed dimer
Rb(TCNQ)	3.16	uncoordinated	column
$(TTP)(TCNQ)_2$	3.22	uncoordinated	dimer
$[Cu(abpt)_2(TCNQ)_2]$	3.22	monodentate	
[Cu(pdto)(TCNQ)]	3.12	bidentate	
$NiL^R(TCNQ)_2]$	3.25	monodentate	
$[Mn(tpa)(TCNQ)(MeOH)](TCNQ)_2MeCN$	3.05, 3.60	monodentate	
$[Mn(TCNQ)(TCNQ\text{-}TCNQ)_{0.5}(MeOH)_2]_\infty$		cis-bidentate	
$[Mn(TCNQ)_2(H_2O)_2]_\infty$	3.1, 3.6*	syn-bidentate	ring-ring,
$[^nBu_4N][TCNQF_4]$	3.206(5)	uncoordinated	ring-external bond

* intralayer and interlayer stacking distances respectively

Table 24. Hydrogen bonds (with esds except for fixed and riding atoms) for $[Mn(TCNQ)_2(H_2O)_2]_\infty$ (10).

D-H	H...A	D...A	<(DHA)	
0.81(3)	2.09(3)	2.896(2)	169(3)	O1-H1W...N3
0.77(4)	2.06(4)	2.819(3)	170(3)	O1-H2W...N1

Table 25. Hydrogen bonds (with esds except for fixed and riding atoms) for $[Mn(TCNQ)(TCNQ\text{-}TCNQ)_{0.5}(MeOH)_2]_\infty$ (9).

D-H	H...A	D...A	<(DHA)	
0.84	1.98	2.822(4)	178.1	O1M-H1M...N16B
0.84	2.04	2.863(4)	166.3	O2M-H2M_a...N14B

Table 26. Hydrogen bonds (with esds except for fixed and riding atoms) for $[Zn(H_2O)_4(\eta^1\text{-}TCNQ)_2 \bullet TCNQ \bullet 2MeCN]_\infty$ (13).

D-H	H...A	D...A	<(DHA)	
0.84	1.99	2.820(4)	167.6	O1_a-H1X_a...N9_a
0.96	2.18	3.057(4)	152.6	O1_a-H1Y_a...N3
0.84	2.02	2.818(4)	159.6	O2_a-H2X_a...N10_a
0.95	2.06	2.931(4)	151.2	O2_a-H2Y_a...N8

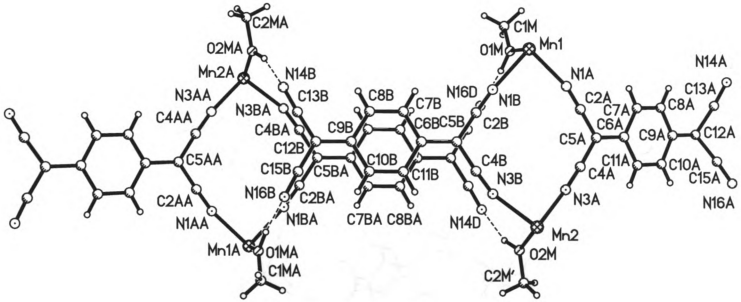


Figure 54. Pluto representation of the $[(TCNQ)_2]^{2-}$ unit in (9) and the hydrogen bonding scheme.

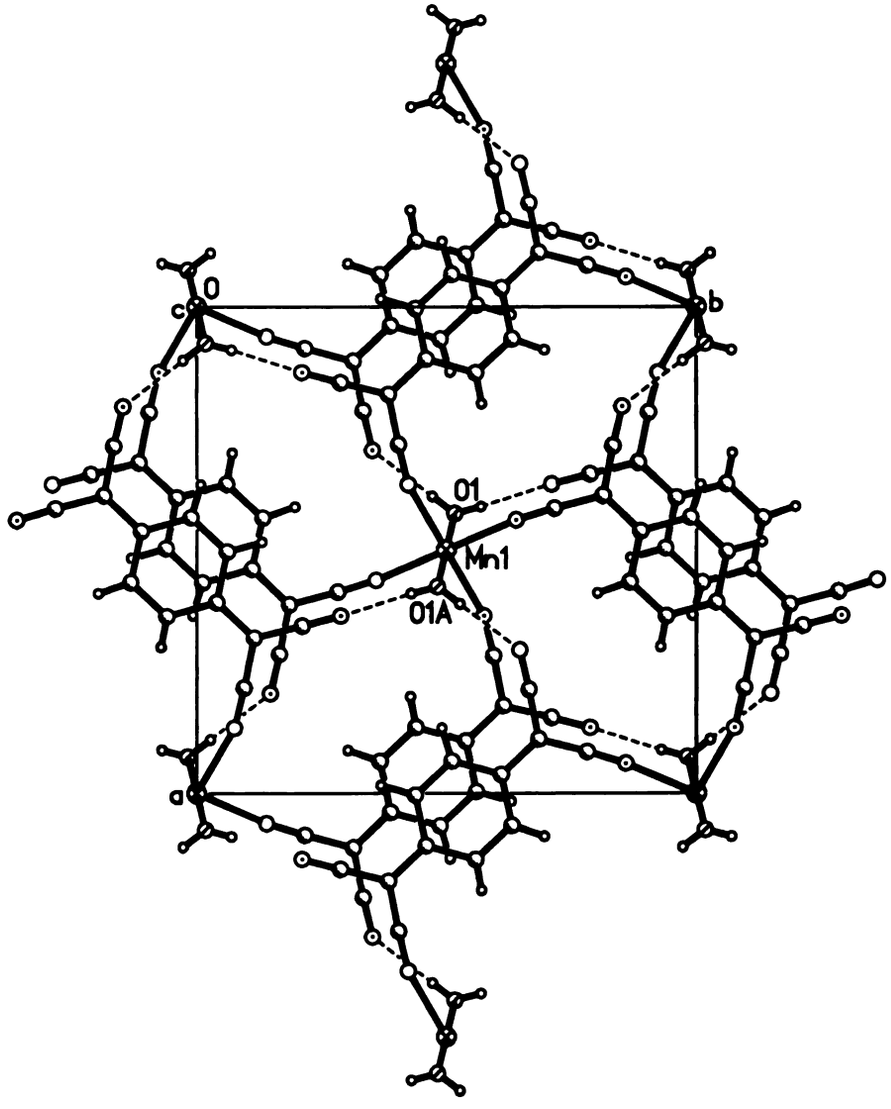


Figure 55. Extended hydrogen bonding networks in $[Mn(TCNQ)_2(H_2O)_4]_\infty$ (10)

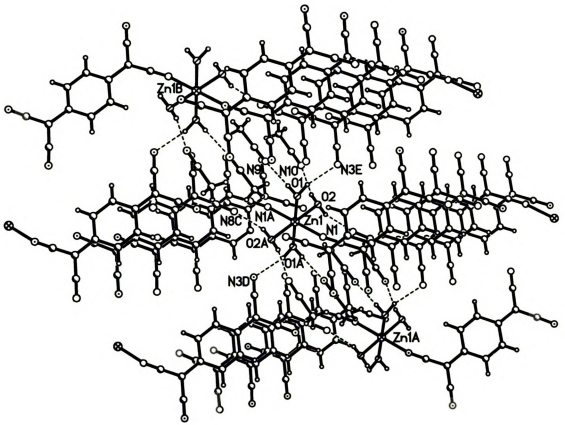
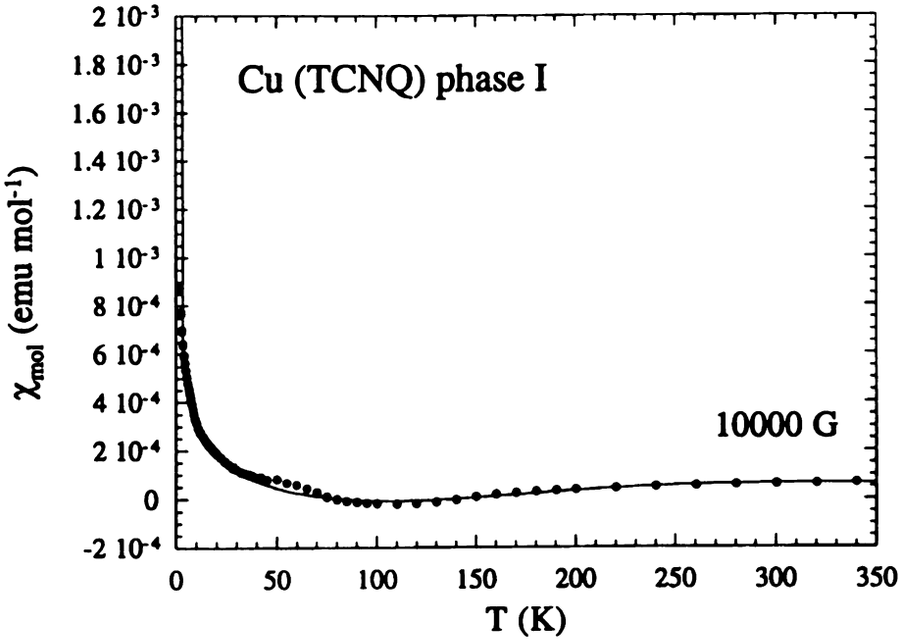


Figure 56. Hydrogen bonding networks in $[Zn(\eta^1\text{-}TCNQ)_2(H_2O)_4(TCNQ) \cdot 2MeCN]_\infty$ (13).

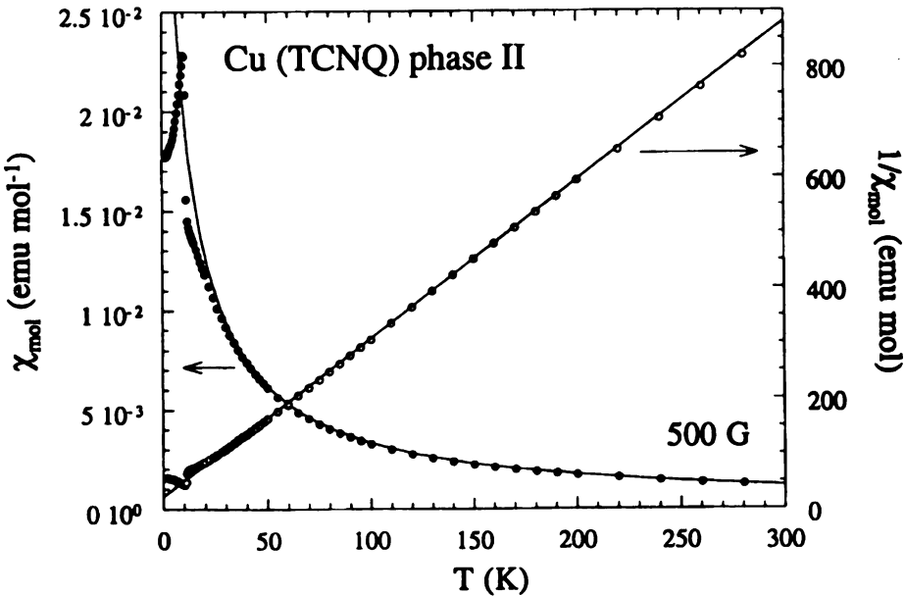
important about this observation, however, are the ramifications that it has in terms of the observed properties of various samples of Cu(TCNQ), especially conductivity and magnetic coupling. The variable temperature magnetic susceptibilities of the samples were measured by the SQUID technique. Plots of χ versus T and μ_{eff} versus T are given in Figures 57 and 58. Phase I shows behavior typical of a TCNQ radical anion salt with TCNQ stacking *viz.*, strong coupling of the unpaired spins. Most simple TCNQ radical anion salts are paramagnetic, but the susceptibilities are only about 10% of that expected for a system with non-interacting spins.[37] The very low susceptibility of phase I (Figure 57) indicates considerable magnetic coupling of the unpaired electrons which renders the sample essentially diamagnetic. This is consistent with early studies on the magnetism of chemically prepared Cu(TCNQ).[38] In phase II, on the other hand, the $TCNQ^{-1}$ radicals behave like isolated paramagnets in the high temperature regime; in fact the μ_{eff} of 1.58 B.M. at 320 K is very close to that of the spin only value for an isolated S = 1/2 system (Figure 57). At low temperatures the effective magnetic moment for phase II begins to slowly decrease, indicating the onset of weak antiferromagnetic interactions between the unpaired spins which at 10 K abruptly changes to an ordering of the ferromagnetic type. In support of an ordering are the results of the zero-field cooled and field-cooled experiments (Figure 58c) and the hysteresis loop observed at 2 K with a coercive field of 500 Gauss (Figure 58d).

(2) Mn samples.

Temperature dependent magnetic susceptibilities (χ) for $[Mn(TCNQ)_2(H_2O)_2]_\infty$ and $[Mn(TCNQ)(TCNQ\text{-}TCNQ)_{0.5}(MeOH)_2]_\infty$ were measured from 5 to 300 K in a d.c. SQUID magnetometer. Plots of χ_{mol}^{corr}, μ_{eff} and $1/\chi_{mol}^{corr}$ versus temperature are provided in Figures 59.

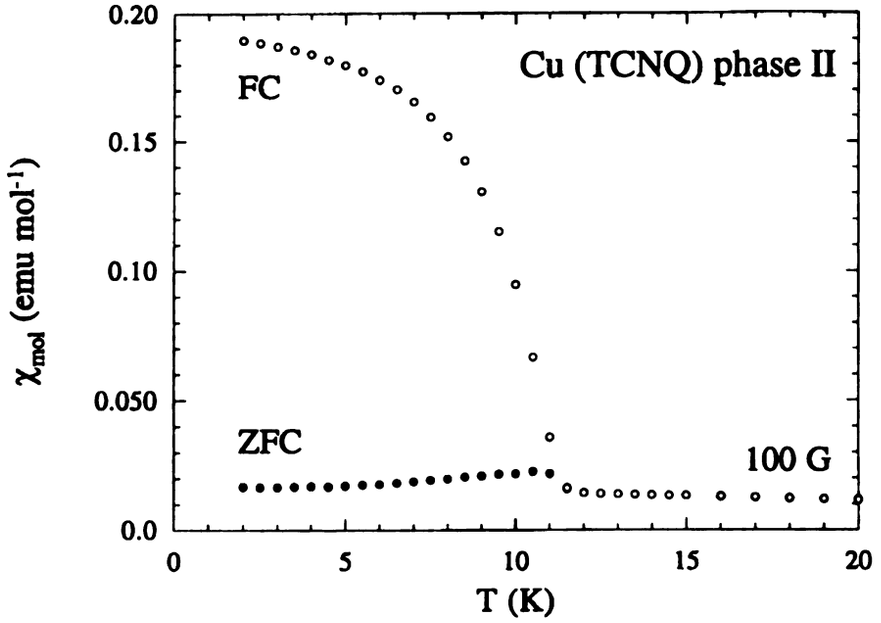


(a)

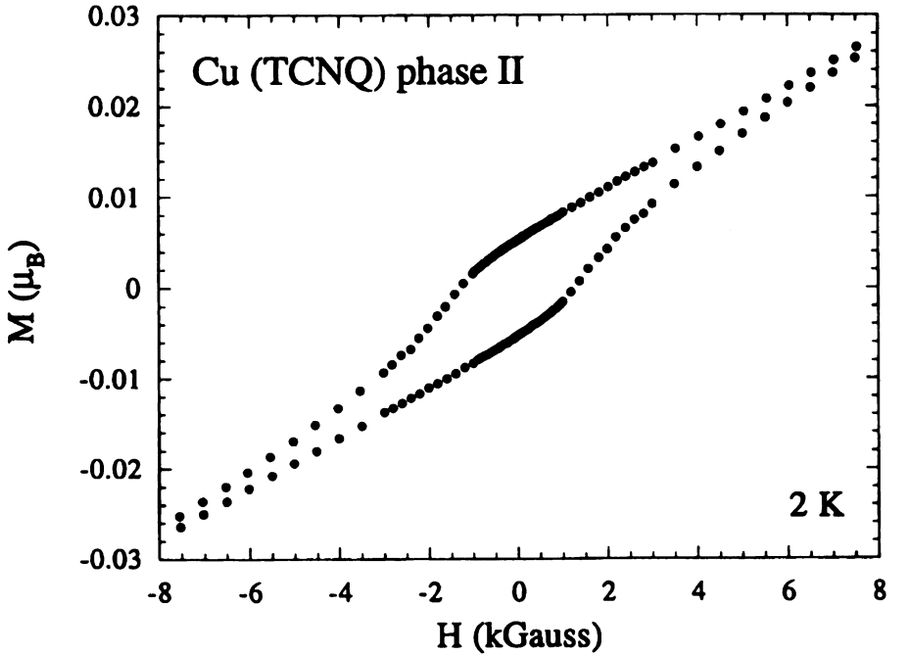


(b)

Figure 57. Variable temperature susceptibility data for Cu(TCNQ) (a) χ versus T for phase I (7); (b) χ and μ_{eff} versus T for phase II (8).



(c)



(d)

Figure 58. Variable temperature susceptibility data for Cu(TCNQ) (c) zero-field cooled and field-cooled χ versus T for phase II (8); (d) hysteresis of phase II(8).

The results of these studies indicate that the Mn compounds exhibit Curie-Weiss behavior (μ_{eff} are ~ 5.9 B.M.) with a small contribution from antiferromagnetic coupling at low temperatures. The conclusion that the TCNQ radicals do not contribute to the magnetism of these compounds is in accord with the X-ray structures that reveal the presence of σ-bonded $[TCNQ\text{-}TCNQ]^{2-}$ and/or π stacked $[TCNQ]^{\cdot-}$ moieties. Both types of TCNQ---TCNQ interactions lead to spin pairing of the radicals. The fact that the π-stacked $[TCNQ]^{\cdot-}$ ligands in the structure of $[Mn(TCNQ)(TCNQ\text{-}TCNQ)_{0.5}(MeOH)_2]_\infty$ are diamagnetic was verified by a measurement of the magnetic susceptibility of the isostructural Zn(II) analog which is rigorously diamagnetic.[39]

F. Charge-Transport Properties TCNQ.

(1) Charge-transport properties of Cu(TCNQ).

The two structural forms of Cu(TCNQ) were subjected to pressed pellet conductivity measurements, and it was found that they exhibit quite different charge-transport properties as illustrated in the plots provided in Figure 60. Both behave as semiconductors, but (7) has a room temperature conductivity of 2.5×10^{-1} Scm^{-1} whereas (8) is nearly insulating with a room temperature conductivity of only 1.3×10^{-5} Scm^{-1}. The band gaps are 0.137 eV and 0.332 eV for phase I and II respectively. It is interesting to note that these values are very close to the corresponding electrical properties of the "unswitched" and "switched" forms of Cu(TCNQ) in the devices. Two separate studies of the conductivity of Cu(TCNQ) prepared by the method of Melby *et. al.*, reported values of σ (r.t.) = $1.6x10^{-2}$ Scm^{-1} and σ(23 °C) = $1x10^{-2}$ $ohm^{-1}cm^{-1}$ and band gaps of 0.11 eV[34a] and E_{gap} = 0.16eV.[40] These data are similar to what was found for phase I in this study. Clearly they

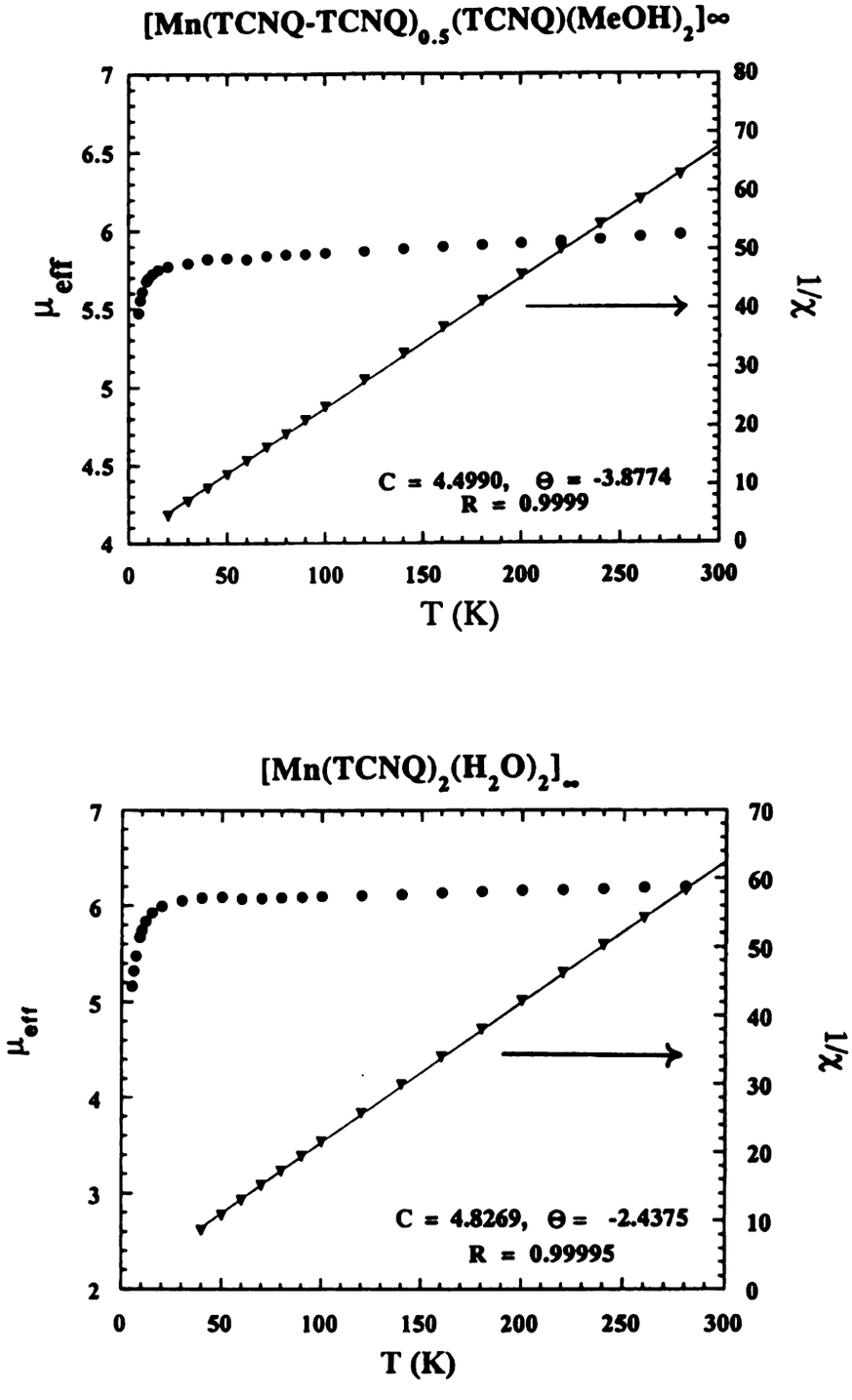


Figure 59. Magnetic data for Mn TCNQ compounds (9),(10).

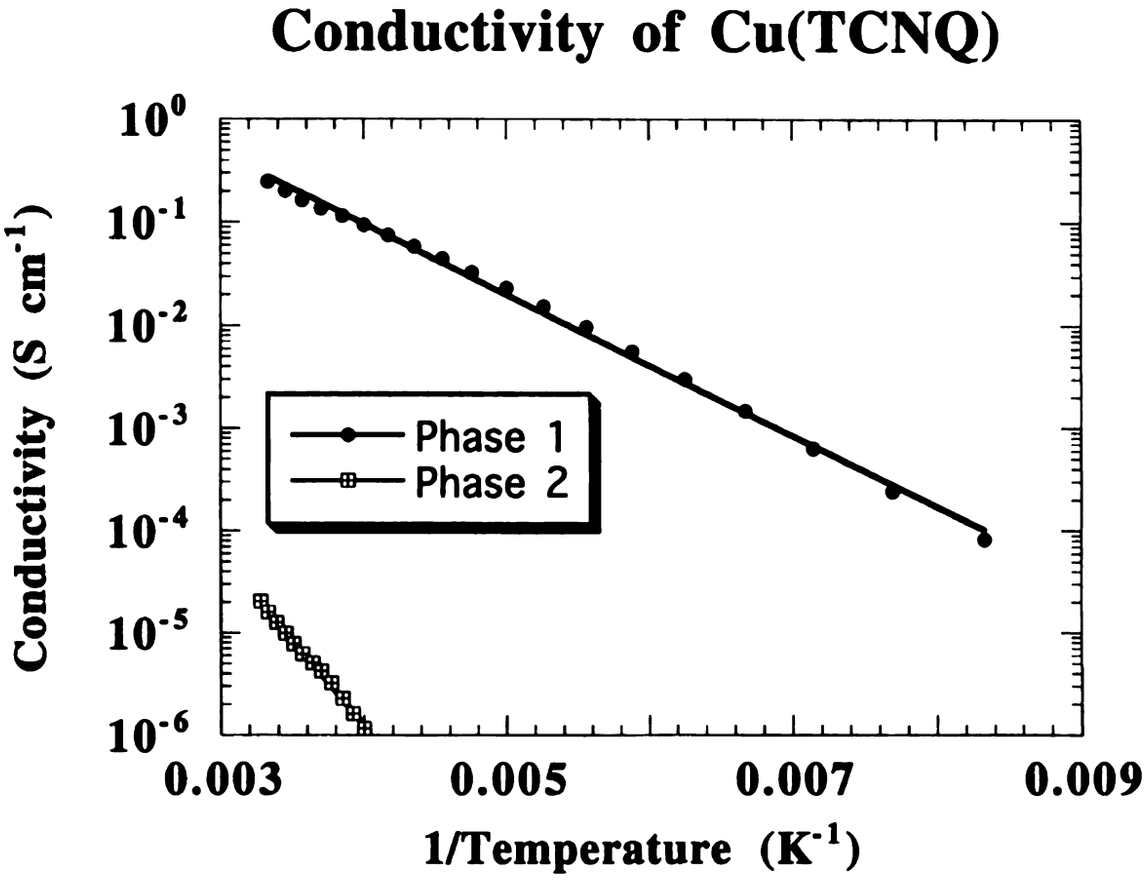


Figure 60. Plot of conductivity σ (S cm^{-1}) versus temperature for bulk Cu(TCNQ) phase I and phase II measured on pressed pellets.

exhibit a much higher conductivity than phase II, which was not recognized as a distinctly different phase prior to the present investigation.

G. Concluding Remarks.

Nearly twenty years ago, it was reported that the application of an electric field to a device consisting of a thin film of Cu(TCNQ) (5-20 μm) sandwiched between a Cu and Al electrode induces a switching of the material from a high to a low resistance state at a critical threshold potential.[8] The device displays a memory effect in that it remains in the low resistance state ("ON" state) for a short period of time in the absence of an applied field. There is a controversy surrounding this phenomenon, however, due to the fact that many researchers have reported an inability to reproduce this behavior. After reviewing the body of literature on the subject, we were led to suspect that subtle changes in the Cu(TCNQ) film preparation could account for the differences in electrical properties of the devices. The results of our investigations establish the existence of two polymorphs of Cu^{I}(TCNQ) by X-ray photoelectron spectroscopy, infrared spectroscopy, powder X-ray diffraction techniques and single crystal X-ray methods. The chemical composition and electronic characteristics of the two phases of Cu(TCNQ) are identical, but the structures and properties are quite different. Powder XRD studies revealed that both phases are present in thin films of Cu(TCNQ) grown on copper substrates but that even subtle differences in reaction conditions can lead to variable quantities of the two phases. This is undoubtedly the cause of the reported inconsistencies in the properties of Cu(TCNQ) devices.[8,17-20] Conductivity data on pressed pellets of bulk samples of the two phases support the conclusion that the material responsible for switching in the films is phase II, which is a very poor

semiconductor. Phase I is a much better conductor; in fact its conductivity is basically the same as that of the Cu(TCNQ) films in the switched state. In our studies, no evidence for switching was observed for the pressed pellets, but this is not unexpected given that the sample thickness is much greater than one can achieve with the films. What we believe is happening in the switching phenomenon is that phase II (centrosymmetric, resting state) converts to another structure (non-centrosymmetric, electrically induced phase) in an electric field. Such a piezoelectrically driven structural changes would not be absurd given how "soft" these materials are. The next step in this work will be to verify that a structural change occurs in the switched state. To do this, one will need a very pure film of phase II for the device, and a diffractometer devoted to measuring the film before, and during, the switching. Technical difficulties have prevented us from performing this experiment to date.

Our investigations of Mn(II) chemistry with $TCNQ^{-1}$ radicals reveal that a major product in methanol is $[Mn(TCNQ)(TCNQ\text{-}TCNQ)_{0.5}(MeOH)_2]_\infty$ with μ_4-$[TCNQ\text{-}TCNQ]^{2-}$ and *cis*-μ-$[TCNQ]^{\cdot-}$ bridges. The latter structure is also exhibited by the Zn(II) derivative and $[Zn(TCNQ)(TCNQ\text{-}TCNQ)_{0.5}(MeOH)_2]_\infty$.[37a] The X-ray structure of the layered material $[Mn(TCNQ)_2(H_2O)_2]_\infty$ revealed yet another type of $TCNQ^{-1}$ binding, namely *syn*-μ-$[TCNQ]^{\cdot-}$ bridges that participate in strong intra-layer π-stacking (~3.1 Å). These results underscore the importance of solvent and the role of supramolecular interactions (hydrogen-bonding and π-interactions) in stabilizing a particular phase. The diamagnetic σ-$[TCNQ\text{-}TCNQ]^{2-}$ and π-$[TCNQ]_2^{2-}$ bridges serve to magnetically isolate the $S = 5/2$ Mn(II) centers, as evidenced by the Curie-Weiss behavior of the compounds between 5 and 300 K (μ_{eff} ~5.9 B.M.).

References

1. (a) Fagan, P. J.; Ward, M. D.; Calabrese, J. C. *J. Am. Chem. Soc.*, **1989**, *111*, 1698. (b) Iwamoto, T. in "*Inclusion Compounds: Inorganic and Physical Aspects of Inclusion*" Iwamoto, T. Atwood, J. L.; Davies, J. E. D.; MacNicol, D. D, Eds., Oxford University Press: Oxford. **1991**, *5*, Ch. 6, 177. (c) Robson, R.; Abrahms, B. F.; Batten, S. R.; Gable, R. W.; Hoskins, B. F.; Liu, J. in *Supramolecular Architecture*; Bein, T.; Ed.; American Chemical Society: Washington, D.C., **1992**, 256. (d) Tannenbaum, R. *Chem. Mater.* **1994**, *6*, 550. (e) Constable, E. C.; *Prog. Inorg. Chem.*, **1994**, *42*, 67. (f) Lu, J.; Harrison, W. T. A.; Jacobson, A. J. *Angew Chem. Int. Ed. Engl.* **1995**, *34*, 2557. (g) Dunbar, K. R., Heintz, K. R. *Prog. Inorg. Chem.*, **1996**, 283. (h) Kawata, S.; Kitagawa, S.; Kumagai, H.; Kudo, C.; Kamesaki, H.; Ishiyama, T.; Suzuki, R.; Kondo, M.; Katada, M. *Inorg. Chem.*, **1996**, *35*, 4449. (i) Whiteford, J. A.; Rachlin, E. M.; Stang, P. J. *Angew. Chem. Int. Ed. Engl.*, **1996**, *35*, 2524. (j) Sharma, C V. K.; Zaworotko, M. J. *Chem. Commun.*, **1996**, 2655. (k) Hirsch, K. A., Wilson, S. R.; Moore, J. S. *Inorg. Chem.*, **1997**, *36*, 2960.

2. (a) Gardner, G. B.; Venkataraman, D.; Moore, J. S.; Lee, S. *Nature*, **1995**, *374*, 792-795. (b) Yaghi, O. M.; Li, G.; Li, H. *Nature*, **1995**, *378*, 703. (c) Whiteford, J. A.; Rachlin, E. M.; Stang, P. J. *Angew. Chem. Int. Ed. Engl.* **1996**, *35*, 2524. (d) Yaghi, O. M.; Li, H. *J. Am. Chem. Soc.*, **1995**, *117*, 10401. (f) Yaghi, O. M.; Li, H. *J. Am. Chem. Soc.*, **1996**, *118*, 295. (g) Venkataraman, D.; Gardner, G. B.; Lee, S.; Moore, J. S. *J. Am. Chem. Soc.*, **1995**, *117*, 11601. (h) Yaghi, O. M.; Li, H.; Groy, T. L. *J. Am. Chem. Soc.*, **1996**, *118*, 9096. (i) Olenyuk, B.; Whiteford, J. A.; Stang, P. J. *J. Am. Chem. Soc.*, **1996**, *118*, 8221.

3. (a) Manriquez, J. M.; Yee, G. T.; McLean, S.; Epstein, A. J.; Miller, J. S. *Science* **1991**, *252*, 1415-1417. (b) Tamaki, H.; Zhuang, Z. J.; Matsumoto, N.; Kida, S.; Koikawa, M.; Achiwa, Hashimoto, Y.; Okawa, H. *J. Am. Chem. Soc.*, **1992**, *114*, 6974. (c) Stumpf, H. O.; Pei, Y.; Kahn, O.; Sletten, J.; Renard, J. P. *J. Am. Chem. Soc.*, **1993**, *115*, 6738. (d) Inoue, K.; Iwamura, H. *J. Am. Chem. Soc.*, **1994**, *116*, 3173. (e) Ohba, M.; Maruono, N.; Okawa, H.; Enoki, T.; Latour, J.-M. *J. Am. Chem. Soc.*, **1994**, *116*, 11566-11567. (f) Kahn, O. in

Molecular Magnetism: From Molecular Assemblies to the Devices: NATO ASI Series. Eds., Coronado, E.; Delhaes, Gatteschi, D.; Miller, J. S. Kluwer Academic, Dordrecht, **1996,** *321*, pp. 243-288. (g) Decurtins, S.; Schmalle, H. W.; Schneuwly, P.; Zheng, Li-M.; Ensling, J.; Hauser, A. *Inorg. Chem.*, **1995**, *34*, 5501. (h) Miyasaka, H.; Matsumoto, N.; Okawa, H.; Re, N.; Gallo, E.; Floriani, C. *Angew. Chem. Int. Ed. Engl.* **1995**, *34*, 1446-1448. (i) Ohba, M.; Okawa, H.; Ito, T.; Ohto, A. *J. Chem. Soc. Chem. Commun.*, **1995**, 1545-1546. (j) Michaut, C.; Ouahab, L.; Bergerat, P.; Kahn, O.; Bousseksou, A. *J. Am. Chem. Soc.*, **1996**, *118*, 3610. (k) de Munno, G. ; Poerio, T.; Viau, G.; Julve, M.; Lloret, F.; Journaux, Y.; Riviere, E. *Chem. Commun.*, **1996**, 2587.

4. (a) Lacroix, P.; Kahn, O.; Gliezes, A.; Valade, L.; Cassoux, P. *Nouv. J. de Chimie*, **1985**, 643-651. (b) Gross, R.; Kaim, W. *Angew. Chem. Int. Ed. Engl.* **1987**, *26*, 251. (c) Bartley, S. L.; Dunbar, K. R. *Angew. Chem. Int. Ed. Eng.* **1991**, *30*, 448. (d) Ballester, L.; Barral, M.; Gutiérrez, A.; Jiménez-Aparicio, R.; Martinez-Muyo, J.; Perpiñan, M.; Monge, M.; Ruiz-Valero, C. *J. Chem. Soc. Chem. Commun.* **1991**, 1396-1397. (e) Humphrey, D.G.; Fallon, G.D.; Murray, K.S. *J. Chem. Soc., Chem. Commun.* **1988**, 1356. (f) Cornelissen, J.P.; van Diemen, J. H.; Groeneveld, L. R.; Haasnoot, J. G.; Spek, A. L.; Reedijk, J. *Inorg. Chem.* **1992**, *31*, 198-202. (g) Oshio, H.; Ino, E.; Mogi, I,; Ito, T. *Inorg. Chem.*, **1993**, *32*, 5697-5703. (h) Ballester, L.; Barral, M.; Gutiérrez, A.; Monge, A.; Perpiñan, M. F.; Ruiz-Valero, C.; Sánchez-Pélaez, A. *Inorg. Chem.* **1994**, *33*, 2142-2146. (i) Dunbar, K. R.; Ouyang, X. *Molecular Crystals Liquid Crystals*, **1995**, *273*, 21-28. (j) Oshio, H.; Ino, E.; Ito, T.; Maeda, Y. *Bull. Chem. Soc. Jpn.*, **1995**, *68*, 889. (k) Dunbar, K. R. *Angew Chem.*, **1996**, *35*, 1659. (l) Decurtins, S.; Dunbar, K. R. ; Gomez-Garcia, C. J.; Mallah, T.; Raptis, R. G.; Talham, D.; Veciana, J. in *Molecular Magnetism: From Molecular Assemblies to the Devices.* (Eds.: E. Coronado, P. Delhaès, D. Gatteschi, J. S. Miller) NATO ASI Series vol. E321 Kluwer, **1996**, 571-582. (m) Dunbar, K. R.; Ouyang, X. *Chem. Commun.*, **1996**, 2427. (n) Zhao, H.; Heintz, R. A.; Rogers, R. D.; Dunbar, K. R. *J. Am. Chem. Soc.*, **1996**, *118*, 12844. (o) Dunbar, K. R.; Ouyang, X. *Inorg. Chem.*, **1996**, *35*, 7188. (p) Azcondo, M. T.; Ballester, L.; Gutiérrez, A.; Perpiñán, F.; Amador, U.; Ruiz-Valero, C.; Bellitto, C. *J. Chem. Soc., Dalton Trans.* **1996**, 3015.

5. (a) Aumüller, A.; Erk, P.; Klebe, G.; Hünig, S.; von Schütz, J.; Werner, H. *Angew. Chem. Int. Ed. Engl.* **1986**, *25*, 740-741. (b) Aumüller, A.; Erk, P.; Hünig, S. *Mol. Cryst. Liq. Cryst. Inc. Nonlin. Opt.* **1988**, *156*, 215-221. (c) Erk, P.; Gross, H.-J.; Hünig, U. L.; Meixner, H.; Werner, H.-P.; von Schütz, J. U.; Wolf, H. C. *Angew. Chem. Int. Ed. Engl.* **1989**, *28*, 1245-1246. (d) Kato, R.; Kobayashi, H.; Kobayashi, A. *J. Am. Chem. Soc.*, **1989**, *111*, 5224-5232. (e) Aumüller, A.; Erk, P.; Hünig, S.; Hädicke, E.; Peters, K.; von Schnering, H. G. *Chem Ber.* **1991**, *124*, 2001.(f) Sinzger, K.; Hünig, S.; Jopp, M.; Bauer, D.; Bietsch, W.; von Schütz, J. U.; Wolf, H. C; Kremer, R. K.; Metzenthin, T.; Bau, R.; Khan, S. I.; Lindbaum, A.; Lengauer, C. L.; Tillmanns, E. *J. Am. Chem. Soc.* **1993**, *115*, 7696. (g) Kato, R.; Kobayashi, H.; Kobayashi, A. *J. Am. Chem. Soc.* **1989**, *111*, 5224.

6. An excellent review on the subject of sigma coordination to TCNX molecules is: Kaim, W.; Moscherosch, M. *Coord. Chem. Rev.* **1994**, *129*, 157.

7. Structure of Ag(TCNQ): Shields, L. *J. Chem. Soc., Faraday Trans. 2* **1985**, *81*, 1.

8. Potember, R. S.; Poehler, T. O.; Cowan, D. O. *Appl. Phys. Lett.* **1979**, *34*, 405.

9. (a) Potember, R. S.; Poehler, T. O.; Hoffman, R. C.; Speck, K.R.; Benson, R. C. In *Molecular Electronic Devices II* Carter, F. L., Ed.; Marcel Dekker: New York. **1987**, 91. (b) Potember, R. S.; Poehler, T. O.; Cowan, D. O.; Carter, F. L.; Brant, P. I *Molecular Electronic Devices* Carter, F. L., Ed.; Marcel Dekker: New York. **1982**, 73. (c) Kamitsos, E. I.; Risen, W. M. Jr. *Solid State Commun.* **1983**, *45*, 165. (d) Potember, R. S.; Poehler, T. O.; Cowan, D. O.; Brant, P.; Carter, F. L.; Bloch. A. N. *Chem. Scripta* **1981**, *17*, 219. (e) Kamitsos, E. I.; Risen, W. M., Jr. *Solid State Commun.* **1982**, *42*, 561.

10. Kamitsos, E.I.; Risen, W.M. *Mol. Cryst. Liq. Cryst.* **1986**, *134*, 31.

11. (a) Poehler, T. O.; Potember, R. S.; Hoffman, R.; Benson, R. C. *Mol. Cryst. Liq. Cryst.* **1984**, *107*, 91. (b) Potember, R. S.; Poeler, T. O.; Benson, R. C. *Appl. Phys. Lett.* **1982**, *41*, 548.

12. Kamitsos, E. I.; Risen, W. M. Jr. *J. Chem. Phys.* **1983**, *79*, 5808.

13. Benson, R. C.; Hoffman, R.C.; Potember, R. S.; Bourkoff, E.; Poehler, T. O. *Appl. Phys. Lett.* **1983**, *42*, 855.

14. (a) Yamaguchi, S.; Viands, C. A.; Potember, R. S. *J. Vac. Sci. Technol.* **1991**, *9*, 1129. (b) Hoffman, R. C.; Potember, R.S. *Applied Optics* **1989**, *28(7)*, 1417. (c) Kamitsos, E.I.; Risen, W. M. Jr. *J. Chem. Phys.* **1983**, *79*, 477.

15. Potember, R. S.; Poehler, T.O.; Rappa, A.; Cowan, D.O.; Bloch, A. N. *Synth. Metals* **1982**, *4*, 371.

16. Potember, R. S.; Poehler, T. O.; Rappa, A.; Cowan, D. O.; Bloch, A. N. *J. Am. Chem. Soc.* **1980**, *102*, 3659.

17. Duan, H.; Mays, M. D.; Cowan, D. O.; Kruger, J. *Synth. Metals* **1989**, *28*, C675.

18. Sato, C.; Wakamatsu, S.; Tadokoro, K.; Ishii, K. *J. Appl. Phys.* **1990**, *68(12)*, 6535. In this work, vapor deposition techniques were used to produce films of Cu on a glass-ceramics substrate which was dipped into a solution of TCNQ in acetone/CH_3CN to yield Cu(TCNQ).

19. Hoagland, J. J.; Wang, X. D.; Hipps, K. W. *Chem. Mater.* **1993**, *5*, 54.

20. (a) Liu, S. G.; Liu, Y.Q.; Wu, P. J.; Zhu, D. B. *Chem. Mater.* **1996**, *8*, 2779. (b) Liu, S.-G; Liu, Y.-Q.; Zhu, D.-B. *Thin Solid Films*, **1996**, *280*, 271. (c) Sun, S. Q.; Wu, P. J.; Zhu, D. B. *Solid State Commun.*, **1996**, *99*, 237. (d) Liu, S. G.; Liu, Y.Q.; Wu, P. J.; Zhu, D. B.; Tian, H.; Chen, K.-C. *Thin Solid Films*, **1996**, *289*, 300.

21. (a) Wakida, S.; Ujihira, Y. *Jpn. J. Appl. Physics* **1988**, *27*, 1314. (b) Hua, Z. Y.; Chen, G. R. *Vacuum* **1992**, *43*, 1019.

22. Duan, H.; Cowan, D. O.; Kruger, J. In *Advanced Organic Solid State Materials* Chiang, L. Y; Chaikin, P.M.; Cowan, D. O. Ed.; Materials Research Society Symposium Proceedings Vol. 173; Materials Research Society: Pittsburgh, Pennsylvania, **1990**; p.165.

23. (a) Melby, L. R.; Harder, R.J.; Hertler, W. R.; Mahler, W.; Benson, R. E.; Mochel, W. E. *J. Am. Chem. Soc.* **1962**, *84*, 3374. (b) Sano, M.; Ohta, T.; Akamatsu, H. *Bull. Chem. Soc. Jpn.* **1968**, *41*, 2204. (c) Ikemoto, I.; Thomas, J. M.; Kuroda, H. *Bull. Chem. Soc. Jpn.* **1973**, *46*, 2237. (d) Bozio, R.; Girlando, A.; Pecile, C. *J. Chem. Soc. Faraday Trans.*, **1975**, *71*, 1237.

24. (a) Acker, D. S.; Harder, R. J.; Hertler, W. R.; Mahler, W.; Melby, L. R.; Bensin, R. E.; Mochel, W. E. *J. Am. Chem. Soc.* **1960**, *82*, 6408. (b) Melby, L. R.; Harder, R. J.; Hertler, W. R.; Mahler, W.; Benson, R. E.; Mochel, W. E. *J. Am. Chem. Soc.* **1962**, *84*, 3374. (c) Torrance, J. B. *Acc. Chem. Res.* **1979**, *12*, 79. (d) Endres H. In *Extended Linear Chain Compounds*; Miller, J. S. Ed.; Plenum: New York. **1983**, Vol. 3, 263-312. (e) Wudl, F. *Acc. Chem. Res.*, **1984**, 17, 227. (f) Jérome, D. *Science* **1991**, *252*, 1509. (e) Bryce, M. R. *Chem. Soc. Rev.* **1991**, *20*, 355. (g) Williams, J. M.; Schultz, A. J.; Geiser, U.; Carlson, K. D.; Kini, A. M.; Wang, H. H.; Kwok, W. -K.; Whangbo, M. -H.; Schirber, J. E. *Science* **1991**, *252*, 1501. (h) Ward, M. D. *Electroanal Chem.* **1988** *16*, 181. (i) Martin, N.; Segura, J. L.; Seoane, C. *J. Mater. Chem.* **1997**, *7*, 1661.

25. The method of Kubas, G.J. *Inorg. Synth.* **1979**, *19*, 90, was used with the modification that 45-50% HBF_4 was used instead of 60-65% HPF_6.

26. Hathaway, B. J.; Holah, D. G.; Underhill, A. E. *J. Chem. Soc.* **1962**, 2444.

27. TWINDX, TWROT, TWUTIL and TWHKL are components of the TWINNING program written by Dr. Robert Sparks, private communication.

28. (a) Dunbar, K. R. *J. Am. Chem. Soc.* **1988**, *110*, 8247. (b) Dunbar, K. R.; Pence, L. E. *Inorg. Chem.*, **1991**, *30*, 2018. (c) Bartley, S. L.; Bernstein, S. N.; Dunbar, K. R. *Inorg. Chim. Acta* **1993**, *213*, 213-231. (d) Dunbar, K. R. *Comments Inorg. Chem.*, **1992**, *13*, 313-357. (e) Dunbar, K. R. *J. Cluster Science*, **1994**, *5*, 125-144.

29. We note that it is not cost effective to use a Cu(II) starting material to

prepare Cu(TCNQ) because it consumes $^{n}Bu_4N(TCNQ)$ as a reducing agent and the product is not as pure as the compound obtained from either of the other two methods, as judged by X-ray powder diffraction techniques.

30. (a) Thompson, R. C.; Gujral, V. K.; Wagner, H. J.; Schwerdtfeger, C. F. *Phys. Stat. Sol.* **1979**, *53*, 181. (b) Chain, E. E.; Kevill, D. N.; Kimball, C. W.; Weber, L. W. *J. Phys. Chem. Solids* **1976**, *37*, 817. (c) Thompson, R. C.; Hoyano, Y.; Schwerdtfeger, C. F. *Solid State Commun.* **1977**, *23*, 633. (d) Kathirgamanathan, P.; Rosseinsky, D. R. *J. C. S. Chem Commun.* **1980**, 839.

31. Ikemoto, I.; Thomas, J. M.; Kuroda, H. *Bull. Chem. Soc., Jpn* , **1973**, *46*, 2237.

32. Brant, P.; Fernando, Q. *J. Inorg. Nucl. Chem.*, **1978**, *64*,45.

33. (a) Kobayashi, A.; Kato, R.; Kobayashi, H.; Mori, T.; Inokuchi, H. *Solid State Commun.*, **1987**, *64*, 45. (b) Yashihiro, Y.; Furukawa, Y.; Kobayashi, A.; Tasumi, M.; Kato, R.; Kobayashi, H. *J. Chem. Phys.*, **1994**, *100*, 2449. (b) Willett, R. D.; Long, G., personal communication.

34. (a) Inoue, M.; Inoue, M. B. *J. Chem. Soc., Faraday Trans. 2* **1985**, *81*, 539. (b) Inoue, M. B.; Inoue, M.; Fernando, Q.; Nebesny, K. W. *J. Phys. Chem.* **1987**, *91*, 527. (c) Inoue, M.; Inoue, M. B. *Inorg. Chem.* **1986**, *25*, 37. (d) Pukacki, W.; Pawlak, M.; Graja, A.; Lequan, M.; Lequan, R. M. *Inorg. Chem.* **1987**, *26*, 1328. (e) Farges, J. P.; Brau, A.; Dupuis, P. *Solid State Commun.* **1985**, *54(6)*, 531. (f) Chappell, J. S.; Bloch, A. N.; Bryden, A.; Maxfield, M.; Poehler, T. O.; Cowan, D. O. *J. Am. Chem. Soc.* **1981**, *103*, 2442. (g) Van Duyne, R. P.; Suchanski, M. R.; Lakovits, J. M.; Siedle, A. R.; Parks, K. D.; Cotton, T. M. *J. Am. Chem. Soc.*, **1979**, *101*, 2832. (h) Lunelli, B.; Pecile, C. *J. Chem. Phys.*, **1970**, *52*, 2375. (i) Bozio, R.; Girlando, A.; Pecile, C. *J. Chem. Far. Trans. II*, **1975**, *71*, 1237.

35. (a) Morosin, B.; Plastas, H. J.; Coleman, L. B.; Stewart J. M. *Acta Cryst.* **1978**, *B54*, 540. (b) Dong, V.; Endres, H.; Keller, H. J.; Moroni, W.; Nöthe, D. *Acta Cryst. Sec. B* **1977**, *B33*, 2428. (c) Hoffmann, S. K.; Corvan, P. J.; Singh, P.; Sethulekshmi, C. N.;

Hatfield, W. E. *J. Am. Chem. Soc.* **1983**, *105*, 4608.

36. Kaim, W. and Moscherosch, M. *Coord. Chem. Rev.* **1994,** *129,* 157.

37. (a) Hoekstra, A.; Spoelder, T.; Vos, A. *Acta Cryst.* **1972**, *B28*, 14. (b) Murakami, M.; Yoshimura, S. *Bull. Chem. Soc. Jpn.* **1975**, 48, 157. (c) Konno, M.; Saito, Y. *Acta Cryst.* **1974**, *B30*, 1294. (d) Konno, M.; Saito, Y. *Acta Cryst.* **1975**, *B31*, 2007. (c) Konno, M.; Ishii, T.; Saito, Y. *Acta Cryst.* **1977**, *B33*, 763. (d) Endres, H. In *Extended Linear Chain Compounds* Vol. 3; Miller, J.S. Ed.; Plenun Press: New York, **1983**; pp. 263-317.

38. (a) Kommandeur, J. In *Low-Dimensional Cooperative Phenomena*; Keller, H.J. Ed.; Plenum Press: New York, **1975**, 65. (b) Schwertdfeger, C.F. *Solid State Commun.* **1977**, *23*, 621. (c) Siratori, K.; Kondow, T. J. Phys. Chem. Solids **1978**, *39*, 225. (d) Kommandeur, J. In The *Physics and Chemistry of Low Dimensional Solids*; Alcácer, L. Ed.; D. Reidel Publishing: Dordrecht, Holland, **1980**, 197. (e) Grossel, M. C.; Weston, S. C. *Chem. Mater.* **1996**, *8(5)*, 977. (f) Grossel, M. C.; Weston, S. C. *J. Chem. Soc., Chem. Commun.* **1992**, 1510. (g) Hynes, R. C.; Morton, J.R.; Preston, K. F.; Williams, A. J.; Evans, F.; Grossel, M. C.; Sutcliffe, L.H.; Weston, S. C. *J. Chem. Soc., Faraday Trans.* **1991**, *87(14)*, 2229. (h) Iida, Y. *Bull. Chem. Soc. Jpn.* **1969**, *42*, 71.

39. (a) Zhao, H,; Heintz, R. A.; Ouyang, X.; Dunbar, K. R.; Campana, C.; Rogers, R. D. *Chem. Mater.* **1999**, *11*, 736-746. (b) Dunbar, K. R.; Cowen, J.; Zhao, H.; Heintz, R. A.; Ouyang, X.; Grandinetti, G. *NATO ASI: Supramolecular Engineering of Synthetic Metallic Materials: Conductors and Magnets* Ed: J. Veciana, Kluwer: Dordrecht, **1999**, in press. (c) O'Kane, S.; Dunbar, K. R. unpublished results.

39. Siemons, W. J.; Bierstedt, P. E.; Kepler, R. G. *J. Chem. Phy.*, **1963**, *39*, 3523.

CHAPTER IV

STRUCTURAL AND MAGNETIC STUDIES OF DINUCLEAR AND TETRANUCLEAR CLUSTERS OF 3-D TRANSITION METAL HALIDES

1. Introduction

High spin polynuclear transition metal compounds are of interest for their magnetic applications in biological[1] as well as materials chemistry.[2] In particular, 3*d* transition metal cations are commonly used as spin carriers in extended arrays with cooperative properties. In spite of the interest in such chemistry, a building block approach to preparing extended structures of metal halide magnetic compounds has not been undertaken. In this work, we report the convenient preparation and X-ray structures of $[M_2X_6]^{2-}$ and $M_4X_8(THF)_6$ precursors. These 3*d* transition metal halide dinuclear anions and tetra nuclear clusters are to be used as building blocks in magnetic mterials. In this chapter, we report the structures and magnetic properties of manganese halide clusters with THF, dimetal compounds of the type $[M_2Cl_6]^{2-}$ and products from reactions of $Fe_4Cl_8(THF)_8$ and $[Fe_2Cl_6]^{2-}$ with nitrogen donor chelates.

2. Experimental Section.

A. Synthesis.

The starting materials $MnCl_2$, $FeCl_2$, and $CoCl_2$ were purchased from Strem Chemicals, Inc., and used without further purification. $[Et_4N]Cl$ (tetraethylammonium chloride) was purchased from Sigma Chemical Co. and [ppn]Cl (ppn = bis(triphenylphosphonium)imminium chloride) was purchased from Aldrich; all were used as received. Acetone was distilled over 3 Å molecular sieves; diethyl ether, hexanes and THF were distilled over sodium-potassium/benzophenone, whereas methanol was distilled over $Mg(OMe)_2$ under a nitrogen atmosphere. Unless otherwise specified, all reactions were carried out under an argon atmosphere by using standard Schlenk-line techniques. Due to the extreme moisture sensitivity of these

compounds, all glassware was pre-treated with the commercially available reagent Glassclad.

(1) Preparation of $[Mn_5Cl_{10}(THF)_8]_\infty$ (16).

(a) Bulk preparation

$MnCl_2$ anhydride (0.500 g, 0.397 mmol) was loaded into a three-necked Schlenk flask with 40 mL of THF, and was refluxed for 24 hours. A white precipitate was collected by filtration and washed with 5 mL of THF followed by 5 mL of diethyl ether and vacuum dried. Yield 0.76g (79% based on $Mn_5Cl_{10}(THF)_8$). IR (CsI, Nujol, cm^{-1}) ν(Mn-Cl) = 361(br).

(b) Single crystal growth

A saturated solution of (16) in 20 mL of acetone/0.5 mL of methanol was carefully layered with 2 mL of a buffer solution (acetone/methanol 40:1 v/v) followed by 10 mL of hexanes in a Schlenk tube. The solution was allowed to stand undisturbed, and after three days a small quantity of needle crystals was obtained. IR (CsI, Nujol, cm^{-1}) ν(Mn-Cl) = 366 (br).

(2) Preparation of $[MnBr_2(THF)_2]_\infty$ (17).

(a) Bulk preparation

$MnBr_2$ anhydride (0.94g) was suspended in 40 mL of THF in a three-necked Schlenk flask and refluxed for 12 hours. The yellow-brown solution was reduced in volume to about one-half and layered with 40 mL of hexanes. The resulting pale pink crystalline product was collected by filtration and washed with 5 mL of THF followed by 5 mL of diethyl ether and finally dried in a vacuum; yield: 1.24g (72%).

(b) Single crystal growth

Pale pink needle crystals of (17) suitable for a crystallographic study were grown by carefully layering 20 mL of a saturated acetone solution of $MnBr_2$•xTHF with 10 mL of hexanes.

(3) Preparation of crystals of $[MnCl_2(MeOH)_2]_\infty$(18).

A saturated solution of $[Mn_5Cl_{10}(THF)_8]_\infty$ in 20 mL of acetone and 0.5 mL of methanol was carefully layered with a 5 mL mixture of acetone and methanol (40:1 v/v) followed by 10 mL of hexanes in a Schlenk tube. The solution was allowed to stand undisturbed, and long needle crystals of $[MnCl_2(MeOH)_2]_\infty$ were observed to form over a three day period. The crystals tend to be severely twinned, and they lose interstitial solvent of crystallization immediately upon removal from the mother liquor. Nujol mull (cm^{-1}), ν(Mn-Cl) = 387 (br).

(4) Preparation of $[Fe_2Cl_4(bpy)_2]$ from $Fe_4Cl_8(THF)_4$ (19).

Stock solutions of 2,2'-bipyridine (10.0 mg, 0.064 mmol 5 mL of acetone) and $Fe_4Cl_8(THF)_6$ (0.400 g, 0.426 mmol 10 mL of acetone) were prepared. A 1 mL aliquot of the $Fe_4Cl_8(THF)_6$ solution was syringed into a 6 mm O.D. Pyrex tube, and carefully layered with 0.5 mL of acetone followed by 1 mL of the 2,2'-bipyridine solution. The tube was flame-sealed under a slight vacuum and allowed to stand undisturbed. After several days, orange crystals suitable for crystallographic study were harvested from the interface region of the tube. IR (CsI, Nujol, cm^{-1}): 417, 359, 317, 250. *Anal.* Calcd.: %C, 42.45; %H, 2.85; %N, 9.90. Found: %C, 41.70; %H, 3.19; %N, 9.17.

(5) Preparation of $[FeCl_2(bpy)]_\infty$ from $Fe_4Cl_8(THF)_4$ (20).

Stock solutions of 2,2'-bipyridine (6.0 mg, 0.038 mmol in 5 mL of acetone) and $Fe_4Cl_8(THF)_6$ (0.380 g, 0.404 mmol in 15 mL of acetone) were prepared. A 1 mL aliquot of the $Fe_4Cl_8(THF)_6$ solution was syringed into a 6 mm O.D. Pyrex tube and carefully layered with 1 mL of acetone followed by 1 mL of the 2,2'-bipyridine solution. The tube was flame-sealed under a slight vacuum and allowed to stand undisturbed. After several days, red

needle crystals suitable for crystallographic study were harvested from the interface region of the tube.

(6) Preparation of $[ppn]_2[Co_2Cl_6]$ (21).

Anhydrous $CoCl_2$ (0.260 g, 2 mmol) and [ppn]Cl (1.144 g, 2 mmol) were dissolved in 60 mL of acetone and stirred at r.t. for 16 hours. A blue solution and a large quantity of blue solid were present at the end of this time. The blue product was collected by filtration, and the filtrate was treated with 40 mL of diethyl ether to yield additional microcrystalline product; combined yield, 1.02 g (67%). Single crystals were grown by slow diffusion of diethyl ether into a solution of the compound in acetone. IR (Nujol, cm^{-1}) 1705 (ms), 1587 (m), 1261 (br), 1111 (m), 1026 (m), 997 (m), 798 (m), 762 (m), 742 (m), 690 (s), 550 (s), 532 (s), 495 (s), 395 (ms), 333 (ms), 306 (ms), 268 (br). *Anal.* Calcd. for $Co_2Cl_6P_4N_2C_{72}H_{60}$: C, 61.43; H, 4.30; Cl, 15.11; N, 1.99. Found: C, 61.46; H, 4.37; N, 1.79.

(7) Preparation of $[ppn]_2[Mn_2Cl_6]$ (22).

Anhydrous $MnCl_2$ (0.252 g, 2 mmol) and [ppn]Cl (1.145 g, 2 mmol) were dissolved in 35 mL of acetone and stirred for 16 hours. The resulting colorless solution was filtered to remove any insoluble particles, and the filtrate was treated with 40 mL of diethyl ether to give a pale yellow-green microcrystalline product which was collected, washed with 5 mL of diethyl ether and dried *in vacuo*; yield, 1.14 g (97%). Single crystals were obtained by dissolving $[ppn]_2[Mn_2Cl_6]$ in 20 mL of acetone and layering with 10 mL of hexanes in a Schlenk tube. Light yellow, rhombohedral crystals were harvested after three days. IR (Nujol, cm^{-1}) 1707 (m), 1587 (m), 1265 (br), 1180 (m), 1113 (m, s), 1026 (m), 997 (s), 800 (m, s), 748 (s), 694 (s), 551 (s), 532 (s), 499 (s), 396 (m, s), 330 (s), 287 (m, s), 248 (m, s), 228 (m, s). *Anal.* Calcd. for $Mn_2Cl_6P_4N_2C_{72}H_{60}$: C, 61.78; H, 4.32; Cl, 15.20; N, 2.00.

Found: C, 61.65; H, 4.56; N, 1.74.

(8) Preparation of $[ppn]_2[NiCl_4]$ (23, 24).

(a) Bulk Preparation.

Samples of anhydrous $NiCl_2$ (0.260 g, 2 mmol) and [ppn]Cl (1.148 g, 2 mmol) were dissolved in 35 mL of acetone and stirred at r.t. for 16 hours. A small quantity of light blue precipitate was removed by filtration and discarded, and the filtrate was treated with 40 mL of diethyl ether to produce a light blue microcrystalline material. The product was collected by filtration, washed with 3 x 5 mL of diethyl ether and vacuum dried. Yield 0.686 g (47%).

(b) Single crystals of phase I (23).

Blue needle crystals of (23) of an orthorhombic form were obtained by dissolving 50 mg of the salt in 20 mL of acetone and layering the solution with 10 mL of diethyl ether.

(c) Composite crystals of a triclinic phase (24) and orthorhombic phase (23).

Blue platelet crystals of a triclinic phase of $[ppn]_2[NiCl_4]$ (24) were grown from layering 10 mL of hexanes on top of 20 mL of an acetone solution that contained 50 mg of the compound.

(9) Preparation of $[Mn_2(bpym)_4(\mu\text{-}F)(\eta^1\text{-}BF_4)(BF_4)_2(MeCN)\bullet 2MeCN]_\infty$ (25).

Single crystals of (25) were grown by layering an acetonitrile solution of $[Mn(MeCN)_4]_2[BF_4]_2$ with a MeCN solution of 2,2'-bypyrimidine. Stock solutions of 2,2'-bipyridine (10 mg in 5 mL of acetonitrile) and $[Mn(MeCN)_4]_2[BF_4]_2$ (0.20 g in 10 mL of acetonitrile) were prepared, and 1 mL of the metal containing solution was syringed into a 6 mm O.D. Pyrex tube and carefully layered with 0.5 mL of acetonitrile followed by 1 mL of

the 2,2'-bipyridine stock solution. The tube was flame-sealed under a slight vacuum and allowed to stand undisturbed. After several days, pale yellow crystals suitable for crystallographic study were harvested from the interface region of the tube.

(10) $[Et_4N]Cl•[Fe_2Cl_4(MeOH)_4(\mu\text{-}2,2'\text{-bpym})]$ (26).

(a) Bulk preparation.

A methanol solution (15 mL) of $[Et_4N]_2[Fe_2Cl_6]$ (26) was added to 15 mL of a methanol solution of 2,2'-bipyrimidine, and the resulting solution was stirred for 12 h to give a pale red solution. The solution was concentrated and treated with diethyl ether (20 mL) to give a black solid; yield: 0.0352 g, 36% based on 2,2'-bpym.

(b) Single crystal growth.

Single crystals of (26) were grown by slow diffusion of a MeOH solution of $[Et_4N]_2[Fe_2Cl_6]$ into a THF solution of 2,2'-bypyrimidine.

B. Structural Studies.

Crystallographic data for (16), (18) and (21) –(26) were collected on a Bruker (Siemens) SMART 1K CCD platform diffractometer. Data for (17), (19) were collected on a Rigaku AFC6S four circle diffractometer. Data for (20) was collected on a Nicolet P3/V four circle diffractometer. Detailed procedures for using a Bruker CCD are described in Appendix A.

(1) Structure of $[Mn_5Cl_{10}(THF)_8]_\infty$ (16).

A colorless, rod-like crystal of approximate dimensions 0.60 x 0.29 x 0.29 mm was mounted on the tip of a glass fiber with Dow Corning silicone grease. Indexing and refinement of 35 reflections from a total of 60 frames with an exposure time of 10 sec/frame gave unit cell parameters for a triclinic unit cell. A hemisphere of data with 1321 frames were collected

with a scan width of 0.3° in ω and an exposure time of 30 sec/frame. Indexing and refinement of 93 reflections from a total of 180 data frames was used to generate a precise cell for data integration which led to 7,753 reflections in the range of $-12 \leq h \leq 7$, $-14 \leq k \leq 14$, $-16 \leq l \leq 15$ with a maximum 2θ angle of 56.96°. Of the 5400 unique reflections, a total of 3786 reflections with $I > 2\sigma(I)$ and $R_{int} = 0.0303$ remained after data reduction. The final cell was produced from the refinement of the XYZ centroids of 5400 reflection with $I/\sigma > 10$. The unit cell parameters are a = 9.4620(2) Å, b = 11.13870(2) Å, c = 12.4763(2) Å, α = 75.2850(10)°, β = 76.3050(10)°, γ = 79.6870(10)° and V = 1225.72(3) Å^3. The data were corrected for beam inhomogeneity, crystal decay and absorption by SADABS[3] which led to a transmission factors ranged from 0.83 to 1.00 and an R_{int}=0.303.

The positions of the non-hydrogen atoms were located by direct methods and refined by full-matrix least squares on F^2 using the SHELXTL 5.04 package. Two disordered THF molecules were modeled at half occupancies in two positions. All non-hydrogen atoms were refined anisotropically except the two disordered THF groups which were refined isotropically. Hydrogen atoms were placed in idealized positions. Crystallographic data for (16) are summarized in Table 27.

(2) Structure of $[MnBr_2(THF)_2]_\infty$ (17).

A pale pink, rod-like crystal of approximate dimensions 0.40 x 0.25 x 0.25 mm was mounted on the tip of a glass fiber with Dow Corning silicone grease. Indexing and refinement of 20 reflections in the 2θ range 25-45 led to an orthorhombic crystal system with the unit cell parameters a = 7.593(2) Å, b = 18.375(4) Å, c = 3.989(1) Å, $\alpha = \beta = \gamma = 90°$, and V = 556.6(2) Å^3. The data were collected in the 2θ-ω scan mode to 50° in the range of $0 \leq h \leq$

9, $0 \leq k \leq 21$, $0 \leq l \leq 4$ with a maximum 2θ angle of 49.91°. The data were corrected for Lorentz and polarization effects which led to $R_{int} = 0.115$ and $R_{sig} = 0.0364$.

Systematic absences indicated two possible orthorhombic space groups, namely *P*nnm and *P*nn2. In the Pnnm space group, the THF molecule is disordered around the mirror plane. In the space groups *P*nn2, the Mn and Br atoms positions were located by direct methods and refined by full-matrix least squares on F^2 using the SHELXTL 5.04 package. Other non-hydrogen atoms were located from alternating difference Fourier maps and least squares refinement. A disordered THF group was isotropically refined in two positions, and the Mn and Br atoms were refined anisotropically. Hydrogen atoms were fixed in idealized positions. Crystallographic data for (17) are summarized in Table 27.

(3) $[MnCl_2(MeOH)_2]_\infty$ (18)

A colorless thin needle crystal of dimensions 0.21 x 0.13 x 0.05 mm was secured on the tip of a glass fiber with Dow Corning silicone grease and placed in a cold N_2(g) stream at 173(2) K. Indexing 80 reflections failed to produce a solution with default parameters in the auto-indexing routine from a total of 60 frames with an exposure time of 10 sec/frame. Reindexing with a reflection percentage fit ratio reduced of 70% (versus 80%) indicated a monoclinic I-centered crystal system with cell parameters a = 24.14(3)Å, b = 3.69(5)Å, c = 22.08(3)Å, β = 97.27(6), and V = 1950.9(3.6)Å^3. A hemi-sphere of data with 1321 frames was collected with a scan width of 0.3 in ω and exposure times of 20 sec/frame. A further indexing after data collection failed to reproduce the monoclinic cell and indicated that crystal might belong to a primitive triclinic system with a = 3.7288(5) Å, b = 15.429(2) Å, c = 17.456(2) Å, α = 83.969(2)°, β = 83.875(2)°, γ = 82.932(2)°, V =

986.64(37) Å^3. However, data integration with the triclinic cell cannot be solved. The final cell was eventually indexed by the TWINNING[4] package which indicated the presence of quadruple rotational twins with a = 3.723(2) Å, b = 5.817(3) Å, c = 7.695(3) Å, α = 94.801(7)°, β = 96.252(8)°, γ = 96.072(8)° and V = 163.96(21) Å^3. The twinning laws for other three solutions related solution A are [-1 0 0, 0.33 1 0, 0 -0.25 -1], [-1 0 0, 0 -1 0, 0.5 0.25 1] and [1 0 0, -0.33 -1 0, -0.5 0 1] respectively. The data were integrated by using the orientation matrix of component A. Laue crystal symmetry constraints were used during data integration, and the cell parameters and orientation matrix were also refined. Summary of data collection and refinement are listed in Table 28.

(4) $Fe_2Cl_4(bpy)_2$ (19).

An orange needle crystal of approximate dimensions 0.20 x 0.20 x 0.30 mm^3 was mounted on the tip of a glass fiber with Dow Corning silicone grease. Indexing and refinement of 20 reflections in the 2θ range 25-45° gave unit cell parameters for a triclinic crystal system, a = 8.205 (2) Å, b = 8.436 (2) Å, c = 8.749 (2) Å, α = 110.25(3)°, β = 105.69(3)°, γ = 93.93 (3)°, and V = 538.2(2) Å^3. The data were corrected for Lorentz and polarization effects. The positions of the non-hydrogen atoms were located by direct methods and refined by full-matrix least square on F^2 using the SHELXTL 5.04 package whereas hydrogen atoms were placed in calculated positions. Key crystallographic data are summarized in Table 29.

(5) $Fe_2Cl_4(bpy)_\infty$ (20).

A red needle crystal of approximate dimensions 0.35 x 0.26 x 0.26 mm was mounted on the tip of a glass fiber with Dow Corning silicone grease. Indexing and refinement of 24 reflections in the 2θ range 15-30° gave unit cell parameters for a monoclinic *C*-centered crystal system

Table 27. Crystal data and structure refinement for $[Mn_5Cl_{10}(THF)_8]_\infty$(16) and $[MnBr_2(THF)_2]_\infty$ (17).

Identification code	(16)	(17)
Empirical formula	$C_{32}H_{64}Cl_{10}Mn_5O_8$	$C_8H_{16}Br_2MnO_2$
Formula weight	603.02	179.48
Temperature	133(2) K	173(2) K
Wavelength	0.71073 Å	0.71073 Å
Crystal system	Triclinic	Orthorhombic
Space group	P-1	Pnn2
Unit cell dimensions	a = 9.4620(2) Å	a = 7.5930(15) Å
	b = 11.13870(10) Å	b = 18.375(4) Å
	c = 12.4763(2) Å	c = 3.9890(8) Å
	α = 75.2850(10)°.	$\alpha = \beta = \gamma = 90°$
	β = 76.3050(10)°.	
	γ = 79.6870(10)°.	
Volume	1225.72(3) Å^3	556.55(19) Å^3
Z	1	2
Density (calculated)	1.634 Mg/m^3	2.142 Mg/m^3
Absorption coefficient	1.840 mm^{-1}	8.332 mm^{-1}
F(000)	615	350
Crystal size (mm^3)	0.60 x 0.29 x 0.29	0.75 x 0.40 x 0.40
Reflections collected	7753	563
Absorption correction	SADABS	Scan
Refinement method	Full-matrix on F^2	Full-matrix on F^2
Data/restraints/parameters	5400 / 100 / 242	563 / 1 / 42
GOF on F^2	0.964	1.113
$R1(wR2)$ [F^2, $I>2\sigma(I)$]	0.0564(0.1446)	0.0506(0.1340)
Largest difference peak and hole	1.024 and -1.407 e$^-$/Å^3	1.566 and -1.021 e$^-$/Å^3
Abs. Structure, Extinction		0.04(7), 0.067(8)

$R1 = \Sigma \, ||F_o| - |F_c|| \, / \, \Sigma \, |F_o|$, $wR2 = \{\Sigma \, [w(F_o^2 - F_c^2)^2] \, / \, \Sigma \, [w(F_o^2)^2]\}^{1/2}$, $GOF = S = \{[w(F_o^2 - F_c^2)^2] \, / \, (n - p)\}^{1/2}$, $w = 1 \, / \, [\sigma^2(F_o^2) + (aP)^2 + bP]$

Table 28. Crystal data and structure refinement for $[MnCl_2(MeOH)_2]_\infty$ (18).

Identification code	(18)
Empirical formula	$C_2H_8Cl_2MnO_2$
Formula weight	189.92
Temperature	143(2) K
Wavelength	0.71073 Å
Crystal system	Triclinic
Space group	P-1
Unit cell dimensions	a = 3.7232(16) Å
	b = 5.817(3) Å
	c = 7.695(3) Å
	α = 94.801(7)°.
	β = 96.252(8)°.
	γ = 96.072(8)°.
Volume	163.96(12) Å3
Z	1
Density (calculated)	1.923 Mg/m3
Absorption coefficient	2.726 mm-1
F(000)	95
Crystal size (mm^3)	0.10 x 0.20 x 0.5
Indexing method	TWINNING
Reflections collected	1025
Absorption correction	SADABS
Refinement method	Full-matrix least-squares on F^2
Data / restraints / parameters	720 / 0 / 34
GOF on F^2	3.703
Final R indices [$I>2\sigma(I)$]	$R1$ = 0.1756, $wR2$ = 0.4677
R indices (all data)	$R1$ = 0.1926, $wR2$ = 0.4721
Largest diff. peak and hole	5.857 and -1.075 e/Å^3

$R1 = \Sigma \, ||F_o| - |F_c|| \, / \, \Sigma \, |F_o|$, $wR2 = \{\Sigma \, [w(F_o^2 - F_c^2)^2] \, / \, \Sigma \, [w(F_o^2)^2]\}^{1/2}$, $GOF = S = \{[w(F_o^2 - F_c^2)^2] \, / \, (n - p)\}^{1/2}$, $w = 1 \, / \, [\sigma^2(F_o^2) + (aP)^2 + bP]$

with a = 17.935(13) Å, b = 9.071(7) Å, c = 6.879(5) Å, α = 90°, β = 113.17(10)°, γ = 90°, and V = 1028.86(1.33) Å^3. Unique data of 1346reflections was collected by the ω-2θ technique between $4 \leq 2\theta \leq 55$. The data were corrected for Lorentz and polarization effects. The positions of the non-hydrogen atoms were located by direct methods and refined by full-matrix least square on F^2 using the SHELXTL 5.04 package whereas hydrogen atoms were placed in calculated positions. Key crystallographic data are summarized in Table 29.

(6) Structure of $[ppn]_2[Co_2Cl_6]$ (21).

Single crystals of $[ppn]_2[Co_2Cl_6]$ were grown by dissolving a bulk sample of $[ppn]_2[Co_2Cl_6]$ in 20 mL of acetone and layering with 10 mL of hexanes in a Schlenk tube. Light blue crystals were harvested after three days. A light blue diamond-shaped crystal of approximate dimensions 0.05 x 0.04 x 0.02 mm was mounted on the tip of a glass fiber with Dow Corning silicone grease and placed in a N_2 cool stream at 173(1)K. Indexing and refinement of 53 reflections from a total of 60 frames with an exposure time of 10 sec/frame indicated a monoclinic crystal system. A hemisphere of data with 1321 frames was collected with a scan width of 0.3° in ω and an exposure time of 30 sec/frame. Indexing and refinement of 221 reflections from a total of 200 data frames generated the precise cell for data integration which led to 40,634 reflections in the range of $-28 \leq h \leq 18$, $-17 \leq k \leq 17$, $-31 \leq l \leq 31$ with a maximum 2θ angle of 56.60°. Final cell parameters were generated from the refinement of the XYZ centroids of 6220 strong reflections with $I > 10\ \sigma(I)$. The unit cell parameters are a = 21.6564(2) Å, b = 13.1996(2) Å, c = 23.8566(1) Å, β= 102.7312(3)°, and V = 6651.90(12) Å^3. The intensities were corrected for beam inhomogeneity and crystal absorption and decay with SADABS which led to transmission factors

Table 29. Crystal data and structure refinement for $Fe_2Cl_4(bpy)_2$ (19) and $[FeCl_2(bpy)]_\infty$(20).

Identification code	(19)	(20)
Empirical formula	$C_{20}H_{16}Cl_4Fe_2N_4$	$C_{10}H_8Cl_2FeN_2$
Formula weight	282.93	282.93
Temperature	193(2) K	173(2) K
Wavelength	0.71073 Å	0.71069 Å
Crystal system	Triclinic	Monoclinic
Space group	P-1	C2/c
Unit cell dimensions	a = 8.205(2) Å	a = 17.935(5) Å
	b = 8.436(2) Å	b = 9.071(5) Å
	c = 8.749(2) Å	c = 6.879(5) Å
	α = 110.25(3)°	α = 90.000(5)°.
	β = 105.69(3)°	β = 113.170(5)°
	γ = 93.93(3)°	γ = 90.000(5)°
Volume	538.2(2) $Å^3$	1028.9(10) $Å^3$
Z	1	4
Density (calculated)	1.746 Mg/m^3	1.827 Mg/m^3
Absorption coefficient	1.860 mm^{-1}	1.946 mm^{-1}
F(000)	284	568
Crystal size (mm^3)	0.30 x 0.20 x 0.20	0.35 x 0.26 x 0.26
Reflections collected	2038	1223
Refinement method	Full-matrix on F^2	Full-matrix on F^2
Data/restraints/parameters	1897 / 0 / 168	1187 / 0 / 70
GOF on F^2	1.074	1.060
Final R indices [I>2σ(I)]	$R1$ = 0.0314, $wR2$ = 0.0850	$R1$ = 0.0776, $wR2$ = 0.1943
Largest diff. peak and hole	0.504 and -0.919 $e^-/Å^3$	1.566 and -2.871 $e^-/Å^3$
Extinction coefficient		0.008(3)

$R1 = \Sigma \| |F_o| - |F_c| \| / \Sigma |F_o|$, $wR2 = \{\Sigma [w(F_o^2 - F_c^2)^2] / \Sigma [w(F_o^2)^2]\}^{1/2}$, $GOF = S = \{[w(F_o^2 - F_c^2)^2] / (n - p)\}^{1/2}$, $w = 1 / [\sigma^2(F_o^2) + (aP)^2 + bP]$

between 0.89 to 1.00. Of the 15565 unique reflections, a total of 8184 reflections with $I > 2\sigma(I)$ and $R_{int} = 0.0332$ remained after data reduction. Equivalent reflections were merged and truncated to 0.85Å resolution to reduce the high R_{sigma} caused by the small size of the crystal. The structure was solved and refined with the SHELXTL 5.04 package. The positions of all non-hydrogen atoms were located by direct methods and refined anisotropically by full-matrix least squares on F^2. Hydrogen atoms were placed in idealized positions. The final full-matrix refinement was based on 11293 unique reflections (merged and truncated) and 775 parameters led to $R1 = 0.0452$ and $wR2 = 0.0789$ ($I > 2\ \sigma$). The goodness-of-fit index was 1.019 and the highest peak in the final difference map was 0.470 $e^-/Å^3$. The crystallographic data for (21) are summarized in Table 30.

(7) $[ppn]_2[Mn_2Cl_6]$ (22).

Single crystals were obtained by dissolving a bulk sample of $[ppn]_2[Mn_2Cl_6]$ in 20 mL of acetone and layering with 10 mL of hexanes in a Schlenk tube. Pale yellow rhombohedral crystals were harvested after three days. A light yellow rhombohedral crystal of approximate dimensions 0.49 x 0.31 x 0.26 mm was mounted on the tip of a glass fiber with Dow Corning silicone grease. Indexing and refinement of 274 reflections from a total of 60 frames with an exposure time of 10 sec/frame gave unit cell parameters. for a monoclinic unit cell. A hemisphere of data with 1321 frames was collected with a scan width of 0.3° in ω and an exposure time of 30 sec/frame. Indexing and refinement of 300 reflections from a total of 100 data frames generated the precise cell for data integration which led to 41,252 reflections in the range of $-18 \leq h \leq 28$, $-17 \leq k \leq 14$, $-31 \leq l \leq 31$ with a maximum 2θ angle of 56.66°. Final cell parameters were generated from the refinement of the centroids of 8192 strong reflections with

$I > 10\ \sigma$, are a = 21.7045(4) Å, b = 13.2667(2) Å, c = 24.0041(3) Å, β= 102.549(1)°, and V = 6746.80(29) Å^3. The reflections were corrected for beam inhomogeneity, crystal absorption and decay with the program SADABS which led transmission factors between 0.83 to 1.00. Of the 15,889 unique reflections, a total of 11,647 reflections with $I > 2\sigma(I)$ and R_{int} = 0.0321 remained after data reduction.

The positions of the non-hydrogen atoms were located by direct methods and refined by full-matrix least squares on F^2 using the SHELXTL 5.04 package. All non-hydrogen atoms were refined anisotropically. Hydrogen atoms were placed in idealized positions. Crystallographic data for (22) are summarized in Table 30.

(8) Structure of $[ppn]_2NiCl_4$ orthorhombic phase (23).

A blue block-shaped crystal of approximate dimensions 0.52 x 0.31 x 0.18 mm was mounted on the tip of a glass fiber with Dow Corning silicone grease and placed in a N_2 cool stream at 173(1) K. A hemisphere of data with 1321 frames was collected with a scan width of 0.3° in ω and an exposure time of 30 sec/frame. Indexing and refinement of 206 reflections from a total of 200 data frames generated the precise cell for data integration which led to 21816 reflections in the range of $-19 \leq h \leq 32$, $-16 \leq k \leq 16$, $-14 \leq l \leq 14$ with a maximum 2θ angle of 56.72°. Final cell parameters were generated from the refinement of the XYZ centroids of strong reflections with $I > 10\ \sigma(I)$. The unit cell parameters are a = 24.467(2) Å, b = 12.6947(8) Å, c = 10.8072(7) Å, $\alpha = \beta = \gamma = 90°$, and V = 3356.8(4) Å^3. The intensities were corrected for beam inhomogeneity, crystal absorption and decay with SADABS which led to transmission factors between 0.808 to 1.00 and R_{int} = 0.0452 for a total of 21,816 reflections (8,375 unique). The structure was solved and refined with the

SHELXTL 5.04 package. The positions of all non-hydrogen atoms were located by direct methods and refined anisotropically by full-matrix least squares on F^2. Hydrogen atoms were placed in idealized positions and not refined. The final full-matrix refinement was based on 4554 unique reflections and 394 parameters led to $R1$ = 0.0396 and $wR2$ = 0.0787 ($I > 2\ \sigma$). The goodness-of-fit index was 1.024 and the highest peak in the final difference map was 0.51 $e^-/Å^3$. The crystallographic data for (23) are summarized in Table 31.

(9) Composite phases of $[ppn]_2NiCl_4$ with orthorhombic and triclinic forms (23b, 24).

A hexagonal platelet of crystal (23b, 24) of approximate size 0.36 x 0.29 x 0.17 mm was examined on a SMART 1K CCD Area Detector and indexed to give the triclinic cell a = 13.620(10) Å, b = 13.646(7) Å, c = 21.443(13) Å, α = 104.52(7)°, β = 95.52(5)°, γ = 115.35(5)°, V = 3390.64(388) $Å^3$. A hemisphere of data was collected at 30sec/frame. Without symmetry constraints the data gave a different cell of a = 14.3861(3) Å, b = 14.1148(1) Å, c = 22.6380(5) Å, α = 90.0000(11)°, β = 90.0000(12)°, γ = 115.9618(6)°, V = 4132.92(15) $Å^3$. After reprocessing the data, one third of the original reflections used for indexing was rejected during the least-square refinement as the error is bigger than tolerance, and the cell reverted from the monoclinic setting back to a triclinic cell.

TWINDX[4] was then used to index the data, and a triclinic cell was indexed with default parameters. A second run with the remaining reflections revealed that the rest of the reflections indexed to an orthorhombic cell which happened to be the same as the cell for (23). This is a very rare case in which one can actually index reflections that belong to different crystal systems. A comparison of the orientation matrices and cell

Table 30. Crystal data and structure refinement for $[ppn]_2[Co_2Cl_6]$ (21) and for $[ppn]_2[Mn_2Cl_6]$ (22).

Identification code	(21)	(22)
Empirical formula	$C_{72}H_{60}Cl_6Co_2N_2P_4$	$C_{72}H_{60}Cl_6Mn_2N_2P_4$
Formula weight	1407.66	1399.68
Temperature	173(2) K	133(2) K
Wavelength	0.71073 Å	0.71073 Å
Crystal system	Monoclinic	Monoclinic
Space group	$P2_1/n$	$P2_1/n$
Unit cell dimensions	a = 21.6564(2) Å	a = 21.7045(4) Å
	b = 13.1996(2) Å	b = 13.2667(2) Å
	c = 23.85660(10) Å	c = 24.0041(3) Å
	β = 102.73°.	β = 102.55°.
Volume	6651.89(12) $Å^3$	6746.79(18) $Å^3$
Z	4	4
Density (calculated)	1.406 Mg/m^3	1.378 Mg/m^3
Absorption coefficient	0.880 mm^{-1}	0.750 mm^{-1}
F(000)	2888	2872
Crystal size, mm^3	0.050x 0.040 x 0.020	0.49 x 0.31 x 0.26
Reflections collected	11293	41252
Absorption correction	Multi-Scan, SADABS	Multi-scan, SADABS
Refinement method	Full-matrix on F^2	Full-matrix on F^2
Data / restraints / parameters	11293 / 0 / 775	15889 / 0 / 775
GOF on F^2	1.020	1.175
Final R indices [$I > 2\sigma(I)$]	$R1$ = 0.0452, $wR2$ = 0.0788	$R1$ = 0.0411, $wR2$ = 0.0815
Largest diff. peak and hole	0.470 and -0.386 $e/Å^3$	0.481 and -0.471 $e/Å^3$

$R1 = \Sigma \, ||F_o| - |F_c|| \, / \, \Sigma \, |F_o|$, $wR2 = \{\Sigma \, [w(F_o^2 - F_c^2)^2] \, / \, \Sigma \, [w(F_o^2)^2]\}^{1/2}$, goodness-of-fit = $S = \{[w(F_o^2 - F_c^2)^2] \, / \, (n - p)\}^{1/2}$, $w = 1 \, / \, [\sigma^2(F_o^2) + (aP)^2 + bP]$

Table 31. Crystal data and structure refinement for $[ppn]_2NiCl_4 \bullet Me_2CO$ (23) and (24).

Identification code	(23)	(24)
Empirical formula	$C_{75}H_{68}Cl_4N_2NiOP_4$	$C_{75}H_{66}Cl_2N_2NiOP_4$
Formula weight	1337.70	1264.79
Temperature	133(2) K	293(2) K
Wavelength	0.71073 Å	0.71073 Å
Crystal system	Orthorhombic	Triclinic
Space group	$P2_12_12$	P-1
Unit cell dimensions	a = 24.4677(15) Å	a = 13.661(3) Å
	b = 12.6947(8) Å	b = 13.712(3) Å
	c = 10.8072(7) Å	c = 21.279(5) Å
	α = 90°.	α= 104.059(4)°.
	β = 90°.	β= 95.699(4)°.
	γ = 90°.	γ= 115.919(4)°.
Volume	3356.8(4) Å^3	3379.9(12) Å^3
Z	2	2
Density (calculated)	1.323 Mg/m^3	1.243 Mg/m^3
Absorption coefficient	0.590 mm^{-1}	0.505 mm^{-1}
F(000)	1392	1320
Crystal size (mm^3)	0.45 x 0.30 x 0.28	0.36 x 0.29 x 0.17
Indexing method	SMART	TWINNING
Reflections collected	21784	20931
Refinement method	Full-matrix on F^2	Full-matrix on F^2
Data/restraints/parameters	7977 / 0 / 394	14764 / 15 / 772
GOF on F^2	1.024	0.853
$R1(wR2)$ [F^2, $I>2\sigma(I)$]	0.0396(0.0787)	0.0867(0.1811)
Abs. Struct. parameter	0.005(14)	
Largest diff. peak and hole	0.51 and -0.33 e.Å^{-3}	0.435 and -0.901 e.Å^{-3}

$R1 = \Sigma \, ||F_o| - |F_c|| \, / \, \Sigma \, |F_o|$, $wR2 = \{\Sigma \, [w(F_o^2 - F_c^2)^2] \, / \, \Sigma \, [w(F_o^2)^2]\}^{1/2}$, $GOF = \{[w(F_o^2 - F_c^2)^2] \, / \, (n - p)\}^{1/2}$, $w = 1 \, / \, [\sigma^2(F_o^2) + (aP)^2 + bP]$

parameters with TWROT indicated that the two solutions are rotated 37° from each another.

Data integration was carried out on the triclinic cell (24) from the TWINDX result with local and global cell constraints. The data were partially contaminated from the orthorhombic data. R_1 = 0.0888, wR_2 = 0.1944 (for $I > 2\sigma(I)$), and R_1 = 0.2881, wR_2 = 0.2507 (for all data).

Data integration for the orthorhombic cell (23b) with a global constraint produced a second data set. The reflections are weaker than those belonging to the triclinic cell. Least-squares refinement on F^2 led to R_1 = 0.1355, wR_2 = 0.1990 (for $I>2\sigma(I)$), and R_1 = 0.3753, wR_2 = 0.2746 (for all data). The crystallographic data for (24) are summarized in Table 31.

(10) [Et_4N]Cl•[$Fe_2Cl_4(MeOH)_4$(μ-2,2'-bpym)] (26)

A dark brownish-green crystal of dimensions 0.49 x 0.22 x 0.13 mm was secured on the tip of a glass fiber with Dow Corning silicone grease and placed in a cold N_2(g) stream at 173(2) K. Indexing and refinement of 39 out of 79 reflections from a total of 60 frames with an exposure time of 10 sec/frame indicated a monoclinic crystal system. A full sphere of data with 2474 frames was collected with a scan width of 0.3 in ω and exposure times -18< h < 18, -20 < k < 20, -20 < l < 20 with a maximum 2θ angle of 56.70°. Re-indexing the data reflection list with the TWINNING[4] package indicated the presence of rotational twins which correspond to 54 independent reflections for component A and 9 independent reflections for component B. Component B is readily transformed into component A by a 180° rotation around the (100) axis in direct or reciprocal space. The twinning law is [1 0 -0.15, 0 -1 0, 0 0 -1]. The data were integrated by using the orientation matrix of component A. Laue crystal symmetry constraints

Table 32. Crystal data and structure refinement for $[Et_4N]Cl{\bullet}Fe_2Cl_4(bpym)(MeOH)_4$. (26)

Identification code	(26)
Empirical formula	$C_{40}H_{84}Cl_{10}Fe_4N_{10}O_8$
Formula weight	1411.07
Temperature	173(2) K
Wavelength	0.71073 Å
Crystal system	Monoclinic
Space group	P2(1)/c
Unit cell dimensions	a = 13.589(2) Å
	b = 15.262(2) Å
	c = 15.423(2) Å
	α= 90°.
	β= 94.318(3)°.
	γ= 90°.
Volume	3189.7(8) Å^3
Z	2
Density (calculated)	1.469 Mg/m^3
Absorption coefficient	1.361 mm^{-1}
F(000)	1464
Crystal size	0.49 x 0.22 x 0.13 mm^3
Indexing method	TWINNING
Reflections collected	37705
Absorption correction	Multiscan (SADABS)
Refinement method	Full-matrix least-squares on F^2
Data / restraints / parameters	7774 / 0 / 325
GOF on F^2	0.910
Final R indices [$I>2\sigma(I)$]	$R1$ = 0.0642, $wR2$ = 0.1396
Largest diff. peak and hole	0.663 and -0.488 e.Å^{-3}

$R1 = \Sigma \, ||F_o| - |F_c|| \, / \, \Sigma \, |F_o|$, $wR2 = \{\Sigma \, [w(F_o^2 - F_c^2)^2] \, / \, \Sigma \, [w(F_o^2)^2]\}^{1/2}$, $GOF = S = \{[w(F_o^2 - F_c^2)^2] \, / \, (n - p)\}^{1/2}$, $w = 1 \, / \, [\sigma^2(F_o^2) + (aP)^2 + bP]$

were used during data integration, and the cell parameters and orientation matrix were refined and updated every 100 frames. All final parameters were generated from the refinement of the XYZ centroids of 6822 strong reflections with I >5 σ, which led to a = 13.589(2) Å, b = 15.262(2) Å, c = 15.423(2) Å, β = 94.318(3)°, V = 3189.7(8) Å^3. The intensities were corrected for beam inhomogeneity absorption and decay with the program SADABS[3] which led to transmission factors between 0.78 to 1.00. Of the 8060 unique reflections, a total of 3241 reflections with I > 2σ (I) and R_{int} = 0.164 remained after data reduction. The structure was solved and refined in the SHELXTL 5.10 package. The position of all non-hydrogen atoms were located by direct methods and refined anisotropically by full-matrix least squares on F^2. Hydrogen atoms were placed in idealized positions. The final full-matrix refinement based on 4774 unique reflection, of which 3241 with $I > 2\sigma$, and 326 parameters led to $R_1 = 0.064$ and $wR_2 = 0.166$ ($I > 2\sigma$). The goodness-of-fit is 0.910 and the highest peak in the final difference map is 0.663 e$^-$/Å^3

3. Discussion

A. X-ray Structural Results and Discussion.

(1) Structure of $[Mn_5Cl_{10}(THF)_8]_\infty$ (16).

Unlike the related clusters $Co_4Cl_8(THF)_6$[5] and $Fe_4Cl_8(THF)_6$[6] that exist as discrete molecular species, the Mn(II) derivative crystallizes as a one-dimensional polymeric chain. The structure of $[Mn_5Cl_{10}(THF)_8]_\infty$ is best described as a one-dimensional chain consisted of alternating $Mn_4Cl_8(THF)_6$ and $MnCl_2(THF)_2$ repeat units linked by chloride bridges. The presence of the mononuclear "$MnCl_2(THF)_2$" bridge allows for six coordination for all the metal ions, as opposed to the Fe and Co clusters in which there are two

five-coordinate and two six-coordinate metal centers. The fact that Mn(II) has a larger radius compared to Co(II) and Fe(II) is likely to contribute to its tendency to form exclusively six-coordinate structures in the absence of steric hindrance.

There are three different types of Mn environments in the structure, namely *trans*-$MnCl_4(THF)_2$, $MnCl_5(THF)$ and *cis*-$MnCl_4(THF)_2$ that exhibit different numbers of shared chlorides. There are also three types of chloride ligands in (16). The two terminal chlorides on the five coordinate sites in the Fe and Co clusters become μ_2-Cl atoms in $[Mn_5Cl_{10}(THF)_8]_\infty$ due to bridging interactions with the $MnCl_2(THF)_2$ unit, while the remaining μ_2-Cl and μ_3-Cl chlorine atoms exhibit similar geometry to the Fe and Co derivatives. The Mn-(μ_2-Cl) distances range from 2.494(1)-2.554(1)Å and the Mn-(μ_3-Cl) distance are from 2.593(1)-2.602(1) Å compared to the M(μ_2-Cl) ranges of 2.355(1)-2.488(2) Å and 2.285(2)-2.46(1) Å for Fe and Co respectively. In these clusters the M(μ_3-Cl) distances range from 2.506(1)-2.737(1) Å in Fe and 2.450(2)-2.844(3) Å in Co. From these comparisons, it is obvious that the μ_3-Cl interactions in (16) are more symmetrical with a more narrow range of observed bond lengths compared to the Fe and Co compounds. Schematic diagrams of the Fe and Mn derivatives are provided in Figure 62. The Mn-Mn separations are longer (Mn1-Mn2 = 3.7622(7) Å, Mn1-Mn1A = 3.7510(10) Å, Mn2-Mn3 = 3.6851(5) Å) than the distances observed in the structures of the Fe and Co derivatives (Co-Co range 3.630(2)-3.686(2) Å and Fe-Fe range 3.649(2)-3.751(2) Å).

(2) Structure of $[MnBr_2(THF)_2]_\infty$ (17)

The solid-state structure of (17) is also a one-dimensional polymeric structure, but in this case there is only one kind of manganese environment,

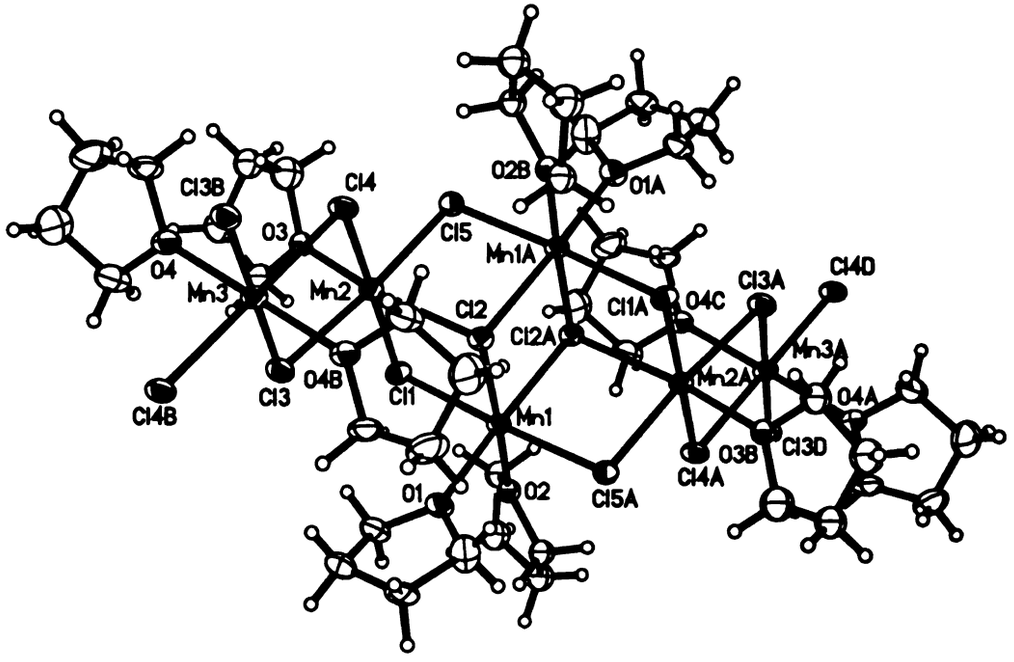
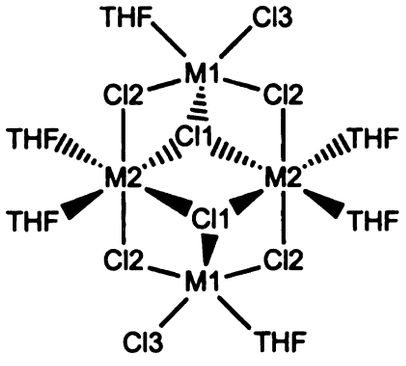
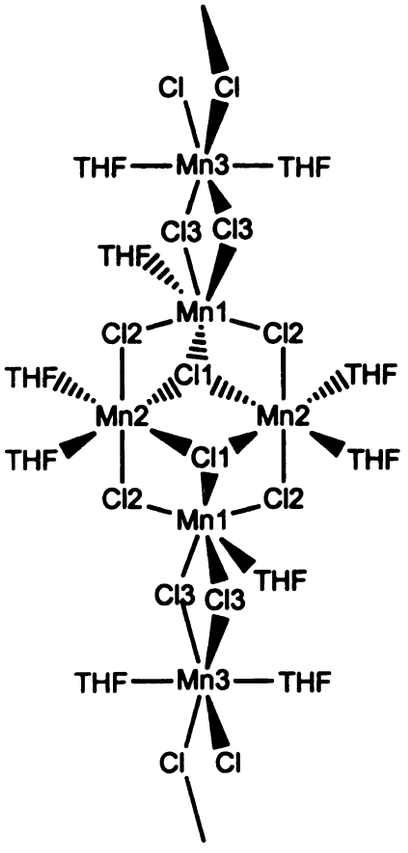


Figure 61. Thermal ellipsoid representation of $\{Mn_5Cl_{10}(THF)_8\}_\infty$(16).



$M_4Cl_8(THF)_6$, M = Fe, Co



$\{Mn_5Cl_{10}(THF)_8\}_n$

Figure 62. Comparison of different types of Mn(II) sites in (16) with the metal sites in $M_4Cl_8(THF)_6$ clusters.

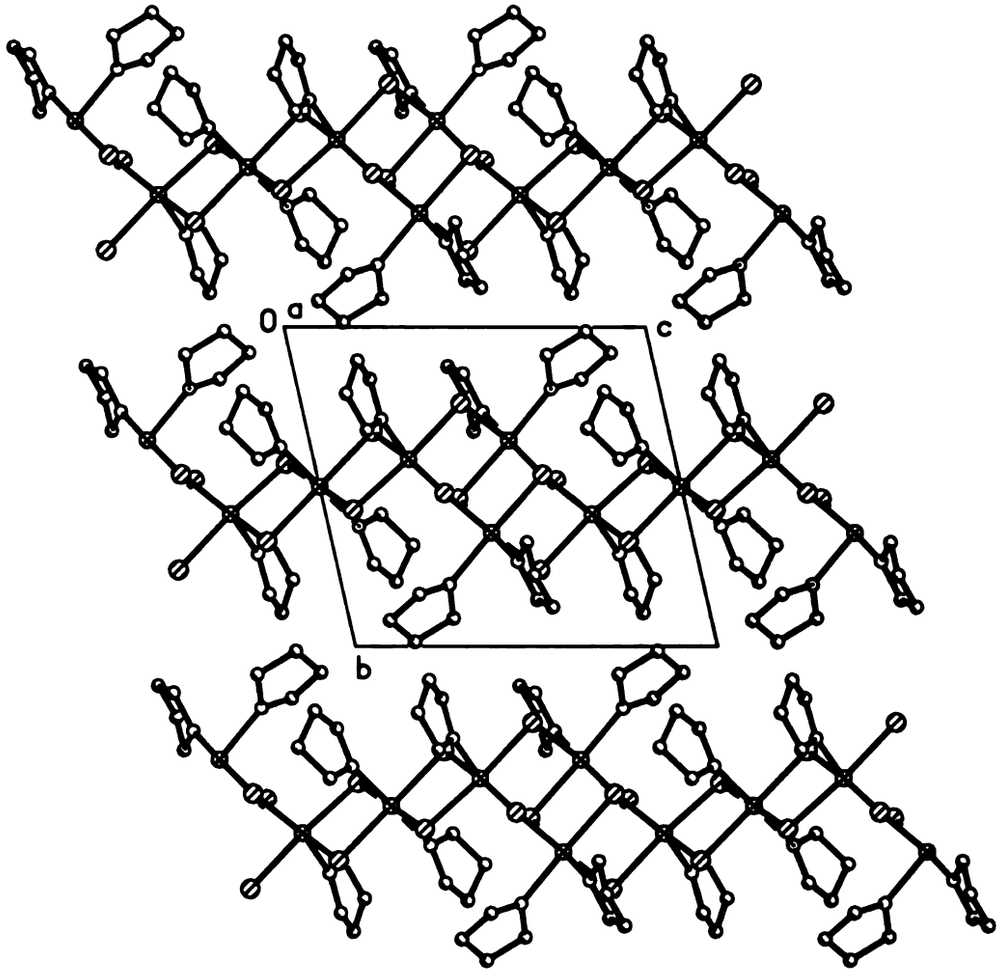


Figure 63. Packing view of $[Mn_5Cl_{10}(THF)_8]_\infty$ (16) down the *b* axis.

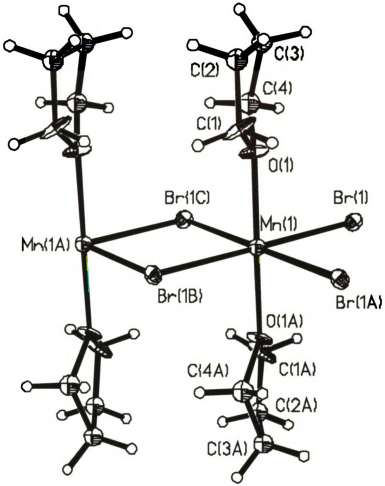


Figure 64. Thermal ellipsoid representation of a portion of the chain compound $[MnBr_2(THF)_2]_\infty$ (17).

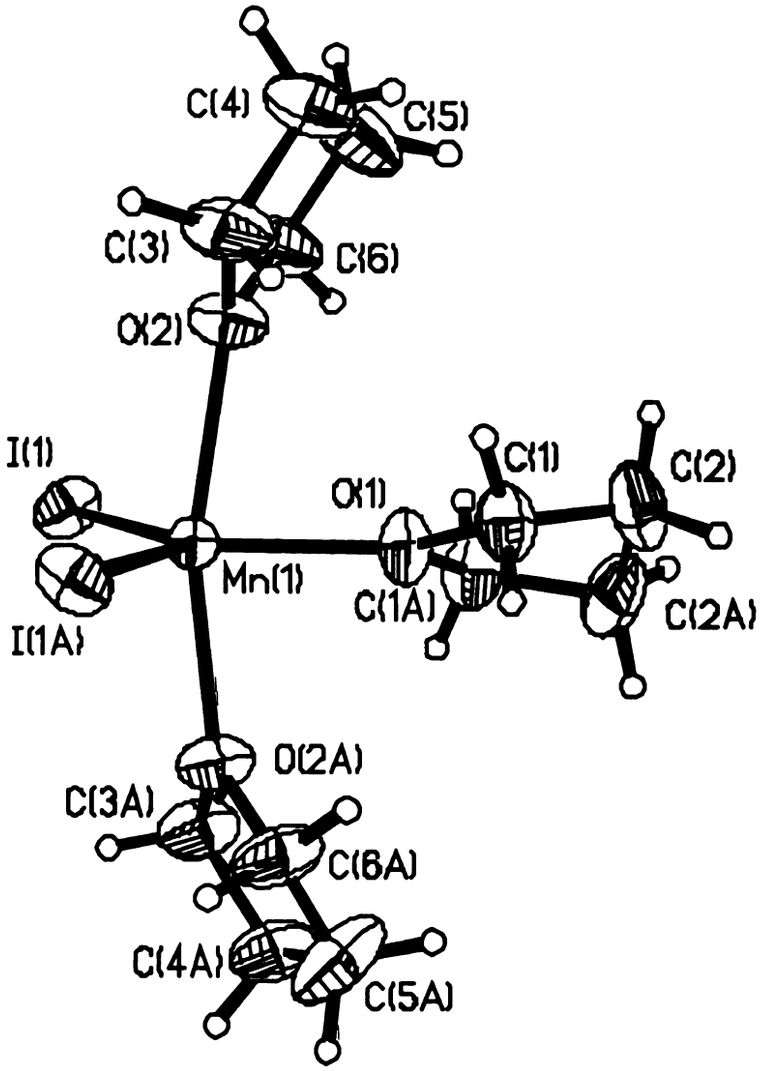


Figure 65. Thermal ellipsoid representation of mononuclear $[MnI_2(THF)_3]$.

namely a *trans*-bis(thf)tetrabromomanganate(II) unit which is the same as the mononuclear bridging moiety in (16). The fact that there is no evidence for the formation of the $Mn_4Br_8(THF)_6$ cluster is probably related to steric effects due to the much larger radius of Br^- as compared to Cl^-. The Mn-Mn separation in (17) is 3.9890(8) Å and the Mn-Br bond length is 2.722(5) Å. As expected, these distances are appreciably longer than those in the Cl compound. The angles Br-Mn-Br and Mn-Br-Mn are 85.9(2)° and 94.25(3)° respectively. The oxygen atoms are related by a two-fold axis through the Mn atom and the O-Mn-O is nearly linear (179.7(15)°).

The steric argument advanced to explain the structural differences in the $MnX_2(THF)_y$ (X = Cl, Br) compounds is further supported by an examination of the iodide derivative.[7] As can be seen from the Thermal ellipsoid diagram in Figure 63, *cis*-$MnI_2(THF)_3$ is a five coordinate trigonal bipyramidal molecule rather than a cluster or an oligomer. Due to the larger size of the iodine atoms, the axial oxygen atoms are bent away from the equatorial positions as evidenced by the angles O-Mn-O is 165.3(3)° and the I-Mn-I angle is 126.89(5)°. The Mn-I bond length is 2.7244(9) Å.

(3) Structure of $Fe_2Cl_4(bpy)_2$ (19).

Compound (19) crystallizes as a dinuclear compound with a square pyramidal geometry resulting from the union of two "$FeCl_2(bpy)$" units with two bridging chloride atoms. The Fe atoms are 0.699(1) Å above the least-square plane of the basal plane of the square pyramid. The angle between the least-squares plane of the bipyridine and the base of the square pyramidal is 21.54(8)°. The least-square plane refinement results are listed in Table 5. The bipyridine molecules from different dimer units stack along the *a* direction of the unit cell with an average intermolecular contact of 3.393(3) Å. A plot of (19) viewed down the *a* direction of the unit cell is

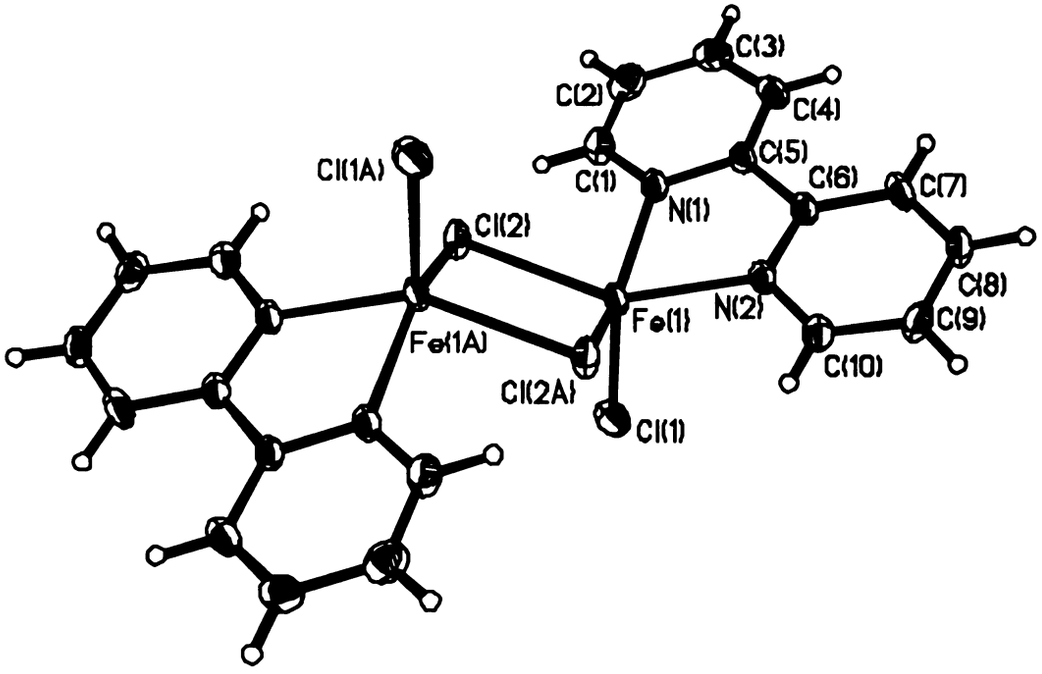


Figure 66. Thermal ellipsoid representation of $[Fe_2Cl_4(bpy)_2]$. (19)

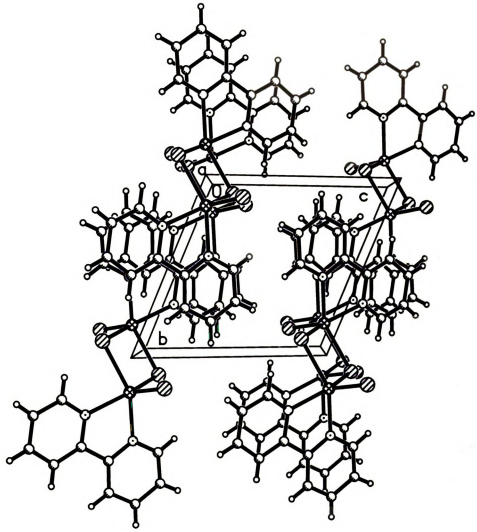


Figure 67. Packing view of $[Fe_2Cl_4(bpy)_2]$(19) down the *a* axis.

shown in Figure 66. It is interesting to note that the structure of the $Fe_2Cl_4(bpy)_2$ differs from that of the corresponding manganese chloride compound of empirical formula "$MnCl_2(bpy)$" which crystallizes in polymeric chains.[8] The dimer feature of (19) versus the one-dimensional chain of $[MnCl_2(bpy)]_\infty$ and (20) may be explained by the fact that the smaller Fe(II) ion does not always prefer six coordination unlike Mn(II). In the event that more sterically demanding ligands than 2,2'-bipyridine are used, Mn(II) adopts the dinuclear structure as in the case of $Mn_2Cl_4(biq)_2$ (biq = 2,2'-biquinolyl).[9] The molecule $Mn_2Cl_4(biq)$ (depicted schematically in Figure 70), possesses a Mn-Mn distance of 3.887(1) Å and a Mn-Cl-Mn angle of 99.8°, compared to the Fe-Fe distance in (19) of 3.7048(17) Å and an Fe-Cl-Fe angle of 97.35(4)°. Although the two structures are very similar, the Fe-Fe distance is shorter and the Fe-Cl-Fe angle is more acute. The bpy ligand deviates only slightly from planarity, while the biq ligand is bent. It appears from these results that the edge sharing square pyramidal dimer structures of $Fe_2Cl_4(bpy)_2$ and $Mn_2Cl_4(biq)_2$ result from primarily steric rather than electronic factors. The existence of another similar dimer metal bipyridyl chloride complex $[CuCl_2(4,4'\text{-}Me_2bpy)_2]_2$[10] also supports such a hypothesis.

(4) Structures of $[ppn]_2[Co_2Cl_6]$ (21) and $[ppn]_2[Mn_2Cl_6]$ (22)

Compound (21) and compound (22) of general formula $[M_2Cl_6]^{2-}$ crystallize as dinuclear anions consisting of two distorted tetrahedra with shared chlorine edges. Both structures are similar to that of $[ppn]_2Fe_2Cl_6$ in that the packing is dominated by the relatively bulky $[ppn]^+$ cations. The two orientations of the $[M_2Cl_6]^{2-}$ anions in the asymmetric unit of (21) and (22) are believed to be the result of a packing effect that forces the chlorine bridges to adopt more acute angles.

Table 33. Bond lengths [Å] and angles [°] for $[FeCl_2(bpy)]_\infty$ (20).

A-B (Å)		A-B (Å)	
Fe(1)-N(3)#1	2.171(3)	N(3)-C(5)	1.341(5)
Fe(1)-N(3)	2.171(3)	N(3)-C(4)	1.350(5)
Fe(1)-Cl(2)	2.4220(12)	C(4)-C(6)	1.391(6)
Fe(1)-Cl(2)#1	2.4220(12)	C(5)-C(7)	1.396(5)
Fe(1)-Cl(2)#2	2.632(2)	C(5)-C(5)#1	1.492(8)
Fe(1)-Cl(2)#3	2.632(2)	C(6)-C(8)	1.378(7)
Cl(2)-Fe(1)#3	2.632(2)	C(7)-C(8)	1.376(6)

A-B-C (°)		A-B-C (°)	
N(3)#1-Fe(1)-N(3)	74.98(18)	Cl(2)#1-Fe(1)-Cl(2)#3	96.62(4)
N(3)#1-Fe(1)-Cl(2)	93.74(10)	Cl(2)#2-Fe(1)-Cl(2)#3	179.92(4)
N(3)-Fe(1)-Cl(2)	162.84(10)	Fe(1)-Cl(2)-Fe(1)#3	96.56(4)
N(3)#1-Fe(1)-Cl(2)#1	162.84(10)	C(5)-N(3)-C(4)	117.7(3)
N(3)-Fe(1)-Cl(2)#1	93.74(10)	C(5)-N(3)-Fe(1)	117.0(3)
Cl(2)-Fe(1)-Cl(2)#1	99.93(6)	C(4)-N(3)-Fe(1)	124.8(3)
N(3)#1-Fe(1)-Cl(2)#2	84.74(9)	N(3)-C(4)-C(6)	123.3(4)
N(3)-Fe(1)-Cl(2)#2	95.19(9)	N(3)-C(5)-C(7)	122.2(4)
Cl(2)-Fe(1)-Cl(2)#2	96.62(4)	N(3)-C(5)-C(5)#1	115.3(2)
Cl(2)#1-Fe(1)-Cl(2)#2	83.44(4)	C(7)-C(5)-C(5)#1	122.5(2)
N(3)#1-Fe(1)-Cl(2)#3	95.19(9)	C(8)-C(6)-C(4)	118.1(4)
N(3)-Fe(1)-Cl(2)#3	84.74(9)	C(8)-C(7)-C(5)	119.2(4)
Cl(2)-Fe(1)-Cl(2)#3	83.44(4)	C(7)-C(8)-C(6)	119.5(4)

Symmetry transformations used to generate equivalent atoms:
#1 -x,y,-z+1/2
#2 x,-y+1,z-1/2
#3 -x,-y+1,-z+1

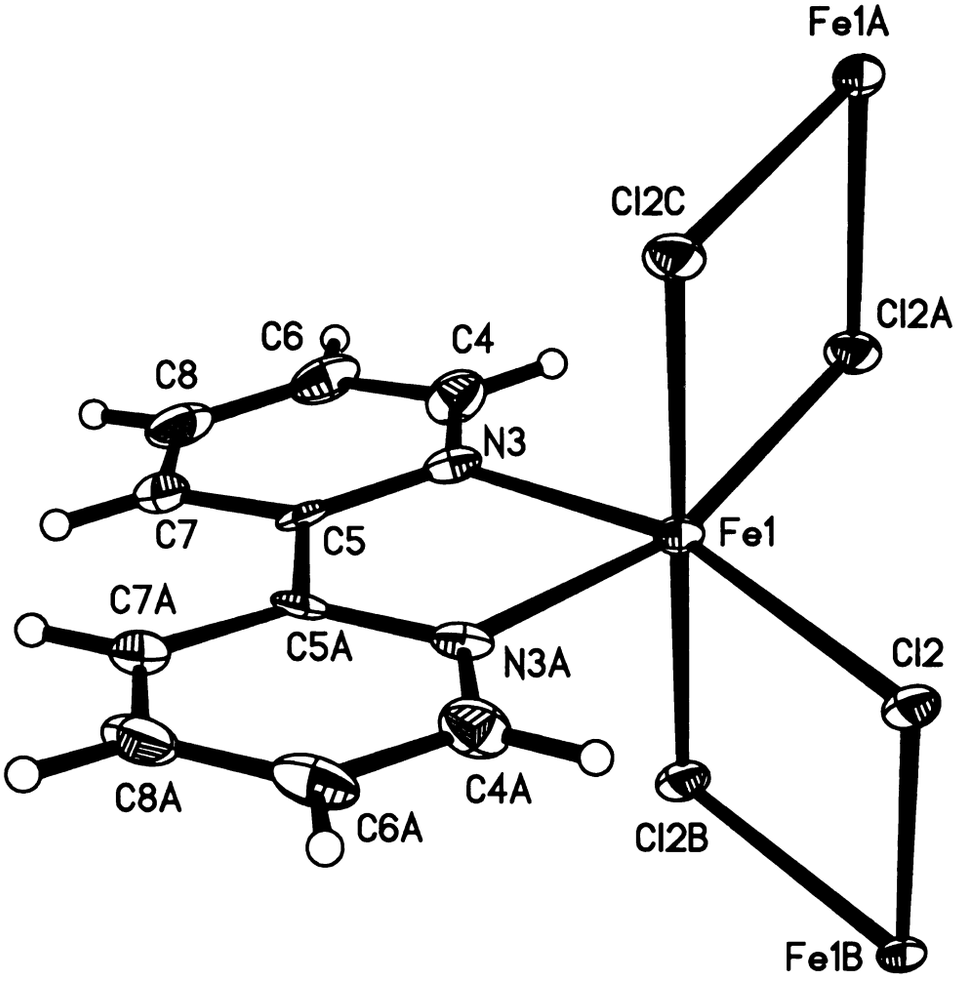


Figure 68. Thermal ellipsoid representation of $[FeCl_2(bpy)]_\infty$ (20.)

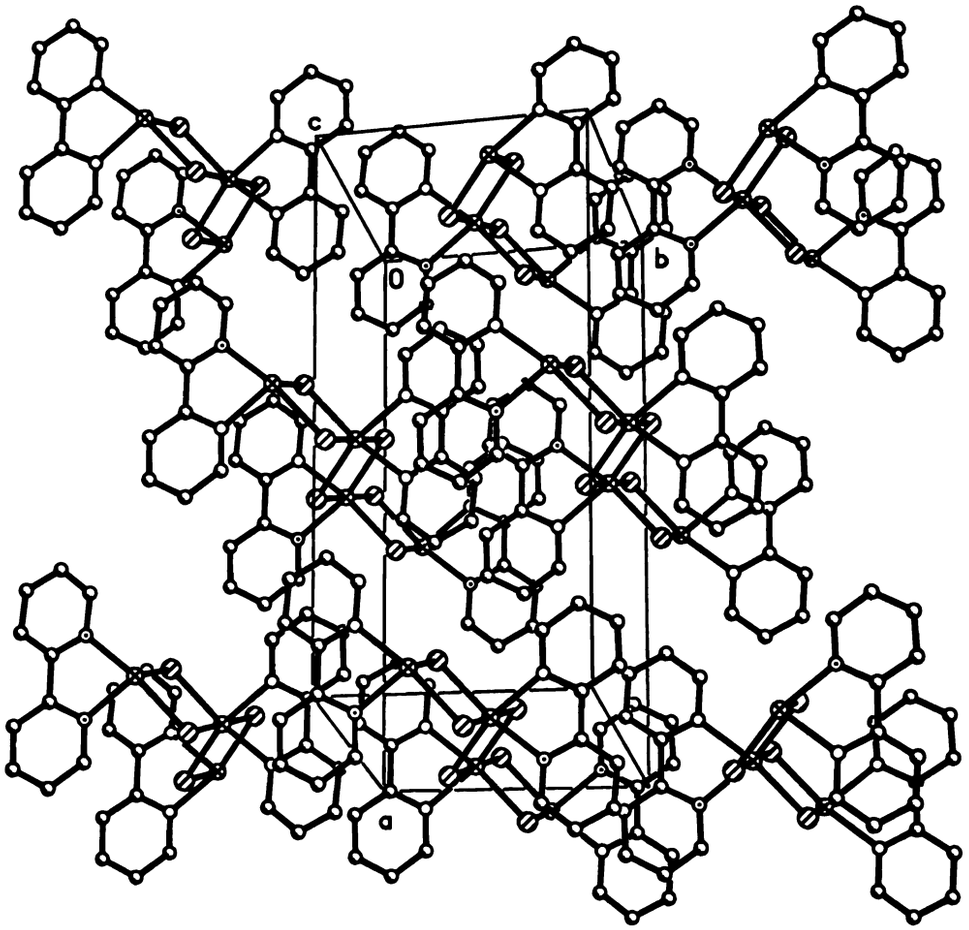
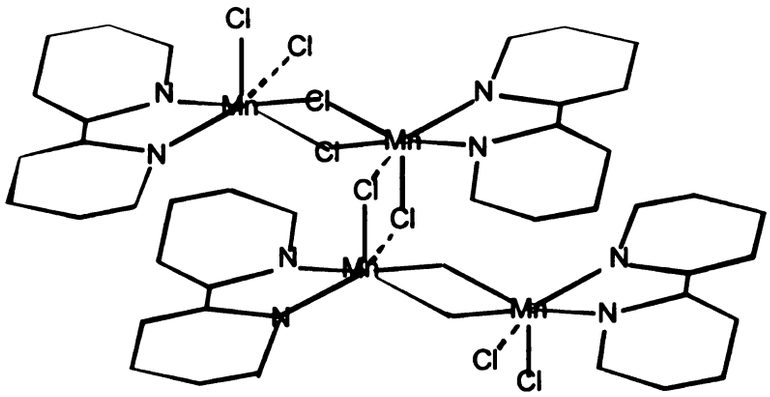
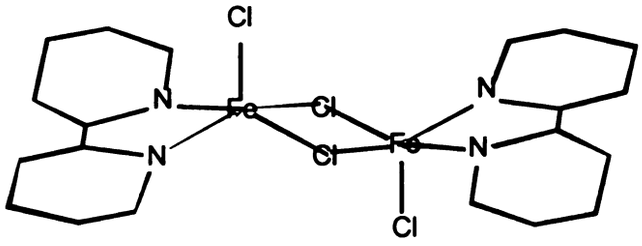


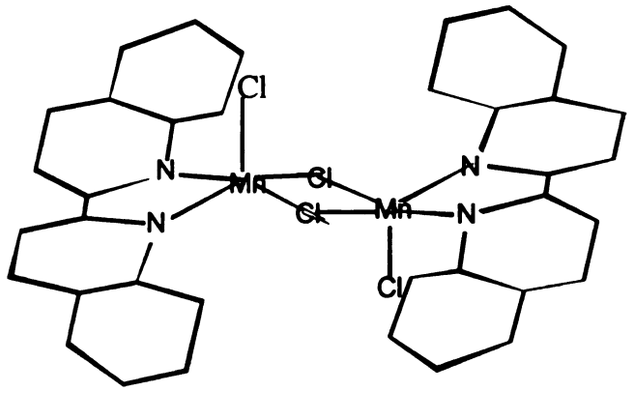
Figure 69. Packing diagram of $[FeCl_2(bpy)]_\infty$ (20) showing the one-dimensional chain along *c* axis.



$[MnCl_2(bpy)]_n$



$[FeCl_2(bpy)]_2$



$[MnCl_2(biq)]_2$

Figure 70. Structures of $[MCl_2(bidentateL)]_2$.

(a) $[ppn]_2[Co_2Cl_6]$ (21).

The $[Co_2Cl_6]^{2-}$ moieties can be viewed as an assembly of two edge-sharing tetrahedral $[CoCl_4]^-$ units related by an inversion center. There are two independent $[Co_2Cl_6]^{2-}$ anions in the asymmetric unit. The average Co-$Cl_{terminal}$ and average Co-$Cl_{bridging}$ distances of 2.224(1) Å and 2.346(1) Å are comparable to the corresponding distances reported in the literature (2.212(3)-2.238(6) Å for distances of Co-$Cl_{terminal}$ and 2.329(5)-2.38 (3) Å for Co-$Cl_{bridging}$).[24] The Co·····Co distance of 3.221(1) Å is shorter than the corresponding distances reported in the literature (3.277 (6)-3.366 (3) Å).[26] The Co1-Cl2-Co1* and Cl2-Co-Cl2* angles of 85.79 and 93.29(3)° are considerably distorted from an ideal tetrahedral geometry due to the formation of the four membered ring. Both of the $[Co_2Cl_6]^{2-}$ units possess Cl-Co-Cl angles larger than 90°. By comparison, in the $[ppn]_2Fe_2Cl_6$ structure, one of the two $[Fe_2Cl_6]^{2-}$ anions exhibits an angle less than 90°. The Co·····Co distance in (21) is the shortest one of the group, and the Co-Cl-Co angle is the smallest in our $[ppn]_2[M_2Cl_6]$ (M = Fe, Co and Mn) series. A projection diagram viewed in the *ac* plane in Figure 71 illustrates the arrangement of the $[ppn]^+$ cations and the $[Co_2Cl_6]^{2-}$ anions in the unit cell.

(b) $[ppn]_2[Mn_2Cl_6$ (22).

The $[ppn]_2[Mn_2Cl_6]$ structure is similar to the Co analogue, with two independent dimetal anion units in the unit cell and a Cl-Mn-Cl angle greater than 90°. The average Mn-$Cl_{terminal}$ and average Mn-$Cl_{bridging}$ distances of 2.309(1) Å and 2.446(1)Å are comparable to analogous distances reported in the literature 2.306(2) Å for distances of Mn-$Cl_{terminal}$ and 2.440(2) Å for distances for Mn-$Cl_{bridging}$.[11] The average Mn·····Mn distance of 3.376(1) Å is the same as the distances reported in the literature for $[Mn_2Cl_6]^{2-}$ anion (3.376(2) Å).[11a] The average Mn1-Cl2-Mn1* and Cl2-Mn-Cl2* angles of

87.25(2)° and 92.75(2)° are considerably distorted from an ideal tetrahedral geometry due to the formation of the four member ring. A projection diagram viewed down the *ac* plane in Figure 74 illustrates the arrangement of the $[ppn]^+$ and the $[Mn_2Cl_6]^{2-}$ units in the unit cell.

(c) $[Et_4N]Cl•[Fe_2Cl_4(MeOH)_4(\mu\text{-}2,2'\text{-bpym})]$ (26).

Cleavage of the $[Fe_2Cl_6]^{2-}$ core is also observed to occur in the reaction of $[Et_4N]_2[Fe_2Cl_6]$ with 2,2'-bpym in MeOH. The compound $[Et_4N]Cl•Fe_2Cl_4(MeOH)_4(\mu\text{-}2,2'\text{-bpym})$ consists of two Fe(II) atoms joined by a bis-chelating 2,2'-bpym ligand that are further bonded to two terminal chlorides and two methanol ligands. The unit cell also contains an equivalent of $[Et_4N]Cl$ that serves to fill void space as well as to assist in connecting the dimeric molecules into an infinite chain through hydrogen bonds between the outer-sphere Cl^- ions and the axial MeOH ligands. The average hydrogen bonding distance between the outer-sphere Cl^- ion and the axial methanols is 2.315(7) Å. There are also weak hydrogen bonding between the terminal chlorides, which bonded to the metal, and 2,2'- bpym ring as well as the tetraethylammonium cation at an average distance of 2.805(5) Å. The 2,2'-bpym ring is slightly out of the plane containing Fe1 and Fe1A by ~0.015 Å. A thermal ellipsoid drawing as well as selected bond distances and bond angles for $[Et_4N]Cl•[Fe_2Cl_4(MeOH)_4(\mu\text{-}2,2'\text{-bpym})]$ are presented in Figure 75 and Table 36. The average Fe-Cl bond distance is 2.383(2) Å. Fe1-N(bridging) bond distances of 2.224(6) Å and 2.239(6) Å differ only slightly differs from Fe2-N(bridging) bond distances at 2.244(6) Å and 2.250(6) Å. The separation between two intramolecular Fe(II) atoms is 5..957 Å. The closest intermolecular Fe$\cdots$Fe contact is 7.964 Å. The occurence of rotational twining hindered previous attempts to solve the structure by point detector data, which was contaminated by twinning

Table 34. Selected bond distances (Å) and bond angles (°) for $[ppn]_2[Co_2Cl_6]$, (21).

Bond Distances

A	B	A-B (Å)	A	B	A-B (Å)	A	B	A-B (Å)
Co1	Co1*	3.191 (1)	Co2	Co2*	3.251 (1)	N1	P1	1.585 (3)
Co1	Cl1	2.224 (1)	Co2	Cl4	2.232 (1)	N1	P2	1.580 (3)
Co1	Cl2	2.347 (1)	Co2	Cl5	2.362 (1)	N2	P3	1.585 (3)
Co1	Cl2*	2.342 (1)	Co2	Cl5*	2.334 (1)	N2	P4	1.578 (3)
Co1	Cl3	2.224 (1)	Co2	Cl6	2.216 (1)			

Bond Angles

A	B	C	A-B-C (°)	A	B	C	A-B-C (°)
Cl1	Co1	Cl3	115.94 (4)	Cl4	Co2	Cl6	115.57 (4)
Cl1	Co1	Cl2	106.86 (4)	Cl4	Co2	Cl5	112.34 (4)
Cl1	Co1	Cl2*	114.34 (4)	Cl4	Co2	Cl5*	113.55 (4)
Cl3	Co1	Cl2	114.81 (2)	Cl6	Co2	Cl5	109.94 (5)
Cl3	Co1	Cl2*	108.76 (4)	Cl6	Co2	Cl5*	110.75 (5)
Cl2	Co1	Cl2*	94.21 (3)	Cl5	Co2	Cl5*	92.37 (3)
Co1	Cl2	Co1*	85.79 (3)	Co2	Cl5	Co2*	87.63 (3)
P1	N1	P2	137.4 (2)	P3	N2	P4	140.6 (2)

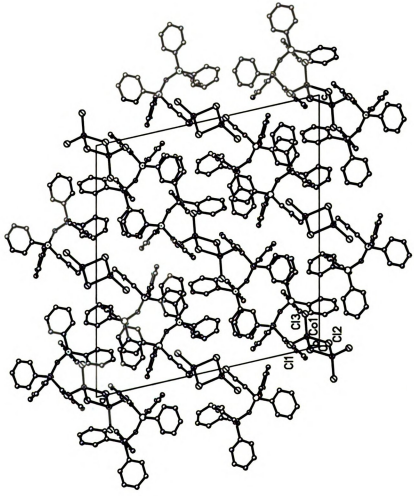


Figure 71. Packing view of $[ppn]_2Mn_2Cl_6$ in the *ac* plane.

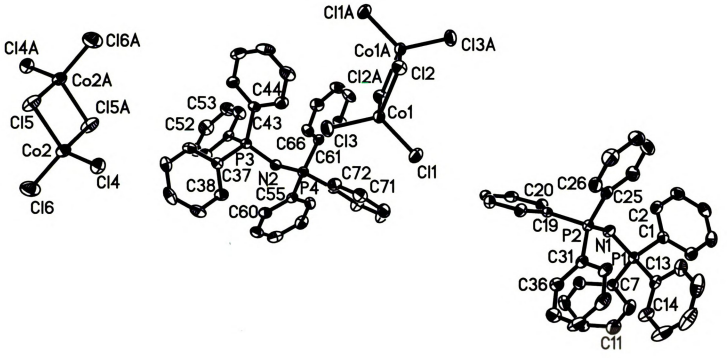


Figure 72. Thermal ellipsoid representation of (21).

and led to severe systematic violations and a high R factor. By using CCD data and the TWINNING[4] package, we were able to integrate the data basically free from twinning contamination (less than 0.1%).

B. Magnetic Studies.

Since one of the goals of this work was to use the dinuclear metal anion $[Fe_2Cl_6]^{2-}$ and the tetranuclear metal cluster $Fe_4Cl_8(THF)_6$ as a source of the diferrous ion in reactions with polydentate ligands, we undertook a comprehensive study of the magnetic properties of various salts of this anion and of analogous anions of Co(II) and high-spin Mn(II). Four complexes containing the $[Co_2Cl_6]^{2-}$ moiety[12] and $[M_2X_6]^{2-}$ salts containing various metals and halides such as $[Fe_2I_6]^{2-}$ and $[Mn_2X_6]^{2-}$ (X = Br, I Cl), have appeared in the literature.[13,14] No magnetism has been detailed for these compounds. In this work, magnetic studies of the different salts of $[M_2Cl_6]^{2-}$ with the metal ions M^{II} = Fe, Co and Mn have been performed. For the Fe compounds, salts containing four different counterions were studied to check for the effect of counterion on magnetic interactions.

(1) Magnetic properties of $[ppn]_2[Co_2Cl_6]$ and $[ppn]_2[Mn_2Cl_6]$.

The magnetic properties of the $[ppn]^+$ salt are depicted in Figures 66, 67 and 68 with plots of χ vs. T and χT vs. T. These data suggest the presence of strong antiferromagnetic exchange interactions between the Co(II) ions. A rounded maximum in χ at 50 K is observed, while χT reveals a continuous decrease from a value of 4.22 emu·K/mole at 300 K to a value close to zero at 2 K. In tetrahedral environments, Co(II) is described by a $^4A_2$ term. Therefore, the Hamiltonian in Eq. 7 was expected to be appropriate to describe its properties,

$$H_o = -2JS_1S_2 + D(S_{z1}^2 + S_{z2}^2) \qquad \text{(Eq. 7)}$$

as it contains an isotropic exchange term supplemented by a zero-field splitting term to account for the single-ion anisotropy of the spin S=3/2 of Co(II). In an initial fitting exercise, we attempted to reproduce the magnetic properties by a fully isotropic Hamiltonian, *i.e.*, by neglecting the single-ion anisotropy contribution. This simple model completely failed to fit the magnetic data. In particular, significant differences between theory and experiment were observed in the region near the maximum in χ (dotted line in Figure 76). In a second step, the ZFS term was taken into account which introduces a magnetic anisotropy. In a manner similar to the treatment of the Fe dimers, the model needs to calculate the two components of the magnetic susceptibility ($\chi_{//}$ and $\chi_{\perp}$) in order to obtain the theoretical curve for a powder ($\chi_{powder} = (\chi_{//} + 2\chi_{\perp})/3$). With this additional term the magnetic behavior is closely reproduced in the whole temperature range from the following set of parameters: J = - 11.6 cm^{-1}, D = 29.0 cm^{-1} and g = 2.25 (solid line in Figures. 76 and 77). A small amount of paramagnetic impurity (0.16 %) was introduced to reproduce the Curie tail observed below 4 K.

In summary, the spin anisotropy is again the dominant contribution (the ratio $\Delta J/\Delta D$ is equal to 0.4), although a stronger antiferromagnetic coupling is present. The large values of D compared to J are a consequence of the bridging angles M-Cl-M which are not far from the orthogonality value which favors weak interactions. An additional effect for a distorted tetrahedral environment is that the ZFS of the ground spin state can mix withexcited states through a second-order spin orbit coupling may be quite significant. The magnetic data for $[ppn]_2[Mn_2Cl_6]$ are plotted in Figure 78. A continuous decrease in χT is observed at lower temperatures which is indicative of dominant antiferromagnetic interactions. In this case the ZFS is expected to be quite small compared to J, as the ground state of Mn(II) is

Table 35. Selected bond distances (Å) and bond angles (°) for $[ppn]_2[Mn_2Cl_6]$, (22).

Bond Distances

A	B	A-B (Å)	A	B	A-B (Å)	A	B	A-B (Å)
Mn1	Mn1*	3.344 (1)	Mn2	Mn2*	3.408 (1)	N1	P1	1.586 (2)
Mn1	Cl1	2.305 (1)	Mn2	Cl4	2.305 (1)	N1	P2	1.583 (2)
Mn1	Cl2	2.447 (1)	Mn2	Cl5	2.466 (1)	N2	P3	1.583 (2)
Mn1	Cl2*	2.439 (1)	Mn2	Cl5*	2.434 (1)	N2	P4	1.582 (2)
Mn1	Cl3	2.310 (1)	Mn2	Cl6	2.316 (1)			

Bond Angles

A	B	C	A-B-C (°)	A	B	C	A-B-C (°)
Cl1	Mn1	Cl3	118.00 (3)	Cl4	Mn2	Cl6	118.21 (3)
Cl1	Mn1	Cl2	105.58 (3)	Cl4	Mn2	Cl5	108.63 (3)
Cl1	Mn1	Cl2*	113.82 (3)	Cl4	Mn2	Cl5*	110.04 (3)
Cl3	Mn1	Cl2	114.49 (3)	Cl6	Mn2	Cl5	111.52 (3)
Cl3	Mn1	Cl2*	108.79 (3)	Cl6	Mn2	Cl5*	113.40 (3)
Cl2	Mn1	Cl2*	93.63 (2)	Cl5	Mn2	Cl5*	91.87 (2)
Mn1	Cl2	Mn1*	86.37 (2)	Mn2	Cl5	Mn2*	88.13 (2)
P1	N1	P2	137.3 (2)	P3	N2	P4	141.2 (1)

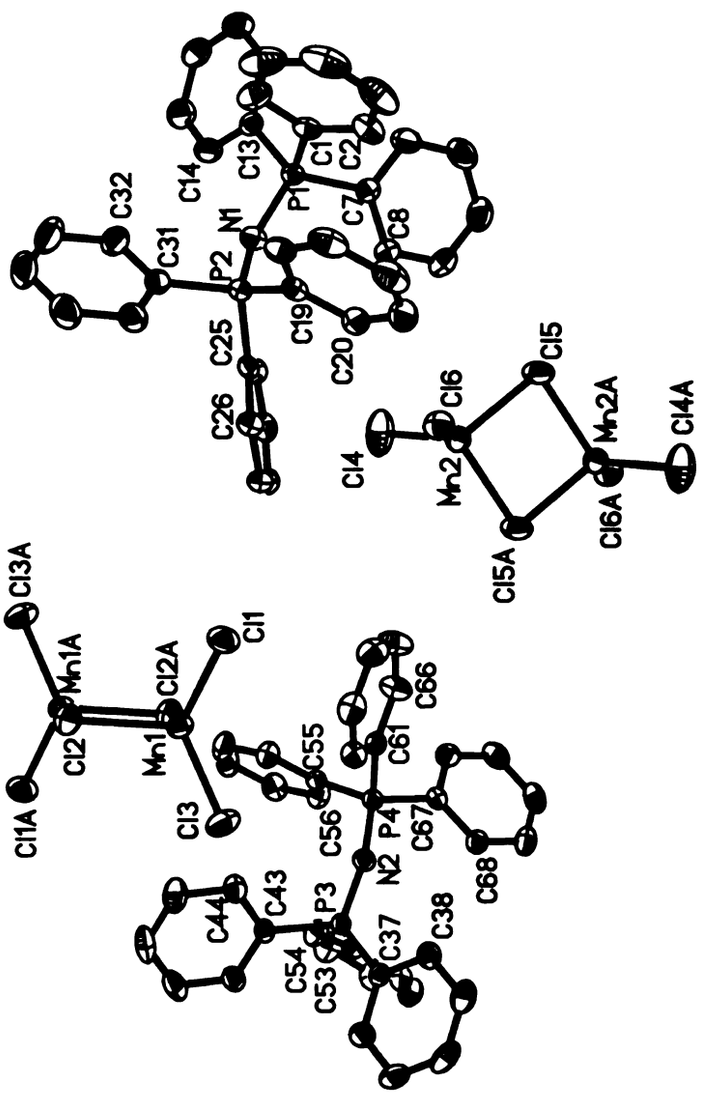


Figure 73. Thermal ellipsoid representation of (22).

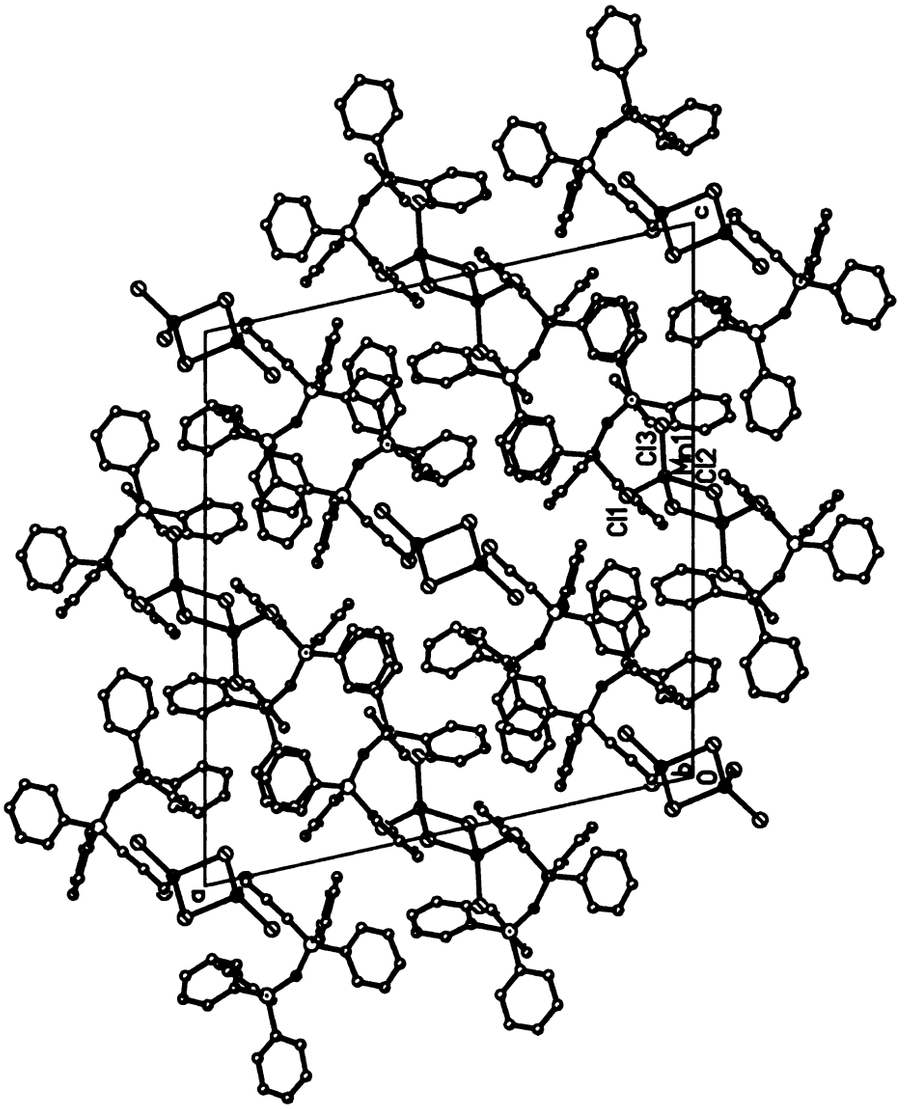


Figure 74. Packing view of $[ppn]_2Mn_2Cl_6$ in the *ac* plane.

described by a $^6A_1$ term. Thus, a fully isotropic Heisenberg Hamiltonian should be suitable for describing the properties. As we can see from the data, however, this model does not satisfactorily reproduce the experimental behavior. A model assuming two antiferromagnetic J parameters of different magnitudes was used to improve this fit. The consideration of a second exchange coupling in this system may be due to the presence of a weak antiferromagnetic coupling between Mn dimers. A simple model that accounts for this effect is that of an alternating J-J' chain of spins 5/2. If these spins are treated as classical, an analytical expression can be obtained. Using this expression, a good fit of the experimental data was obtained. The best fit (solid line in Figure 78) corresponds to the following parameter values: J = -15.6 cm^{-1}, J' = - 0.69 cm^{-1} and g = 2.32. In order to reproduce the data a paramagnetic impurity has been introduced (3%).

(2) Magnetic fitting of Mn(II) chains of (17).

In order to fit the magnetic properties of these linear chains, the well-known Fisher expression for classical spins was used.[13] The best fit gives[J = -0.17 K and g = 2.06. Unfortunately, the data are contaminated with oxygen just in the region where the χT product starts to decreases which makes it difficult to obtain a precise fit. Another sample needs to be measured for this to be a reliable fit.

(3) $[Mn_5Cl_{10}(THF)_8]_\infty$chain of (16)

With the classical model, fitting parameters were obtained with g equal to 2.28 and J equals to –0.70 K. A cluster approximation with the definition of the exchange pathways (as shown in Figure 70-73).

(4) Magnetism of the Mn cluster (16)

In the cluster approximation the best fitting parameters are obtained when J'/J is small (J'/J = 0.1, J' = J" and J = -0.4K). When compared to the

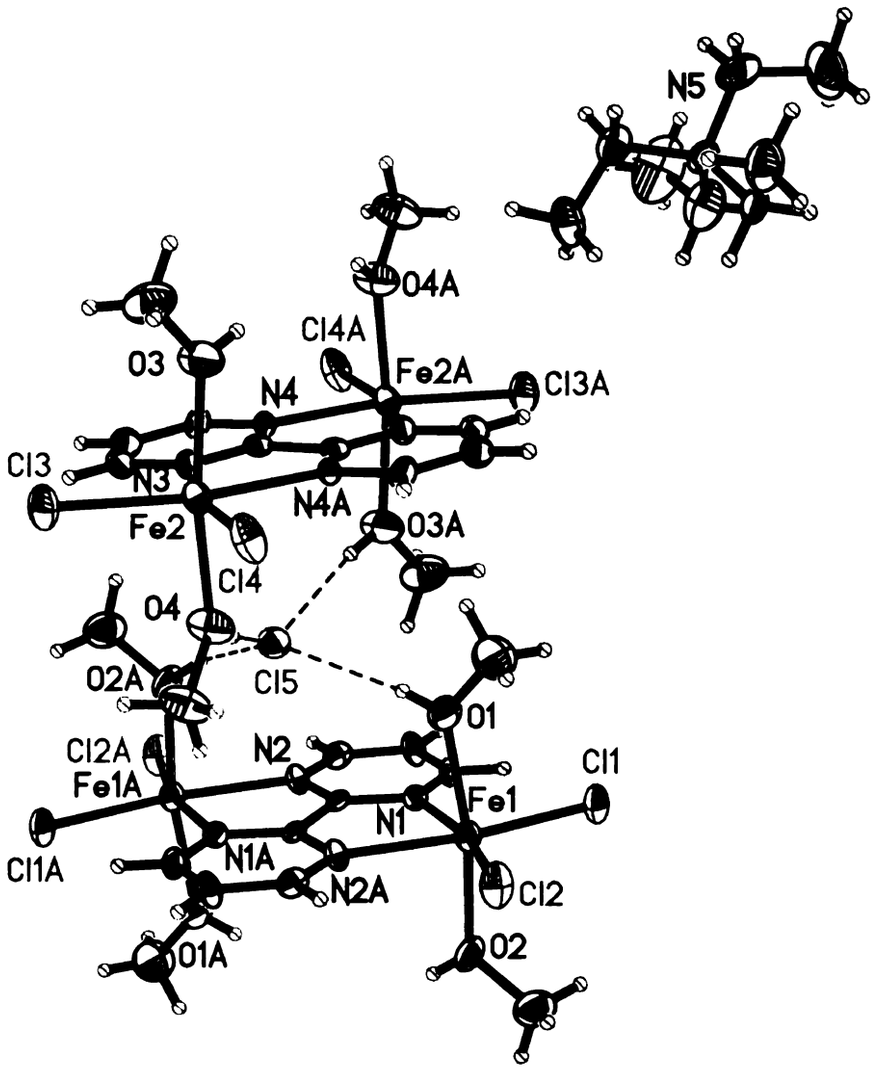


Figure 75. Thermal ellipsoid representation of $[Et_4N]Cl\cdot[Fe_2Cl_4(MeOH)_4(\mu\text{-}2,2'\text{-bpym})]$ (26) illustrates the hydrogen bond between the iron dimer units and the chloride ion.

Table 36. Selected bond distances (Å) and bond angles (°) for $[Et_4N]Cl\bullet[Fe_2Cl_4(MeOH)_4(\mu\text{-}2,2'\text{-bpym})]$, (26).

Bond Distances

A	B	A-B (Å)	A	B	A-B (Å)
Fe1	O2	2.137(6)	Fe2	O4	2.151(6)
Fe1	O1	2.168(6)	Fe2	O3	2.164(6)
Fe1	N1	2.239(6)	Fe2	N3	2.244(6)
Fe1	Cl1	2.379(2)	Fe2	Cl3	2.386(2)
Fe1	Cl2	2.388(2)	Fe2	Cl4	2.381(2)

Bond Angles

A	B	C	A-B-C (°)	A	B	C	A-B-C (°)
N2*	Fe1	N1	74.6(2)	N3	Fe2	N4*	73.8(2)
O2	Fe1	N1	86.8(2)	O4	Fe2	N3	85.6(2)
O1	Fe1	N1	84.7(2)	O3	Fe2	N3	85.7(2)
O1	Fe1	Cl1	92.77(18)	O3	Fe2	Cl3	94.36(18)
N1	Fe1	Cl1	90.61(18)	N3	Fe2	Cl3	92.95(18)
Cl1	Fe1	Cl2	102.22(8)	Cl4	Fe2	Cl5	102.43(9)

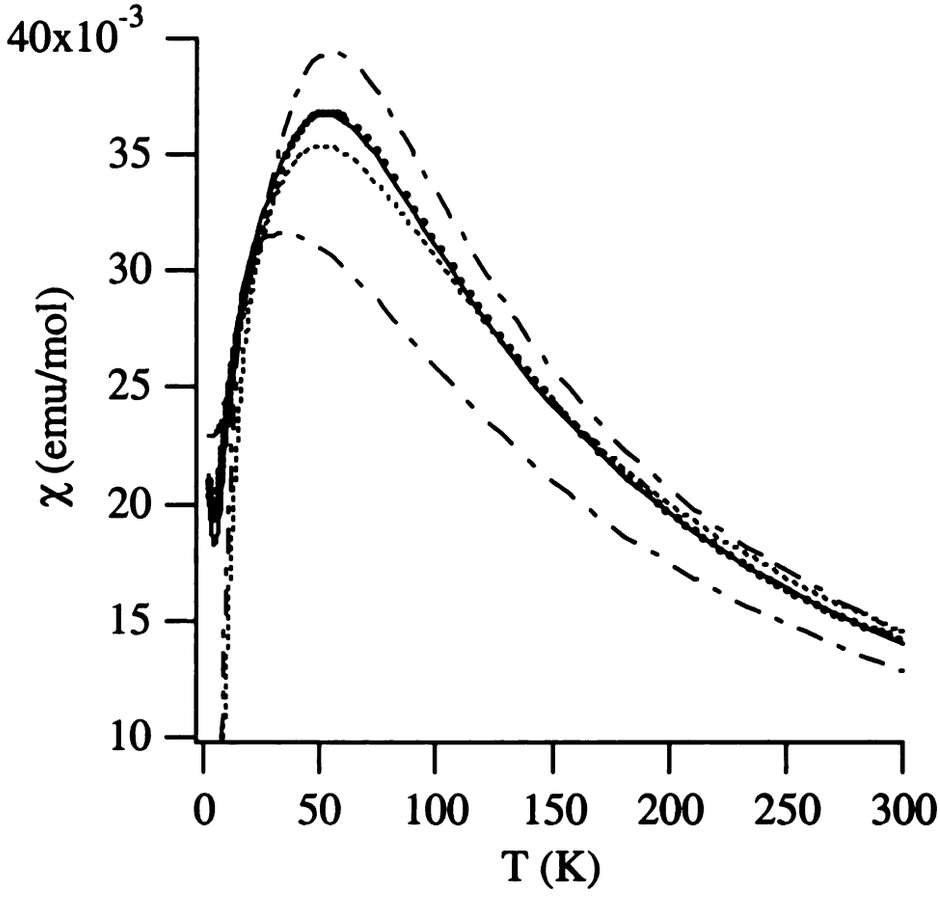


Figure 76. Thermal dependence of the susceptibility for the $[ppn]_2[Co_2Cl_6]$ dimer (filled circles) and the best fit to the experimental data obtained (solid line). Dashed-dotted lines represent the perpendicular (upper) and parallel (lower) susceptibility. The theoretical behavior of a fully isotropic antiferromagnetic Co(II) dimer is shown as dotted line.

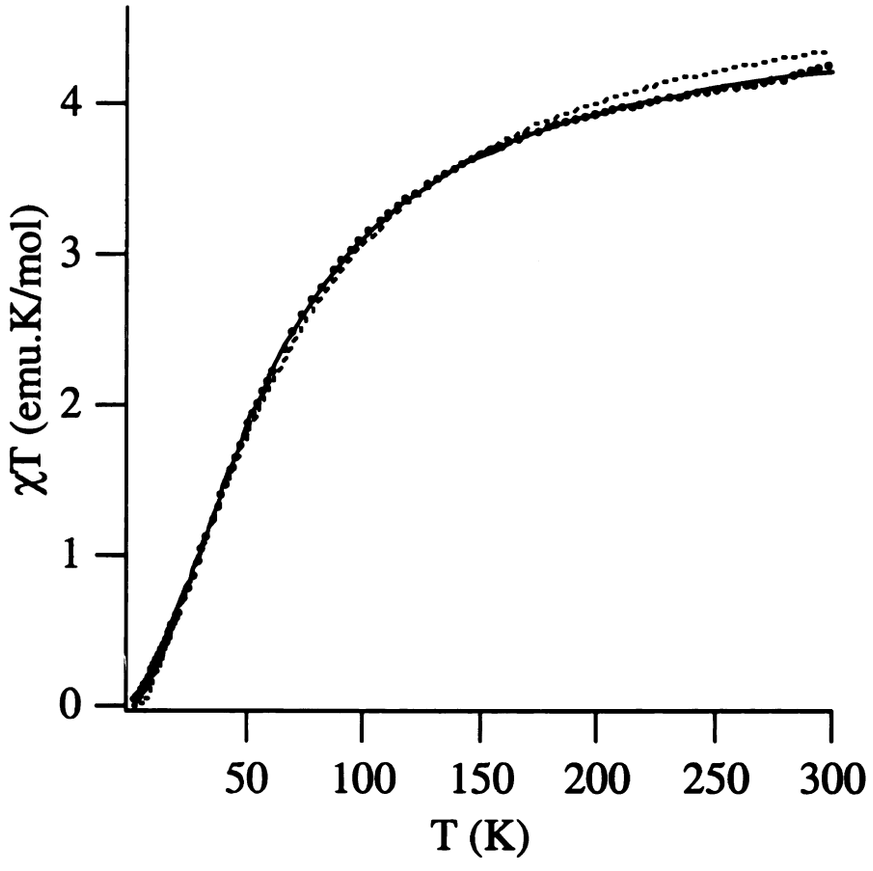


Figure 77. Thermal dependence of the product χT for $[ppn]_2[Co_2Cl_6]$ (filled circles) and the best fit to the experimental data obtained (solid line). The theoretical behavior of a fully isotropic antiferromagnetic Co(II) dimer is shown as dotted line.

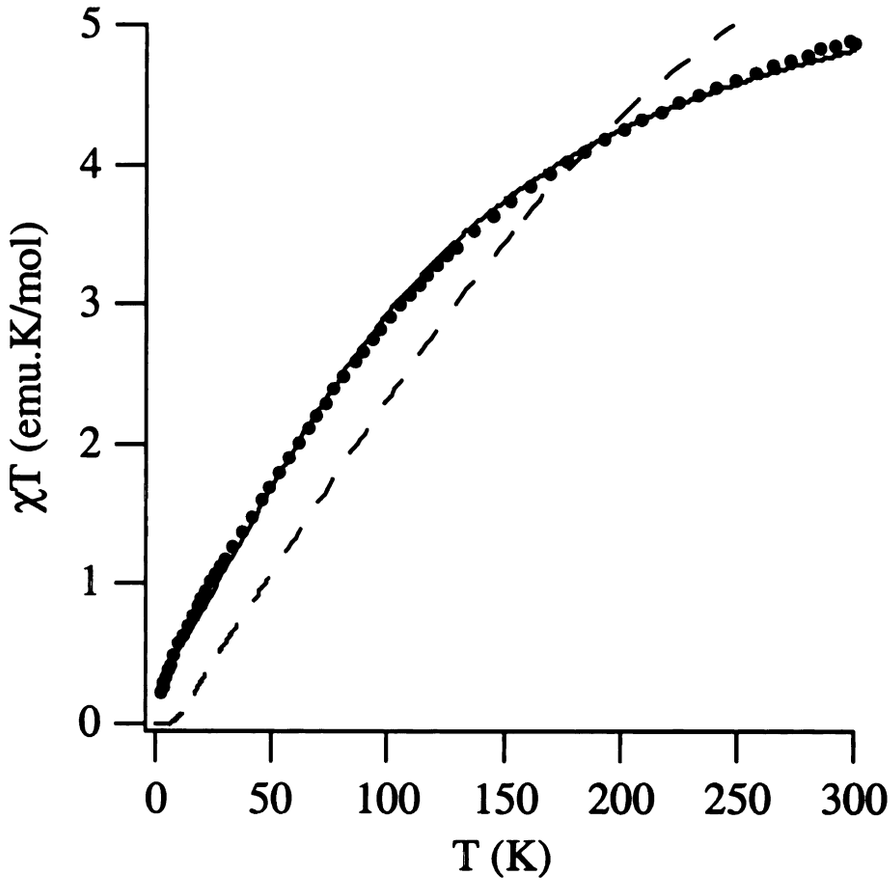


Figure 78. Thermal dependence of the susceptibility for [ppn][Mn_2Cl_6] (filled circles) and the best fit to the experimental data obtained (solid line). The theoretical behavior of a fully isotropic antiferromagnetic Mn(II) dimer is shown as dotted line.

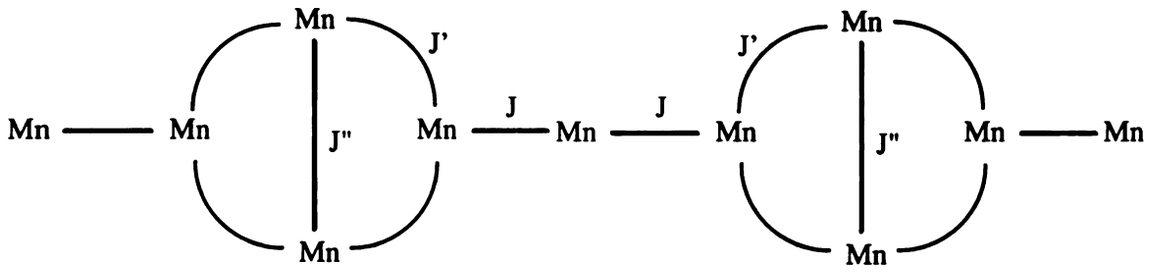


Figure 79. Polymeric chain of $MnCl_2$ units in (16).

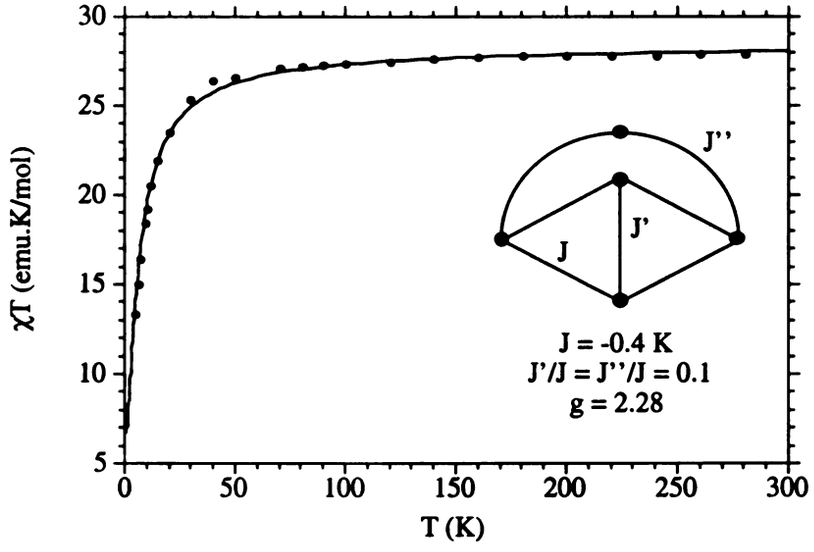


Figure 80. Fitting with the cluster model of magnetic measurement data of (16).

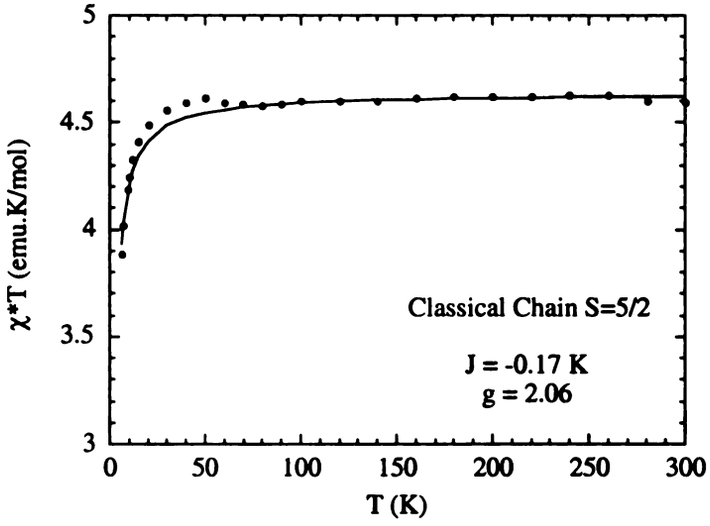


Figure 81. Magnetic data fitting of $[MnBr_2(THF)_2]_\infty$ (17).

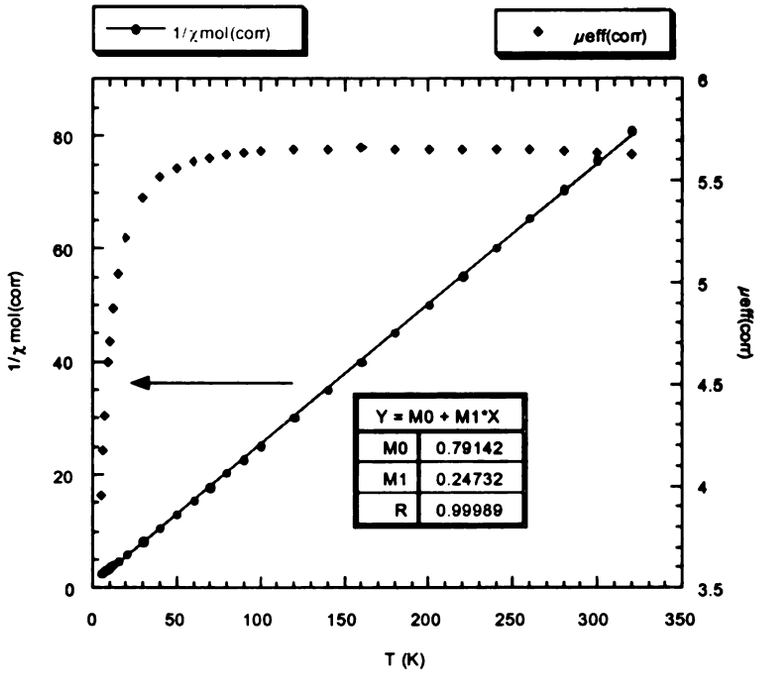


Figure 82. The Curie-Weiss behavior of $[MnCl_2(MeOH)_2]_\infty$ (18). Solid line is the Curie-Weiss fit, dot is the $1/\chi$ and diamond dot is the μ_{eff} plot.

classical model, the data can be interpreted with a simple cluster model (tetramer plus an isolated Mn(II)). The interaction between isolated Mn and the tetramer is weaker than the interaction of Mn within the tetramer (J > J').

4. Conclusion

Metal halide complexes of 3d metals with simple solvent molecules like THF and MeOH have the potential be used as building block for molecular arrays with their tendency to form multinuclear clusters, solubility in common organic solvents, and the presence of unpaired spins. Although their synthesis and structures may be simple, their solid-state characterizations is not as easy as one might think due to their tendency to lose solvent and/or twinning. However, their structural information is important in understanding the basic magnetic interactions of clusters, which leads to a better understanding of more complicated molecular arrays.

References

1. (a) Holm, R. H. *Acc. Chem. Res.* **1977**, *10*, 427. (b) Holm, R. H. *Chem. Soc. Rev.* **1981**, *10*, 455. (c) Papaefthymiou,V.; Girerd, J.J.; Moura, I.; Moura, J.J.G.; Münck, E. *J. Am. Chem. Soc.* **1987**, *109*, 4703. (d) Taft, K. L.; Lippard, S. J. *J. Am. Chem. Soc.* **1990**, *112*, 9629.(e) Ménage, S.; Vincent, J. M.; Lambeaux, C.; Chottard, G.; Grand, A.; Fontecave, M. *Inorg. Chem.* **1993**, *32*, 4766. (f) Taft, K. L.; Papaefthymiou, G. C.; Lippard, S. J. *Science* **1993**, *259*, 1302. (g) Zang, Y.; Jang, H. G.; Chiou, Y. M.; Hendrich, M. P.; Que, L. Jr. *Inorg. Chim. Acta* **1993**, *213*, 41. (h) Hendrich, M. P.; Day, E. P.; Wang, C. -P.; Synder, B. S.; Holm, R. H.; Münck, E. *Inorg. Chem.* **1994**, *33*, 2848 and references therein. (i) Powell, A. K.; Heath, S. L. Comments *Inorg. Chem.* **1994**, *15*, 255 and references therein. (j) Goldberg, D. P.; Tesler, J.; Bastos, C. M.; Lippard, S. J. *Inorg. Chem.*, **1995**, *34*, 3011.

2. (a) Willett, R. D.; Landee, C. P.; Gaura, R. M., Swank, D. D.; Groenedijk, H. A.; van Duynevelt, A. J. *J. Mag. Mag. Mater.* **1980**, *15-18*, 1055. (b) Groenedijk, H. A.; van Duynevelt, A. J.; Blöte, H. W. J.; Gaura, R. M., Willett, R. D. *Physica* **1981**, *106B*, 47. (c) Kitajima, N.; Amagai, H.; Tamura, N.; Ito, M.; Moro-oka, Y.; Heerwegh, K.; Pénicaud, A.; Mathur, R.; Reed, C. A.; Boyd, P. D. W. *Inorg. Chem.* **1993**, *32*, 3583. (d) Taft, K. L.; Delfs, C. D.; Papaefthymiou, G. C.; Foner, S.; Gatteschi, D.; Lippard, S. J. *J. Am. Chem. Soc.* **1994**, *116*, 823 and references therein. (e) Elmali, A.; Elerman, Y.; Svoboda, I.; Fuess, H.; Griesar, K.; Haase, W. *Z. Naturforsch.* **1994**, *49B*, 365. (f) Mathonière, C.; Carling, S. G.; Yusheng, D.; Day, P. *J. Chem. Soc., Chem. Commun.* **1994**, 1551. (g) Klose, A.; Solari, E.; Floriani, C.; Chiese-Villa, A.; Rizzoli, C.; Re, N. *J. Am. Chem. Soc.* **1994**, *116*, 9123. (h) Aromi, G.; Claude, J. P.; Knapp, M. J.; Huffman, J. C.; Hendrickson, D. N.; Christou, G. *J. Am. Chem. Soc.*, **1998**, *120*, 2977.

3. Sheldrick, G. M., *SADABS*. Siemens Area Detector Absorption (and other) Correction, 1998. University of Gttingen, Germany.

4. Sparks, R. A. *TWINNING* (TWINDX, TWUTIL, TWROT and TWHKL), Program for processing twinned data. Bruker AXS Instrument, Madison, WI.

5. Sobota, P.; Olejnik Z.; Utko, J. and Lis, T. *Polyhedron*, **1993**, *12*, 613.

6. (a) Bel'skii, V. K.; Ishchenko, V. M.; Bulychev, B. M.; Protskii, A. N.; Soloveichik, G. L.; Ellert, O. G.; Seifulina, Z. M.; Rakitin, Y. V.; Novotortsev, V. M. *Inorg. Chim. Acta*, **1985**, *96*, 123. (b) Cotton, F. A.; Luck, R. L.; Son, K.-A. *Inorg. Chim. Acta*, **1991**, *179*, 11.

7. Stolz, P. and Pohl, S. *Z. Natuurforsch., Teil, B.*, **1988,** *43*, 175.

8. Lubben, M.; Meetsema, A.; Feringa, B. L. *Inorg. Chim. Acta*, **1995**, *230,* 169.

9. Sinn, E. *J. C. S. Dalton*, **1976**, 162.

10. González, O.; Atria, A. M.; Spodine, E.; Manzur, J.; Garland, M. T. *Acta Cryst. C* **1993**, 1589.

11. (a) Pampaloni, G.; Englert, U. *Inorg. Chim. Acta* **1995,** *231,* 167. (b) Brass, C.; Robert, R.; Bachet, B. and Chevalier, R. *Acta Crystallogr., Sect. B.* **1976,** *32,* 1371. (c) Goodyear, J.; Ali, E. M. and Shutherland, H. H. *Acta Crystallogr., Sect. B.* **1978,** *34,* 2671.

12. (a) Harrison, W.; Trotter, J. *J. Chem. Soc. Dalton Trans.* **1973**, 61. (b) Olson, W. L.; Dahl, L. F. *Acta Cryst.* **1986**, *C42*, 541. (c) Kireeva, O. K.; Bulychev, B. M.; Streltsova, N. R.; Belsky, V. K.; Dunin, A. G. *Polyhedron*, **1992**, *11*, 1801.

13. (a) Saak, W.; Haase, D.; Pohl, S. Z. *Naturforsch.* **1988**, *43B*, 289. (b) Ruhlandt-Senge, K.; Müller, U. Z. *Naturforsch.* **1992**, *47B*, 1075.

14. Pohl, S.; Saak, W.; Stolz, P. Z. *Naturforsch.* **1988**, *43B*, 171.

15. Khan O. *Molecular Magnetism.* **1993** 258.

CHAPTER V

THE USE OF THE CCD AREA DETECTOR X-RAY INSTRUMENT TO RESOLVE TWINNING PROBLEMS

1. Introduction

Crystallography has become an essential component of both chemical and biological research.[1] New structures are emerging in the literature at an ever-increasing rate, thanks to technical advances in radiation sources, detectors, computing and to improved structure-determination methods. The recent introduction of Charge Coupled Device (CCD) area detectors for single crystal X-ray analysis has contributed to a recent "structural explosion".[1] As evidence for this, a new structure is deposited in the Cambridge Structure Data Base (CSD), on average, approximately every forty minutes, with the total number of crystal structures determined reaching 190,000 in 1998.[2,3] With the new techniques being put to use, researchers can now obtain crystallographic results much more quickly than ever before. In the past, it was not uncommon for data to be collected over the course of weeks, but comparable structures can now be determined in less than 24 hours, including solution and least-square refinement and preparation of tables and diagrams for publication. In spite of these remarkable advances, the practitioner of modern crystallography soon learns what "seasoned" crystallographers have been warning,[2] namely that you need to have an even deeper understanding of the underlying crystallographic principles in the CCD era. Diffractometers equipped with CCD area detectors are being widely used in small molecule crystallography in place of the conventional serial detectors, and data collections on microcrystals and weakly diffracting, mosaic crystals have become more common. A typical crystallography lab equipped with a CCD area detector may collect three to four hundred data sets a year, of which as many as 10% are for problem crystals with twinning or other problems. In this chapter,

specific strategies for handling problematic crystal data in terms of data collection and processing, as well as solution and refinement of twinning and other problematic crystals will be discussed.

A. Background

(1) A brief history of diffractometers

In the first X-ray diffraction experiment (Figure 83), performed by Laue, Friedrich and Knipping in 1912[3], it was demonstrated that a crystal lattice is able to diffract X-rays in a manner much like a fine metal grid diffracts light. The size of the grid corresponds to the wavelength of the diffracted beam. This result implied to scientists that we may actually be able to "see" atoms by virtue of their diffraction pattern. The first successful crystal structure to be solved was carried out on sodium chloride by Bragg.[4] It is interesting to point out that the diffraction pattern was recorded on a photographic film, which is the first type of area detector; in fact, the experimental setup is essentially the same as the one used today. Today's equipment is obviously more elaborate, but the essential components are still an X-ray source, a crystal bathed in the incident beam, and a detector to measure the intensity of diffracted X-ray beams. From the early days of Bragg, various film techniques dominated the X-ray diffractometers until these gave way to scintillation detectors in the 1960's. Scintillation detectors (serial or point detectors) use electronic devices for direct counting of diffracted photons for more rapid and accurate intensity measurements[5] as compared to the difficult to obtain (and usually less accurate) intensities measured by film methods. Protein crystallography, which rapidly developed in the 1980's, requires the collection of hundreds of thousands of reflections for a data set, which would take months to collect with a serial

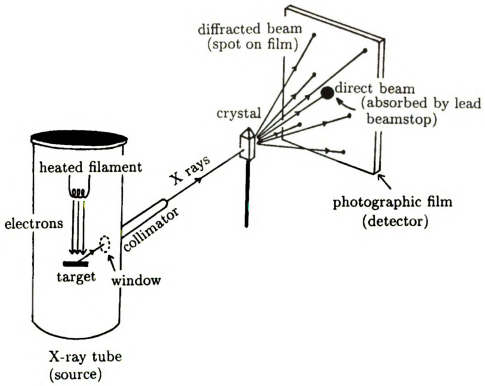


Figure 83. The experimental setup used by Laue, Friedrich and Knipping to measure X-ray diffraction intensities. This same general experimental setup is still currently used, although the source of X rays and the detection system are now much more sophisticated.

detector, thus crystallographers in this field are forced to use film and other area detector techniques.

(2) Modern area detectors and CCD techniques

The desire to collect large numbers of data sets or to collect from crystals with very large unit cells has lured crystallographers back to area detectors that can collect multiple reflections simultaneously when the detector cuts through the Ewald sphere. Area detectors developed from the old film technique use electronic devices, such as image plates and multi-wire area detectors, to record X-ray photons. While these have been very useful, these area detector techniques usually suffer from slow readout time.

The CCD (Charge Coupled Device) detector was developed in the mid 1980's as an electronic camera, and it soon found an application in crystallography. The CCD camera is an area detector that measures the X-ray intensity of slices of reciprocal space. The area detector collects intensities for many reflections simultaneously, resulting in shorter data collection times as compared to serial diffractometers. The CCD detector contains a phosphor screen located immediately behind a beryllium window. The screen converts incoming X-ray photons into optical photons. Because of the greater energy of X-ray photons compared to optical photons, hundreds of optical photons are produced for each incident X-ray photon. A fiber-optics taper transmits the optical photons to the CCD chip, where they are converted to stored electrons. The detector is very sensitive, permitting the measurement of useful data from small specimens, like microcrystals that are much smaller than samples that can be collected with a serial diffractometer.

Because CCD area detectors collect all data contained in planes of reciprocal space, it provides the opportunity for studying superstructures,

twinning, and crystal defects.

B. The Advantages and Disadvantages of Area Detectors.

One advantage of CCD area detectors is that they can read out data much faster than other area detectors, thus the collection of thin slices of data is practical. The area detector collects data from crystal of medium to large unit cells in a fraction of the time required for serial scintillation detectors to perform the same operation. On the other hand, (for the average crystallographer) there is also a disadvantage to the CCD area detector in that it allows for the collection of all the data which includes reflections from twinning components, from tiny daughter crystals. These problems are ordinarily solved by using slits to cut off the background signal or twinning replications in the serial detector instruments, but this hardware option is no longer possible for area detectors. In fact most of the "old tricks" used with scintillation diffractometers cannot be used with area detectors. The manipulation of the data, then, must rely on powerful new software options, which is a different strategy than most crystallographers have been accustomed to using.

C. New Problems in the CCD Era

(1) The problem of twinning

(a) Definition of twinning

Twinning may be classified according to the symmetry relation of the twin components or to the origin of the twins. As defined in the *International Table of Crystallography Vol C*:[6]

> A *twin* consists of two or more single crystals of the same species but in different orientations. *Twin components* are intergrown in such way that at least some of their lattice

directions are parallel. The *twinning law* describes the geometrical relation between *twin components*. It specifies a symmetry operation, the *twin operation* that brings one of the twin components into parallel orientation with the other. The corresponding symmetry element is called the *twin element.*

The biggest problem with twinning is that it may not be easy to distinguish between twinning and disorder.[7] Although this is the case, pursuing the possibility of twinning is advantageous. As George Sheldrick has suggested, "You only need two more parameters to test if there is twinning, but you may spend a long time struggling with a disorder model."[8]

Below are the equations that describe the structure factor relationship to reflections in the case of twinning or disorder:

$$F(h) = \sum_i f_i(h)\exp(2\pi i \mathbf{h}^T \mathbf{x}_i) + g\sum_j f_j(h)\exp(2\pi i \mathbf{h}^T \mathbf{x}_j) + (1-g)\sum_k f_k(h)\exp(2\pi i \mathbf{h}^T \mathbf{x}_k) \quad \text{Eq. 5}$$

$$F_1(h_1) = \sum_i f_i(h_1)\exp(2\pi i \mathbf{h}_1^T \mathbf{x}_i) \quad \text{Eq. 6}$$

$$F_2(h_2) = \sum_i f_i(h_2)\exp(2\pi i \mathbf{h}_2^T \mathbf{x}_i) \quad \text{Eq. 7}$$

$$F(h) = \{g[F_1(h_1)]^2 + (1-g)[F_2(h_2)]^2\}^{1/2} \quad \text{Eq. 8}$$

Where the x_i's are the position coordinates and the $f_i(h)$'s are the scattering factors for the non-disordered atoms, the x_j's are the position coordinates and the $f_j(h)$'s are the scattering factors for the disordered atoms in the first position and the x_k's are the position coordinates and the $f_k(h)$'s are the scattering factors for the disordered atoms in the second position. The g parameter is the fraction of disordered atoms in the first position and 1-g is the fraction of disordered atoms in the second position (Eq. 5).

In the twinning expression (Eq. 8), *g* is proportional to the volume of the first component and 1-*g* is proportional to the volume of the second

component. Note how this expression differs from the expression for disorder. Often when a disordered model does not refine well (good R-values cannot be obtained), it may be that the sample is twinned instead of disordered.

Most types of crystallographic twins are merohedral/pseudo-merohedral or rotational twins. For merohedral twins and pseudo-merohedral twins there is an exact overlap of the twinning lattice and the real lattice, thus no special data collection or integration procedures are needed. For rotational twins, however, the twinning lattice does not exactly overlap with the original lattice, thus the indexing routine attempts to include reflections that belong to different twinning components in determining the unit cell of a single component. In many cases, the program cannot find a solution.

D. Manipulation of Data for Twinned Crystals - Why not Grow a Better Crystal?

The progression of crystallography from being the tool of an elite group of highly trained crystallographers to becoming the tool of the everyday scientist has led to a new way of viewing the importance of a data set. Rather than insisting on "perfect" crystals, many modern crystallographers seek to solve a chemical problem in a practical manner and in a timely fashion using the available crystals. Structural determination by single crystal X-ray methods is important to nearly every chemist, and to inorganic chemists in particular. The Cambridge Structure Data Base (CSD) has witnessed a tremendous increase in the number of deposited structures during the past decade. Many of these problems are being pursued because of the need to address physical properties of new materials, often of

marginal crystal quality. Conventional crystallographers are finding themselves at odds with their training when asked to handle crystals they consider unacceptable. The conventional wisdom "garbage in, garbage out" may not apply in the same sense as when structures were being evaluated for their "crystallographic merit" as opposed to their "chemical information merit". The problems of small, twinned, strongly absorbing crystals are falling into the hands of synthetic chemists who often have more incentive than professional crystallographers to resolve these issues because the success of their project depends on knowing the answer.

Before the age of the automated serial diffractometers when film techniques were still in use, (1950's and 1960's), there were many publications in the literature devoted to theoretical aspects of twinning. After the advent of scintillation detectors, the number of papers that dealt with this topic dropped to only an occasional paper because these machines can't deal with twinning easily.[9] The process has come full circle now with the widespread use of the CCD, and more researchers are tackling twinning problems with renewed interest. The reason for this resurgence of interest is that area detectors collect more data than a point detector, and one cannot ignore data once it is obtained.

(1) Indexing of twinned crystals:

There are a number of ways one may index reflections from a twinned crystal. These are summarized in the following sections.

(a) Simple algorithm method.

In the system software for various diffractometers, there is a built-in routine to index reflections when twinning is suspected. The routine is not very sophisticated, however, and is essentially a simple approach such as indexing odd numbered reflections only or even number reflections, or some

other arithmetic combination.

(b) Difference vector and related methods.

There is a widely used program called DIRAX[10] written by A. J. M. Duisenberg, which sorts out the projection of reflections into so called T vectors. Another program is Robert Sparks' TWINNING[11] package which is distributed with the SMART 1000 CCD platform diffractometer and beta tested by SMART users before the NT version release. In Sparks' program, there are two strategies for indexing. One uses the difference vector method, and the other uses a full vector method. The SMART system uses difference vectors for its indexing routine. If twinned data are encountered, many cross vectors will be generated between different twinning components, which makes it difficult to generate reasonable cell parameters. By reducing the "fraction of difference vectors which must fit" number, a temporary cell usually can be generated, and the XYZ coordinates of reflections calculated. By loading the file that contains the temporary cell, orientation matrix and the XYZ coordinates of reflections to TWINDX, one can quickly check if the reflections belong to a unique domain or to twinned domains. When running TWINDX, the shortest 100 difference vectors will be generated and sorted by decreasing number of difference vectors in a group. The program will ask for the number of difference vectors in a group to be used in the indexing. Because the first three non-coplanar vectors may not be from the same crystal, the program generates many combinations of three non-coplanar vectors from the list of difference vectors. It can be shown that for at least one such combination, all three difference vectors will come from reflections from the same twin component. The program then outputs a summary file which contains the cell parameters, orientation matrices and a brief summary of fitted reflections with a combined figure of merit and a

detailed reflection fitting file. TWUTIL is then used to remove the indexed reflections for solution A and prepare input file for indexing in the subsequent run. TWINDX is run again with the new set of reflections. After removal of reflections that fit solution A, it is easier for the rest of the reflections to be indexed since they may now fit the same solution. From the list of possible solutions, the one with the same cell parameters as solution A is of interest. TWUTIL generates a new input file with only independent reflections after comparing two indexing results. A further run of TWINDX with only these reflections is preferred in order to obtain a refined solution with all independent data. Finally, TWUTIL can be run again to generate a file with cell parameters, an orientation matrix and the independent reflection list for a specific solution. Finally, TWROT is run to determine the rotation angle and the twinning law between a special pair of solutions.

E. Data Integration and Deconvolution.

After obtaining the indexing results from the TWINDX program, there are several considerations for data integration, depending on the type of problem encountered.

(1) A rotational twin.

A pair of rotational twins is usually rotated 180° from each other. There may be some partial overlapping reflections which will affect the refinement of the cell parameters and crystal orientation. A tight constraint with integrated cell refinement turned off will generate a desired result. If one of the components is of a much lower percentage than the other (as judged by the number of independent reflections contributing to that cell), a tightly constrained integration with global cell refinement will be satisfactory.

(2) A nearly perfect twin.

In the case of a twin in which one solution only differs from the other by a small angle, nearly all of the reflections are overlapped. By using a loosely constrained or unconstrained integration window to accommodate diffraction spots of both fragments, one has the best chance for a stable integration. Essentially, the data are being treated as if they are broad reflections with a high degree of mosaic spread.

F. Structure solution and refinement.

Structure solution for a rotational twin can be handled in the same way as normal data, with SHELXS and the corresponding XS generating satisfactory results. In the case of severely affected data, SIR92[12] or SIR97 is the program of choice to produce a reasonable solution by a default procedure. SHELXL97 and SHELXTL can use twinned data in HKLF 5 format and allow the BASF parameter (twinning volume ratio) to be refined. Other crystallographic packages such as CRSTAL[13] by David Watkin can also refine structures with twinned data. Merohedrally and pseudo-merophedrally twinned data can be used directly in the standard SHELX HKLF 4 format with refinement of the twinning batch (BASF) parameter.

2. Mastering the CCD Technique for Special Needs

The chemical and structural details of the crystals for the data sets presented here are discussed in the individual chapters. The discussions in this chapter are limited to the type of twinning problem that was evident and to the solution of the problems.

A. Problematic Structures: Seven Case Studies.

(1) Example 1: Large cell, "small molecule" data set: of

$\{[Mo_2(O_2CCMe_3)_3(NC)2CC(CN)CONH] \cdot 8CH_2Cl_2\}_\infty$ (3)

A point detector can only collect one reflection at a time, thus it takes weeks for data collections from crystals with large unit cells. Unfortunately, if the crystal is not stable in the X-ray beam, the crystal may not survive. One such case is a compound prepared at low temperature and with a huge quantity of incorporated solvent.

Single crystals of (3) were grown from the low temperature crystallization of a reaction mixture of $Mo_2(O_2CBu^t_3)_4$ with TCNE in dichloromethane. The crystals are red hexagonal platelets of typical size 0.3 x 0.3 x 0.2 mm. Due to twinning and the presence of large channels that contain numerous disordered solvent molecules, the data are very weak. Repeated attempts to improve the technique of crystallization were not able to yield a better crystal.

Data set 1 was collected at Michigan State using a Nicolet P3/V diffractometer controlled by a VAX 3520 workstation. Cell refinement from 14 well-centered reflections gave a hexagonal cell, with $a = b = 27.101(4)$ Å, $c = 22.861(5)$ Å, $\alpha = \beta = 90°$, $\gamma = 120°$ and $V = 14541.07$ Å^3. T = -100 ± 1 °C. The cell belongs to the hexagonal system space group P6/mcc or P6cc. The observed reflections comprised only 14% of the entire data set, and their average intensity $I/\sigma = 4$. The structure was partially solved in the space group of P6/mcc with the program DIRDIF84.[14]

Data set 2 was collected by Fr. Charles Campana at Siemens (Bruker) using a SMART CCD 1K diffractometer equipped with a LT2 low temperature device at –160(1) C. The cell indexed as a hexagonal system,

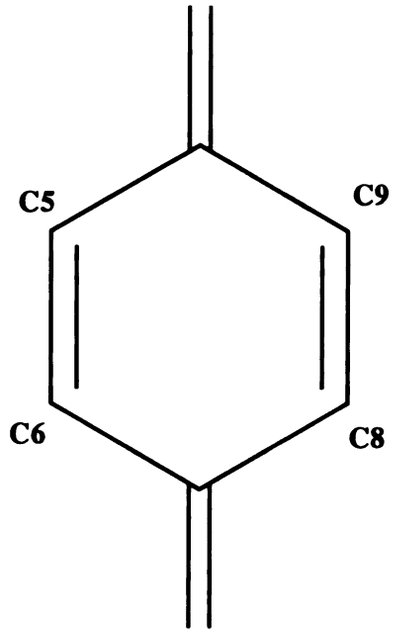
but the cell volume was three times larger than the one obtained using the point detector instrument, with a = 46.8862(4) Å, b = 46.8862(4) Å, c = 22.7568(4) Å, $\alpha = \beta = 90°$, $\gamma = 120°$, V = 43324.3(9) Å^3. The space group could not be selected with confidence due to twinning and a large amount of disorder. The structure was refined in several different space groups and with different combinations of twinning laws. The differences between the choice of space group are mainly based on the degree of disordered methylene chloride.

(2) Example 2: A Pseudo-Merohedral twin: $[Mn_2(\mu^4\text{-}\sigma\text{-TCNQ-TCNQ})_2(\mu\text{-cis-TCNQ})_2(MeOH)_2]_\infty$ (9)

Crystals of (9) were grown by a layering reaction of $[Mn(MeCN)_4](BF_4)_2$ in acetonitrile with LiTCNQ in MeOH. The first data set was collected using the Rigaku AFC6S instrument at -100 ± 1 °C. The automatic peak search routine indicated an orthorhombic crystal system with

a = 14.470(3) Å, b = 27.373(6) Å, c = 13.148(3) Å, $\alpha = \beta = \gamma = 90$, V = 5207.8(18) Å^3. There was a problem, however, with the solution. The two space groups that met the systematic absence check are Cmcm and Aba2. In these space groups, the TCNQ fragment resides on a mirror plane that bisects the molecule. When the structure was expanded, the TCNQ fragment became highly distorted as one side of the quinone ring is smaller than the other side.

A second data set was collected on a SMART CCD area detector by Dr. D. Powell at the University of Wisconsin, Madison. The solution turned out to be a pseudo-merohedral twin in a monoclinic space group with the beta angle just 0.05 off the perfect 90°. The twinning ratio was found to be 30:70.



C5 and C9, C6 and C8, which are related by local symmetry, are assigned the same thermal parameters in the refinement

Figure 84. Using local symmetry to reduce independently refined parameters.

The original data were then re-refined as pseudo-merohedrally twinned data. This led to $R1$ = 0.0565 for 1078 $Fo > 4\sigma(F_o)$ and 0.2463 for all 3069 data and $wR2$ = 0.2089, GOF = 0.982. Heavy constraints were introduced during the refinement because of the low data to parameter ratio. Only one-half of the atoms that form the TCNQ ring were refined independently (Figure 84). The other half of the atoms in the TCNQ quinone ring were constrained to have the same atomic displacement parameters as the refined one by introduction of a mirror plane.

(3) Example 3: A rotational twin:

$[Et_4N]Cl{\cdot}Fe_2Cl_4(MeOH)_4(bpym)_3$ (26).

(a) A data set from a scintillation detector compared to a data set from CCD detector.

The first data set was collected on a Rigaku AFC6S diffractometer.

The unit cell was generated from the precise refinement of 20 well-centered reflections in the two theta range from 14 – 30°. A standard quadrant of data was collected according to convention. Three standard reflections were periodically measured to monitor the decay of the crystal after every 150 reflections. The structure solution was from DIRDIF/SHELXS86 and refined against F^2 in Texsan V5.0 to give R = 0.112 (wR = 0.129) for 310 variables.

(b) Using a rotational twinning matrix in the refinement

It was noted that there are systematic absence violations to the *c* glide plane in the category of h0l (l = 2n). The unit cell parameter has a β angle equal to 94° (close to 90°), with *b* and *c* being nearly equal. This situation usually leads to rotational twinning. When the twinning matrix [1 0 0.15, 0 - 1 0, 0 0 -1] was used in the refinement, the twinning ratio was refined to about 1% contamination from the possible twins. The systematic absence violation was resolved by this strategy.

A CCD data set was then collected in a monoclinic cell setting. The unusually high *R1* and systematic violation to the glide plane suggested the possibility of twinning. The data frames were examined, but no visual splitting of the reflections was noted. The preliminary orientation matrix was then loaded to the TWINDX program. A pair of solutions from default runs revealed that the crystal is indeed rotationally twinned. There were 54 out of 71 reflection indexed as independent reflections for twin domain one, and 9 for twin domain two. There remained 12 completely overlapping reflections and four diffraction spots that failed to be indexed. The orientation of domain two was transformed to domain one by the transformation matrix. The rotation angle is 180° between domain one and two. The rotation axis is along a* (1 0 0) in reciprocal space or a (1 0 0) in

Table 37. Rotational transformation of $[Et_4N]Cl{\bullet}Fe_2Cl_4(MeOH)_4(bpym)_3$ (26). from orientation A_1 to orientation A_2.

Orientation Matrix A_1 from solution 1 (jas10a0.p4p)
Orientation Matrix A_2 from solution 2 (jas10b0.p4p)

Orientation matrix and unit cell parameters for A_1

0.05160	0.01662	0.04700			
0.04626	0.01563	-0.04526			
-0.02556	0.06128	-0.00166			
13.5790	15.2931	15.3667	89.612	94.447	90.198

Orientation matrix and unit cell parameters for A_2

-0.05247	-0.01658	0.04028			
-0.04511	-0.01576	-0.05265			
0.02471	-0.06139	0.00366			
13.6468	15.2672	15.1025	89.119	94.152	90.827

Transform matrix from orientation 1 to 2 (twinning law)

A_2(inverse) * A_1 [transforms h1 to h2] =

-1.00375	0.00008	-0.15045
0.01109	-0.99810	0.02493
-0.02190	0.00190	0.98111

Rotation axis in reciprocal space = -0.07630 0.00990 1.00000
Angle of rotation around -0.08 0.01 1.00 = -179.72050
Rotation axis in direct space = -0.01002 0.00317 1.00000

Table 38. Indexing result of rotationally twinned $[Et_4N]Cl{\bullet}Fe_2Cl_4(MeOH)_4(bpym)_3$ (26).

Name of files: jas10aa.twx / jas10bb.twx

figures of merit/reflections indexed/reflections used:
0.00155/54/54 0.00339/9/9

unit cells:

13.579	15.293	15.367		13.647	15.103	15.267	
0.008	0.006	0.008		0.249	0.275	0.119	
89.612	85.553	89.802	3181.43	89.119	89.173	85.848	3137.68
0.040	0.047	0.042	2.92	1.141	1.145	1.425	82.42

Refl#	H	K	L	Flags	H	K	L
1	-5.011	1.001	-6.025	1 - 1 -	-4.104	5.987	1.094
2	-0.017	2.987	-3.008	1 + 0 -	0.455	2.914	3.056
3	3.000	5.995	-0.990	1 + 0 -	3.180	0.862	6.042
4	4.000	6.999	1.009	1 + 0 -	3.884	-1.122	7.005
5	-1.992	6.998	-6.976	1 + 0 -	-0.930	6.843	7.137
6	-5.008	1.992	-7.017	1 - 1 -	-3.952	6.959	2.108
7	0.807	1.984	-1.074	0 - 1 +	0.991	1.001	2.017
8	4.001	7.997	0.011	1 + 0 -	4.034	-0.145	8.027
9	2.012	7.000	-2.985	1 + 0 -	2.489	2.840	7.084
10	0.990	4.989	-2.992	1 + 0 -	1.464	2.873	5.066
11	0.795	1.871	-1.131	0 - 1 +	0.988	1.057	1.905
12	1.993	3.994	-1.002	1 + 0 -	2.171	0.900	4.034
13	-4.608	-1.049	-4.010	0 - 1 +	-4.003	4.006	-0.997
14	2.978	2.994	1.975	1 + 0 -	2.711	-2.041	2.973
15	0.991	2.996	-2.014	1 + 0 -	1.318	1.917	3.052
16	0.970	2.054	-0.971	1 + 0 -	1.139	0.896	2.086
17	0.013	7.000	-4.985	1 + 0 -	0.783	4.845	7.112
18	-1.002	4.995	-5.995	1 + 0 -	-0.084	5.863	5.124
19	1.981	2.999	-0.025	1 - 1 -	2.012	-0.056	3.016
20	-0.001	3.997	-4.004	1 + 0 -	0.621	3.889	4.089
.....							
66	2.009	-4.002	2.016	1 + 0 -	1.732	-2.046	-4.022
67	2.014	-1.979	2.027	1 + 0 -	1.736	-2.060	-2.003
68	3.558	0.061	3.967	0 - 1 +	2.994	-4.002	0.002
69	3.010	-2.003	3.023	1 + 0 -	2.586	-3.060	-2.041
70	0.999	-4.995	1.004	1 - 1 -	0.871	-1.029	-4.999
71	-4.000	-6.993	-2.007	1 + 0 -	-3.694	2.038	-6.973
72	3.984	-7.002	4.998	1 + 0 -	3.266	-5.009	-7.069
73	1.132	-1.974	1.000	0 - 1 +	1.005	-1.033	-1.982
74	1.130	-2.017	0.918	0 - 1 +	1.016	-0.953	-2.023
75	-2.986	-3.986	-1.989	1 + 0 -	-2.679	1.992	-3.961
76	6.004	-1.003	8.005	1 + 0 -	4.841	-8.015	-1.133
77	3.010	-2.996	3.025	1 + 0 -	2.585	-3.060	-3.032
78	-0.011	-8.006	0.984	1 + 0 -	-0.140	-0.982	-8.015
79	0.993	-5.859	1.124	0 - 0 -	0.846	-1.145	-5.864

Summary of indexing result (Flags):

0+0+	0+0-	0+1+	0+1-	0-0+	0-0-	0-1+	0-1-	1+0+	1+0-	1+1+	1+1-	1-0+	1-0-	1-1+	1-1-
0	0	0	0	0	4	9	0	0	54	0	0	0	0	0	12

Note for flags(fitting code):
0-0-: Refl not been indexed and not used for indexing;
1+0-: Independent reflections for cell 1;
0-1+: Independent reflections for cell 2;
1+1+: Non-independent reflection used in indexing;
1-1-: Non-independent reflections fitted to both solution, but not been used in indexing.

direct space. The cell parameters are a = 13.558(3) Å, b = 15.229(3) Å, c = 15.390(3) Å, β = 94.30(3)°. The orientation file was subjected to TWINDX treatment which resulted in two orientation cells with 54 and 6 independent reflection respectively (see Table 38). Because the second domain was relatively weak, data were reintegrated with tight cell constraints for integration and global cell refinement. Cell refinement was set to run on every 100 frames, with only the strong reflections ($I/\sigma > 20$) to avoid influence from the minor twinning domain. The reprocessed data refined to a final $R1$ = 0.0633, $wR2$ = 0.1392 on 2473 ($I > 2\sigma(I)$) against 326 parameters and $R1$ = 0.1826, $wR2$ = 0.1670 (all data) for all 3895 reflections.

(4) Examples 4a and 4b: Nearly perfect twins:

(a) $Mn_2(bpym)_2(\mu\text{-}F)(\eta^1\text{-}BF_4)(BF_4)_2(MeCN)\cdot 2MeCN$ (25).

Crystals of (25) were grown from a layering reaction of $[Mn(MeCN)_4][BF_4]_2$ and 2,2'-bypyrimidine in acetonitrile. A crystal of size 0.3 x 0.35 x 0.45 mm was mounted on the tip of a glass fiber with Dow Corning Silicone grease. Examination of 45 preliminary frames indicated that the crystal belongs to the triclinic system. A hemisphere of data was collected with 25 sec/frame. The following cell parameters were indexed from 45 preliminary frames: a = 12.299(5) Å, b = 12.480(4) Å, c =12.690(6) Å, α = 100.98(5)°, β = 116.63(3)°, γ = 101.02(4)°, V = 1622.23(98) Å^3.

The predicted reflection positions matched poorly with the data frames. Slightly split reflections were found after careful examination of the frame data. The XYZ coordinates of 38 strong reflections were saved to an input file and R. Sparks' TWNNING package was used to deconvolute the data. Two similar cells with different orientation matrices were indexed with 17 and 12 reflections separately. The relation of the orientation matrices is as shown in Table 39. The rotation angle from solution 1 to

solution 2 is only 1.5°

Data integration was carried out with triclinic constraints, with only global cell refinement. The resulting integrated data were processed by TWHKL to generate the reflection file in HKLF 5 format, which indicated that there are 2,478 single reflections and 11,340 completely overlapping reflections; 6,228 partially overlapped reflections were rejected. Structural solution and refinement was carried out by using the SHELXTL package. All non-hydrogen atoms were located from the XS output and refined with XL on F^2. The *R1* values with and without TWHKL processing are 14.3% (5272 $Fo > 4\sigma(Fo)$ unique reflections) and 18% (6605 unique reflections) respectively.

(b) Structure of $Mn(\eta^1\text{-}TCNQ)_2(TCNQ)(HOCH_2CH_2OH)_3$ (28).

For this data set, the TWROT indicates that the two orientation matrices of the split crystal are separated by only ~1°. Inspection of the frames indicated that some of the reflection spots are well separated, (about 3–4 frames apart in the z direction) while some frames are not. To better refine the structure, the following strategy was used:

(i) Big box integration.

In the big box integration, the integration box was set to be very large so as to include both reflection mates. The box (peak shape) refinement was turned on. This method treats the total intensity of both crystals as the intensity of an averaged, but single, mosaic crystal.

(ii) Small box integration.

In the small box integration, several options may be used which lead to different results.

(1) Refine and update the orientation of the cell every 200 frames, and refine the box (peak shape) as well.

Table 39. Rotational transformation of $Mn_2(bpym)_2(\mu\text{-}F)(\eta^1\text{-}BF_4)(BF_4)_2(MeCN)\bullet 2MeCN$ (25) from orientation A_1 to orientation A_2.

Orientation Matrix A1 from solution 1 (twin11.p4p)
Orientation Matrix A2 from solution 2 (twin22.p4p)

Orientation matrix and unit cell parameters for A1

-0.01138 -0.06826 0.01943
-0.06702 -0.05150 -0.08071
0.05394 -0.03308 -0.04773
12.3459 12.8265 12.3121 116.679 101.227 100.477

Orientation matrix and unit cell parameters for A_2

-0.01200 -0.06871 0.01901
-0.06562 -0.05272 -0.08209
0.05557 -0.03091 -0.04578
12.3795 12.8417 12.2807 116.575 100.726 101.494

Transform matrix from orientation 1 to 2 (twinning law)

A_2(inverse) * A_1 [transforms h1 to h2] =

0.99070 -0.03093 -0.02947
-0.00053 1.00144 0.00079
0.02473 0.00895 1.00619

Rotation axis in reciprocal space = 0.76207 -5.00000 2.15606
Angle of rotation around 0.76 -5.00 2.16 = -1.46653
Rotation axis in direct space = -0.02766 -1.00000 -0.00931

Table 40. Rotational transformation of $Mn(TCNQ)_2(TCNQ)(HOCH_2CH_2OH)_3$ (28) from orientation A_1 to orientation A_2.

Orientation Matrix A1 from solution 1 (sao6a.p4p)
Orientation Matrix A2 from solution 2 (sao6b.p4p)

Orientation matrix and unit cell parameters for A_1

0.00456	-0.06331	-0.02571			
0.00176	0.03669	-0.06280			
0.09500	-0.00100	0.00211			
10.5244	13.8093	14.8698	82.128	89.394	87.314

Orientation matrix and unit cell parameters for A_2

0.00575	-0.06356	-0.02453			
0.00138	0.03578	-0.06284			
0.09465	0.00066	0.00242			
10.5518	13.8540	14.9611	81.968	89.713	87.879

Transform matrix from orientation 1 to 2 (twinning law)

A_2(inverse) * A_1 [transforms h1 to h2] =

1.00343	-0.01718	-0.00354
0.01751	1.00015	0.01516
0.00401	-0.01480	1.00790

Rotation axis in reciprocal space = 1.25372 0.83509 -3.00000
Angle of rotation around 1.25 0.84 -3.00 = 1.32474
Rotation axis in direct space = 3.86700 2.11682 -5.00000

(2) Refine only the orientation of the cell with a fixed box size.

(3) Use the orientation matrix from the TWINDX without further peak shape or orientation matrix refinement. A global cell refinement is performed when the integration is finished with only those reflections with $I/\sigma > 10$.

Because some diffraction spots were not sufficiently well separated, peak shape refinement led to incorrect cell parameters and the data could not be used. Data from method (1) were ultimately used to solve the structure. The refinement led to $R1 = 0.102$ for 3846 $Fo > 4\sigma(Fo)$ and 0.203 for all 9938 data and $wR2 = 0.263$, GOF = 0.975.

(5) **Example 5: Crystal movement during data collection:**

Structure of $Rh_2(pynp)_2(O_2CCH_3)_2(BF_4)_2 \cdot C_7H_8$ (27).

Crystals of (27) were grown from the layering reaction of $Rh_2(O_2CCH_3)_2(MeCN)_6(BF_4)_2$ and a toluene solution of pynp (pynp = bis(pyridylnaphthyridine)). Preliminary data indicated that the crystal was monoclinic. The final data, however, failed to reproduce the cell with the autoindex routine in SMART. After reducing the required reflection ratio for indexing from 80% (default) to 70%, a temporary cell was obtained, which enabled the indexing/least-square routine to calculate the XYZ coordinates of the reflections. SMART was re-run in the debug mode to produce the XYZ coordinates of the reflections which were manually edited to remove the temporary indexes. These were saved as a raw file for use in the TWINNING program. Two solutions had similar cell parameters but different orientation matrices. TWINDX yielded two cells with a rotational angle of ~37° between them. Careful inspection of the indexed reflection list revealed that the first cell is associated with the first half of the data while the second cell is associated with the second half of the

Table 41. Rotational transformation of $Rh_2(O_2CMe)_2(pynp)_2.(BF_4)_2 \bullet C_7H_8$ (27) from orientation A_1 to orientation A_2.

Orientation Matrix A_1 from solution 1 (rh11r.p4p)
Orientation Matrix A_2 from solution 2 (rh22r.p4p)

Orientation matrix and unit cell parameters for A_1

-0.05238 -0.03188 0.00858
-0.01790 0.02133 0.06063
-0.05031 0.02560 -0.03982

13.4185 21.6846 13.7409 90.000 94.922 90.000

Orientation matrix and unit cell parameters for A_2

-0.02631 -0.04084 -0.02498
-0.05100 0.00047 0.04946
-0.04842 0.02170 -0.04809

13.3652 21.6223 13.6780 90.000 94.828 90.000

Transform matrix from orientation 1 to 2 (twinning law)

A_2(inverse) * A_1 [transforms h1 to h2] =
0.80066 -0.27547 -0.32054
0.48593 0.87310 -0.55440
0.45912 0.13885 0.90063

Rotation axis in reciprocal space = 2.13 -5.00 2.99
Angle of rotation around 2.13 -5.00 2.99 = -37.62720
Rotation axis in direct space = 3.92954 -3.13519 5.00000

Table 42. Comparison of two TWINDX solutions of (27).

Name of files:rh11.twx/ rh22.twx

figures of merit/reflections indexed/reflections used:
0.00169/77/77 0.00233/55/55
unit cells:

Refl#	H	K	L	Flags	H	K	L
1	-3.005	1.993	-2.007	1 + 0 -	-1.955	3.206	-1.562
2	-3.007	2.990	-2.011	1 + 0 -	-1.611	4.284	-1.891
3	-3.002	1.997	0.002	1 + 0 -	-1.068	3.870	0.262
4	-2.975	2.029	6.005	1 + 0 -	1.603	5.864	5.698
5	-1.986	1.022	4.010	1 + 0 -	0.967	3.571	3.949
				.....			
81	-2.992	-2.985	-6.990	1 + 0 -	-5.876	-3.826	-4.466
82	-7.056	-6.317	6.853	0 - 0 -	-3.374	-0.620	10.294
83	-2.992	-4.003	0.008	1 + 0 -	-3.149	-2.624	2.226
84	-5.001	-6.007	0.998	1 + 0 -	-4.614	-3.352	4.320
85	-7.009	-7.998	-1.000	1 + 0 -	-7.391	-5.049	3.695
86	-5.987	-6.041	4.021	1 + 0 -	-3.885	-1.846	7.344
87	-8.994	-8.962	-8.004	1 + 0 -	-12.000	-7.295	-1.821
88	-1.964	2.727	-6.306	0 - 1 +	-2.970	2.008	-5.988
89	-2.706	1.462	-5.730	0 - 0 -	-3.602	1.240	-4.851
90	-7.524	-4.169	-5.157	0 - 0 -	-8.196	-1.989	-1.196
91	-9.258	-3.374	-7.154	0 - 0 -	-9.837	-0.824	-2.804
92	-2.063	3.819	-7.041	0 - 1 +	-2.972	3.001	-6.986
93	-0.361	5.293	-6.001	0 - 1 +	-0.982	3.995	-6.980
94	-4.689	-0.297	-7.085	0 - 1 +	-5.998	-0.008	-4.975
95	-3.699	1.380	-6.942	0 - 0 -	-4.758	1.304	-5.659
96	-4.931	-4.829	-7.715	0 - 1 +	-8.000	-4.983	-4.001
97	-2.246	-1.837	-6.994	0 - 1 +	-5.032	-2.999	-5.045
98	-3.942	-3.320	-7.973	0 - 1 +	-6.995	-3.985	-4.994
99	-0.243	1.185	-7.446	0 - 1 +	-2.978	-0.991	-6.981
100	1.381	4.162	-7.744	0 - 0 -	-1.100	1.231	-8.661
				.....			
155	4.093	9.567	-6.486	0 - 1 +	2.962	5.986	-10.014
156	8.244	4.570	-10.386	0 - 1 +	1.988	-3.005	-13.039
157	8.521	5.208	-8.977	0 - 1 +	2.998	-2.005	-12.042
158	7.694	5.414	-8.033	0 - 1 +	2.990	-1.014	-11.030
159	0.023	0.017	-0.043	1 - 1 -	0.035	0.035	0.056

Summary of indexing result (Flags):

0+0+	0+0-	0+1+	0+1-	0-0+	0-0-	0-1+	0-1-	1+0+	1+0-	1+1+	1+1-	1-0+	1-0-	1-1+	1-1-
0	0	0	0	0	25	55	0	0	77	0	0	0	0	0	2

Note for flags(fitting code):
0-0-: Refl not been indexed and not used for indexing;
1+0-: Independent reflections for cell 1;
0-1+: Independent reflections for cell 2;
1+1+: Non-independent reflection used in indexing;
1-1-: Non-independent reflections fitted to both solution, but not been used in indexing.

data. This is a clear indication that the crystal moved during data collection. After examining the data frames with the two orientation matrices, a third orientation matrix was needed to integrate a hundred data frames obtained after the time that the crystal moved. In the end, about 100 frames (10% of the total data) were unusable. This is thought to be related to a large movement that was ongoing during these frames before the crystal finally settled into a new position.

Data integration was carried out separately on the two orientation matrices. The first cell was used for the first part of the data (about one third of the total frames), and the second cell was used to treat the second half of the data. A third cell was used to integrate a hundred data frames during the time the crystal was moving. The final data were corrected for inhomogeneity, decay and absorption with SADABS and then merged by XPREP and truncated to a resolution of 0.95 Å ($2\theta = 47°$) to suppress effects of solvent and anion disorder.

The structure was solved by SIR97.[12] A main structure fragment and the disordered toluene were refined without problem. The disordered $[BF_4]^-$ anions, however, posed a major problem in further refinement. Both $[BF_4]^-$ anions are near 2-fold symmetry elements, and were modeled at 50% occupancy. The final *R1* is 8.9% based on 1,399 reflections ($I/\sigma > 4$) and *R1* = 14.2% with all 2,341 data refined against 293 parameters.

(6) Example 6: A quadruply twinned crystal:CuTCNQ phase II (8).

CuTCNQ phase II was grown by a diffusion reaction between CH_3CN solution of CuI and TCNQ in a 3-compartment fritted cell. Details of the crystallization technique are described in Chapter 4. The habit of the crystals is square platelet with a typical size being 0.13 x 0.13 x 0.01 mm.

The first data set was collected by Dr. Charles Campana of Siemens (Bruker) on a SMART 1K platform CCD diffractometer. There were problems during the indexing, and the final cell was indexed by selectively removing reflections introduced by possible twinning components. Data integration was carried out with the program SAINT on the indexed cell with cell parameters a = 5.3337(8) Å, b = 5.3312(8) Å, c = 18.875(3) Å, β = 94.036(3)° and V = 535.38(14) Å^3. Systematic absences indicated that the space group is P2. Structure solution was obtained from XS and refined against F^2. The MISYMM program in the PLATON software package indicated that an inversion center exists in the structure model. This result, however, is contradicted by the systematic absences to the data. Rotational twinning or multiple twinning was proposed, and a four-fold rotation twinning law [0 1 0, -1 0 0, 0.25 0.25 1] was used in the refinement to model the twinning in space group P2/n. The off diagonal terms are the contributions from the non 90 degree β angle. The *R1* dropped from 20% to 16% after refinement. The twinning volume ratio for individual twinning components are refined as 52%, 8%, 15%, 25%.

A second data set was collected at MSU on a SMART 1K CCD diffractometer equipped with an Oxford Cryostream LT device. A platelet crystal of approximate dimensions 0.13 x 0.13 x 0.05 mm was mounted on the tip of a glass fiber with Dow Corning Silicone grease. The crystal was also found to be severely twinned. A full sphere data set was collected over a 72-hour period with an exposure time of 90 sec/frame. Of the total reflections, 253 reflections with $I/\sigma > 20$ were selected, but the indexing routine was unable to produce a reasonable cell. The XYZ coordinates of the reflections were subjected to the treatment of the TWINDX routine. By using 100 reflections and fitting ratio of 20%, TWINDX gave three solutions

with different orientations. Solution B is rotated 90° from solution A and C while solution C is rotated 180° from solution A. When the results were discussed with Dr. V. Young of the University of Minnesota and Dr. R. Sparks of Siemens, Dr. Young pointed out that there might exist a fourth solution related to solution B. Dr. Sparks offered to process the data with an updated version of his TWINDX routine that he redimensioned to handle this data set, which contained more than two twinned domains for the normal routine. In this manner, a fourth solution was determined and confirmed by the SMART indexing routine with the following relation to the first three.

$$A_4 = A_2 * A_1^{-1} * A_3$$

The 238 reflections that were used for the indexing are distributed among the four twinning domains according to the numbers 99, 100, 88 and 83 respectively. There remained 71 reflections (of maximum intensity $I/\sigma <$ 5) that did not fit any of the four solutions.

The data were integrated separately with four orientation matrices. A revised version of TWHKL was then used to process the four sets of integrated data together. Due to the complicated twinning situation and the exclusion of partial overlapping reflections, however, the combined data processing did not improve the refinement. After careful examination of the relations between the four twins, an alternative method was used to generate a set of HKLF 5 formatted data from a single integrated data set by one of the following conditions, which are derived from the twinning law. The orientation matrices of other cells could be transformed from one cell by the 3 x 3 matrix (0 -1 0, 1 0 0 0.25 0.25 1), which rotates 90° successively along the (0 0 1) axis in reciprocal space. Thus the following relationships related the other twins to the solution A:

h' = k, k' = -h, l' = (h-k)/4 +l;

h" = -h, k" = -k, l" = h/2 +l.

h"' = -k, k"' = h, l"' = (h+k)/4 +l

A simple FOTRAN routine was written to treat the integrated reflection data from solution A. A new data set with the HKLF 5^{15} format for overlapping reflection were given different batch numbers according to their relationship, partial overlapped reflection was removed. The structure was solved and refined with SHELXTL in the monoclinic space group P2/n with a final *R1* of 15.9% and *wR2* of 34.5% (*Fo*>4 σ(*Fo*)). The volume ratio of the twinning domains were refined to be 0.35, 0.19, 0.25, and 0.21.

(7) Example 7: A composite of two polymorphic crystals: Two morphologies of $[ppn]_2NiCl_4 \cdot Me_2CO$, (23, 24).

A hexagonal platelet of crystal (24) was examined on a SMART 1K CCD Area Detector and indexed to give the triclinic cell a = 13.620(10) Å, b = 13.646(7) Å, c = 21.443(13) Å, α = 104.52(7)°, β = 95.52(5)°, γ = 115.35(5)°, V = 3390(4) Å^3. A hemisphere of data was collected at 30 sec/frame. Without symmetry constraints the data integration gave a different cell of a = 14.3861(3) Å, b = 14.1148(1) Å, c = 22.6380(5) Å, α = 90.0000(11)°, β = 90.0000(12)°, γ = 115.9618(6)°, V = 4132.92(15) Å^3. After reprocessing the data, one third of the 465 reflections for indexing was removed from the least-square refinement as their error in indices are much bigger than allowed tolerance, and the cell reverted from the monoclinic setting back to a triclinic cell.

To identify the cause of the problem, TWINDX was then used to index the data, and a triclinic cell was indexed from 355 out of 464 reflections. A second run with the remaining reflections revealed that the rest of the reflections indexed to an orthorhombic cell which is the same as

(23). This is a very rare case in which one can actually index reflections that belong to different crystal systems. A comparison of the orientation matrices and cell parameters with TWROT indicated that the two solutions are rotated 37° from each another.

Data integration was carried out on the triclinic cell from the TWINDX result with local and global cell constraints. The data were partially contaminated from the orthorhombic data. The final statistics were $R1 = 0.0888$, $wR2 = 0.1944$ (for $I > 2\sigma(I)$), and $R1 = 0.2881$, $wR2 = 0.2507$ (for all data).

Data integration for the orthorhombic cell with a global constraint produced a second data set. It should be noted that the reflections are weaker than those belonging to the triclinic cell. Least-squares refinement on F^2 led to $R1 = 0.1355$, $wR2 = 0.1990$ (for $I > 2\sigma(I)$), and $R1 = 0.3753$, $wR2 = 0.2746$ (for all data).

B. Discussion

(1) Considerations before data collection.

It is important to select the best crystal for a crystallographic experiment! When problems such as twinning and fragmentation occur due to crystal defects or stress during growth, some precautions may be taken to avoid these problems. A quick rotational photograph typically reveals problems for a crystal of normal size. For microcrystals, a longer exposure time is needed to examine the quality of the candidate for data collection. In the event that performing a still photograph is not sufficient, one may collect all the data at longer exposure times. Sometimes the dilemma becomes whether to conduct an exhaustive search for the best crystal and versus collecting data for the "less than perfect" crystal in hand.

(2) Data collection.

With a CCD area detector, data may be collected even without successful indexing of a unit cell. This is especially helpful when the crystal is very weak. To be able to handle potential twinning problems, a full sphere of data is preferred.

(3) Data processing.

When using a serial detector to collect data for a problem crystal, one may vary options such as using a narrow slit. Precise crystal centering can also be used to reduce the effect of twinning or to prevent the collection of data on small daughter crystals. When CCD detectors are used, hardware options are not available. Nevertheless, the software options during data integration such as the integration box size, and peak-shape profile refinement are useful resources when facing problem data collection. Narrowing or widening the integration window is one of the options that can have major effects on the quality of the final data. In the case of small angles between the twinning domains, one can widen the integration window to allow for the chance to treat the nearly perfectly overlapped reflections as one with broad mosaic spread. When a bigger separation of reflections is encountered, one can narrow the window to avoid the daughter crystal reflections altogether so as to be able to treat the data as a small single crystal. It is still important, however, to select the best crystal and carefully choose data collection parameters to give one a chance to obtain the best data.

(4) Structure solution and refinement.

It is common for twinning laws to contain off-diagonal terms when a monoclinic system exhibits a β angle ~ 90° and the a and b are nearly equal. A 180° rotation along the (0 0 1) axis will generate a twinning law of

Table 43. Rotational transformation of $[ppn]_2[NiCl_4]\bullet Me_2CO$ (23b, 24) from orientation A_1 to orientation A_2.

Orientation Matrix A_1 from solution 1 (40ctra.p4p)
Orientation Matrix A_2 from solution 2 (40ctrb.p4p)

Orientation matrix and unit cell parameters for A_1

0.06467 0.07256 0.00044
-0.02006 -0.02616 -0.04989
-0.04898 0.03680 0.00080

13.6943 13.7336 21.2670 104.039 95.809 115.908

Orientation matrix and unit cell parameters for A_2

-0.04288 -0.03938 0.02990
0.07211 0.01337 0.02502
-0.03930 0.06670 0.01278

10.7946 12.7217 24.3727 90.163 90.291 90.246

Transform matrix from orientation 1 to 2 (twinning law)

A_2(inverse) * A_1 [transforms h1 to h2] =

-0.26483 -0.75304 -0.42303
-0.98377 -0.11981 -0.09892
0.48735 1.18885 -0.72199

Rotation axis in reciprocal space = -3.00000 2.97493 1.10602
Angle of rotation around -3.00 2.97 1.11 = 144.57920
Rotation axis in direct space = -2.98588 4.00000 1.18486

Table 44. Comparison of indexing results of the two TWINDX solutions of ppn]$_2$[NiCl$_4$]•Me$_2$CO (23b, 24).

Name of files: 40tr00.twx/40tr01.twx

figures of merit/reflections indexed/reflections used:

0.00334/355/355 0.00243/94/94

unit cells:

13.694	13.734	21.267		10.795	12.722	24.373	
0.009	0.006	0.011		0.007	0.013	0.019	
104.039	95.809	115.908	3390.44	90.163	90.291	90.246	3346.94
0.036	0.045	0.039	2.94	0.074	0.058	0.069	4.82

Refl#	H	K	L	Flags	H	K	L
1	5.971	-3.987	-3.962	1 + 0 -	3.121	-5.013	1.007
2	-0.973	0.966	11.047	1 + 0 -	-5.119	-0.259	-7.326
3	2.990	-1.000	2.046	1 + 0 -	-0.880	-3.032	-1.233
4	6.003	-2.020	5.008	1 + 0 -	-2.163	-6.167	-3.116
5	6.017	-2.028	6.002	1 + 0 -	-2.582	-6.279	-3.836
.....							
456	1.993	-5.789	-2.636	0 - 1 +	4.971	-1.015	-4.031
457	0.517	4.398	-10.481	0 - 1 +	1.009	-0.007	13.024
458	-0.029	-1.032	-7.935	1 + 0 -	4.166	0.929	4.464
459	0.868	-2.261	-5.886	0 - 1 +	3.987	-0.009	1.961
460	-0.435	2.451	-8.750	0 - 1 +	1.995	0.992	8.995
461	0.980	-3.033	-5.908	1 + 0 -	4.548	-0.025	1.115
462	0.821	-3.045	-4.458	0 - 1 +	3.986	-0.011	-0.025
463	-0.068	-1.045	-4.931	1 + 0 -	2.914	0.671	2.262
464	-0.077	-1.065	-5.923	0 - 0 -	3.352	0.781	2.950

Summary of indexing result (Flags):

0+0+	0+0-	0+1+	0+1-	0-0+	0-0-	0-1+	0-1-	1+0+	1+0-	1+1+	1+1-	1-0+	1-0-	1-1+	1-1-
0	0	0	0	0	14	94	0	0	355	0	0	0	0	0	1

Note for flags(fitting code):

0-0-: Refl not been indexed and not used for indexing;
1+0-: Independent reflections for cell 1;
0-1+: Independent reflections for cell 2;
1+1+: Non-independent reflection used in indexing;
1-1-: Non-independent reflections fitted to both solution, but not been used in indexing.

[-1 0 0, 0 -1 0, .5 0 1] (Example 6). The off-diagonal term can readily be calculated from the formula $2c\cos\beta/b$.[9] In the case where *b* and *c* are nearly equal, the rotation will be around (1 0 0) (Example 3). Structure solution for a twinned crystal is not as straightforward as for a non-twinned crystal. Sometimes the Patterson methods can be used to locate the heavy element position. Structure refinement for twinned crystal data from merohedral twins and pseudo-merohedral twins (Example 2) could be handled by using the built-in capacity of a refinement program such as SHELXL97[8] or CRYSTAL.[13] Solutions for crystal with *rotational twins* may be obtained by using data set integrated from one of the twinned orientation. To achieve the best results for refinement, reflection data that contain both orientations should be used. However, unless special programs like UNTWIN[16] or TWHKL5[17] are used to handle the partially overlapping reflections, the refinement residual index (*R1*) is usually much higher than for an non-twinned crystal.

3. Conclusions

With the help of a CCD X-ray instrument, graduate students that depend on single crystal structures can be more productive when crystallography is routinely needed for their research. Considerable effort, however, is still required in order to handle problem crystals that are more frequently encountered when using the high resolution and sensitivity of a CCD camera. Basic education and training in handling problem crystals, especially those that suffer from twining, should become a standard teaching procedure in CCD equipped X-ray facilities.

References

1. Baker T. *IUCr Newslett.* **1997**, *5*, 1.

2. Baker, T. *IUCr Newslett.* **1999**, *7* ,1

3. Friedrich, W., Knipping, P., and Laue, M. *Sitzungsberichte der mathenatisch-physikalischen Klasse der Königlichen Bayerischen Akademie der Wissenschaften zu München.* **1912**, 303-322. **English translation:** Stezowski, J. J. In: *Structural Crystallography in Chemistry and Biology.* (Ed., Glusker, J. P.) Hutchinson & Ross: Stroudsburg, PA. **1981**, 23.

4. Bragg, W. L. *Proc. Roy. Soc. (London)* **1913**, *A89*, 248.

5. *X-ray Structure Determination—A Practical Guide,* Stout, G. H. and Jensen L. H. 2nd Ed. John Wiley & Sons, Inc. USA **1989** 173.

6. Wilson, A. J. C., Ed., *International Tables for Crystallography, Volume C,* Kluwer Academic Publishers, Dordrecht, The Netherlands, 1995.

7. (a) Hoenle, W. and von Schnering, H. G. *Z. Krist.*, **1988** *184*, 301. (b) *SHELXTL V5 Reference Manual.* **1997**, Ch8. Siemens Energy & Automation, Inc. Analytical Instrumentation.

8. *SHELX97* [Includes SHELXS97, SHELXL97, CIFTAB (and SHELXA)] - Programs for Crystal Structure Analysis (Release 97-2). Sheldrick, G.M., Institüt für Anorganische Chemie der Universität, Tammanstrasse 4, D-3400 Göttingen, Germany, 1998.

9. Watkin, D. *Twinning. Don't give up -- yet.* Presented at BCA Autumn Meeting, Bristol, November 12th 1997. http://darkstar.xtl.ox.ac.uk/refs_bris97.html. Online published: Jan 28, 1998, Site Visited: Mar 26, 1998.

10. (a) Duisenberg, A. J. M. *J. Appl. Cryst.* **1992**, *25*, 92. (b) *DIRAX,* Duisenberg, A. J. M.Private communication.

11. Sparks R. A. *TWINNING* (TWINDX, TWUTIL, TWROT and TWHKL), Program for processing twinned data. Bruker AXS Instrument, Madison, WI.

12. (a) *SIR92* –A program for crystal structure solution. A. *J. Appl. Cryst.* **1993**.*26*, 343. (b) *SIR97*, Altomare, A., Cascarano, G., Giacovazzo, C. and Guagliardi **1997.**

13. Watkin,D. *Crystals32* Release 10 user's manual.

14. DIRDIF84 - Beurskens, P. T.-Direct Methods for Difference Structures; Technical Report **1984**/1, Crystallography Laboratory, Toernooiveld, 6525 Ed Nijmegen, Netherlands.

15. Reflection format that contains h, k, l F^2, σ and a batch number, the batch number indicated whether a relation is an independent reflection or overlapping reflection. Volume ratio of twinning domains could be refined in least-square refinement.

16. Young, V. G. Jr. *New Strategies in the Refinement of Rotationally Twinned Materials*, Poster presentation in ACA 1998 Meeting St. Louis, MO.

17. *TWHKL5,* Sparks R. A. and Young G. V. Jr. Program for processing twinned reflection data based on *UNTWIN* and *TWHKL,* private communication.

APPENDICES

APPENDIX A

GENERAL PROCEDURES FOR DATA COLLECTION

1. Data collection procedure for Siemens CCD platform diffractometer

Data collection procedures on a Siemens CCD platform diffractometer involved the following steps:

A. Crystal mounting and preliminary data collection.

Crystals were secured on the tip of a short glass fiber typically (1/8 of an inch) with Dow Corning silicone grease and inserted into a copper pin on a goniometer. The instrument is a Siemens SMART[1] 1K CCD platform diffractometer with graphite-monochromated Mo Kα radiation source ($\lambda\alpha$ = 0.71073 Å) powered at 50 kV and 40 mA. The crystal was bathed in a cold stream of nitrogen, which serves to solidify the grease, with an Oxford Cryosystem Cryostream cooling device. Intensity data were collected with 0.3° frames by the ω-scan technique with a detector-to-crystal distance of 5 cm. Initial cell parameters and an orientation matrix were generated from a set of preliminary data collection of 10 sec frames, from three detector positions (detector was positioned at $2\theta = \pm 26°$, when $\phi = 0°$, and $2\theta = -26°$ when $\phi = 90°$, 15 frames were taken for each detector position).

B. Data collection.

Data collection was performed according to the Laue symmetry of the preliminary data. For crystal systems of monoclinic and higher symmetry, only a hemisphere of data was collected. In the case of triclinic systems, a full sphere of data was collected to ensure sufficient redundancy for the absorption correction (Described in Step three). For a hemisphere data collection, the detector was successively set to three initial positions $\phi = 0$, 90 and 180, with $2\theta = \omega = -28$. Frames were measured at 30 sec for all ϕ positions; 606 frames were measured for the first ϕ position, and 453 and 230 for the second and third ϕ position to ensure sufficient coverage for a

resolution of 0.75 Å and redundancy above 2 for a hemisphere. An extra 50 frame set at the first detector position was recollected at the end of data collection check for crystal decay. When collecting a full sphere of data, another detector position with $\phi = 270$ was added. A total of 606 frames were collected for all detector positions.

C. Data integration.

Post data collection cell parameters and a second orientation matrix were obtained by refining reflections from ~ 30-50 frames in six to eight groups, which were evenly distributed among all data frames. Diffraction was carefully checked against locations predicted by the new orientation matrix for signs of mosaic spread, twinning, split crystals or crystals that moved during data collection. The new orientation matrix was used in data integration. All frames were then integrated with the new orientation matrix with appropriate global and local constraints according to the Laue symmetry. Final cell parameters and the orientation matrix were obtained from the XYZ centroids of up to 8192 integrated reflections with $I > 10\sigma(I)$.

D. Beam inhomogeneity, crystal decay and absorption correction.

The intensities of integrated reflections were corrected for beam inhomogeneity, crystal decay and absorption with the program SADABS according to the algorithm described by Blessing,[2] which is applied when high redundancy data such as CCD data are used.

References

1. SMART: Area-Detector Software Package, **1993.** Siemens Industrial Automation, Inc.: Madison, WI.
2. Blessing J. *Acta Cryst.* **1995,** *A51,* 33 .

APPENDIX B

ATOM POSITIONS TABLES

Table 45. Atomic coordinates (x 10^4) and equivalent isotropic displacement parameters ($Å^2$x 10^3) for $[Mo_2(O_2CCF_3)_4(TCNQ)•2m\text{-}C_8H_{10})]_\infty$•·$[Mo_2(O_2CCF_3)_4•2m\text{-}C_8H_{10})]_\infty$ (1).

	x	y	z	U(eq)
Mo(1)	9719(1)	8628(1)	7660(1)	27(1)
Mo(2)	11516(1)	8673(1)	7671(1)	27(1)
Mo(3)	5091(1)	5362(1)	5501(1)	28(1)
O(1)	9660(4)	6901(3)	8049(3)	35(1)
O(2)	11557(4)	6965(3)	8053(3)	33(1)
O(3)	11590(4)	10387(3)	7270(3)	36(1)
O(4)	9692(4)	10344(3)	7258(3)	34(1)
O(5)	9101(3)	8605(3)	9055(3)	32(1)
O(6)	10997(4)	8625(3)	9080(3)	32(1)
O(7)	12121(4)	8728(4)	6278(3)	34(1)
O(8)	10212(4)	8675(4)	6270(3)	34(1)
O(9)	6930(4)	5101(3)	5217(3)	32(1)
O(10)	5404(4)	6913(3)	4555(3)	33(1)
O(11)	3261(4)	5664(3)	5842(3)	32(1)
O(12)	4793(4)	3843(3)	6512(3)	33(1)
N(1)	17436(5)	8542(5)	7787(4)	44(2)
N(2)	13631(5)	8881(5)	7883(4)	37(1)
C(7)	11304(6)	8729(5)	5887(5)	34(2)
C(9)	5373(5)	6965(5)	3761(4)	32(1)
C(11)	2669(5)	5380(5)	5381(4)	32(2)
C(13)	16493(6)	8763(5)	8122(4)	31(1)
C(14)	15347(5)	9079(5)	8560(4)	26(1)
C(15)	14382(5)	8954(5)	8181(4)	28(1)
C(17)	16138(5)	9646(5)	9644(4)	32(2)
C(18)	15977(5)	10118(5)	10319(4)	32(2)
C(16)	15168(5)	9519(5)	9272(4)	28(1)
C(1)	10603(6)	6466(5)	8154(4)	32(1)
C(3)	10664(6)	10837(5)	7127(4)	32(2)
C(5)	9895(6)	8587(5)	9449(4)	31(1)

Table 45. (cont'd).

	x	y	z	U(eq)
C(2)	10604(5)	5234(5)	8441(4)	45(2)
F(1A)	11520(9)	4882(6)	7861(6)	36(3)
F(2A)	9610(9)	4754(8)	8470(13)	56(3)
F(3A)	10816(14)	4867(8)	9255(6)	46(3)
F(1B)	9489(7)	4832(11)	8921(12)	47(5)
F(2B)	11255(17)	4888(14)	9025(12)	62(6)
F(3B)	10957(20)	4818(13)	7747(8)	70(6)
F(1C)	9945(18)	4792(12)	8042(15)	27(6)
F(2C)	11698(10)	4873(22)	8174(23)	82(11)
F(3C)	10177(29)	4779(19)	9338(6)	76(10)
C(4)	10756(5)	12060(5)	6743(4)	45(2)
F(4A)	9853(27)	12462(26)	6405(30)	55(13)
F(5A)	11754(25)	12398(33)	6067(23)	94(19)
F(6A)	10752(35)	12532(18)	7397(14)	20(9)
F(4B)	11718(14)	12513(11)	6845(15)	39(5)
F(5B)	9811(13)	12529(13)	7150(15)	55(6)
F(6B)	10894(23)	12372(13)	5845(6)	47(6)
F(4C)	11335(16)	12528(6)	7164(10)	51(3)
F(5C)	9676(5)	12469(6)	6814(11)	46(3)
F(6C)	11335(13)	12310(7)	5855(4)	51(3)
C(6)	9484(4)	8472(4)	10472(4)	39(2)
F(7A)	8353(6)	8676(9)	10768(7)	56(3)
F(8A)	10158(8)	9097(7)	10715(7)	37(3)
F(9A)	9659(8)	7443(5)	10895(6)	46(2)
F(7B)	10311(8)	8847(9)	10760(8)	56(4)
F(8B)	9171(9)	7449(5)	10959(6)	55(3)
F(9B)	8508(6)	9044(7)	10672(6)	42(2)
C(10)	5506(5)	8076(5)	3077(4)	49(2)
F(10A)	6206(8)	8069(9)	2256(5)	51(3)
F(11A)	6023(9)	8789(7)	3355(6)	55(3)
F(12A)	4457(7)	8430(9)	2987(8)	64(3)
F(10B)	5557(9)	8894(7)	3433(6)	55(3)

Table 45. (cont'd).

	x	y	z	U(eq)
F(11B)	4550(7)	8236(8)	2744(7)	55(3)
F(12B)	6461(8)	8160(10)	2369(6)	60(4)
C(12A)	1371(7)	5673(8)	5495(7)	34(5)
F(13A)	1083(10)	6397(8)	5973(7)	42(4)
F(14A)	682(8)	4772(7)	5902(7)	45(3)
F(15A)	1162(9)	6143(8)	4697(6)	50(3)
C(12B)	1328(7)	5555(8)	5676(7)	33(5)
F(13B)	924(8)	5894(8)	4941(6)	41(2)
F(14B)	1042(10)	6256(8)	6181(7)	41(4)
F(15B)	697(8)	4646(6)	6206(6)	39(2)
C(8)	11724(5)	8856(4)	4862(5)	50(2)
F(16A)	12251(9)	9809(6)	4365(7)	66(3)
F(17A)	10799(7)	8687(9)	4570(7)	56(3)
F(18A)	12533(7)	8111(7)	4691(6)	48(2)
F(16B)	10977(8)	8370(8)	4582(8)	57(3)
F(17B)	12804(7)	8500(9)	4587(8)	70(3)
F(18B)	11764(9)	9931(5)	4450(6)	54(3)
C(19A)	6880(11)	6397(13)	6704(11)	31(4)
C(20A)	6619(14)	7420(13)	6218(12)	32(5)
C(21A)	5429(14)	7660(13)	6291(12)	26(6)
C(22A)	4528(14)	6866(13)	6830(11)	28(5)
C(23A)	4776(16)	5856(13)	7322(12)	35(5)
C(24A)	5964(14)	5630(14)	7249(11)	32(4)
C(25A)	8139(12)	6045(14)	6675(12)	46(4)
C(26A)	5280(21)	8778(15)	5706(16)	44(6)
C(19B)	6697(14)	6136(13)	6937(12)	34(4)
C(20B)	6676(15)	7165(15)	6377(13)	36(5)
C(21B)	5674(15)	7688(15)	6199(14)	38(7)
C(22B)	4597(15)	7099(12)	6643(11)	29(5)
C(23B)	4586(13)	6069(14)	7214(11)	27(4)
C(24B)	5608(15)	5583(14)	7378(12)	37(5)
C(25B)	7886(15)	5693(17)	7018(14)	64(5)

Table 45. (cont'd).

	x	y	z	U(eq)
C(26B)	5566(25)	8804(19)	5588(20)	74(10)
C(27A)	5564(13)	6583(16)	10070(13)	37(6)
C(28A)	4883(16)	6949(18)	10804(15)	44(7)
C(29A)	3663(18)	7152(20)	10944(14)	50(7)
C(30A)	3084(18)	7007(17)	10324(13)	56(6)
C(31A)	3712(17)	6616(16)	9602(15)	52(5)
C(32A)	4934(19)	6419(16)	9475(13)	43(6)
C(33A)	6861(14)	6375(16)	9974(14)	62(5)
C(34A)	2935(28)	7518(28)	11748(20)	116(13)
C(27B)	5499(15)	6676(18)	10269(14)	46(7)
C(28B)	4630(19)	7031(19)	10902(15)	49(7)
C(29B)	3476(17)	7101(20)	10844(15)	51(7)
C(30B)	3241(17)	6821(15)	10131(12)	41(5)
C(31B)	4086(18)	6513(15)	9467(12)	46(5)
C(32B)	5228(16)	6412(16)	9547(14)	47(6)
C(33B)	6779(15)	6530(16)	10293(14)	61(5)
C(34B)	2625(19)	7453(19)	11611(15)	64(6)

U(eq) is defined as one third of the trace of the orthogonalized U_{ij} tensor.

Table 46. Atomic coordinates (x 10^4) and equivalent isotropic displacement parameters ($Å^2$x 10^3) for $[Mo_2(O_2CCF_3)_4(DM\text{-}DCNQI)\bullet C_6H_6]_\infty$ (2).

	x	y	z	U(eq)
Mo(1)	-433(1)	576(1)	-283(1)	19(1)
O(1)	-257(4)	-1497(5)	559(6)	30(2)
O(2)	-1153(4)	-256(5)	-1(6)	26(2)
O(3)	-338(4)	-1164(4)	-1562(6)	24(1)
O(4)	-1267(4)	51(4)	-2174(6)	23(1)
C(1)	-905(6)	-1142(7)	315(8)	21(2)
C(2)	-1436(6)	-1810(6)	437(8)	25(2)
F(1)	-1325(12)	-2694(12)	249(22)	45(6)
F(2)	-1207(15)	-1752(20)	1561(14)	55(7)
F(3)	-2240(11)	-1601(21)	-398(23)	80(11)
F(1')	-980(17)	-2064(24)	1647(16)	70(9)
F(2')	-2120(13)	-1401(20)	72(25)	67(9)
F(3')	-1651(14)	-2647(15)	-191(22)	61(9)
C(3)	-1042(6)	-717(7)	-2366(9)	22(2)
C(4)	-1707(6)	-1209(7)	-3680(9)	28(2)
F(4)	-2102(4)	-1903(4)	-3589(5)	34(1)
F(5)	-1332(4)	-1609(4)	-4076(5)	35(1)
F(6)	-2277(3)	-583(4)	-4545(5)	34(1)
N(1)	-1390(5)	2055(6)	-1283(7)	24(2)
C(5)	-1348(5)	2879(6)	-1327(8)	16(2)
N(2)	-1403(5)	3861(5)	-1480(7)	21(2)
C(6)	-705(5)	4389(6)	-740(8)	16(2)
C(7)	131(6)	3981(7)	218(8)	22(2)
C(8)	833(6)	4567(7)	963(8)	22(2)
C(9)	1705(6)	4179(7)	1948(9)	26(2)
C(1S)	0	-3485(11)	-2500	29(3)
C(2S)	-748(7)	-3990(8)	-3364(9)	32(2)
C(3S)	-743(6)	-4999(8)	-3365(9)	30(2)
C(4S)	0	-5498(12)	-2500	39(4)

Table 47. Atomic coordinates (x 10^4) and equivalent isotropic displacement parameters ($Å^2$x 10^3) for $\{[Mo_2(O_2C(CH_3)_3)_3((NC)_2C(CN)CCONH)]\cdot 6CH_2Cl_2\}_\infty$ (3).

	x	y	z	U(eq)
Mo(1)	4045(2)	2387(2)	9291(9)	16(2)
Mo(2)	4231(2)	2908(2)	9303(9)	17(2)
Mo(3)	2600(2)	936(2)	9152(9)	8(2)
Mo(4)	2417(2)	419(2)	9145(9)	16(2)
Mo(5)	4647(2)	893(2)	9438(9)	15(2)
Mo(6)	4985(2)	708(2)	9391(9)	16(2)
O(1)	4526(14)	2448(14)	9315(28)	7(13)
O(2)	4708(15)	3007(15)	9410(30)	11(14)
O(3)	3762(23)	2821(23)	9229(43)	28(25)
N(7A)	3762(23)	2821(23)	9229(43)	28(25)
O(4)	4100(25)	2379(24)	8420(44)	42(25)
O(5)	4296(21)	2922(20)	8380(37)	29(20)
O(6)	4020(16)	2376(16)	10241(30)	8(15)
O(7)	4225(17)	2915(17)	10251(32)	16(17)
O(8)	2131(15)	863(15)	9044(30)	13(15)
O(9)	1907(14)	322(14)	9086(28)	6(13)
O(10)	2879(15)	495(16)	9217(29)	0(16)
N(3A)	2879(15)	495(16)	9217(29)	0(16)
O(11)	2583(17)	944(16)	8254(32)	11(17)
O(12)	2381(16)	410(16)	8291(30)	11(15)
O(13)	2554(15)	931(14)	10110(27)	0(14)
O(14)	2347(15)	398(14)	10092(27)	0(12)
O(15)	5038(14)	1376(14)	9430(28)	3(12)
O(16)	5379(16)	1193(16)	9368(30)	12(15)
O(17)	4623(15)	233(15)	9406(31)	0(16)
N(9A)	4623(15)	233(15)	9406(31)	0(16)
O(18)	4642(20)	938(20)	8557(37)	27(20)
O(19)	5006(20)	742(21)	8528(38)	29(21)
O(20)	4674(18)	921(19)	10400(37)	23(19)

Table 47. (cont'd).

	x	y	z	U(eq)
O(21)	5028(19)	730(18)	10298(36)	18(18)
N(1)	3787(16)	1767(16)	9191(31)	0(14)
N(2)	4315(18)	1214(18)	9408(36)	9(17)
N(3)	3070(15)	1049(16)	9258(29)	6(16)
O(10A)	3070(15)	1049(16)	9258(29)	6(16)
N(4)	3572(21)	404(21)	9522(40)	23(19)
N(5)	2859(17)	1563(17)	9158(32)	3(15)
N(6)	2339(25)	2110(25)	9156(48)	31(24)
N(7)	3580(17)	2283(17)	9263(32)	13(17)
O(3A)	3580(17)	2283(17)	9263(32)	13(17)
N(8)	3030(23)	2910(23)	9088(45)	26(22)
N(9)	4262(22)	420(22)	9490(42)	38(25)
O(17A)	4262(22)	420(22)	9490(42)	38(25)
N(10)	3470(19)	-282(19)	9587(36)	14(17)
N(11)	4600(24)	-473(24)	9273(43)	26(23)
N(12)	3552(20)	-1001(19)	9374(38)	13(18)
C(1)	3753(20)	1495(20)	9297(37)	0(17)
C(2)	3746(27)	1218(26)	9272(50)	23(25)
C(3)	4089(24)	1228(24)	9331(46)	12(22)
C(4)	3457(25)	868(25)	9361(48)	19(23)
C(5)	3161(20)	826(19)	9195(37)	0(17)
C(6)	3543(27)	615(27)	9349(52)	24(25)
C(7)	2867(29)	1786(29)	9213(54)	26(28)
C(8)	2874(20)	2125(20)	9139(40)	2(17)
C(9)	2591(19)	2106(19)	9115(39)	0(17)
C(10)	3177(25)	2442(25)	9143(50)	16(23)
C(11)	3535(22)	2526(22)	9175(43)	9(19)
C(12)	3125(24)	2703(24)	9077(47)	15(22)
C(13)	4304(34)	169(33)	9427(65)	38(33)
C(14)	4062(20)	-164(20)	9470(38)	2(17)
C(15)	3732(26)	-214(25)	9530(48)	18(24)
C(16)	4095(20)	-426(20)	9374(39)	0(17)

Table 47. (cont'd).

	x	y	z	U(eq)
C(17)	4378(21)	-440(21)	9378(42)	5(18)
C(18)	3769(27)	-768(27)	9373(51)	20(24)
C(19)	4765(19)	2764(32)	9320(59)	34(32)
C(20)	5098(15)	2808(16)	9414(32)	10(19)
C(21)	5367(21)	3146(16)	9562(43)	23(24)
C(22)	5132(48)	2739(31)	8787(34)	169(135)
C(23)	5130(32)	2566(21)	9791(54)	61(40)
C(24)	4225(25)	2653(25)	8110(29)	17(23)
C(25)	4305(17)	2674(16)	7475(30)	69(51)
C(26)	4584(20)	2611(22)	7400(53)	36(30)
C(27)	4393(20)	2994(16)	7190(39)	12(21)
C(28)	4009(19)	2406(19)	7176(53)	39(32)
C(29)	4166(19)	2645(19)	10527(26)	0(17)
C(30)	4238(19)	2653(19)	11165(28)	31(29)
C(31)	4253(29)	2943(21)	11465(61)	58(42)
C(32)	3985(24)	2347(20)	11459(56)	51(36)
C(33)	4565(22)	2674(32)	11219(73)	83(59)
C(34)	1884(15)	575(19)	9106(38)	0(17)
C(35)	1552(17)	531(19)	9000(33)	35(30)
C(36)	1282(41)	202(20)	9194(57)	129(98)
C(37)	1495(32)	582(28)	8375(31)	48(35)
C(38)	1543(27)	790(23)	9366(39)	32(28)
C(39)	2510(52)	619(52)	7921(47)	89(62)
C(40)	2471(22)	672(21)	7289(42)	41(33)
C(41)	2738(28)	631(37)	7020(117)	172(144)
C(42)	2491(35)	978(23)	7052(76)	73(51)
C(43)	2147(23)	385(24)	7122(69)	62(42)
C(44)	2413(43)	649(45)	10326(37)	63(48)
C(45)	2339(15)	668(15)	10956(29)	14(21)
C(46)	2598(20)	953(20)	11292(53)	45(35)
C(47)	2278(25)	357(19)	11247(60)	58(42)
C(48)	2030(17)	684(21)	10966(44)	20(23)

Table 47. (cont'd).

	x	y	z	U(eq)
C(49)	5352(26)	1440(20)	9375(71)	49(38)
C(50)	5637(15)	1781(15)	9381(29)	17(22)
C(51)	5545(25)	2025(24)	9169(52)	0(33)
C(52)	5904(27)	1800(32)	9001(46)	18(42)
C(53)	5762(38)	1866(40)	9995(32)	38(57)
C(51')	5570(38)	2056(29)	9493(95)	0(52)
C(52')	5648(86)	1738(75)	8735(35)	186(310)
C(53')	5963(45)	1870(57)	9638(133)	51(136)
C(54)	4849(24)	875(23)	8230(27)	11(21)
C(55)	4889(17)	918(17)	7584(28)	28(27)
C(56)	4861(23)	626(19)	7270(43)	21(23)
C(57)	5226(19)	1204(21)	7486(71)	81(59)
C(58)	4644(23)	998(24)	7334(51)	34(30)
C(59)	4893(22)	861(22)	10618(31)	7(20)
C(60)	4967(23)	941(23)	11251(33)	30(28)
C(61)	4657(32)	861(46)	11565(97)	148(114)
C(62)	5214(38)	1294(23)	11358(109)	167(132)
C(63)	5095(37)	732(35)	11492(73)	68(49)
Cl(1)	4328(8)	1679(11)	8138(22)	64(12)
C(1S)	4715(11)	1746(29)	8342(33)	38(32)
Cl(2)	5018(7)	1969(9)	7817(18)	48(9)
Cl(3)	2262(8)	1516(9)	8061(20)	47(9)
C(2S)	1951(22)	1617(28)	8021(69)	59(50)
Cl(4)	1617(8)	1340(10)	7594(21)	54(10)
Cl(5)	3382(9)	647(11)	5659(27)	59(14)
C(3S)	2964(12)	472(32)	5824(81)	68(63)
Cl(6)	2718(8)	110(9)	5433(20)	32(10)
Cl(9)	1604(8)	1367(11)	10647(22)	57(11)
C(5S)	1927(15)	1598(30)	10160(45)	43(35)
Cl(10)	2276(9)	1568(12)	10306(24)	66(12)
Cl(11)	1520(10)	3491(10)	5829(22)	60(11)
C(6S)	1654(22)	3288(23)	5358(23)	22(25)

Table 47. (cont'd).

	x	y	z	U(eq)
Cl(12)	1883(12)	3140(11)	5720(23)	67(12)
Cl(13)	4768(15)	136(15)	5901(29)	95(18)
C(7S)	5000	0	5518(44)	40(44)
Cl(15)	6939(8)	1967(9)	5911(18)	45(9)
C(8S)	7013(10)	1724(18)	5424(35)	14(21)
Cl(16)	7420(7)	1807(8)	5449(17)	37(8)
Cl(17)	5954(8)	1059(8)	8214(19)	52(10)
C(9S)	6343(17)	1400(15)	8335(47)	44(36)
Cl(18)	6427(9)	1729(8)	7868(19)	52(10)
Cl(19)	5920(9)	1068(9)	10404(21)	60(11)
C(10S)	6331(11)	1385(16)	10417(36)	21(24)
Cl(20)	6404(10)	1681(8)	10952(20)	59(11)
Cl(23)	3235(34)	283(34)	5597(55)	61(18)
C(12S)	3340(56)	248(50)	6318(54)	0(61)
Cl(24)	3460(56)	-48(52)	6395(83)	105(23)
Cl(25)	3539(13)	-586(9)	8029(26)	88(16)
C(13S)	3843(44)	-236(14)	7669(53)	101(74)
Cl(26)	3973(12)	124(9)	8075(25)	82(14)
Cl(29)	3994(9)	848(11)	10776(23)	68(12)
C(15S)	3689(11)	949(26)	10915(152)	166(131)
Cl(30)	3292(9)	616(13)	10810(25)	80(14)
Cl(33)	3493(11)	1431(12)	7757(23)	72(13)
C(17S)	3385(27)	1692(25)	8121(27)	34(31)
Cl(34)	3164(11)	1816(11)	7677(23)	70(13)
Cl(35)	3409(9)	705(12)	12661(24)	81(14)
C(18S)	3029(12)	548(38)	12307(43)	81(57)
Cl(36)	2704(8)	250(10)	12724(21)	61(11)
Cl(37)	5358(10)	221(10)	7798(21)	58(11)
C(19S)	5000	0	8214(37)	46(50)
Cl(39)	5471(27)	2534(26)	6416(49)	111(40)
C(20S)	5434(73)	2774(63)	6965(102)	80(92)
Cl(40)	5603(135)	3062(116)	7533(178)	644(348)

Table 47. (cont'd).

	x	y	z	U(eq)
Cl(41)	4370(9)	575(9)	5888(20)	61(10)
C(21S)	3925(24)	377(45)	5797(188)	289(263)
Cl(42)	3757(11)	-41(12)	6050(29)	106(18)
Cl(43)	3688(18)	751(19)	7850(34)	49(17)
Cl(44)	3337(21)	188(21)	7170(38)	59(21)

U(eq) is defined as one third of the trace of the orthogonalized U_{ij} tensor.

Table 48. Atomic coordinates (x 10^4) and equivalent isotropic displacement parameters ($Å^2$x 10^3) for $\{[Mo_2(O_2C(CH_3)_3)_3((NC)_2C(CN)CCONH)]\cdot 0.5C_6H_6\}_\infty$ (4).

	x	y	z	U(eq)
Mo(1)	1647(1)	6639(1)	12085(1)	36(1)
Mo(2)	1795(1)	8216(1)	11523(1)	36(1)
O(3)	1135(4)	8313(9)	10846(5)	43(3)
O(2)	968(3)	6671(9)	11421(5)	38(3)
O(6)	1786(3)	5572(9)	11222(5)	40(3)
O(4)	1589(4)	9332(9)	12319(6)	43(3)
O(7)	1924(3)	7187(9)	10623(5)	40(3)
O(5)	1436(3)	7651(9)	12903(5)	35(3)
C(1)	2590(8)	7349(18)	12659(12)	64(6)
O(1)	2298(5)	6554(14)	12750(6)	74(6)
N(1)	2445(4)	8207(12)	12156(7)	46(4)
C(2)	3023(7)	6992(19)	13215(12)	37(7)
C(3)	3403(8)	7710(20)	13206(13)	38(7)
N(1A)	2298(5)	6554(14)	12750(6)	74(6)
O(1A)	2445(4)	8207(12)	12156(7)	46(4)
C(2A)	3076(8)	7720(30)	12909(17)	7(9)
C(3A)	3330(14)	7010(30)	13542(19)	21(11)
N(4)	4167(5)	7153(17)	14102(9)	101(7)
N(3)	3451(4)	9528(12)	12414(7)	46(4)
N(2)	3078(4)	5193(13)	14130(7)	49(4)
C(4)	3810(7)	7337(15)	13754(10)	55(5)
C(5)	3098(6)	6032(16)	13778(10)	46(5)
C(6)	3359(5)	8682(14)	12698(9)	37(4)
C(7)	858(6)	7517(14)	10939(9)	43(5)
C(8)	372(6)	7584(12)	10421(9)	58(5)
C(9)	211(8)	6291(19)	10182(16)	92(11)
C(10)	102(7)	8347(19)	10855(12)	61(8)
C(11)	383(8)	8130(30)	9634(12)	95(11)
C(9A)	68(10)	6830(60)	10790(30)	60(30)

Table 48. (cont'd).

	x	y	z	U(eq)
C(10A)	311(13)	8810(30)	10000(30)	40(20)
C(11A)	354(13)	6950(60)	9655(19)	40(20)
C(12)	1871(6)	6057(15)	10666(9)	40(4)
C(13)	1913(6)	5316(14)	9961(9)	48(5)
C(14)	1413(7)	4947(17)	9533(10)	69(6)
C(15)	2190(6)	4149(16)	10263(10)	63(5)
C(16)	2129(5)	6029(13)	9437(8)	38(4)
C(17)	1433(5)	8777(14)	12822(8)	32(4)
C(18)	1221(6)	9532(14)	13342(9)	44(4)
C(19)	1203(6)	8827(14)	14080(9)	50(5)
C(20)	1508(7)	10740(20)	13607(12)	88(7)
C(21)	729(6)	9801(15)	12844(10)	63(5)
C(1S)	0	5600(50)	2500	190(20)
C(2S)	-422(10)	4770(30)	2446(15)	138(10)
C(3S)	-383(8)	3540(20)	2471(13)	99(8)
C(4S)	0	2930(30)	2500	91(10)

U(eq) is defined as one third of the trace of the orthogonalized U_{ij} tensor.

Table 49. Atomic coordinates (x 10^4) and equivalent isotropic displacement parameters ($Å^2$x 10^3) for $[Re_2Cl_4(dppm)_2]_2(TCNQ)$ (5).

	x	y	z	U(eq)
Re(1)	5380(1)	3931(1)	2800(1)	28(1)
Re(2)	6786(1)	4190(1)	3253(1)	28(1)
P(1)	3936(2)	5481(1)	2880(1)	34(1)
Cl(1)	3883(2)	3605(1)	2237(1)	39(1)
Cl(3)	6391(2)	3934(1)	4307(1)	41(1)
Cl(2)	4316(1)	3201(1)	3699(1)	36(1)
P(3)	6487(2)	2288(1)	2639(1)	34(1)
P(2)	5973(2)	5956(1)	3214(1)	32(1)
Cl(4)	8237(2)	4573(1)	2487(1)	41(1)
P(4)	7965(2)	2491(1)	3480(1)	34(1)
N(1)	5934(5)	4583(4)	1934(3)	35(1)
N(2)	7666(8)	6542(7)	431(4)	94(3)
C(1)	6123(6)	4899(6)	1484(4)	41(2)
C(2)	6268(7)	5356(6)	829(3)	51(2)
C(3)	7053(8)	6008(7)	619(3)	61(2)
C(4)	5629(7)	5178(5)	407(3)	45(2)
C(5)	4861(7)	4511(5)	611(3)	48(2)
C(6)	4262(7)	4346(6)	213(3)	53(2)
C(7)	4438(6)	6002(5)	3397(3)	36(2)
C(8)	7964(6)	2074(5)	2807(3)	39(2)
C(9)	2514(6)	5348(5)	3214(3)	41(2)
C(10)	2187(7)	5298(6)	3817(4)	56(2)
C(11)	1097(8)	5181(7)	4067(4)	69(3)
C(12)	324(8)	5118(7)	3703(5)	69(3)
C(13)	629(7)	5173(6)	3111(5)	68(3)
C(14)	1720(7)	5281(6)	2872(4)	57(2)
C(15)	3626(6)	6485(5)	2186(3)	39(2)
C(16)	3354(7)	7501(5)	2189(4)	56(2)
C(17)	3047(9)	8238(6)	1659(4)	73(3)
C(18)	3037(10)	7997(7)	1134(4)	88(3)

Table 49. (cont'd).

	x	y	z	U(eq)
C(19)	3295(8)	6998(6)	1130(4)	64(2)
C(20)	3598(6)	6250(5)	1654(3)	45(2)
C(21)	6077(6)	7050(5)	2570(3)	38(2)
C(22)	5665(7)	8014(5)	2656(3)	51(2)
C(23)	5742(8)	8846(6)	2188(4)	64(3)
C(24)	6214(9)	8761(6)	1634(4)	71(3)
C(25)	6614(8)	7818(6)	1530(3)	63(3)
C(26)	6549(7)	6948(5)	2005(3)	45(2)
C(27)	6423(6)	6331(5)	3817(3)	33(2)
C(28)	5730(7)	6446(5)	4322(3)	45(2)
C(29)	6131(8)	6699(6)	4780(3)	56(2)
C(30)	7223(8)	6833(6)	4718(3)	53(2)
C(31)	7922(7)	6711(6)	4215(3)	50(2)
C(32)	7520(6)	6466(5)	3762(3)	42(2)
C(33)	6634(7)	2210(5)	1858(3)	42(2)
C(34)	7429(8)	2651(7)	1437(3)	63(2)
C(35)	7522(10)	2578(9)	843(4)	89(4)
C(36)	6829(12)	2074(9)	680(4)	97(4)
C(37)	6045(12)	1676(6)	1084(4)	88(4)
C(38)	5932(9)	1744(6)	1670(3)	63(3)
C(39)	5977(7)	1161(5)	3068(3)	37(2)
C(40)	6741(7)	240(5)	3273(3)	48(2)
C(41)	6315(9)	-607(6)	3599(4)	64(3)
C(42)	5171(10)	-549(6)	3719(4)	67(3)
C(43)	4416(8)	350(6)	3514(4)	63(2)
C(44)	4820(7)	1211(5)	3191(3)	47(2)
C(45)	7656(6)	1442(4)	4115(3)	35(2)
C(46)	6566(6)	1461(5)	4387(3)	38(2)
C(47)	6308(7)	619(5)	4829(3)	48(2)
C(48)	7182(8)	-225(6)	5005(4)	62(2)
C(49)	8262(8)	-243(6)	4740(4)	68(3)
C(50)	8515(7)	586(6)	4298(3)	54(2)

Table 49. (cont'd).

	x	y	z	U(eq)
C(51)	9440(6)	2492(5)	3572(4)	44(2)
C(52)	10318(7)	2425(6)	3138(4)	59(2)
C(53)	11404(8)	2460(7)	3246(6)	82(3)
C(54)	11588(8)	2592(8)	3782(6)	88(4)
C(55)	10730(9)	2647(7)	4209(5)	83(3)
C(56)	9620(7)	2626(6)	4114(4)	57(2)
O(1)	2962(6)	8171(5)	3618(3)	87(2)
C(57)	2385(10)	7928(8)	4197(4)	102(4)
C(58)	1319(9)	8616(9)	4191(5)	104(4)
C(59)	1432(10)	9473(8)	3660(5)	99(4)
C(60)	2304(10)	9036(8)	3257(4)	89(3)
O(2)	8922(16)	3660(20)	-421(7)	257(11)
C(61)	9740(20)	3120(14)	-761(12)	253(14)
C(62)	9801(19)	3813(19)	-1334(7)	198(11)
C(63)	9380(20)	4813(15)	-1277(9)	201(11)
C(64)	8950(30)	4676(18)	-686(13)	330(20)
O(3)	12390(20)	2290(18)	1331(11)	338(13)
C(65)	12642(19)	1295(17)	1749(12)	237(13)
C(66)	11640(20)	984(12)	1800(12)	247(14)
C(67)	10729(14)	1868(19)	1675(10)	189(8)
C(68)	11230(20)	2480(30)	1189(13)	460(30)
O(4)	9417(8)	9522(8)	2622(5)	124(3)
C(69)	9074(17)	9739(11)	2041(7)	156(7)
C(70)	9386(18)	8850(17)	1855(8)	179(8)
C(71)	9310(20)	8090(13)	2403(10)	218(12)
C(72)	9449(15)	8473(13)	2860(8)	150(6)
O(5)	6090(20)	353(16)	109(8)	129(8)
C(73)	6530(30)	-550(20)	-73(15)	161(17)
C(74)	5570(50)	-860(40)	-140(30)	320(50)
C(75)	4560(30)	-110(30)	-50(30)	250(40)
C(76)	4980(30)	750(30)	-97(15)	145(18)
O(6)	10560(70)	-390(50)	-240(40)	400(60)

Table 49. (cont'd).

	x	y	z	U(eq)
C(77)	9530(40)	230(40)	-90(40)	260(40)
C(78)	9860(50)	1060(40)	-20(40)	430(60)
C(79)	11050(50)	760(50)	110(30)	310(40)
C(80)	11470(40)	40(40)	-200(20)	240(30)

U(eq) is defined as one third of the trace of the orthogonalized U_{ij} tensor.

Table 50. Atomic coordinates (x 10^4) and equivalent isotropic displacement parameters ($Å^2$x 10^3) for $[Re_2Cl_4(dppm)_2]_2$(DMDCNQI) (6).

	x	y	z	U(eq)
Re(1)	320(1)	3863(1)	2812(1)	31(1)
Re(2)	1712(1)	4137(1)	3286(1)	30(1)
Cl(1)	-1187(2)	3509(2)	2233(1)	46(1)
Cl(2)	-746(2)	3164(2)	3690(1)	40(1)
Cl(4)	3171(2)	4479(2)	2548(1)	45(1)
Cl(3)	1286(2)	3950(2)	4333(1)	43(1)
P(4)	-1138(2)	5421(2)	2883(1)	38(1)
P(3)	896(2)	5906(2)	3221(1)	35(1)
P(2)	2903(2)	2452(2)	3531(1)	39(1)
P(1)	1458(2)	2229(2)	2650(1)	41(1)
N(1)	858(6)	4484(5)	1971(3)	39(2)
N(2)	1162(7)	5209(6)	911(3)	51(2)
C(1)	2936(8)	2011(7)	2841(4)	45(2)
C(2)	-631(7)	5982(6)	3391(4)	36(2)
C(3)	965(8)	4794(7)	1477(5)	43(2)
C(4)	584(9)	5099(7)	456(4)	54(3)
C(5)	-183(10)	4449(8)	577(4)	55(3)
C(6)	-776(9)	4362(8)	132(4)	51(3)
C(7)	-1588(12)	3677(10)	253(5)	94(5)
C(8)	943(9)	1095(7)	3058(4)	48(2)
C(9)	-187(10)	1152(8)	3176(4)	56(3)
C(10)	-583(12)	308(9)	3482(5)	71(3)
C(11)	167(15)	-558(9)	3681(5)	83(4)
C(12)	1302(13)	-644(8)	3574(6)	78(4)
C(13)	1712(11)	188(7)	3262(5)	62(3)
C(14)	1635(10)	2148(7)	1870(5)	58(3)
C(15)	990(12)	1649(9)	1657(5)	82(4)
C(16)	1101(17)	1614(10)	1068(7)	113(6)
C(17)	1876(17)	2060(12)	678(6)	112(6)
C(18)	2509(13)	2576(11)	872(6)	99(5)

Table 50. (cont'd).

	x	y	z	U(eq)
C(19)	2384(10)	2602(9)	1462(5)	71(3)
C(20)	4342(8)	2458(7)	3655(5)	49(3)
C(21)	5253(9)	2364(8)	3239(5)	64(3)
C(22)	6346(9)	2411(9)	3363(6)	73(4)
C(23)	6479(10)	2598(9)	3896(7)	77(4)
C(24)	5598(11)	2699(9)	4320(6)	73(4)
C(25)	4503(8)	2640(7)	4194(5)	53(3)
C(26)	2612(8)	1431(7)	4151(4)	40(2)
C(27)	1511(8)	1462(7)	4410(4)	41(2)
C(28)	1271(9)	640(8)	4833(4)	53(3)
C(29)	2133(10)	-195(7)	5016(5)	60(3)
C(30)	3222(11)	-240(8)	4769(5)	79(4)
C(31)	3462(9)	568(7)	4343(5)	59(3)
C(32)	1374(8)	6335(6)	3802(4)	37(2)
C(33)	715(8)	6470(7)	4321(4)	45(2)
C(34)	1134(9)	6756(8)	4761(5)	60(3)
C(35)	2224(10)	6880(8)	4696(5)	61(3)
C(36)	2899(9)	6734(7)	4196(5)	57(3)
C(37)	2470(8)	6449(7)	3744(4)	44(2)
C(38)	998(8)	6924(6)	2557(4)	38(2)
C(39)	1370(8)	6761(7)	2005(4)	49(3)
C(40)	1406(11)	7563(9)	1508(5)	77(4)
C(41)	1063(12)	8538(9)	1572(5)	83(4)
C(42)	682(12)	8690(9)	2125(6)	85(4)
C(43)	653(10)	7908(7)	2622(5)	62(3)
C(44)	-1473(8)	6393(7)	2195(4)	42(2)
C(45)	-1472(8)	6139(8)	1653(4)	54(3)
C(46)	-1756(10)	6868(8)	1128(5)	70(3)
C(47)	-2056(11)	7840(8)	1136(5)	74(4)
C(48)	-2016(12)	8114(9)	1667(6)	88(4)
C(49)	-1730(9)	7396(8)	2189(4)	58(3)
C(50)	-2554(8)	5311(7)	3218(5)	49(3)

Table 50. (cont'd).

	x	y	z	U(eq)
C(51)	-3357(9)	5232(8)	2871(6)	67(3)
C(52)	-4427(11)	5120(9)	3117(8)	85(4)
C(53)	-4742(11)	5080(9)	3704(7)	79(4)
C(54)	-3931(11)	5164(9)	4069(6)	83(4)
C(55)	-2851(9)	5264(8)	3817(5)	66(3)
O(1)	-2162(9)	8149(7)	3599(5)	115(4)
C(56)	-2799(14)	9012(12)	3245(7)	122(6)
C(57)	-3678(14)	9470(11)	3650(7)	138(7)
C(58)	-3773(12)	8623(13)	4165(6)	124(6)
C(59)	-2676(15)	7953(12)	4181(6)	135(7)
O(2)	4363(12)	-644(12)	2588(7)	165(6)
C(60)	3960(20)	-351(15)	2009(9)	182(10)
C(61)	4320(20)	-1215(19)	1757(10)	237(14)
C(62)	4270(20)	-2021(15)	2288(11)	215(12)
C(63)	4390(20)	-1675(16)	2790(9)	195(11)
O(3)	-5840(20)	5860(40)	880(20)	790(40)
C(69)	-5110(50)	6460(20)	534(18)	540(30)
C(70)	-3980(30)	5860(40)	700(20)	680(50)
C(71)	-4290(30)	5170(30)	1258(15)	450(30)
C(72)	-5160(50)	4860(30)	1020(20)	540(40)
O(4)	-2720(30)	2080(30)	1614(19)	640(30)
C(73)	-3800(40)	2450(20)	1357(19)	560(40)
C(74)	-4390(20)	1700(30)	1708(15)	331(18)
C(75)	-3420(40)	930(30)	2014(18)	520(40)
C(76)	-2460(30)	1060(30)	1596(17)	430(30)
O(5)	1250(30)	80(30)	50(20)	240(20)
C(77)	60(40)	480(30)	90(20)	141(18)
C(78)	-440(40)	-370(50)	190(30)	220(30)
C(79)	530(50)	-1170(30)	80(30)	300(40)
C(80)	1380(40)	-680(40)	-260(20)	210(30)
O(6)	-3640(60)	11140(50)	-210(30)	700(60)
C(82)	-3430(40)	10140(50)	110(20)	360(30)

Table 50. (cont'd).

	x	y	z	U(eq)
C(83)	-4390(80)	9810(40)	-20(40)	400(60)
C(84)	-5300(40)	10720(70)	-70(30)	310(30)
C(85)	-4800(70)	11510(40)	-50(30)	560(60)

U(eq) is defined as one third of the trace of the orthogonalized U_{ij} tensor.

Table 51. Atomic coordinates (x 10^4) and equivalent isotropic displacement parameters ($Å^2$x 10^3) for Cu(TCNQ) phase I (7).

	x	y	z	U(eq)
Cu(1)	7270(60)	2525(6)	3428(18)	64(3)
N(1)	5690(100)	3850(30)	2650(30)	20(8)
C(8)	3810(40)	6030(20)	1910(20)	29(7)
C(5)	-4150(50)	8950(20)	4940(20)	20(8)
C(9)	1860(30)	6720(30)	2677(17)	24(8)
C(10)	490(40)	6340(20)	3799(17)	18(9)
C(11)	-1470(40)	7100(30)	4509(17)	28(10)
C(12)	-2200(40)	8290(30)	4150(30)	39(9)
C(13)	-820(70)	8670(20)	3020(30)	36(11)
C(14)	1140(60)	7910(30)	2310(20)	19(10)
C(1)	4320(110)	4780(30)	2320(40)	12(8)
N(2)	-4310(110)	8320(30)	7100(30)	20(9)
C(2)	-5560(150)	8550(80)	6110(30)	22(11)
N(4)	-4260(130)	11140(30)	4100(40)	43(13)
C(4)	-3380(100)	10190(20)	4550(30)	17(9)
N(3)	4010(100)	6650(40)	-100(30)	25(9)
C(3)	5640(100)	6290(40)	760(30)	19(8)
Cu(1A)	2320(70)	2520(6)	3435(19)	88(4)
N(3A)	5680(120)	6580(40)	-170(30)	43(9)
C(8A)	5550(40)	5950(20)	1910(30)	32(7)
C(5A)	13200(50)	8880(20)	4950(30)	20(7)
C(9A)	7410(30)	6660(20)	2645(19)	60(9)
C(10A)	8630(40)	6280(20)	3785(19)	49(10)
C(11A)	10530(40)	7030(30)	4515(18)	7(8)
C(12A)	11330(40)	8220(30)	4160(30)	41(8)
C(13A)	10110(70)	8610(20)	3030(30)	30(10)
C(14A)	8210(60)	7860(30)	2290(20)	34(8)
N(2A)	13910(100)	8310(40)	6980(40)	32(10)
C(2A)	15290(160)	8540(100)	6020(40)	33(13)
C(3A)	4120(100)	6350(40)	750(30)	24(8)

Table 51. (cont'd).

	x	y	z	U(eq)
N(4A)	14230(80)	11030(20)	4130(30)	0(6)
C(4A)	14460(90)	10070(20)	4620(30)	0(7)
N(1A)	3520(80)	3980(30)	2660(30)	27(7)
C(1A)	5730(90)	4690(30)	2330(30)	23(8)

U(eq) is defined as one third of the trace of the orthogonalized U_{ij} tensor.

Table 52. Atomic coordinates (x 10^4) and equivalent isotropic displacement parameters ($Å^2$x 10^3) for Cu(TCNQ) phase II (8).

	x	y	z	U(eq)
Cu(1)	-2500	11732(5)	7500	24(1)
N(1)	-348(23)	9759(19)	6916(5)	21(3)
C(1)	1292(26)	8940(24)	6636(6)	20(3)
N(2)	5431(22)	4041(20)	6886(6)	24(3)
C(2)	4421(27)	5743(26)	6604(7)	28(4)
C(3)	3215(26)	7839(23)	6257(6)	20(3)
C(4)	4204(24)	8933(23)	5628(6)	20(3)
C(5)	2925(27)	11070(26)	5308(6)	30(3)
C(6)	3828(24)	12080(26)	4700(6)	27(3)

U(eq) is defined as one third of the trace of the orthogonalized U_{ij} tensor.

Table 53. Atomic coordinates (x 10^4) and equivalent isotropic displacement parameters ($Å^2$x 10^3) [Mn(TCNQ-TCNQ)$_{0.5}$(TCNQ)(MeOH)$_2$]$_\infty$ (9).

	x	y	z	U(eq)
Mn(1)	5000	5514(1)	7500	16(1)
O(1M)	4838(2)	5532(1)	9150(2)	29(1)
C(1M)	4020(3)	5497(2)	9746(3)	40(1)
N(1A)	6092(2)	4965(1)	7533(2)	22(1)
C(2A)	6750(2)	4739(1)	7688(2)	17(1)
N(3A)	9000(2)	5028(1)	7898(2)	26(1)
C(4A)	8371(2)	4768(1)	7891(2)	21(1)
C(5A)	7569(2)	4478(1)	7882(2)	17(1)
C(6A)	7565(2)	3966(1)	8180(2)	16(1)
C(7A)	6738(2)	3701(1)	8247(2)	20(1)
C(8A)	6729(2)	3226(1)	8598(2)	22(1)
C(9A)	7547(3)	2996(1)	8885(2)	21(1)
C(10A)	8381(2)	3246(1)	8774(2)	22(1)
C(11A)	8391(2)	3726(1)	8429(2)	20(1)
C(12A)	7531(3)	2485(1)	9371(2)	22(1)
C(13A)	6708(3)	2207(1)	9029(3)	25(1)
N(14A)	6036(2)	2016(1)	8792(2)	36(1)
C(15A)	8384(2)	2209(1)	9130(3)	25(1)
N(16A)	9072(2)	2016(1)	8970(2)	34(1)
Mn(2)	10000	5591(1)	7500	18(1)
O(2M)	10620(2)	5631(1)	9023(2)	31(1)
C(2M')	11564(6)	5552(4)	9295(7)	40(3)
C(2M")	11330(8)	5358(5)	9492(8)	40(3)
N(1B)	6080(2)	6081(1)	7788(2)	24(1)
C(2B)	6692(2)	6327(1)	8014(2)	19(1)
N(3B)	8994(2)	6146(1)	8073(2)	23(1)
C(4B)	8327(2)	6367(1)	8176(2)	18(1)
C(5B)	7469(2)	6616(1)	8272(2)	17(1)
C(6B)	7405(2)	7122(1)	8529(2)	17(1)

Table 53. (cont'd).

	x	y	z	U(eq)
C(7B)	6532(2)	7365(1)	8549(2)	18(1)
C(8B)	6468(2)	7846(1)	8795(2)	19(1)
C(9B)	7272(2)	8126(1)	9044(2)	19(1)
C(10B)	8140(2)	7884(1)	9014(2)	19(1)
C(11B)	8207(2)	7398(1)	8769(2)	19(1)
C(12B)	7208(2)	8631(1)	9309(2)	20(1)
C(13B)	6350(2)	8875(1)	9363(2)	22(1)
N(14B)	5629(2)	9058(1)	9416(2)	33(1)
C(15B)	8018(2)	8910(1)	9488(2)	22(1)
N(16B)	8699(2)	9125(1)	9628(2)	31(1)

U(eq) is defined as one third of the trace of the orthogonalized U_{ij} tensor.

Table 54. Atomic coordinates (x 10^4) and equivalent isotropic displacement parameters ($Å^2$x 10^3) $[Mn(TCNQ)_2(H_2O)_2]_\infty$ (10).

	x	y	z	U(eq)
Mn(1)	0	0	0	25(1)
N(1)	3647(2)	2886(1)	1856(2)	45(1)
C(1)	3442(1)	2116(2)	1944(2)	29(1)
N(2)	1348(1)	758(1)	643(2)	34(1)
C(2)	3199(1)	1153(1)	2032(2)	24(1)
N(3)	7949(1)	-1476(1)	6179(2)	37(1)
C(3)	2170(1)	951(1)	1239(2)	27(1)
N(4)	5617(1)	-3597(1)	4980(2)	34(1)
C(4)	3925(1)	399(1)	2790(2)	22(1)
C(5)	4964(1)	611(1)	3699(2)	22(1)
C(6)	5667(1)	-116(1)	4393(2)	22(1)
C(7)	5388(1)	-1109(1)	4242(2)	21(1)
C(8)	4341(1)	-1322(1)	3338(2)	24(1)
C(9)	3643(1)	-598(1)	2641(2)	24(1)
C(10)	6120(1)	-1858(1)	4954(2)	24(1)
C(11)	7137(1)	-1662(1)	5649(2)	26(1)
C(12)	5858(1)	-2828(1)	4958(2)	25(1)
O(1)	-751(2)	174(1)	-2200(2)	47(1)

U(eq) is defined as one third of the trace of the orthogonalized U_{ij} tensor.

Table 55. Atomic coordinates (x 10^4) and equivalent isotropic displacement parameters ($Å^2$x 10^3) $[Bu_4N][TCNQ]$ (11).

	x	y	z	U(eq)
N(1)	2488(2)	-785(1)	3067(1)	47(1)
N(2)	5106(2)	-1088(1)	1026(1)	45(1)
N(3)	-2346(2)	2280(1)	-104(1)	49(1)
N(4)	373(2)	1956(1)	-2110(1)	42(1)
N(5)	-1246(2)	1782(1)	-5151(1)	25(1)
C(1)	2646(2)	-664(1)	2357(2)	30(1)
C(2)	2888(2)	-504(1)	1496(1)	26(1)
C(3)	4114(2)	-828(1)	1236(1)	30(1)
C(4)	2078(2)	15(1)	962(1)	23(1)
C(5)	869(2)	350(1)	1216(1)	28(1)
C(6)	102(2)	852(1)	702(1)	29(1)
C(7)	478(2)	1066(1)	-103(1)	24(1)
C(8)	1707(2)	739(1)	-352(1)	26(1)
C(9)	2468(2)	234(1)	158(1)	26(1)
C(10)	-322(2)	1589(1)	-637(1)	28(1)
C(11)	-1452(2)	1963(1)	-352(1)	33(1)
C(12)	40(2)	1788(1)	-1455(2)	29(1)
C(13)	-2423(2)	1229(1)	-5286(1)	28(1)
C(14)	-3979(2)	1464(1)	-5644(1)	32(1)
C(15)	-5021(2)	850(1)	-5710(2)	38(1)
C(16)	-6593(2)	1034(1)	-6109(2)	45(1)
C(17)	-1533(2)	2272(1)	-4427(1)	27(1)
C(18)	-386(2)	2827(1)	-4157(1)	32(1)
C(19)	-856(2)	3322(1)	-3495(1)	34(1)
C(20)	193(2)	3927(1)	-3301(2)	46(1)
C(21)	-1243(2)	2200(1)	-5993(1)	28(1)
C(22)	-1181(2)	1787(1)	-6826(1)	39(1)
C(23)	-1109(2)	2277(1)	-7598(2)	44(1)
C(24)	424(3)	2520(1)	-7630(2)	62(1)

Table 55. (cont'd).

	x	y	z	U(eq)
C(25)	244(2)	1433(1)	-4895(1)	28(1)
C(26)	497(2)	1023(1)	-4038(1)	36(1)
C(27)	2065(2)	774(1)	-3815(2)	47(1)
C(28)	2371(3)	368(1)	-2954(2)	74(1)

U(eq) is defined as one third of the trace of the orthogonalized U_{ij} tensor.

Table 56. Atomic coordinates (x 10^4) and equivalent isotropic displacement parameters ($Å^2$x 10^3) $[Bu_4N][TCNQF_4]$ (12).

	x	y	z	U(eq)
F(4)	-69(2)	7356(1)	505(1)	44(1)
F(2)	9(3)	4718(2)	-1384(1)	49(1)
F(3)	-2288(3)	6229(2)	808(1)	50(1)
F(1)	-2195(3)	3597(2)	-1078(1)	52(1)
N(9)	5531(3)	10781(2)	1809(1)	30(1)
C(8)	-580(4)	6421(3)	106(2)	32(1)
C(4)	-2378(4)	4842(3)	-118(2)	31(1)
C(7)	96(4)	6112(3)	-461(2)	29(1)
N(10)	-2792(3)	5975(2)	3268(2)	32(1)
C(5)	-1702(4)	4531(3)	-683(2)	32(1)
C(9)	-1740(4)	5833(3)	258(2)	32(1)
C(12)	1963(5)	7733(3)	-244(2)	37(1)
C(11)	1886(5)	6428(3)	-1226(2)	37(1)
C(6)	-554(4)	5123(3)	-837(2)	33(1)
C(29)	4372(4)	10455(3)	2209(2)	32(1)
C(3)	-4255(5)	4531(3)	614(2)	41(1)
C(10)	1302(4)	6727(3)	-622(2)	32(1)
C(38)	3976(4)	11513(3)	1194(2)	37(1)
N(4)	2555(4)	8543(3)	19(2)	53(1)
C(25)	6455(4)	11808(2)	2200(2)	33(1)
N(1)	-4947(4)	2456(3)	-685(2)	58(1)
C(2)	-3564(4)	4215(3)	46(2)	34(1)
C(1)	-4300(5)	3245(3)	-368(2)	42(1)
C(34)	7792(4)	10355(3)	1363(2)	34(1)
C(37)	4857(4)	10797(3)	1150(2)	34(1)
C(41)	-2916(4)	6162(3)	4001(2)	34(1)
C(30)	3271(4)	9470(3)	1891(2)	36(1)
C(33)	6435(4)	10062(3)	1668(2)	33(1)
C(51)	-6489(4)	4048(3)	2377(2)	43(1)
N(2)	-4854(4)	4742(3)	1064(2)	58(1)

Table 56. (cont'd).

	x	y	z	U(eq)
C(49)	-3955(4)	5053(3)	2834(2)	35(1)
C(35)	8615(4)	9587(3)	1286(2)	41(1)
C(45)	-1340(4)	5831(3)	3114(2)	38(1)
C(31)	2290(5)	9257(3)	2389(2)	46(1)
C(46)	-20(4)	6666(3)	3491(2)	42(1)
C(26)	7347(4)	11934(3)	2849(2)	41(1)
C(39)	3263(5)	11396(3)	512(2)	43(1)
C(50)	-5524(4)	5045(3)	2831(2)	41(1)
N(3)	2401(4)	6260(2)	-1701(2)	53(1)
C(53)	-2990(4)	6874(3)	3123(2)	37(1)
C(32)	1202(5)	8268(3)	2172(2)	59(1)
C(42)	-2537(5)	5427(3)	4291(2)	43(1)
C(54)	-2918(5)	6875(3)	2414(2)	45(1)
C(36)	9954(4)	9839(3)	959(2)	48(1)
C(40)	2410(5)	12134(3)	534(2)	57(1)
C(27)	8275(5)	12992(3)	3142(2)	52(1)
C(47)	1368(4)	6403(3)	3348(2)	54(1)
C(43)	-2877(5)	5627(3)	4998(2)	52(1)
C(55)	-3154(6)	7804(4)	2334(3)	64(1)
C(28)	9075(6)	13223(3)	3828(2)	75(2)
C(44)	-2676(5)	4841(3)	5287(2)	69(2)
C(52)	-8081(5)	3979(3)	2313(2)	70(2)
C(48)	2694(5)	7217(4)	3748(3)	78(2)
C(56)	-4625(7)	7905(4)	2455(3)	103(2)
F(5)	191(2)	200(2)	3450(1)	49(1)
F(6)	-4(2)	-927(2)	4183(1)	50(1)
F(7)	4741(3)	2196(2)	4710(1)	78(1)
F(8)	4538(3)	1079(2)	5456(2)	94(1)
C(23)	933(5)	-1410(3)	5183(2)	40(1)
C(18)	1192(4)	-160(3)	4323(2)	39(1)
C(16)	2498(4)	1244(3)	4015(2)	37(1)

Table 56. (cont'd).

	x	y	z	U(eq)
C(17)	1294(4)	422(3)	3935(2)	38(1)
C(19)	2273(5)	3(3)	4862(2)	42(1)
C(15)	3890(5)	2608(3)	3654(2)	46(1)
N(7)	-36(4)	-2070(3)	5142(2)	57(1)
C(14)	2642(4)	1832(3)	3608(2)	36(1)
C(13)	1585(5)	1672(3)	3057(2)	44(1)
C(21)	3550(5)	1415(3)	4565(2)	52(1)
C(22)	2161(5)	-595(3)	5273(2)	46(1)
N(5)	820(5)	1595(3)	2601(2)	68(1)
N(6)	4863(5)	3245(3)	3656(2)	71(1)
C(24)	3243(6)	-429(4)	5806(3)	68(2)
C(20)	3445(5)	835(3)	4949(2)	56(1)
N(8)	4089(5)	-345(4)	6246(3)	99(2)

U(eq) is defined as one third of the trace of the orthogonalized U_{ij} tensor.

Table 57. Atomic coordinates (x 10^4) and equivalent isotropic displacement parameters ($Å^2$x 10^3) for $[Zn(TCNQ)_2(H_2O)_4(TCNQ)_2(MeCN)_4]_\infty$ (13).

	x	y	z	U(eq)
Zn(1)	0	0	0	21(1)
O(1)	1564(2)	-471(2)	1059(2)	30(1)
O(2)	-536(2)	-1935(2)	718(2)	28(1)
C(1)	-1618(3)	114(3)	2260(2)	19(1)
C(2)	-2371(3)	-91(3)	3280(2)	18(1)
C(3)	-3033(3)	1008(3)	3358(2)	22(1)
C(4)	-2462(3)	-1326(3)	4169(2)	18(1)
C(5)	-1754(3)	-2401(3)	4090(3)	19(1)
C(6)	-1838(3)	-3588(3)	4951(3)	19(1)
C(7)	-2638(3)	-3791(3)	5961(2)	20(1)
C(8)	-3342(3)	-2711(3)	6038(2)	20(1)
C(9)	-3253(3)	-1526(3)	5185(2)	19(1)
C(10)	-2746(3)	-5008(3)	6856(3)	21(1)
C(11)	-2055(3)	-6116(3)	6833(3)	25(1)
C(12)	-3587(3)	-5214(3)	7831(3)	25(1)
C(13)	-462(3)	-6466(3)	3296(3)	27(1)
C(14)	210(3)	-7571(3)	3227(3)	22(1)
C(15)	1015(3)	-7360(3)	2211(3)	26(1)
C(16)	105(3)	-8771(3)	4096(3)	21(1)
C(17)	-688(3)	-8962(3)	5129(3)	23(1)
C(18)	-794(3)	-10121(3)	5984(3)	22(1)
C(19)	4553(3)	-1487(3)	3220(3)	25(1)
C(20)	5260(3)	-2589(3)	3201(2)	19(1)
C(21)	6125(3)	-2410(3)	2234(3)	22(1)
C(22)	5133(3)	-3788(3)	4090(2)	18(1)
C(23)	5844(3)	-4894(3)	4054(3)	19(1)
C(24)	5711(3)	-6056(3)	4924(2)	19(1)
C(25)	4486(3)	-1528(4)	-410(3)	38(1)
C(26)	5454(4)	-2065(4)	-961(3)	44(1)

Table 57. (cont'd).

	x	y	z	U(eq)
C(27)	1780(4)	-4082(4)	-391(4)	41(1)
C(28)	2693(4)	-4693(4)	-929(3)	46(1)
N(1)	-991(2)	259(2)	1437(2)	25(1)
N(2)	-3554(3)	1909(3)	3413(2)	34(1)
N(3)	-1537(3)	-7035(3)	6832(3)	37(1)
N(4)	-4293(3)	-5353(3)	8599(2)	35(1)
N(5)	-1000(3)	-5584(3)	3349(3)	40(1)
N(6)	1666(3)	-7178(3)	1401(2)	37(1)
N(7)	3978(3)	-618(3)	3255(3)	39(1)
N(8)	6838(3)	-2287(3)	1481(2)	30(1)
N(9)	3743(3)	-1107(4)	30(3)	61(1)
N(10)	1070(4)	-3592(4)	26(4)	66(1)

U(eq) is defined as one third of the trace of the orthogonalized U_{ij} tensor.

Table 58. Atomic coordinates (x 10^4) and equivalent isotropic displacement parameters ($Å^2$x 10^3) $[Ni(DMSO)_6][TCNQ]_3$ (14).

	x	y	z	U(eq)
Ni(1)	5000	0	5000	22(1)
S(2)	8271(2)	-1765(2)	5409(1)	30(1)
S(3)	6483(2)	1202(2)	3272(1)	24(1)
O(5)	5038(5)	619(4)	3828(2)	26(1)
O(6)	4753(5)	-1924(4)	4706(2)	28(1)
O(7)	7626(5)	-469(4)	4924(2)	32(1)
C(8)	6362(9)	2886(6)	3498(4)	34(2)
C(17)	8471(7)	4319(5)	-1350(3)	19(1)
C(14)	10221(7)	3391(5)	-8(3)	20(1)
C(19)	11138(7)	3660(6)	-765(3)	23(1)
C(11)	10230(7)	2608(6)	1400(4)	25(1)
N(3)	9190(8)	5233(6)	-3399(3)	47(2)
C(20)	7602(7)	4736(6)	-2020(3)	24(1)
N(1)	9547(7)	2323(6)	2025(3)	40(1)
N(2)	14394(7)	2435(6)	567(3)	41(1)
C(16)	7557(7)	4043(5)	-588(3)	22(1)
N(4)	4330(7)	4953(6)	-1953(3)	42(2)
C(12)	11087(7)	2913(5)	648(3)	21(1)
C(18)	10310(7)	4118(6)	-1406(3)	22(1)
C(21)	8493(8)	5011(6)	-2779(4)	31(2)
C(15)	8376(7)	3611(5)	55(3)	20(1)
S(4)	5791(4)	-2255(3)	3939(2)	38(1)
C(9)	6467(17)	-4005(10)	4114(8)	72(4)
C(10)	4284(18)	-2379(15)	3281(8)	66(4)
S(4')	4552(11)	-2253(10)	3870(4)	26(3)
C(10')	6640(20)	-2520(30)	3356(16)	34(7)
C(9')	4160(30)	-3962(16)	3989(16)	35(8)
S(4")	4830(20)	-3010(20)	4132(12)	48(8)
C(10")	6840(40)	-3280(70)	3540(30)	60(20)
C(9")	3660(60)	-2090(50)	3400(30)	24(14)

Table 58. (cont'd).

	x	y	z	U(eq)
C(27)	8200(8)	218(6)	68(4)	27(1)
C(24)	8405(8)	969(6)	-1341(4)	30(2)
C(22)	5785(8)	4864(6)	-1974(4)	30(1)
C(13)	12913(8)	2658(6)	596(3)	26(1)
C(26)	9177(8)	493(6)	-677(4)	27(1)
C(25)	9340(9)	1263(7)	-2098(4)	36(2)
C(28)	8971(8)	-268(6)	715(4)	30(2)
C(23)	6557(9)	1163(6)	-1330(4)	35(2)
N(6)	5102(8)	1309(6)	-1345(4)	51(2)
N(5)	10029(9)	1502(7)	-2709(4)	58(2)
C(7)	5602(9)	1491(7)	2363(3)	38(2)
C(6)	9084(8)	-1230(7)	6228(4)	39(2)
C(5)	10249(8)	-2371(8)	4849(4)	45(2)

U(eq) is defined as one third of the trace of the orthogonalized U_{ij} tensor.

Table 59. Atomic coordinates (x 10^4) and equivalent isotropic displacement parameters ($Å^2$x 10^3) for $[Mn_5Cl_{10}(THF)_8]_\infty$ (16).

	x	y	z	U(eq)
Mn(1)	4059(1)	3554(1)	5529(1)	19(1)
Mn(2)	3574(1)	5864(1)	7365(1)	20(1)
Mn(3)	5000	5000	10000	22(1)
Cl(1)	1993(1)	4803(1)	6581(1)	23(1)
Cl(2)	5774(1)	4621(1)	6246(1)	20(1)
Cl(3)	3152(1)	4276(1)	9219(1)	26(1)
Cl(4)	5270(1)	6722(1)	8199(1)	26(1)
Cl(5)	3844(1)	7614(1)	5576(1)	24(1)
O(1)	4116(3)	1933(2)	7015(2)	28(1)
C(1)	2880(4)	1632(4)	7907(3)	30(1)
C(2)	3530(5)	813(4)	8882(3)	36(1)
C(3)	4944(5)	147(3)	8322(3)	35(1)
C(4)	5243(5)	880(4)	7110(3)	45(1)
O(2)	2547(8)	2663(6)	4982(8)	22(2)
C(5)	1210(11)	3257(8)	4609(11)	31(3)
C(6)	372(10)	2227(9)	4602(13)	40(3)
C(7)	1605(9)	1235(8)	4298(11)	34(3)
C(8)	2885(9)	1465(7)	4675(11)	26(2)
O(2A)	2361(9)	2603(7)	5213(9)	21(2)
C(5A)	1014(12)	3210(8)	4838(12)	23(3)
C(6A)	225(10)	2116(9)	4964(13)	31(3)
C(7A)	1369(12)	1046(11)	4763(16)	47(3)
C(8A)	2680(11)	1342(8)	5046(13)	30(3)
O(4)	3221(3)	6242(2)	10843(2)	30(1)
C(13)	3440(4)	7421(3)	11023(4)	34(1)
C(14)	1928(5)	7972(4)	11532(5)	52(1)
C(15)	1227(5)	6836(5)	12223(4)	50(1)
C(16)	1844(4)	5867(4)	11528(4)	38(1)
O(3)	1535(9)	7111(6)	7875(10)	22(2)
C(9)	1643(12)	8367(10)	7937(17)	43(4)

Table 59. (cont'd).

	x	y	z	U(eq)
C(10)	114(11)	8942(9)	8169(14)	35(3)
C(11)	-807(12)	7914(10)	8683(16)	43(4)
C(12)	95(11)	6766(9)	8343(14)	33(3)
O(3A)	1682(7)	7057(5)	8115(8)	22(2)
C(9A)	1733(8)	8275(7)	8252(10)	28(2)
C(10A)	187(10)	8881(8)	8510(13)	49(3)
C(11A)	-637(9)	7815(8)	9079(11)	39(3)
C(12A)	221(8)	6722(7)	8597(9)	27(2)

U(eq) is defined as one third of the trace of the orthogonalized U_{ij} tensor.

Table 60. Atomic coordinates (x 10^4) and equivalent isotropic displacement parameters ($Å^2$x 10^3) for $[MnBr_2(THF)_2]_\infty$ (17).

	x	y	z	U(eq)
Br(1)	6908(1)	4372(1)	3533(4)	16(1)
Mn(1)	5000	5000	8545(17)	15(1)
O(1)	3207(8)	4058(4)	8560(70)	20(2)
C(1)	1290(15)	4082(6)	8900(60)	24(3)
C(2)	614(15)	3370(6)	9020(50)	22(3)
C(3)	2144(13)	2833(6)	8190(50)	19(3)
C(4)	3731(16)	3336(6)	9140(40)	23(3)

U(eq) is defined as one third of the trace of the orthogonalized U_{ij} tensor.

Table 61. Atomic coordinates (x 10^4) and equivalent isotropic displacement parameters ($Å^2$x 10^3) [$Fe_2Cl_4(\mu$-2,2'-bpy)$_2$] (19).

	x	y	z	U(eq)
Fe(1)	1856(1)	1758(1)	741(1)	19(1)
Cl(2)	531(1)	-984(1)	-1707(1)	25(1)
Cl(1)	4308(1)	1384(1)	2446(1)	30(1)
N(1)	2522(3)	2867(3)	-932(3)	21(1)
N(2)	1710(3)	4438(3)	1867(3)	20(1)
C(1)	2982(4)	1991(4)	-2310(4)	27(1)
C(2)	3514(4)	2762(4)	-3292(4)	30(1)
C(3)	3578(4)	4517(4)	-2845(4)	29(1)
C(4)	3107(4)	5444(4)	-1425(4)	25(1)
C(5)	2592(3)	4590(3)	-493(3)	20(1)
C(6)	2125(3)	5462(3)	1089(3)	20(1)
C(7)	2145(4)	7222(4)	1759(4)	27(1)
C(8)	1776(4)	7947(4)	3278(4)	30(1)
C(9)	1392(4)	6901(4)	4102(4)	29(1)
C(10)	1350(4)	5157(4)	3345(4)	25(1)

U(eq) is defined as one third of the trace of the orthogonalized U_{ij} tensor.

Table 62. Atomic coordinates (x 10^4) and equivalent isotropic displacement parameters ($Å^2$x 10^3) for $[FeCl_2(\mu\text{-}2,2'\text{-bpy})]_\infty$ (20).

	x	y	z	U(eq)
Fe(1)	0	4142(1)	2500	16(1)
Cl(2)	-851(1)	5860(1)	3390(2)	18(1)
N(3)	735(2)	2243(4)	2484(5)	16(1)
C(4)	1511(2)	2308(4)	2661(7)	22(1)
C(5)	425(2)	909(4)	2563(6)	16(1)
C(6)	1999(3)	1069(5)	2938(7)	25(1)
C(7)	871(3)	-385(4)	2770(6)	22(1)
C(8)	1666(3)	-292(5)	2985(7)	27(1)

U(eq) is defined as one third of the trace of the orthogonalized U_{ij} tensor.

Table 63. Atomic coordinates (x 10^4) and equivalent isotropic displacement parameters ($Å^2$x 10^3) for $[Et_4N]Cl\cdot[Fe_2Cl_4(MeOH)_4(\mu\text{-}2,2'\text{-bpym})]$ (26).

	x	y	z	U(eq)
Fe(1)	4897(1)	8535(1)	1266(1)	22(1)
Fe(2)	-310(1)	8727(1)	-1465(1)	23(1)
Cl(1)	5009(1)	8624(1)	2810(1)	31(1)
Cl(2)	4618(1)	7007(1)	1022(1)	36(1)
Cl(3)	-511(1)	8991(1)	-2992(1)	36(1)
Cl(4)	-464(1)	7176(1)	-1384(1)	37(1)
Cl(5)	2482(1)	10010(1)	-371(1)	30(1)
O(1)	3341(3)	8852(3)	1161(3)	41(1)
O(2)	6457(3)	8416(3)	1196(3)	35(1)
O(3)	-1835(3)	9002(3)	-1252(3)	47(1)
O(4)	1271(3)	8614(3)	-1440(3)	39(1)
N(1)	5113(3)	9983(3)	1170(3)	19(1)
N(2)	5156(3)	11177(3)	152(3)	19(1)
N(3)	-38(3)	10147(3)	-1156(3)	21(1)
N(4)	176(3)	11167(3)	6(3)	15(1)
N(5)	-2527(4)	9882(3)	4678(3)	30(1)
C(1)	5258(4)	10573(4)	1811(4)	25(2)
C(2)	5348(5)	11452(4)	1667(4)	25(2)
C(3)	5307(4)	11719(4)	817(4)	23(2)
C(4)	5073(4)	10323(4)	358(4)	17(1)
C(5)	2567(5)	8505(5)	1623(5)	55(2)
C(6)	7086(5)	7849(4)	1732(5)	46(2)
C(7)	61(4)	10805(4)	-1731(4)	24(2)
C(8)	216(4)	11642(4)	-1448(4)	28(2)
C(9)	262(4)	11816(4)	-578(4)	25(2)
C(10)	35(4)	10359(4)	-318(4)	19(1)
C(11)	-2704(5)	8859(5)	-1779(5)	51(2)
C(12)	1837(5)	8018(4)	-1916(5)	46(2)
C(13)	-2182(5)	8944(4)	4844(4)	36(2)

Table 63. (cont'd).

	x	y	z	U(eq)
C(14)	-2942(6)	8242(5)	4629(5)	53(2)
C(15)	-1663(6)	10454(5)	4948(5)	53(2)
C(16)	-1847(7)	11427(5)	4828(6)	87(3)
C(17)	-2864(5)	10020(4)	3714(4)	34(2)
C(18)	-2104(6)	9853(5)	3099(4)	45(2)
C(19)	-3415(6)	10080(5)	5181(5)	53(2)
C(20)	-3237(8)	9961(6)	6156(5)	89(4)

U(eq) is defined as one third of the trace of the orthogonalized U_{ij} tensor.

MICHIGAN STATE UNIVERSITY LIBRARIES
3 1293 02092 7129